

**Latent free radical polymerization of bulk methacrylates: Organic visible-light
photocatalysis and supramolecular effects**

A Thesis Submitted to the Faculty of the Graduate School of
the University of Colorado Boulder

by

Alan Aguirre-Soto

B.S., Instituto Tecnológico y de Estudios Superiores de Monterrey, 2009

B.S., Hochschule Reutlingen, 2009

M.S., University of Colorado Boulder, 2011

In partial fulfillment of the requirement
for the degree of Doctor of Philosophy
Department of Chemical and Biological Engineering

2015

This thesis entitled:

Latent free radical polymerization of bulk methacrylates: Organic visible-light photocatalysis and supramolecular effects

written by Alan Aguirre-Soto

has been approved for the

Department of Chemical and Biological Engineering

Dr. Jeffrey W. Stansbury

Dr. Christopher N. Bowman

Date _____

The final copy of this thesis has been examined by the signatories, and we find that both the content and the form meet acceptable presentation standards of scholarly work in the above mentioned discipline.

Aguirre-Soto, Alan (Ph.D., Department of Chemical and Biological Engineering)

Latent free radical polymerization of bulk methacrylates: Organic visible-light photocatalysis and supramolecular effects

Thesis directed by Professor Jeffrey W. Stansbury.

Light-activated polymerizations are important because they allow spatially and temporally controlled synthesis of polymers and polymer-based materials under ambient conditions. This capability is greatly valued in numerous applications, such as coatings, adhesives, sealants, electronics, diagnostics, dental materials, and biomaterials. Hence, the amount of precursors and synthetic routes available increases every year. However, there is limited understanding of the often intricate mechanisms via which many of these reactions work. As a consequence, this technology has not been exploited to its fullest. As a result, a need exists for the elucidation of refined mechanisms and kinetic models that aid in better understanding, predicting, and controlling such immensely valuable reactions for the production of practically relevant materials and devices.

The present work delves into the refinement of the theoretical framework of free radically initiated chain growth polymerizations in solvent-free (bulk) monomer(s). This project originated to explain an unexpectedly long-lasting (>2000 s) latent polymerization observed after briefly exposing certain (meth)acrylic monomers, like 2-hydroxyethyl methacrylate, to visible-light in the presence of an organic photocatalysis composition including Methylene blue (MB^+), Hünig's base and an Iodonium salt. Free radical chain growth photopolymerizations in bulk typically stop shortly (< 17 s) after irradiation is extinguished. Thus, it was clear that the available kinetic models and theories were not sufficient to account for this atypical, and potentially advantageous, phenomenon.

We simultaneously monitored the photocatalyst (MB^+) and monomer concentrations with UV-Vis and FT-IR spectroscopy, respectively, under several irradiation regimes. EPR spectroscopy was used to determine the nature and lifetime of the light-generated radical intermediates. Rheology confirmed that the vinyl groups consumed in the dark are in fact being polymerized. Quantum chemical calculations

guided the experiments and supported the proposal of a photocatalytic mechanism via which reactive initiating free radicals can be produced long after the irradiation is extinguished. With these results, the unusually extended latent polymerization was explained by two mechanistic conclusions: 1) organic photocatalysis using MB^+ /Hünig's base/Iodonium salt stores energy during irradiation in the form of Leuco Methylene Blue via an $e^-/\text{H}^+/e^-$ transfer process instead of the typical single e^- transfer; then, LMB is later used to produce radicals upon reaction with the Iodonium salts for even thousands of seconds after light cessation, and 2) hydrogen bonding exacerbates the Trommsdorff-Norrish effect via which bimolecular termination is hindered, thus resulting in the extension of the vinyl polymerization in the dark by the well-documented radical occlusion process.

To my wife and rock Tere,
To my parents Gloria and Hector
And to my grandmother Elda
For their support, unconditional love, enthusiasm,
And encouragement.
Without these things this
Thesis would not have been possible.

Acknowledgments

First, I would like to express my gratitude to my advisor Dr. Jeffrey W. Stansbury who guided me through this journey of ups and downs. I greatly appreciated the conversations, the ideas, the encouragement and the freedom to give this dissertation a personal touch. Secondly, I would like to thank my wife Teresa Arizpe for her persistent and unconditional support, patience, and motivation to strive to become a better man and a better researcher. This dissertation would not have been possible without your shoulder to rest on at times of weakness. I am incredibly fortunate to have you with me. I would like to extend my gratitude and appreciation as well to the member of my scientific committee: Dr. Christopher N. Bowman, Dr. Charles B. Musgrave, Dr. Wayne Mahoney, Dr. Robert McLeod, and Dr. Douglas Gin; your feedback, patience, support, ideas, passion for science, time, and insightful conversations have been of immense value to me. This dissertation contains some of the knowledge that you all shared with me throughout these years. Furthermore, I would like to thank my collaborators and friends: Chern-Hooi Lim, Kaja Kaastrup, David Glugla, James Wydra, Weixian Xi, Dr. Annette Erbse, Sandra Ledem, Caroline Szczepanski, Eric Dailing, JianCheng Liu, Matthew Barros, and Steven Lewis. I greatly appreciated the personal and scientific support, the (often-lengthy) brainstorming sessions, the MATLAB coding sessions, and, in general, the shared passion for polymers, materials, photochemistry, and science. Lastly, I would like to thank all the members of the Stansbury and Bowman groups, University of Colorado Boulder, the funding agencies (IUCRC Photopolymerizations, the National Institute of Health, and the National Institute for Dental and Craniofacial Research(NIH/NIDCR)).

CONTENTS

CHAPTER	Page
1	INTRODUCTION
	1.1 General significance 1
	1.2 Background..... 3
	1.2.1 Polymer chemistry 3
	1.2.2 Photochemistry applied to the synthesis of polymers..... 13
	1.3 Initial observation of latent polymerization..... 23
	1.4 Project scope and significance within the Polymer chemistry field 26
	1.5 Thesis statement 29
	1.6 References 30
2	OBJECTIVES
	2.1 Specific aims of the present thesis..... 37
	2.2 Roadmap of the thesis..... 39
3	VISIBLE-LIGHT ORGANIC PHOTOCATALYSIS FOR LATENT RADICAL-INITIATED POLYMERIZATION VIA $2e^-/1H^+$ TRANSFERS: INITIATION WITH PARALLELS TO PHOTOSYNTHESIS..... 41
	3.1 Introduction 42
	3.2 Experimental section 45
	3.2.1 Materials..... 45
	3.2.2 Light source..... 45
	3.2.3 Fourier transform-infrared spectroscopy (FT-IR)..... 46
	3.2.4 Ultraviolet-visible (electronic) spectroscopy (UV-Vis)..... 46

3.2.5	Electrospray ionization mass spectrometry (ESI-MS)	47
3.2.6	Quantum chemical calculations	47
3.2.7	Lateral polymerization experiments	47
3.2.8	Thick disc polymerization experiments	48
3.2.9	Methylene blue extraction from poly-HEMA gel	48
3.3	Results and discussion	49
3.3.1	Fast radical production in MB ⁺ /DIPEA/DPI ⁺ formulations	49
3.3.2	PET reaction of MB ⁺ /DIPEA generates colorless LMB	50
3.3.3	Radical production from LMB/DPI ⁺ reaction	54
3.3.4	Stored energy in LMB extends radical production after irradiation	56
3.3.5	Photocatalysis cycle mimics photosynthesis	57
3.3.6	Spatial extension of radical production beyond the irradiation site	57
3.3.7	Photo-activated synthesis of thicker polymers	60
3.4	Conclusions	61
3.5	References	63
3.6	Supplemental Information	67
4	MONITORING DYNAMIC INITIATOR/MONOMER INTERACTIONS AND PHOTOPOLYMERIZATION PERFORMANCE WITH SIMULTANEOUS REAL-TIME UV-VIS/FT-NIR SPECTROSCOPY	78
4.1	Introduction	79
4.2	Experimental section	86
4.2.1	Materials	86
4.2.2	Light source	87
4.2.3	Coupling of FT-NIR and UV-VIS spectroscopy	88

	4.2.4 Spectral analysis.....	89
	4.3 Results and discussion.....	90
	4.3.1 Validation of the analytical device.....	90
	4.3.2 Deconvoluting monomer effects on photoinitiation and polymerization	94
	4.3.3 Determination of overall polymerization efficiency	96
	4.3.4 Amine structure effect on CQ and monomer consumption	97
	4.3.5 calculation of quantum yield of radical production and polymerization.....	98
	4.4 Conclusions	99
	4.5 References	100
5	EFFECTS OF OXIDANT ADDITION TO THE CAMPHORQUINONE/AMINE PHOTOREDUCTION PAIR	109
	5.1 Introduction	110
	5.2 Experimental section	114
	5.2.1 Materials.....	114
	5.2.2 Light source.....	115
	5.2.3 Simultaneous UV-Vis and FT-NIR monitoring.....	115
	5.2.4 Spectral processing	116
	5.3 Results and discussion	117
	5.3.1 Effect of oxidant addition	117
	5.3.2 Oxidant concentration effect.....	120
	5.3.3 Effect of oxidant chemistry.....	122
	5.4 Conclusions	123
	5.5 References	124
6	GROUND STATE COMPLEX FORMATION AS TOOL FOR CONTROLLING PHOTOREDOX CATALYSIS.....	128

6.1	Introduction	129
6.2	Experimental section	133
6.2.1	Materials.....	133
6.2.2	Crystallization of methylene blue (MB ⁺) and [MB ⁺ ...amine] complexes.....	133
6.2.3	Polarized light microscopy for visualization of crystals.....	134
6.2.4	UV-Vis spectroscopy for determination of complex formation.....	135
6.2.5	Coupled UV-Vis/FT-NIR full spectrum real-time monitoring	136
6.2.3	Quantum chemical calculation.....	136
6.3	Results and discussion	136
6.3.1	MB ⁺ readily forms ground state complex with <i>i</i> Pr ₂ NEt.....	136
6.3.2	Ru(bpy) ₃ ²⁺ only forms complex with <i>i</i> Pr ₂ NEt in polar aprotic solvents.....	136
6.3.3	Ground state complexes are close enough for hydrogen atom abstraction	140
6.3.4	Free radical polymerization is absent when photocatalyst/amine complex is present.....	142
6.4	Conclusions	147
6.4.1	Guidelines to favor e ⁻ /H ⁺ /e ⁻ transfer over single e ⁻ transfer in photoredox catalysis.....	142
6.5	References	148
7	LONG-LIVED MACRORADICALS STABILIZED BY HYDROGEN BONDING: SELF-ORGANIZATION AND THE TROMMSDORFF-NORRISH EFFECT	154
7.1	Introduction	155
7.2	Experimental section	159
7.2.1	Materials.....	159
7.2.2	Light source.....	159

7.2.3	Fourier Transform-Infrared Spectroscopy	160
7.2.4	Electron paramagnetic spectroscopy (EPR).....	160
7.3	Results and discussion	161
7.3.1	Dependence of the latent polymerization on the radical production rate	161
7.3.2	Latent polymerization as a function of the conversion-at- light-shut-off and temperature	163
7.3.3	Effect of physical mobility restrictions on the extent of the latent vinyl consumption	166
7.3.4	Long-lived propagating radicals formed in monomers with alcohol groups	169
7.3.5	Importance of methyl group in the methacrylate monomers	170
7.3.6	Pre-organization (C=C templating) theory vs mobility theory	172
7.4	Conclusions	174
7.5	References	175
8	CONCLUSIONS AND FUTURE DIRECTIONS	179
8.1	Conclusions	
8.1.1	Summary of the key points from each chapter	179
8.1.2	Answer to the central question: role of each component latent vinyl polymerization	181
8.2	Future directions	184
8.2.1	Addition of photobase	184
8.2.2	Simultaneous rheology/initiation/polymerization monitoring ..	186
8.3	References	188
	BIBLIOGRAPHY	189
	APPENDIX	
A.	APPLICATIONS OF THE COUPLED UV-VIS/FT-NIR	

MONITORING DEVICE	
Real-time detection of fluorophore diffusion from polymers	
Determination of quantum yields of base generation	
Elucidation of the radical production mechanisms by eosin/amine	
Elucidation of the photocatalysis cycles involving Acridine Orange for the reduction of CO ₂ into methanol	

FIGURES

Figure	Page
1.1. Three-dimensional representation of linear polymer chain and classification of the mechanism used in polymer synthesis	5
1.2. Kinetics of chain growth polymerization	8
1.3. Polymer materials produced from photopolymerization of acrylate and (meth)acrylate monomers	12
1.4. Components of photopolymerizable formulations and Jablonski diagram for common photochemical transitions of photoinitiators	15
1.5. Key parameters that determine the performance of photopolymerizable formulations.....	18
1.6. Bond dissociation energies in common organic molecules and most probable photochemical pathways	19
1.7. Molecular orbital theory and typical photochemical interactions in carbonyl compounds	21
1.8. Result from initial discovery of latent polymerization in (meth)acrylate formulations containing Methylene blue/Hünig's base/onium salt	23
1.9. Summarization of all formulations tested during the initial discovery of the latent polymerization	25
1.10. Components of model formulation selected for analysis of the unusually prolonged latent polymer consumption	27
3.1. Free radical production requires the presence of the onium salt when irradiating MB ⁺ /amine formulations in bulk (meth)acrylates	48

3.2. Photoredox catalysis scheme for light harvesting that leads to the latent polymerization.....	49
3.3. Quantum chemical calculations for the thermodynamic feasibility of the reaction between an <i>i</i> Pr ₂ NEt-based α -amino alkyl radical & HEMA	51
3.4. Dearomatization of MB ⁺ thiazinic center responsible for the loss of the characteristic blue color.....	52
3.5. Activation energy of MB ⁺ regeneration step matches the activation energy for the initiation of the free radical polymerization	54
3.6. Latent free radical generation in the dark allows extension of the polymerization beyond the spatial and temporal reach of the photons	57
3.S1. Quantum chemical calculations details for the Gibbs Free Energy of the reaction between the <i>i</i> Pr ₂ NEt-based radicals and HEMA	65
3.S2. Vinyl fraction conversion vs time for the light-induced polymerization of HEMA with MB ⁺ and three different aliphatic tertiary amines	72
3.S3. Electro-spray ionization mass spectrometry results for characterization of the closed shell products from the reaction between MB ⁺ and <i>i</i> Pr ₂ NEt.....	73
3.S4. Calculations for the determination of the activation energy of initiation for the free radical polymerization of HEMA in the presence of MB ⁺ , <i>i</i> Pr ₂ NEt and an iodonium salt	73
3.S5. Changes in latent polymerization profile with various doses.....	74
3.S6. Negative control for the polymerization of thick polymer materials using CQ/EDMAB in HEMA showing lack of polymerization	75
3.S7. Extraction of methylene from a HEMA hydrogel to show capability of removing the residual color after polymerization.....	75

4.1. Picture and data output from the coupled UV-Vis/FT-NIR technique developed for mechanistic analysis of photopolymerization, and model formulation for the initial studies on CQ/amine photoinitiator combinations	81
4.2. Top view of the analytical diagram of the apparatus build for the simultaneous probing of initiator and monomer in real-time	84
4.3. Typical data output from both the UV-Vis and the FT-NIR spectrophotometers.....	87
4.4. Determination of the rate of photon absorption, initiator consumption, conversion, rate of polymerization and quantum yields from the same set of experiments	92
4.5. Interesting results for quantum yields, polymerization kinetics, CQ photoreduction, and photosensitivity of CQ/amine formulations in dental monomers.....	94
5.1. Components for the analysis of the effect of addition of onium salts as oxidants to CQ/amine formulations	107
5.2. Redox potentials for the oxidants selected for the studies.....	108
5.3. Comparison of the effect of the presence of an onium salt on the polymerization rate and the CQ consumption using the coupled UV-Vis/FT-NIR analytical device	110
5.4. Refined mechanism for the free radical production using CQ/aliphatic amine/onium salt as photoinitiating system	111
5.5. Refines mechanism for the free radical production using CQ/amino acid/onium salt as photoinitiating system.....	113
5.6. Effect of the concentration of oxidant to both the rate of polymerization and the consumption of CQ under continuous irradiation.....	114
5.7. Effect of the structure of the oxidant on the rate of polymerization and the consumption of CQ.....	115
6.1. $e^-/H^+/e^-$ vs e^- transfer correlates to the formation of ground state complexes between photocatalysts (like MB^+) and iPr_2NEt	129

6.2. MB ⁺ and Ru(bpy) ₃ ²⁺ form ground state complexes with <i>i</i> Pr ₂ NEt and Et ₃ N depending on the solvent polarity.....	132
6.3. Complex formation correlates with production of radicals due to the reaction via e ⁻ /H ⁺ /e ⁻ transfer instead of single e ⁻ transfer	136
6.4. Effect of complex formation on reaction pathway explains the numerous report on the uniquely high performance and unexpected results obtained with <i>i</i> Pr ₂ NEt-containing photoredox catalysis formulations.....	138
6.S1. Microscope images of MB ⁺ and ground state complex crystals grown from ethanol solutions.....	142
6.S2. Changes in UV-Vis absorbance of CQ upon drop-wise addition of <i>i</i> Pr ₂ NEt in ethanol.....	142
6.S3. Formation of Leuco Methylene Blue from UV-Vis analysis of MB ⁺ /amine solution in ethanol during irradiation with 660 nm red LED.....	143
6.S4. Photocatalyst and monomer consumption vs time for CQ/ <i>i</i> Pr ₂ NEt and MB ⁺ / <i>i</i> Pr ₂ NEt solutions in HEMA.....	143
7.1. Structures of monomers and photoinitiators used for the analysis of the slow latent polymerization observed with HEMA in the absence of the MB ⁺ /amine/onium salt photoinitiator system	149
7.2. Observations of latent polymerization with different photoinitiators and temperature effect on the rate of polymerization under continuous irradiation	152
7.3. Latent polymerization with DMPA photoinitiator in HEMA and the effect of temperature on the rate of the latent polymerization.....	155
7.4. Effect of sampler pressure on the latent polymerization	158
7.5. Electron paramagnetic resonance spectroscopy result of the partial exposure of DMPA solution in EMA and HEMA showed a long-lived radical with hydrogen bonding present	160

7.S1. Photorheology experiments confirm that the mechanical properties change in the dark after short irradiation is oxygen is removed from system	167
A.1. Photoinduced release of fluorophore from polymer network.....	203
A.2. Mechanism for photobase generation.....	204
A.3. Quantum yields of base generation with a series of photobase generators	205
A.4. Mechanism for the photoreduction of eosin by amines.....	206
A.5. UV-Vis result showing the photobleaching of eosin under irradiation in the presence of triethanolamine in water.....	207
A.6. Photoreduction of eosin and regeneration monitoring with couple UV-Vis/FT-NIR technique	208
A.7. Decay of Acridine Orange and formation of Leuco Acridine Orange by appearance of a new absorbance peak centered in the UV region	209

Chapter I

Introduction

1.1 General significance

Polymerizations are chemical reactions that involve the linking of many relatively small molecules, ‘monomers’, into bigger molecules called ‘polymers’, from the ancient Greek *mono*, *polus*, and *meros* meaning “one”, “many or much”, and “parts”, respectively (Berzelliuss, 1833). The increase in molecular size caused by polymerizations often correlates with a perceptible change in phase from liquid to solid state. These polymers, also referred to as ‘macromolecules’ (Figure 1.1- Left), are arguably one of the most important current topics in science, technology and engineering because of two main realizations: first, that materials composed of or containing polymers, mainly in their solid state, are uniquely advantageous in terms of versatility, accessible control of the molecular structure, broad set of attainable properties, and accessibility (including their use in conjunction with ceramics and semiconductors); and secondly, that Materials Science and Engineering in general is and has been paramount in the accelerated progress of humanity since the 1800’s (from the Industrial Revolution to the Materials Genome Initiative^a). As a consequence, polymer-based materials and bulk polymeric materials have permeated into arguably almost every field of the physical sciences, engineering, and, most currently, biology and medicine; as well as into almost every aspect of our everyday life.

Currently, most efforts in research and development of polymers are being targeted towards the synthesis of rationally designed or tailor-made organic macromolecular architectures via new polymerization routes and with novel monomers as building blocks^{1,2}, as well as towards the engineering of hybrid materials (which combine more than one class of materials: ceramics, metals, polymers, etc.) that enable or enhance a broad array of technologies such as conductive polymers for solar energy

^a The Materials Genome Initiative is a multi-agency initiative designed to create policies, resources, and infrastructure to support U.S. institutions in an effort to discover, manufacture and deploy advanced materials twice as fast and at a reduced cost. (<http://www.whitehouse.gov/mgi>)

harvesting, photonics for optoelectronic devices, detection of biological molecules, and medical diagnostics, to name a few. However, this growth in the library of materials and synthetic approaches inherently opens up opportunities in areas related to the elucidation of the reaction mechanisms via which both conventional and novel polymers are synthesized. The latter is important because the development of advanced materials is strongly dependent on the availability of experimental data and theoretical models that describe how materials are and can be created as well as how the material properties depend on the molecular structure, reaction conditions, and post-processing, among other factors. Hence, elucidation of the working mechanisms and structure-property relationships serves as platform for the rational design and accelerated deployment of the next generations of advanced materials. We definitely have made progress in understanding how many of these polymerizations work, but there is most certainly a lot that can still be accomplished in this endeavor.

Additional contributions to the set of theoretical and physical frameworks employed to predict and control such multitude of polymer syntheses has an immense practical value. With this in mind, we embarked into the elucidation of the polymerization mechanisms by which certain types of polymeric materials are produced using light (which is thought of as being composed of units called ‘photons’) as energy source; thus working at the interface of polymer chemistry and photochemistry. This research project originated after the discovery (which will be described later in this *Introduction*) of an unusual, and potentially advantageous, latency in some photo-induced polymerization reactions; where latency can be generally defined as the time-delay in or prolongation of the polymerization of the reacting monomer(s) after activation by a relatively short initial exposure to light. After an initial exposure to light, certain free radical-based polymerizations were found to continue over intervals (> 2000 s) much greater than the expected lifetime or typical duration (< 17 s) of light-activated solvent-free polymerizations under ambient conditions, as will be described. Hence, the main objective of this thesis was simply answering the fundamental question: what reaction mechanisms are responsible for the uniquely long-lasting polymerization of the monomers presented herein after initial exposure to light? To answer this

question we had designed and built a novel analytical device that allowed us to expand the capabilities in terms of the mechanistic analysis that can be performed *in-situ* during polymerization reactions. The application of this unexpected phenomenon will be introduced both as proof of the proposed polymerization mechanisms and as motivator for the undertaking of the present research project. These mechanisms are also placed in the context of Material Science and Engineering, and their significance within the field of polymer chemistry is identified throughout the chapters of this thesis.

1.2 Background

1.2.1 Polymer chemistry

In practical terms, the use of organic polymers dates back to the Egyptians, as they employed photochemically (using sunlight) induced reactions to solidify or harden liquid coatings made with bitumen of Judea (which contains nature-derived polymerizable compounds) as part of their mummification process³. Then, the Mayans were documented in the 1500's to have recognized the utility of the polymerization of liquid latex from trees into natural rubber to produce the first solid bouncing ball for its unique mechanical properties, namely its elasticity. However, it was not until 1839 that Charles Goodyear discovered that the vulcanization process improves durability and properties of natural rubber (polymer of isoprene: 'polyisoprene') via crosslinking modification of its chemical structure, thus initiating the industrial era of polymers with the introduction of elastomeric materials, specifically for automobile tires. Then, in 1907 Leo Bakeland developed the first purely synthetic polymer, Bakelite (a glassy material), as an electrical insulator. A few decades later (1917-1927) researchers finally gathered enough evidence, e.g. X-ray crystallography, to support Staudinger's theory (1920) about the concatenation or addition of small molecules into macromolecules via the formation of covalent bonds (by the sharing of electrons between atoms). In most cases, this concatenation of small(er) repeat molecular units into high-molecular-weight covalently bonded macromolecules correlates with a significant increase in viscosity (and a change of phase in some instances): a low-viscosity liquid turns

into a solid precipitate (if in solution), or into a rubbery or glassy (higher-viscosity) solid if in bulk. Staudinger was awarded the Nobel Prize in 1953 as it became evident that his theory provided the physical framework to explain how the linking of monomer molecules occurs, and to understand the connection between the macromolecular architecture (e.g. linear chains, branched chains, networks, dendrimers or star-shaped) and the macroscopic properties of the final polymer material. Ultimately, the experimental and theoretical work of Staudinger, Carothers and Flory (1974 Nobel Laureate) established the fundamental relationships between the increase in molecular weight, the kinetics of polymerization reactions, and the observed changes in the physical properties associated with the increase in molecular weight from reactants to products: solubility, chemical resistance, toughness, refractivity, light scattering, and viscosity, for example. Due to the latter, and aided by discoveries in other fields, like physics, organic, analytical and theoretical chemistry, polymer research and development dramatically increased between 1927 and 1980, culminating in an industrial shift from metals (steel, aluminum, copper) to polymers in the USA, and subsequently world-wide. The theoretical set of rules designed by these pioneers constitutes the foundations for the analysis of the polymerization reactions pertinent to this research.

Efforts during the twentieth century also paved the way towards the classification of polymerization reactions. Two types of classifications came into use: one, based on the structure of the macromolecules formed⁴, and the other, based on the reaction mechanism by which they are produced⁵. The former divides polymerization reactions into condensation and addition polymers. The latter divides them into step growth and chain growth mechanisms. Although the respective terms may often be used interchangeably because most condensation polymers are produced via step growth and most addition polymers are formed by chain growth mechanisms, these terms are not always synonymous^{6,7}, as in the free radically initiated step growth polymerization of thiols with vinyl monomers⁸.

Carothers, the pioneer of step growth reactions, proposed that condensation polymerization includes polymers formed from multi-functional (bearing more than one reactive group per molecule)

monomers by one of several condensation reactions of organic chemistry (polycondensations) with the elimination of small molecule by-products, e.g. water. One example is the synthesis of polyamides from reaction of diamines with diacids. Reactions that do not obey this principle were considered to form addition polymers. However, it quickly became evident that this approach was not appropriate as several cases were found that do not fall into Carothers' definition for condensation-type reactions, but that should be classified as such. As a result, a more rigorous definition was brought to use: a polymer can be classified as condensation polymer if its synthesis involves the elimination of small molecules, or it contains functional groups as part of the macromolecular chain, or its repeating units lack certain atoms that were present in the precursor monomer(s). If the polymer does not fulfill at least one of these criteria, then it is thought to be an addition polymer⁶. Note there are a few rare cases in of chain growth polymers with functional groups in their backbone structure. This approach is still confusing and might not be applicable to some of the ever-evolving routes for macromolecular synthesis.

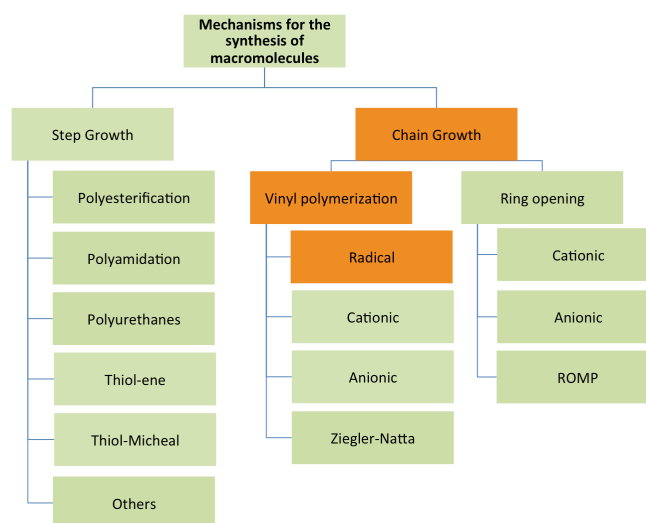
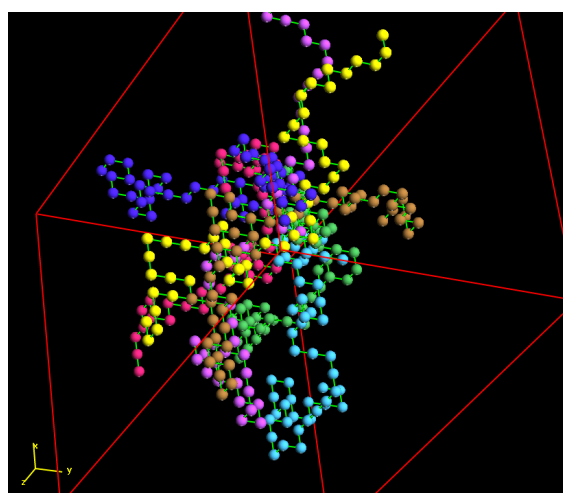


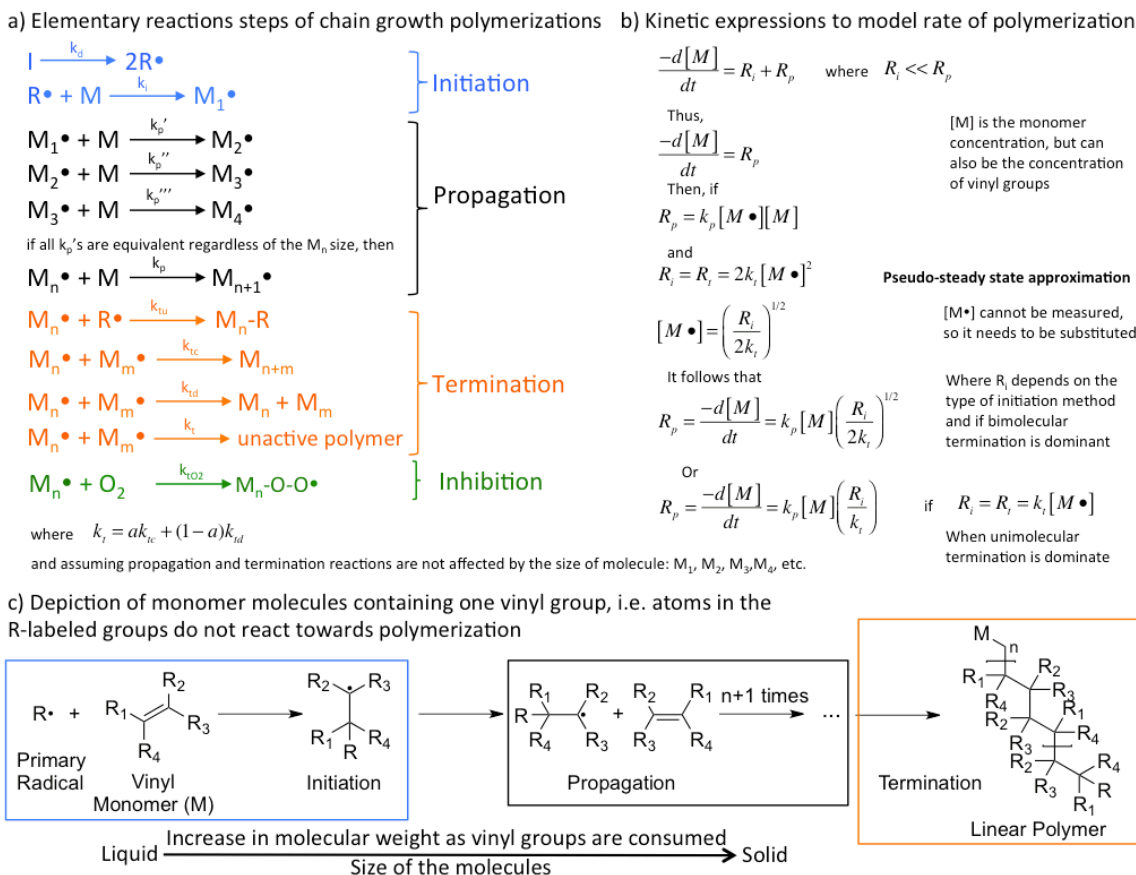
Figure 1.1 Left- Three-dimensional (3D) representation of entangled linear polymer chains or macromolecules composed of small molecular units (monomers) depicted as beads. Right- Classification of the most ubiquitous mechanisms for the synthesis of polymers. Emphasis of the present work is the polymerization of vinyl monomers (containing at least one carbon-carbon double bond) using free radicals, also called 'radicals', to initiate the polymerization reaction- labeled with orange boxes.

A more recent and arguably more useful classification is the one proposed by Flory⁹ based on the mechanism via which the macromolecules are built-up: step growth or chain growth. This approach makes the distinction based on several features, but the most important ones are perhaps the identities of the reactants, and the dependence of the molecular weight of the macromolecules formed on the extent of conversion (defined as the fraction of reactive functional groups consumed at a given point in time, and labeled as ρ or χ). Step polymerizations proceed by the stepwise reaction between the functional groups of the monomers, like in the A-A + B-B type addition to form -A-A-B-B- units. As a result of such mechanism, the size of the macromolecules increases at a relatively slow rate as a function of monomer conversion. This classification is important because the polymerization reactions displaying the unusual latent polymerization fall clearly in the chain growth category, and hence must display the particular characteristics associated with this reaction mechanism (Figure 1.1).

In chain growth polymerizations, on the other hand, an initiator molecule (referred to simply as ‘initiator’) forms a reactive center (free radical, cation, anion, base, or acid), which starts the addition of monomer in a chain reaction mechanism (Figure 1.1). In contrast, step growth polymerizations are typically not initiated by reactive centers. However, examples have been reported in which this is not the case, such as in thiol-ene polymerizations that react via a step growth mechanism despite being initiated by free radicals^{8,10,11}. Formation of the reactive centers can be induced thermally, chemically, electrochemically, or photochemically (using radiation). Then, addition of hundreds, thousands, or even hundreds of thousands and millions of monomer molecules proceeds due to the so called ‘propagation’ of the reactive centers in a successive fashion; where the reactive centers are regenerated after addition of each monomer unit (Figure 1.2-a and c). This addition of many molecules per reactive center is termed ‘chemical amplification’. Finally, the growth of the macromolecules ceases when the reactive center is ‘killed’ or ‘terminated’ by one of the plausible termination reactions, such as radical-radical quenching, hydrogen abstraction, or acid-base (Figure 1.2-a). Termination (with rate constant values on the order of $k_t \sim 10^7 \text{ L}\cdot\text{mol}^{-1}\cdot\text{s}^{-1}$) is kinetically and thermodynamically more feasible than propagation ($k_p \sim 10^3 \text{ L}\cdot\text{mol}^{-1}\cdot\text{s}^{-1}$).

$l*s^{-1}$) in conventional free radical chain growth polymerizations. Hence, if initiation is ceased and no more reactive centers are produced, termination quickly reduces the concentration of the propagating radicals to zero (or effectively zero in most cases), halting the propagation process as a consequence, and stopping the polymerization reaction shortly thereafter (which was expected to occur in the polymerizations discussed herein). However, if initiation does not cease, radical concentrations are kept orders of magnitude lower ($\sim 10^{-8}$ M) than the usual monomer concentrations (10^{-1} M), and thus the propagation of monomer can proceed at steady-state^b rates of polymerization (R_p): $10^{-6} < R_p < 10^{-4}$ L \cdot mol $^{-1}$ \cdot s $^{-1}$ (see Figure 1.2). The distinguishing characteristic of chain polymerizations is that polymer growth takes place only by the reaction between monomer and the propagating reaction center(s). Monomer does not react with in-activated monomer molecules, and the macromolecular species formed at a given point in time do not react between each other. As a result, chain growth polymerizations will lead to the formation of high-molecular-weight macromolecules from the very early stages of the reaction, as opposed to the step-growth mechanism in which high-molecular-weight macromolecules are only present towards the very end of the reaction. In consequence, kinetics are typically affected by the rapid growth in molecular size from the early stages of the polymerization reaction. The four essential assumptions on which this theoretical framework is founded are: 1) steady-state concentration of reactive centers prevails throughout the reaction, 2) radical reactivity is independent of the chain-length (size of the macromolecules), 3) no chain transfer reaction(s) occur, and 4) no auto-acceleration or gel-effect occur (defined in the next paragraph). If any of these assumptions is not valid, then the associated kinetic expressions (Figure 1.2- b) have to be re-examined. In this work, we will discuss how modifications to these assumptions could explain the unusually prolonged polymerization observed so long (> 2000 s) after initiation is expected to cease.

^b A pseudo-steady state approximation is most often valid, which means that the rate of initiation can be assumed equal to the rate of termination, as depicted in Figure 1.2-b.



c) Depiction of monomer molecules containing one vinyl group, i.e. atoms in the R-labeled groups do not react towards polymerization

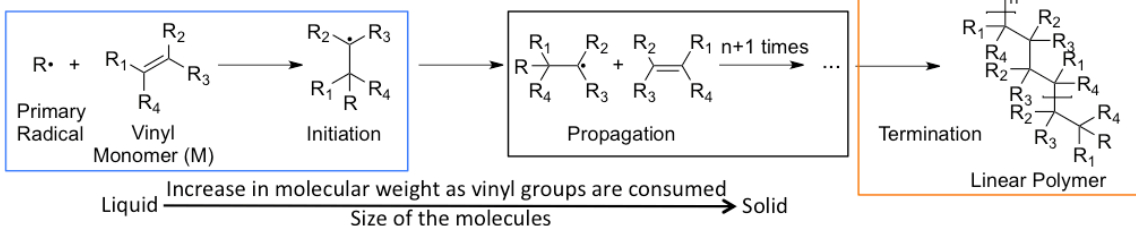


Figure 1.2 Elemental reaction steps, kinetic expressions and depiction of chain growth polymerization reactions of monomers containing vinyl groups (C=C double bonds). This constitutes the basic theoretical framework to explain and predict the formation of macromolecules via the chain growth mechanism.

The validity of these assumptions and of the associated kinetic model of chain growth polymerizations are also dependent on the experimental conditions at which the reactions are performed, e.g. bulk (monomer only), in solution, in suspension, or emulsion. For example, modifications to this general construct of chain growth polymer synthesis (Figure 1.2- b) have been proposed to explain atypical experimental results observed in bulk polymerizations; namely the increase in the rate of polymerization (R_p), called ‘auto-acceleration’, that is due to the accumulation of propagating radicals (deviating from the pseudo-steady state approximation) as a result of the increase in mobility restrictions associated with the change in viscosity and free volume when the material solidifies. The latter preferentially decreases the termination rate constant (k_t) for the dominant bimolecular radical-radical

quenching reactions because bigger macromolecular propagating radicals have lower probability of colliding as they are the most sensitive to increasing diffusion restrictions (Figure 1.2-a). The latter is normally referred to as the *Trommsdorff-Norrish* or gel effect. The polymerizations analyzed for this work are performed in bulk conditions, and thus are not expected to obey the pseudo-steady state assumption at all conversions due to this gel-effect.

Probably the only important ambiguities with the classification of step and chain growth mechanisms are the cases in which a linear increase in molecular weight with conversion of monomer to polymer is observed for some chain growth reactions, e.g. ‘living’ polymerizations, ring-opening polymerizations, and in protein synthesis. In these cases, relatively minor alterations to the general working mechanism for chain growth polymerization are responsible for the linear dependence of polymer growth on the conversion or extent of the reaction, e.g. termination reactions are absent or initiation is significantly faster than termination of the reactive centers. As a result, living polymerizations and ring-opening polymerizations are classified as chain growth mechanisms despite such a discrepancy. A subset of the living polymerizations category was then created, which is called controlled radical polymerizations (CRP). This refers to reactions that work via a chain growth mechanism in which very slow termination reactions allows sufficient control over the polymer growth to make more uniform sizes and macromolecular architectures, as opposed to the stochastic growth in molecular weight associated with typical free radical initiated polymerizations due to competing propagation and termination reactions. CRP’s is relevant to the present work because this type of reactions is characterized by having a hindered termination process (as will be detailed in Chapter 7), which could partially explain the unusual latency observed in the polymerizations analyzed for this research.

Ultimately, the polymerization reactions that display the unusual latency fall into the free radical initiated chain growth classification (Figure 1.1); and, hence would be expected to function via the general mechanism described above (Figure 1.2). However, the prolonged polymerization of the monomer after the expected cease of initiation indicates that some modifications to this general

framework might be required. A plausible theory is that initiation is not ceasing when it is expected to. A slightly altered initiation mechanism in the present polymerizations could lead to an extended production of primary radicals, as will be discussed in Chapters 3, 4 and 6. On the other hand, if termination becomes hindered by mobility restrictions, or is kinetically less feasible due to the formation of a dormant state (as in controlled radical polymerizations), or due to competitive reactions, like chain transfer, then propagation of the free radicals will not stop as quickly as expected after light cessation, discussed in Chapter 7.

In chain growth polymer synthesis, vinyl monomers are by far the most commonly used⁶. These are defined as monomers that contain one or more carbon-carbon double (called ‘pi’ or π) bonds, commonly referred to as ‘unsaturations’, for example: ethylene, α -olefins, styrene, vinyl esters, methacrylic esters, and vinyl ethers. Polymerization of vinyl monomers via reaction of the π -bonds with either free radical, cationic, or anionic reactive centers has been reported. Monomer reactivity towards any of these reactive centers depends on inductive and resonance effects, which alter the electron density of the molecule, imposed by the substituent(s) attached to the carbon-carbon double bond, C=C, and is based on thermodynamic and kinetic considerations. However, initiation of the chain growth polymerization of vinyl monomers by free radicals is the most ubiquitous. As the reactive centers propagate they convert every pi-bond into two sigma bonds after successive monomer additions (every double bond can add two monomer molecules, one in each side, as opposed to what happens in step growth polymerization), as depicted in the blue box in Figure 1.2- c. As a result, the backbone of most of these macromolecules is exclusively composed of carbon atoms, which contributes to the often-useful mechanical properties of materials composed from these polymers.

Vinyl monomers with one double bond per molecule (mono-vinyl) normally form linear or branched polymer chains (Figure 1.1), whereas multi-vinyl monomers produce crosslinked polymer networks shown in Figure 1.2. Differences in macromolecular architecture greatly influence what the properties of the final material will be (Figure 1.3): typically crosslinked polymers are ‘thermosets’

(meaning that once the polymer is created it can not be modified by thermal post-processing), whereas non-crosslinked macromolecules tend to be soluble ‘thermoplastics’ (meaning that they can be melted and reshaped, e.g. by extrusion). Regardless of their architecture though, bulk solid polymer materials can be classified by their mechanical properties as well, namely viscosity, glass transition temperature (T_g -temperature at which a material transitions from a glassy to a rubbery behavior), moduli (rubbery or glassy, loss or storage, Young’s). Thus, crosslinked polymer networks can have either rubbery or glassy character. As will be shown later, the polymeric materials synthesized for this research project are sometimes referred to as ‘densely crosslinked polymer networks’, which tend to extend the glassy (high modulus) state to higher temperatures while providing higher rubbery modulus above the T_g . These are different than the loosely crosslinked networks, which include hydrogels and typically form rubbery solids or gels. The density of these networks will become important due to the *Trommsdorff-Norrish* effect: kinetics of the polymerization reaction are significantly affected by the mobility of the propagating radicals as the transition from a low-viscosity ‘liquid’ into a high-viscosity solid occurs, i.e. changes in viscosity and free volume depend on the rate of polymerization (R_p), but also affect the evolution of R_p themselves by effecting k_p and k_t ¹²⁻¹⁶.

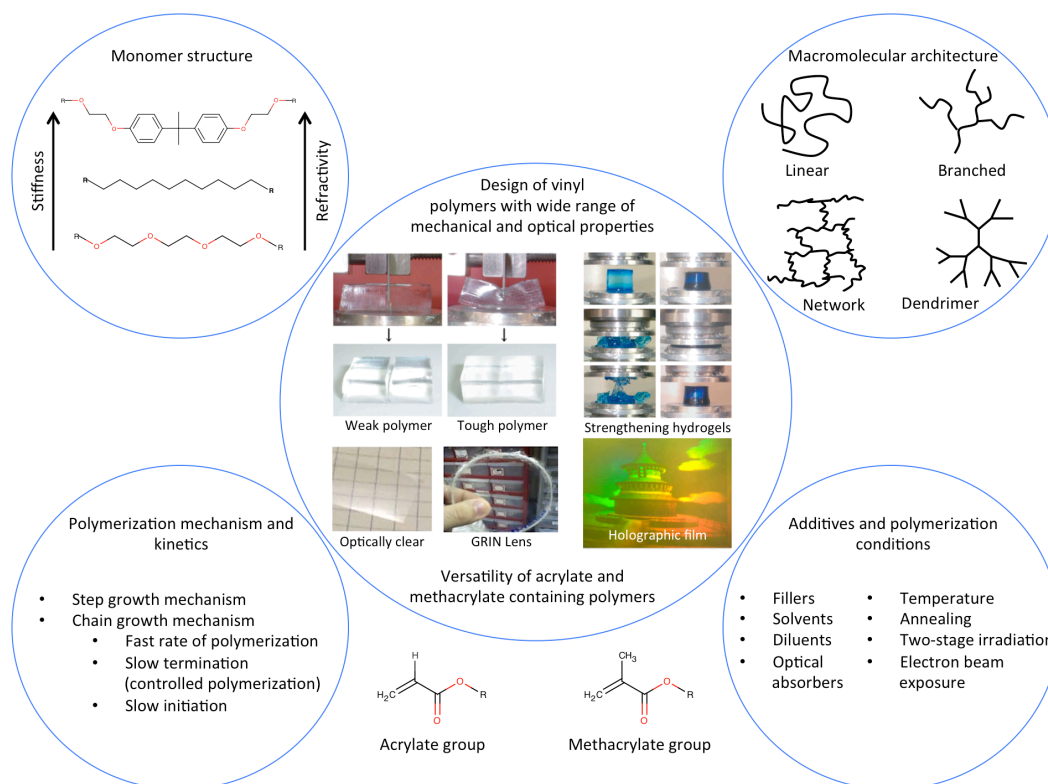


Figure 1.3 Versatility of polymer materials containing made with monomers containing vinyl groups. Monomer structure, macromolecular architecture, polymerization mechanism, kinetics, processing conditions and additives are the most important parameters that can be used to tailor the properties of the polymer-based materials.

Acrylates and methacrylates, referred to as ‘(meth)acrylic’ monomers from this point on, are used widely as vinyl monomers^c to produce predominately linear polymer from monovinyl monomers as well as densely crosslinked networks, which offer a variety of mechanical and optical properties (Figure 1.3), when di- or multi-vinyl monomers are involved. These are preferred in applications such as coatings¹⁷, dental materials¹⁸, photolithography for electronics manufacturing¹⁹, 3D prototyping²⁰, holography²¹, biomaterials^{22,23}, adhesives²⁴, sealants, contact and other lenses²⁵, micro device fabrication (integrated circuits)^{21,26}, to name some. These polymer networks are useful because of their chemical resistance (thermally stable and solvent resistant), mechanical strength and toughness (glassy materials) and optical

^c (Meth)acrylic monomers contain a C=C double bond that is conjugated to an ester group (-CO-O-R).

clarity^{21,27}. Methacrylates (which generally display a slower rate of polymerization but higher T_g compared with acrylate analogs) are often preferred in dental and biomaterials where strength and durability are major issues²⁸⁻³¹, whereas acrylates are most widely employed for electronics and optical materials since high strength is not a primary requirement, and their higher reactivity facilitates production efficiency^{27,32}. Herein we discuss the synthesis of crosslinked networks as macromolecular architectures built from acrylates and methacrylates; but focusing primarily on the latter. As a result, the present work, although fundamental in nature, will pertain to the use of polymers as dental and orthopedic materials^{20,33-36} but extends to many other application areas as well. The bulk polymerization of (meth)acrylic monomers employed in these applications has been documented to generally obey the reaction mechanism of free radical initiated chain growth polymerizations described above. Modifications have been proposed to explain most of the existent experimental data^{13,14,37,38}. However, the currently available theoretical framework and models sometimes fail to correlate with experimental results; as for the unusually prolonged latent polymerizations presented herein. The central problem addressed by this thesis is then to explain the unusual latency in polymerization of mono-vinyl hydroxylated methacrylate monomer, such as 2-hydroxyethyl methacrylate (HEMA), by refining the mechanistic framework introduced in this section to account for discrepancies from the conventionally accepted mechanistic standards.

1.2.2 Photochemistry applied to the synthesis of polymers

Photochemically induced initiation of chain-growth polymerizations of acrylates and methacrylates has been exploited since the 1940's³⁹. The integration of polymer chemistry and photochemistry is usually highly effective and practically advantageous since photochemical reactions readily produce free radicals that efficiently initiate polymerization of (meth)acrylic monomers (Figure 1.2). Photoinitiated polymerizations (called 'photopolymerizations' from this point onward) of (meth)acrylic monomers belong to the chain growth category, and thus, their reaction mechanism should

obey the fundamental principles introduced in the *Polymer Chemistry* sub-section (above). Hence, the role of the photochemical reaction(s) in a photopolymerization is most often restricted to the production of primary radicals, labeled herein as ‘primary’ to differentiate them from monomer-based ‘propagating’ radicals (Figure 1.2). Immediately after the photochemical step, primary radicals initiate monomer molecules that quickly turn into ‘propagating radicals’, which concatenate as vinyl groups add to the macromolecules. It is important to note that radicals produced from the photochemical reactions are typically highly reactive towards a variety of functional groups and molecules. Hence, initiation of polymerization is typically inhibited at least slightly by the presence of molecular oxygen or any other molecules that can compete with the vinyl groups for the reaction with the free radicals produced. Finally, propagating radicals are neutralized or ‘killed’ by unimolecular and bimolecular termination processes⁴⁰⁻⁴² via radical-radical quenching, radical scavenging by oxygen to form more stable peroxy radicals^{43,44} (Figure 1.2-a), and hydrogen abstraction (in a few cases). Almost always, photochemical production of free radicals ceases completely when irradiation is extinguished. If in fact, no more radicals are produced when the light is extinguished, then the propagation should be halted by termination, and the polymerization should stop shortly after the extinction of irradiation. It is thus plausible that, in the cases studied in this work, initiation does not cease when irradiation is no longer present. Hence, Chapters 3, 5 and 6 examine the photochemical mechanisms via which primary radicals are produced in the formulations that display the long-lasting polymerization in the ‘dark’ (after irradiation is no longer present), in order to assess whether or not primary radicals are somehow produced after an initial exposure to irradiation.

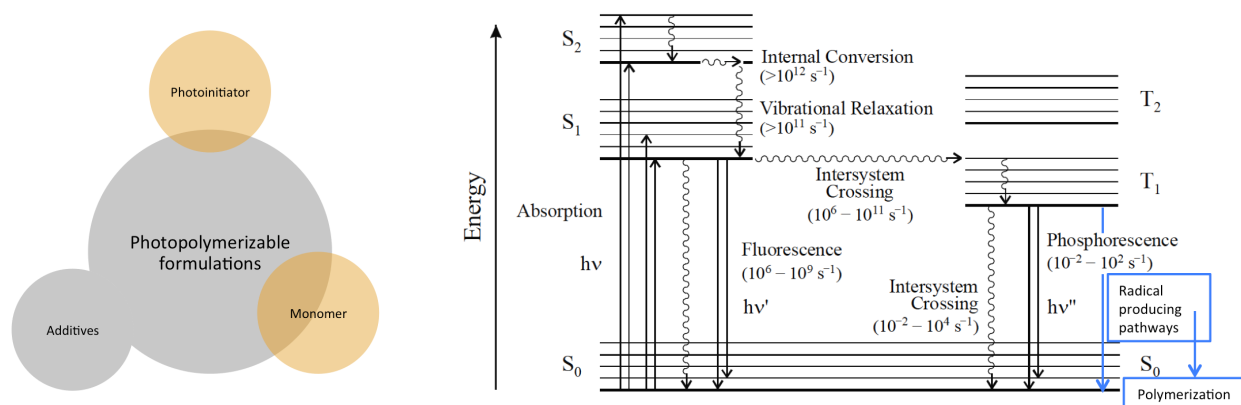


Figure 1.4 Left- Components of a photopolymerizable formulation. The focus of this work is on the reactions involving initiator(s) and the monomer(s). Right- General Jablonski diagram for photochemical and photophysical transitions. Primary radicals are most often produced from the triplet state (T₁) following intersystem crossing from the initially formed singlet excited state of the photoinitiator molecule.

The photochemical and photophysical pathways of a chromophore are shown in the form of a Jablonski diagram (Figure 1.4- Right). The atoms in the chromophore molecule are associated via the interactions of their respective electrons. Depending on the energy level at which these electrons are found, several ‘electronic states’ can be devised: S₀, S₁, S₂, T₁, T₂, and so on. The nomenclature of said states describes the spin multiplicity of the entire molecule, where S stands for singlet, and T stands for triplet. The subscript then describes the ranking of a particular state relative to its energy. Thus, S₀ is the singlet state with the lowest energy, also referred to as ground state. All other states are excited states in which at least one electron ‘jumped’ to a higher energy orbital, S₂ and S₁ for example, after the absorption of one photon by the molecule. These electronic states are not discrete, but rather manifolds of several states that are energetically close to each other. The absorption of one, or in some cases two, photon(s) corresponds to the transition from the ground state singlet S₀ to a higher energy excited state singlet, like S₂. From S₂, several decay pathways can occur by which the absorbed energy is essentially released: radiative, radiationless, or quenching processes. Radiative processes are those in which a photon of equal

or lower energy is emitted by the excited molecule, such as fluorescence and phosphorescence. Radiationless processes include internal conversion, vibrational relaxation, and intersystem crossing, from which the absorbed energy from light is then released as heat. Intersystem crossing involves a change in the spin of the electron found in the excited state. Any transition that involves a spin flip is said to be spin-forbidden, and usually occurs at relatively lower rates. From any of the excited states, S_1 or T_1 for example, a molecule can undergo bond cleavage, if the energy of said state is equal or higher than the bond dissociation energy of a particular bond in the molecule (Figure 1.6-Left), or it can be quenched by a ground state molecule. Quenching processes involve the reaction of a molecule in an excited state with another molecule. Most frequently the other molecule is in its ground state. Quenching typically occurs from one of the triplet states since they are longer lived due to the fact that the transition from a triplet T_1 back to the original ground state manifold S_0 is spin forbidden. In some cases, quenching of one of the singlet states, S_1 or S_2 , can occur despite the shorter lifetimes of these states. Triplet state quenching of chromophores by amines (Figure 1.4- Right) typically leads to primary radicals, and will be analyzed in detail in Chapters 3, 5, and 6. Analysis of such photochemical and photophysical pathways will allow us to scrutinize the free radical production process to assess its effect on the latent vinyl polymerization.

Photochemical production of primary radicals to initiate polymerizations has several advantages over thermal, chemical (redox) and electrochemical initiation: 1) polymerization proceeds rapidly under ambient conditions, 2) polymer synthesis can be controlled spatially and temporally, 3) higher energy-efficiency, and 4) no requirement for solvents (which are usually employed to control temperature of the reaction)⁴⁵. The spatiotemporal control attained in the photopolymerization of (meth)acrylic monomers is mainly due to the fact that these reactions are chain growth processes, initiated by free radicals, and activated photochemically^d. Given this unique set of characteristics, photoinitiated free radical chain growth polymerization of acrylates and methacrylates has been the preferred polymer synthesis method

^d Radical production is restricted to where and when photons are present, free radicals are very short lived, and high-molecular weight macromolecules are quickly formed. Thus, polymerization is restricted spatially and temporally to the presence of photons. The role of these factors will be discussed throughout the thesis chapters.

where materials need to be formed *in-situ* or *in-vivo* under ambient conditions with no or little solvent present (except for hydrogels^{46,47}), and with control over when and where the reaction occurs. However, photopolymerizations have arguably not been utilized to their full potential due to a generally limited understanding of the polymerization process, as well as to unresolved issues, such as oxygen or water inhibition (oxygen quenches radicals while water quenches anions and cations), volumetric shrinkage and stress development (most important in solvent-free systems), and presence of potentially leachable unreacted monomer⁴⁵. The goal of this research is not solving any of the latter practical issues, but rather contributing to the better understanding of how these photopolymerizations function and offer potential opportunities for expanding the scope of how photocuring can be employed. Even though no direct attempts were made to improve or eliminate any of the practical concerns just mentioned, some connections will be drawn as we describe the mechanisms associated with the delayed polymerization of monomer after initial irradiation exposures.

Photopolymerization of (meth)acrylic monomers (sometimes called ‘resins’) has mostly been performed with ultra-violet (UV) irradiation, which includes the range of the electromagnetic spectrum between 10 and 380 or 400 nm. Although, the practical wavelength range is 300 to 400 nanometers since most organic molecules absorb light at shorter (< 300 nm) wavelengths, i.e. control over or specificity of the light absorption is lost. This type of radiation is advantageous (as in photopatterning for electronic and optical materials) because the relatively shorter wavelengths (considering the diffraction limit) readily allow production of patterns on the micron scale, and more recently even on the nanometer scale¹⁹. Additionally, the light emission from the sun at the earth’s surface and conventional lamps (use for everyday human activities) has a relatively low intensity in the ultraviolet region. As a result, UV photopolymerizable formulations are more photochemically stable than those that are visible-light sensitive. Furthermore, UV sensitive components inherently lack color. Hence, optically clear polymers required for many applications can be readily produced (except when yellow by-products are produced).

Lastly, UV-initiated systems tend to have a sufficiently long shelf life under ambient dark conditions, typically upon the customary additional of stabilizers or radical inhibitors.

However, demand has risen to design photoinitiators that can efficiently initiate chain growth polymerization via production of free radicals in response to the lower energy, more benign visible-light⁴⁸⁻⁵⁰, corresponding to wavelengths between 400 and 700 nm. One example is dental and other biomaterials applications that typically use light in the 400-500 nm range due to the more stringent requirements associated with these, and to the greater penetration of longer-wavelength visible-light through the sample as a result of less scattering. Both industrial and academic efforts have been undertaken to design photopolymerizable formulations that can be activated by these longer wavelengths. While it has been confirmed that longer wavelength (lower energy) photons have a significantly lower photo-toxicity, several issues have clearly been identified. First, visible-light sensitive photoinitiators are inherently colored. Thus, for applications in which clear polymer materials are desired these are not preferred. Secondly, these photoinitiators tend to be photochemically and thermally less stable than UV-sensitive systems. Lastly, in most cases these photoinitiators require a combination of at least two reactants and/or reagents in order to produce free radicals at competitive rates. The latter makes the photochemical mechanisms more intricate. Finally, there seems to be a limited understanding of the complex reaction mechanisms involved in the primary radical production, and how to design visible-light multi-component photoinitiators that have a longer shelf life, polymerize monomers at fast rates, and that can potentially be used to make optically clear polymer materials.

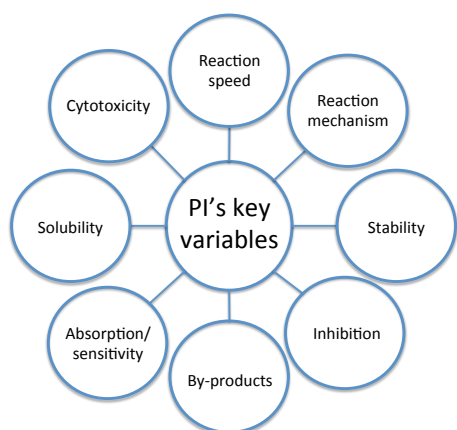


Figure 1.5 Most important factors determining the performance of photoinitiators (PI's) for the synthesis of polymer materials.

Having stated the differences between photoinitiators based on the type of light they are sensitive to, we can now classify them based on the photochemical pathways by which they tend to react (Figure 1.6- Left). This classification divides photoinitiators into Type I and Type II. The former involves light absorbing molecules (called ‘chromophores’) that cleave into smaller molecules upon excitation by a photon. This process is referred to as ‘cleavage’, since one or more atomic bonds (typically sigma C-C bonds) are broken upon light absorption. The breaking of a covalent bond (homolysis) produces two free radicals, which are typically both used to initiate the polymerization. So far, these initiators have been synthesized to react only upon absorption of UV and blue light (UV-470 nm). Despite many recent efforts, the synthesis of blue light (400-470 nm) sensitive chromophores is still complex and generally more costly than the synthesis of UV (300-400 nm) sensitive photoinitiators. This typically requires the synthesis of molecules containing heavier atoms, such as germanium. As a result, Type I photoinitiators have not successfully displaced the Type II PI’s in applications where the use of UV light is preferentially avoided, such as in dental materials⁵¹. Examples of Type I photoinitiators are bis-acyl phosphine oxides and acetophenones.

λ (nm)	Photon energy (kcal/mol)	Species	BDE; T_1 (kcal/mol)
200	143	Ketone (C=O)	173
250	114	O ₂ (O=O)	119
300	95	ROH (H-O)	105
350	82	Ketones (C-C)	80
400	71	ROOH (H-O)	88
450	64	H ₂ O ₂ (H-O)	88
500	57	C-Br	65
550	52	S-S	52
600	48	H ₂ O ₂ (O-O)	51
650	44	C-I	45
700	40	Polyaromatics	40 (T_1)
800	36	R ₂ O ₂ (O-O)	37
1,000	27	-	-

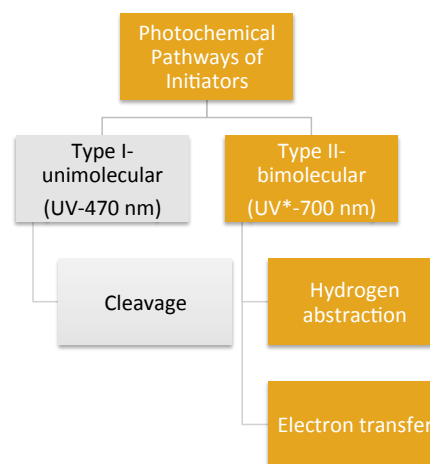


Figure 1.6 Left- Table comparing Bond Dissociation Energies of typical organic compounds with triplet state energies from most important functional groups in photochemistry. Right- classification of photoinitiators by their primary photochemical pathways.

In contrast, Type II photoinitiators cannot undergo cleavage after light absorption, but rather require the reaction with an additional ground state molecule (sometimes called a co-initiator). By utilizing these bimolecular photochemical reactions, primary radicals can be produced with lower energy photons from visible-light chromophores at practically competitive rates. Chromophores employed for these photoinitiating systems are most often easier to synthesize and readily accessible, like quinones and organic dyes, than Type I photoinitiators. After a photon is absorbed by the chromophore, bimolecular reactions can occur if the excited state(s) is sufficiently long-lived to allow for the collision with the non-excited (or ground state) co-initiator. Examples of some of the most ubiquitous reactions subsequent to the absorption of one visible-light photon are hydrogen abstraction and electron transfer (Figure 1.7-Right). Some of the most plausible photochemical pathways for molecules excited via $n \rightarrow \pi^*$ and $\pi \rightarrow \pi^*$ (where n stands for non-bonding orbital, π stands for the bonding pi-orbital, and π^* stands for the anti-bonding pi-orbital) transitions are describe in Figure 1.7-Left. The probability of each one of the plausible pathways that follow after the initial photochemical step depends primarily on the nature of the light-absorbing functional group, the structure of the co-initiator, and the medium in which the reaction is performed. An example of a Type II photoinitiator is the combination of camphorquinone as a chromophore, and an amine as a reductive co-initiator; this system is still the standard for the *in-situ* photopolymerization of (meth)acrylic monomers used as dental restorative materials⁵¹⁻⁵⁵.

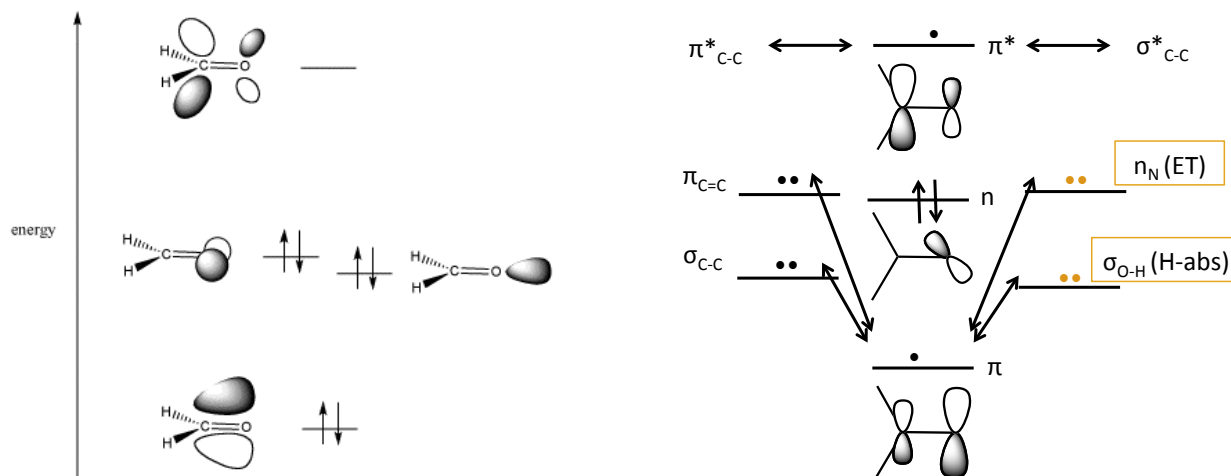


Figure 1.7 Left- Frontier molecular orbitals in a carbonyl compound. Right- Plausible photochemical pathways for molecules excited from the via the electron jump from a π orbital to a π^* orbital.

Around the 1970's, it was identified that in many cases the addition of a third component, e.g. an onium salt as an oxidant, to the conventional Type II chromophore/reductant combinations most often leads to an increase in the rate of polymerization and also often in the final limiting conversion achieved. Since the rate of polymerization and final extent of polymerization are probably the most important practical parameters, these so-called 'three-component' (as they require at least three different molecules) photoinitiators immediately attracted interest within the photopolymerizations community^{56,57}. However, it was not realized until 2010 that these photoinitiators usually fall into the field of organic and organometallic photocatalysis (also called photoredox catalysis). Detailed mechanistic studies of three-component initiator systems were reported in our lab beginning in 2009 but it is recognized that Fouassier and coworkers review publication on this class of photoinitiating compositions made the first reported connection between these two topics⁵⁸. Such realization is important because of two main reasons: first, photocatalysis has recently gained much attention in organic chemistry due to the development of better catalysts for more efficient and 'greener' synthesis of pharmaceuticals, fuels, and important organic precursors; secondly, the photochemical mechanisms involved in the synthesis of small organic molecules in solution using photocatalysis can serve as guideline for what can be expected to occur in polymer

synthesis. Production of reactive centers for polymer synthesis via visible-light organic photocatalysis has thus become arguably the most important topic in current photoinitiators literature. However, due to the inherently complex reaction mechanisms involving photochemical and ground state reaction steps, and to the almost infinite amount of possible photoinitiating combinations of three (or more) components, there are still considerable challenges involving unresolved mechanisms. The unusually prolonged latency was observed in photopolymerizable formulations containing a few of these combinations, including one composed of an organic dye as the photocatalyst, a tertiary aliphatic amine as a reductant co-initiator, and an onium salt as an oxidant. Hence, a significant effort was made herein to elucidate how the present organic photocatalysis photoinitiating system(s) produces the radicals involved in the polymer synthesis.

1.3 Initial observation of latent consumption of vinyl groups

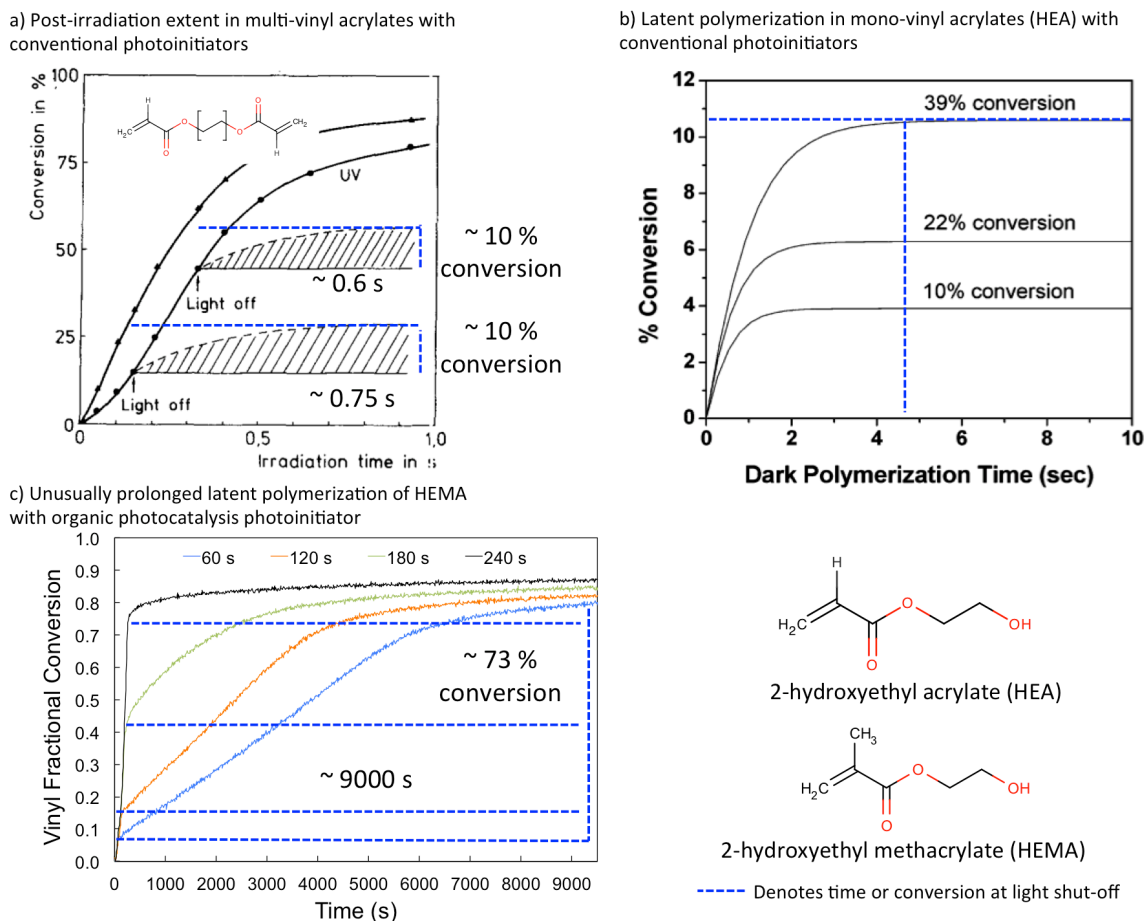


Figure 1.8 Comparison of typical duration of a chain growth free radically initiated polymerization reaction and the unusual prolonged latency observed for some visible-light organic photocatalysis photoinitiators in (meth)acrylic monomers in bulk. a) shows the extent of the post-irradiation vinyl consumption seen in dimethacrylates that are typically used for coatings applications⁵⁹. b) shows the dark polymerization obtained for mono-vinyl hydroxylated acrylate monomers after the extinction of irradiation at different conversions⁶⁰. c) shows the uniquely prolonged latent polymerization seen when 2-hydroxy ethyl methacrylate is irradiated for different exposure times when containing a visible-light photocatalytic photoinitiator that is introduced below.

Due to concerns about the photo-toxicity of UV and even blue light to some extent, a portion of the research efforts in our laboratory have been aimed at the study and development of these three-component photocatalytic photoinitiators that can polymerize dental (meth)acrylic monomers at competitive rates upon activation with wavelengths greater than 470 nm. Some of the initiator components are fairly polar salt compounds that display quite limited solubility in many traditional non-

polar monomers. Thus, slightly polar hydroxylated (meth)acrylic monomers were required to test the photoinitiating combinations. Around 2008-2009^{61,62}, it was observed that polymerization of some of these mono-vinyl hydroxylated methacrylates, such as 2-hydroxyethyl methacrylate (HEMA), in bulk and initiated by >500 nm light in the presence of photocatalytic (three-component) photoinitiators, e.g. Methylene blue/Hünig's base/Onium salt, displayed an unusually prolonged latency after an initial irradiation with a broad-band halogen lamp: 100 W quartz halogen (Oriol) and a dental halogen lamps (Coltolux 75)^e, as shown in Figure 1.9. The unusually prolonged polymerization in the dark was determined by quantifying the concentration of vinyl groups in real-time with Fourier-Transform Near-Infrared Spectroscopy (FT-NIR). The use of this technique to analyze the kinetics of photopolymerization reactions will be presented in Chapter 4 as we describe the design of a spectroscopy apparatus for the improved kinetic analysis of the reactions involved in these polymerizations. Using FT-NIR it was observed that the monomer continues to polymerize for over 5000 s after an initial 10 to 60 s irradiation period. To put this in perspective, the post-irradiation consumption of vinyl groups is expected to last in general for roughly 0.1-17 s, base on reported kinetic constants and rate values, after the production of primary radicals has ceased at light extinction in conventional bulk free radical photopolymerizations via the chain growth mechanism, as confirmed previously by Decker and by Hoyle and coworkers (Figure 1.8- a and b)^{59,60}. Hence, these initial experiments seemed to indicate that some unique mechanisms might be in play in these photopolymerizable formulations. The most plausible scenario based on the known mechanisms introduced herein are: first, that production of primary radicals is sustained long after the irradiation has ceased; secondly, that the termination of the propagating radicals is somehow slower than in conventional reactions; and finally, that both conditions synergistically contribute to the unusually prolonged duration of the reaction after the initial irradiation.

The set of formulations analyzed in the initial testing and discovery of the latent polymerization (before the start of the present project) are listed below:

^e Halogen lamps are typically used for applications in which visible-light emission is desired. The emission spectrum of these lamps will be described in Chapters 3-6 of this thesis.

	Chromophore (Photocatalyst)	Reductant	Oxidant	Monomer	Intensity (mW/cm ²)	Lamps used
Formulations showing signs of latent polymerization						
Formulation 1	Zn-ttp	DABCO	DPI-AsF ₆	HEMA	0.15	Quartz Halogen & Dental Lamps Effective emission 400-800 nm
Formulation 2	Zn-ttp	DABCO	DPI-PF ₆	HEMA	0.15	
Formulation 3	Zn-ttp	DABCO	DPI-Cl	HEMA	0.15	
Formulation 4	Zn-ttp	DABCO	DPI-SbF ₆	HEMA	0.15	
Formulation 5	Zn-ttp	DIPA	DPI-AsF ₆	HEMA	0.15	
Formulation 6	Zn-ttp	MDEA	DPI-AsF ₆	HEMA	0.15	
Formulation 7	Zn-ttp	NaOH	DPI-Cl	HEMA	440	
Formulation 8	Rose bengal	DABCO	DPI-AsF ₆	HEMA	0.15	
Formulation 9	Rose bengal	DABCO	DPI-AsF ₆	HEA	0.15	
Formulation 10	Methylene Blue	Hünig's Base	DPI-Cl	HEA	500	
Formulation 11	Methylene Blue	Hünig's Base	DPI-Cl	HEMA	0.15	
Formulation 12	Methylene Blue	Hünig's Base	DPI-Cl	HEMA	500	
Formulation 13	Methylene Blue	Hünig's Base	DPI-Cl	HEMA	0.15	
Formulation 14	Methylene Blue	Hünig's Base	DPI-AsF ₆	HEMA	500	
Formulation 15	Methylene Blue	Hünig's Base	DPI-PF ₆	HEMA	500	
Formulation 16	Methylene Blue	TEA	DPI-Cl	HEMA	500	
Formulation 17	Methylene Blue	DIPA	DPI-Cl	HEMA	500	
Formulation 18	RF	Hünig's Base	DPI-Cl	HEMA	500	
Formulation 19	RZ	Hünig's Base	DPI-Cl	HEMA	500	
Formulations showing conventional duration of polymerization post-irradiation						
Formulation 20	CQ	DABCO	DPI-AsF ₆	HEA	440	Quartz Halogen & Dental Lamps Effective emission 400-800 nm
Formulation 21	CQ	EDMAB	-	HEA	500	
Formulation 22	Zn-ttp	Hünig's Base	DPI-Cl	HEMA	500	
Formulation 23	RB	Hünig's Base	DPI-Cl	HEMA	500	
Formulation 24	Methylene Blue	TEA	-	HEA	500	
Formulation 25	Methylene Blue	Hünig's Base	TPS	HEMA	500	
Formulation 26	Methylene Blue	Hünig's Base	Triazine	HEMA	500	
Formulation 27	Methylene Blue	Hünig's Base	DPI-Cl	TEGDMA	500	
Formulation 28	Methylene Blue	Hünig's Base	DPI-Cl	HDDA	500	
Formulations with several degrees of latent polymerization						
Formulation 29	Methylene Blue	Hünig's Base	DPI-Cl	HEMA/HDDA	500	

Figure 1.9 Table listing of the formulations tested for the discovery and assessment of the prolonged latency in the polymerization of methacrylate monomers HEMA and HEA. Formulations inside the black box displayed the longest latent polymerization of vinyl groups in bulk monomer after brief irradiation.

Conclusions derived from the initial assessment of the latent monomer consumption:

1. HEMA shows more latent polymerization than its non-methylated analog: HEA

2. Other monomers, such as TEGDMA and HDDA show no latent polymerization as expected
3. Presence of the electron donor (iodonium salt) leads to latent polymerization, absence of this component causes no monomer consumption after light extinction (CQ/EDMAB)
4. Increasing the counter-anion size of the iodonium salt oxidant increases solubility, thus leading to more latent polymerization
5. The combination of Methylene Blue/Hünig's Base/DPI-Cl in HEMA gives the highest latent polymerization, whereas Methylene Blue/Triethylamine showed none
6. Lower light intensity increases the duration of the latent monomer consumption
7. The rate of polymerization immediately after light cessation changes based on the conversion at the time of light shut-off

1.4 Project scope and significance within the field of polymer chemistry

The present work focuses on the mechanism of free radical chain growth polymerization of (meth)acrylic monomers in bulk and initiated by visible-light organic photocatalysis with methylene blue as photocatalyst (or chromophore), Hünig' base (N-N-diisopropyltheylamine) as a reductant and diphenyliodonium salts as oxidant. We chose this particular three-component combination because it displayed the most extensive latent polymerization in the initial experiments. Additionally, the three components are readily accessible and are not as expensive as most of the organometallic photocatalysts, such as zinc, ruthenium and iridium complexes. The latter seems more appropriate for applications in which the photocatalyst is not recoverable, as is the case for bulk photopolymerizations.

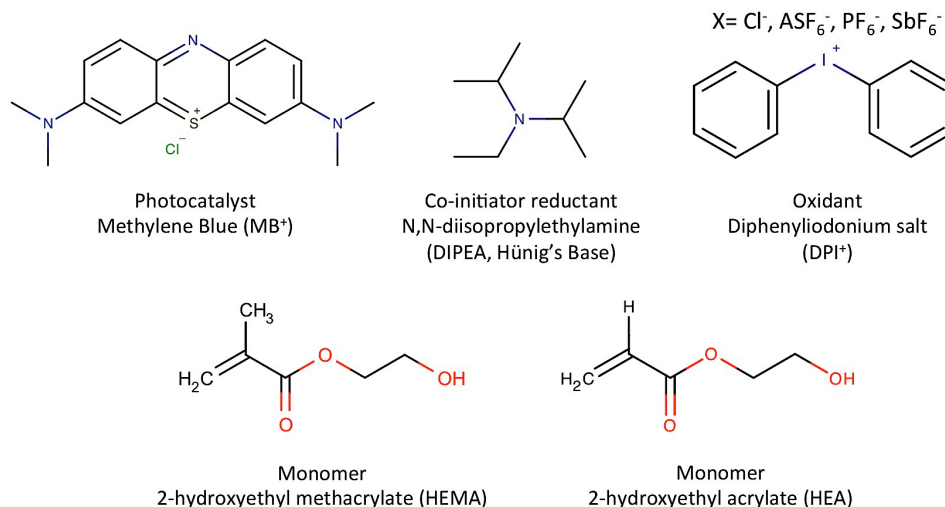


Figure 1.10 Components of the model formulations studied in the present thesis. The combination of MB⁺/DIPEA/DPI⁺ in HEMA leads to the most extensive latent monomer polymerization after an initial irradiation.

Methylene blue belongs to the class of thiazine dyes. Thiazine dye/amine combinations have been reported to initiate polymerization of vinyl monomers in solution since the middle of the twentieth century, but limited mechanistic information has been gathered for bulk polymerizations, and for MB⁺/amine/oxidant combinations used in free radical chain growth polymerizations in general⁶³⁻⁶⁹. The Hünig's base (DIPEA) is a very useful non-nucleophilic base for organic synthesis. However, its use as a ground state reductant co-initiator for photoinitiating systems has remained nearly non-existent. Iodonium salts are typically utilized as UV-sensitive cationic photoinitiators. However, their use as oxidants for three-component systems to initiate both radical and cationic polymerizations as well as dual network and hybrid polymers has been reported on numerous occasions.

As introduced in the previous sections, free radical initiated photopolymerizations are characterized by rapid cessation of polymerization when the irradiation is extinguished. Continuous irradiation is necessary to sustain the polymerization up to its completion since the reactive centers have a very short lifetime due to highly favorable termination reactions. In contrast, cationic photopolymerizations allow significant latent polymerization due to the longer lifetime of this type of

active center. Thus, the latent monomer conversion, also referred to as dark cure, is a signature trait of cationic photopolymerizations. However, monomers that are suitable for polymerization via cationic reactive centers are less common and typically more expensive to synthesize. There are a few examples of (meth)acrylic monomers that react via free radical chain growth photopolymerization and exhibit a longer than usual latent polymerization⁷⁰. These are also characterized by other unusual properties, such as significantly higher reactivity than typically encountered, and formation of a certain amount of unexpected crosslinks perhaps due to chain transfer reactions. However, these monomers are not commercially available. As a result, the prospect of bringing the latent polymerization capability to the free radical photopolymerization of readily accessible monomers is highly significant within the field of polymer chemistry because of the following reasons: 1) reduced processing times could be attained, 2) required photoinitiator concentrations may be lowered, 3) polymerization in shadowed regions adjacent to irradiated areas could be achieved, 4) enhanced depth of cure, and 5) photopolymerization of pigmented or highly filled (optically opaque) materials might be allowed. Fundamentally, the elucidation of the mechanisms that cause the unique attributes of these monomers and of methods to control this latent polymerization could open new vistas for the application of free radical chain growth photopolymerizations to unexplored areas and needs.

Over the past three or four decades, developments in organic chemistry, quantum chemistry, synthesis, catalysis, and supramolecular chemistry have shaped current polymer science and engineering. Currently, the question is not whether we can synthesize macromolecules efficiently, but rather, if we can achieve ever better control of the polymerization reaction, and the macromolecular architecture; thus attaining unprecedented levels of precision in terms of the physical properties of the final material; the ultimate goal being the design of entire libraries of materials with precise control of the properties from the (nano-) molecular scale to the macroscopic scale. This comes from the realization that with the current developments in processing techniques, characterization devices, and synthetic tools we have the capabilities and the knowledge to direct molecular assembly, reaction, and/or interactions in specific ways

as needed to create materials with a defined set of properties and desired performance, e.g. molecular devices, layer by layer assembly, nanogels, dendrimers, DNA-mimics, among others. We hope this fundamental work will contribute to the understanding of how to achieve such level of control in order to design high-performance materials relevant for the future of the field of polymer chemistry and humanity.

1.5 Thesis statement

Despite the initial efforts to characterize the uniquely prolonged duration of monomer consumption after relatively brief irradiation, the explanation of these phenomena was not found. The hypothesis discussed in the following chapters is as follows:

“The unusually prolonged latent polymerization of the vinyl groups in the methacrylate monomer molecules is due to synergistic contributions from the visible-light organic photocatalysis photoinitiating system and from the secondary functionality of the mono vinyl methacrylates utilized. On one hand, the photocatalytic cycle of Methylene Blue allows the very efficient storage of the light energy in the form of meta-stable intermediates. This energy is then utilized slowly to produce free radicals from ground state redox reactions over extended intervals in the dark. On the other hand, the intermolecular hydrogen bonding associated with the secondary functionality of the methacrylate monomer reduces the mobility of the system and the free volume. Leading to a somewhat unique Trommsdorff-Norrish effect as a result of hindered termination reactions.”

Hence, the focus of this research project was determining the role of both the photocatalytic photoinitiating system and the hydroxylated monovinyl methacrylate monomers, and the extent to which each one of these contributes to the latent polymerization observed. Along with this, an improved

analytical technique that monitors both initiator and monomer consumption kinetics was developed to help characterize the complex initiation/polymerization relationships involved here.

1.6 References

1. Hawker, C. J. & Wooley, K. L. The Convergence of Synthetic Organic and Polymer Chemistries. *Science* **309**, 1200–1205 (2005).
2. Barner-Kowollik, C., Lutz, J. F. & Perrier, S. New methods of polymer synthesis. *Polym. Chem.* (2012). doi:10.1039/c1py00443c
3. Decker, C. *UV-curing chemistry: past, present, and future.* (JCT, 1987).
4. Carothers, W. H. Studies on polymerization and ring formation. I. An introduction to the general theory of condensation polymers. *J. Am. Chem. Soc.* **51**, 2548–2559 (1929).
5. Flory, P. J. The Configuration of Real Polymer Chains. *J. Chem. Phys.* **17**, 303 (1949).
6. Odian, G. *Principles of Polymerization.* 1–839 (Wiley Interscience, 2004).
7. Cowie, J. M. G. *Polymers.* (CRC Press, 1991).
8. Hoyle, C. E. & Bowman, C. N. Thiol-Ene Click Chemistry. *Angew. Chem. Int. Ed.* **49**, 1540–1573 (2010).
9. Flory, P. J. *Principles of polymer chemistry.* (1953).
10. Cramer, N. B. *et al.* Investigation of thiol-ene and thiol-ene–methacrylate based resins as dental restorative materials. *Dental Materials* **26**, 21–28 (2010).
11. Cramer, N. B. *et al.* Properties of methacrylate-thiol-ene formulations as dental restorative materials. *Dental Materials* **26**, 799–806 (2010).
12. Goodner, M. D. & Bowman, C. N. *ACS Symposium Series.* **713**, 220–231 (American Chemical Society, 2009).
13. Goodner, M. D. & Bowman, C. N. Development of a comprehensive free radical photopolymerization model incorporating heat and mass transfer effects in thick films. *Chemical Engineering Science* **57**, 887–900 (2002).
14. Goodner, M. D. & Bowman, C. N. Modeling Primary Radical Termination and Its Effects on Autoacceleration in Photopolymerization Kinetics. *Macromolecules* **32**, 6552–6559 (1999).
15. Goodner, M. D., Lee, H. R. & Bowman, C. N. Method for determining the kinetic parameters in diffusion-controlled free-radical homopolymerizations. *Ind. Eng. Chem. Res.* **36**, 1247–1252 (1997).

16. Anseth, K. S., Kline, L. M., Walker, T. A. & Anderson, K. J. Reaction kinetics and volume relaxation during polymerizations of multiethylene glycol dimethacrylates. ... **28**, 2491–2499 (1995).
17. Maurin, V., Croutxé-Barghorn, C. & Allonas, X. Photopolymerization process of UV powders. Characterization of coating properties. *Progress in Organic Coatings* **73**, 250–256 (2011).
18. Stansbury, J. W. Curing dental resins and composites by photopolymerization. *J Esthet Dent* **12**, 300–308 (2000).
19. Scott, T. F., Kowalski, B. A., Sullivan, A. C., Bowman, C. N. & McLeod, R. R. Two-Color Single-Photon Photoinitiation and Photoinhibition for Subdiffraction Photolithography. *Science* **324**, 913–917 (2009).
20. Rengier, F. *et al.* 3D printing based on imaging data: review of medical applications. *Int J CARS* **5**, 335–341 (2010).
21. EATON, D. Nonlinear optical materials. *Science* **253**, 281–287 (1991).
22. DeForest, C. A. & Anseth, K. S. Cytocompatible click-based hydrogels with dynamically tunable properties through orthogonal photoconjugation and photocleavage reactions. 1–7 (2011). doi:10.1038/nchem.1174
23. DeForest, C. A., Polizzotti, B. D. & Anseth, K. S. Sequential click reactions for synthesizing and patterning three-dimensional cell microenvironments. *Nature Materials* **8**, 659–664 (2009).
24. Yang, D. B., Wolf, D., Wakamatsu, T. & Holmes, M. Characterization of cure profiles of anaerobic adhesives by real-time FT-IR spectroscopy. Part II. Surface activation. *Journal of Adhesion Science and Technology* **9**, 1369–1379 (1995).
25. Lai, Y. C. Effect of crosslinkers on photocopolymerization of N-vinylpyrrolidone and methacrylates to give hydrogels. *J. Appl. Polym. Sci.* **66**, 1475–1484 (1997).
26. Eaton, D. F. *Dye Sensitized Photopolymerization. Advances in Photochemistry* **13**, 427–487 (John Wiley & Sons, Inc., 1986).
27. Kloosterboer, J. G. *Network formation by chain crosslinking photopolymerization and its applications in electronics.* 1–61 (Springer, 1988).
28. Anseth, K. S., Wang, C. M. & Bowman, C. N. Reaction behaviour and kinetic constants for photopolymerizations of multi (meth) acrylate monomers. *Polymer* (1994). doi:10.1016/0032-3861(94)90129-5
29. Stansbury, J. W. Difunctional and multifunctional monomers capable of cyclopolymerization. *Macromolecules* **24**, 2029–2035 (1991).
30. Stansbury, J. W. & Dickens, S. H. Determination of double bond conversion in dental resins by near infrared spectroscopy. *Dental Materials* **17**, 71–79 (2001).
31. Stansbury, J. W. Dimethacrylate network formation and polymer property evolution as determined

- by the selection of monomers and curing conditions. *Dental Materials* **28**, 13–22 (2012).
32. Kilambi, H. *et al.* Design, Development, and Evaluation of Monovinyl Acrylates Characterized by Secondary Functionalities as Reactive Diluents to Diacrylates. *Macromolecules* **40**, 6112–6118 (2007).
 33. Shalaby, S. W. & Salz, U. *Polymers for Dental and Orthopedic Applications*. (CRC Press, 2006).
 34. Ramakrishna, S., Mayer, J., Wintermantel, E. & Leong, K. W. Biomedical applications of polymer-composite materials: a review. *Composites Science and Technology* **61**, 1189–1224 (2001).
 35. Ifkovits, J. L. & Burdick, J. A. Review: Photopolymerizable and Degradable Biomaterials for Tissue Engineering Applications. *Tissue Engineering* **13**, 2369–2385 (2007).
 36. Young, J. S. J., Gonzales, K. D. K. & Anseth, K. S. K. Photopolymers in orthopedics: characterization of novel crosslinked polyanhydrides. *Biomaterials* **21**, 1181–1188 (2000).
 37. Bowman, C. N. & Peppas, N. A. Coupling of kinetics and volume relaxation during polymerizations of multiacrylates and multimethacrylates. *Macromolecules* **24**, 1914–1920 (1991).
 38. Bowman, C. N. The Effects of Light Intensity, Temperature, and Comonomer Composition on the Polymerization Behavior of Dimethacrylate Dental Resins. **78**, 1469–1476 (1999).
 39. Decker, C. Photoinitiated crosslinking polymerisation. *Progress in Polymer Science* **21**, 593–650 (1996).
 40. Ibrahim, A. *et al.* Investigation of termination reactions in free radical photopolymerization of UV powder formulations. *European Polymer Journal* **48**, 1475–1484 (2012).
 41. Tian, Y., HAMIELEC, A. E. & Eaton, D. R. Termination of trapped radicals at elevated temperatures during copolymerization of MMA/EGDMA. *Polymer* **31**, 1726–1734 (1990).
 42. Berchtold, K. A., Lovell, L. G., Nie, J. & Hacıoğlu, B. The significance of chain length dependent termination in cross-linking polymerizations. *Polymer* (2001).
 43. Decker, C. & Jenkins, A. D. Kinetic approach of oxygen inhibition in ultraviolet-and laser-induced polymerizations. *Macromolecules* (1985).
 44. Decker, C. A novel method for consuming oxygen instantaneously in photopolymerizable films. *Die Makromolekulare Chemie* **180**, 2027–2030 (1979).
 45. Bowman, C. N. & Kloxin, C. J. Toward an enhanced understanding and implementation of photopolymerization reactions. *AIChE J.* **54**, 2775–2795 (2008).
 46. Kloxin, A. M., Tibbitt, M. W., Kasko, A. M., Fairbairn, J. A. & Anseth, K. S. Tunable Hydrogels for External Manipulation of Cellular Microenvironments through Controlled Photodegradation. *Adv. Mater.* **22**, 61–66 (2010).
 47. Tibbitt, M. W. & Anseth, K. S. Hydrogels as extracellular matrix mimics for 3D cell culture.

- Biotechnol. Bioeng.* **103**, 655–663 (2009).
48. Fouassier, J. P., Loughnot, D.-J. & Pilot, T. Visible laser light in photoinduced polymerization. I. A quantitative comparison with UV laser irradiation. *Journal of Polymer Science: Polymer Chemistry Edition* **23**, 569–573 (1985).
 49. Valdes-Aguilera, O., Pathak, C. P., Shi, J. & Watson, D. Photopolymerization studies using visible light photoinitiators. ... **25**, 541–547 (1992).
 50. Avens, H. J., Randle, T. J. & Bowman, C. N. Polymerization behavior and polymer properties of eosin-mediated surface modification reactions. *Polymer* **49**, 4762–4768 (2008).
 51. Ilie, N. & Hickel, R. Can CQ be completely replaced by alternative initiators in dental adhesives? *Dent Mater J* **27**, 221–228 (2008).
 52. Shintani, H., Inoue, T. & Yamaki, M. Analysis of camphorquinone in visible light-cured composite resins. *Dental Materials* (1985). doi:10.1016/S0109-5641(85)80002-6
 53. Jakubiak, J., Allonas, X., Fouassier, J. P. & Sionkowska, A. Camphorquinone–amines photoinitiating systems for the initiation of free radical polymerization. *Polymer* (2003). doi:10.1016/S0032-3861(03)00568-8
 54. Nie, J. *et al.* A reappraisal of the photopolymerization kinetics of triethyleneglycol dimethacrylate initiated by camphorquinone-N,N-dimethyl-p-toluidine for dental purposes. *Acta Polymerica* **49**, 145–161 (1998).
 55. Cook, W. D. Photopolymerization kinetics of dimethacrylates using the camphorquinone/amine initiator system. *Polymer* **33**, 600–609 (1992).
 56. Oxman, J. D. & Jacobs, D. W. Ternary photoinitiator system for curing of epoxy/polyol resin composition. (2001).
 57. Oxman, J. D. *et al.* Evaluation of initiator systems for controlled and sequentially curable free-radical/cationic hybrid photopolymerizations. *J. Polym. Sci. A Polym. Chem.* **43**, 1747–1756 (2005).
 58. Lalevée, J. *et al.* Photoredox catalysis for polymerization reactions. *Chimia (Aarau)* **66**, 439–441 (2012).
 59. Decker, C. & Moussa, K. A new method for monitoring ultra-fast photopolymerizations by real-time infra-red (RTIR) spectroscopy. *Die Makromolekulare Chemie* **189**, 2381–2394 (1988).
 60. Lee, T. Y., Roper, T. M., Jonsson, E. S., Guymon, C. A. & Hoyle, C. E. Influence of Hydrogen Bonding on Photopolymerization Rate of Hydroxyalkyl Acrylates. *Macromolecules* **37**, 3659–3665 (2004).
 61. Kim_Stansbury_Patent_1_2009. 1–25 (2010).
 62. Kim_STansbury_Patent_2_2009. 1–51 (2010).

63. Padon, K. S. & Scranton, A. B. A mechanistic investigation of a three-component radical photoinitiator system comprising methylene blue, N-methyldiethanolamine, and diphenyliodonium chloride. *J. Polym. Sci. A Polym. Chem.* **38**, 2057–2066 (2000).
64. Sirovatka Padon, K. & Scranton, A. B. The effect of oxygen on the three-component radical photoinitiator system: Methylene blue, N-methyldiethanolamine, and diphenyliodonium chloride. *J. Polym. Sci. A Polym. Chem.* **38**, 3336–3346 (2000).
65. Kim, D. & Scranton, A. The role of diphenyl iodonium salt (DPI) in three-component photoinitiator systems containing methylene blue (MB) and an electron donor. *J. Polym. Sci. A Polym. Chem.* **42**, 5863–5871 (2004).
66. Kim, D., Scranton, A. B. & Stansbury, J. W. Effect of the electron donor structure on the shelf-life of visible-light activated three-component initiator systems. *J. Appl. Polym. Sci.* **114**, 1535–1542 (2009).
67. WEIL, L. ON THE MECHANISM OF THE PHOTO-OXIDATION OF AMINO ACIDS SENSITIZED BY METHYLENE BLUE. *Arch. Biochem. Biophys.* **110**, 57–68 (1965).
68. Chaberek, S. & Allen, R. J. Dye-Sensitized Photopolymerization Processes. 1a II. A Comparison of the Photoactivities of Thionine and Methylene Blue. *J. Phys. Chem.* **69**, 647–656 (1965).
69. Nilsson, R., Merkel, P. B. & Kearns, D. R. Kinetic properties of the triplet states of methylene blue and other photosensitizing dyes. *Photochem Photobiol* **16**, 109–116 (1972).
70. Kilambi, H., Reddy, S. K., Schneidewind, L., Stansbury, J. W. & Bowman, C. N. Copolymerization and dark polymerization studies for photopolymerization of novel acrylic monomers. *Polymer* **48**, 2014–2021 (2007).

Chapter 2

Objectives

2.1 Aims of the present thesis

Several papers were found discussing the photoreduction of Methylene Blue and other thiazine dyes by amines upon visible-light irradiation, but no reports were identified dealing with the photoreduction by the Hünig's base. This presented the first challenge since there are indications of a strong influence of the structure of the reductant on light-induced single-electron transfer reactions. Hence, it was clear that this initial photochemical step was highly important to understand where the primary radicals are coming from. On the other hand, despite the relatively more abundant literature on MB⁺ photochemical, chemical, and electrochemical reductions, there seems to be a disconnect between some of the mechanistic aspects reported. Based on this, one of the key aspects of this work was to investigate the photoredox catalysis cycle involving the photobleaching and potential regeneration of MB⁺, as was theorized for other systems.

At the same time it was identified that monomer solutions containing MB⁺/DIPEA/DPI⁺ eventually lead to spontaneous polymerization when stored at room temperature in the absence of light. This is evidence of ground-state redox reactions leading to the production of primary radicals. This shows an example of the intricacies of the reaction mechanisms of these three-component photoinitiators due to the combination of multiple reactants, which can be involved in several reaction pathways. By judicious selection of the concentrations of the initiator components, suitable stability was achieved to allow valid study of the photo-activated processes of interest here. Such experimental findings were taken into account when designing theoretical models and making quantum chemical calculations to support the proposal of a photocatalysis mechanism that accounts for all previous and present experimental observations.

While analyzing the probable reaction pathways related to the photocatalysis combination (MB⁺/DIPEA/DPI⁺), it was necessary to obtain appropriate controls, including those for the

polymerization of the monomers with other conventional photoinitiators. These experiments lead to the finding that there was a lower, but still substantial latent polymerization associated with the conventional photoinitiators, which did not display any spontaneous redox radical production in the dark after initial exposure to light (as does the $\text{MB}^+/\text{DIPEA}/\text{DPI}^+$ combination). Thus, the effect of the monomer on the termination kinetics and on the latent polymerization had to be deconvoluted from that of the photocatalyst.

Taking all this into consideration, the present thesis was divided into three major specific aims, as follows:

Specific aim 1: Elucidate the mechanism via which the organic photocatalysis combination methylene blue/Hünig's base/iodonium salt produces primary radicals, and identify if and how this contributes to the unusual latent polymerization.

Specific aim 2: Build an apparatus for the simultaneous monitoring of the initiator (MB^+) and monomer (vinyl group from the acrylates or methacrylates) consumption during photopolymerization reactions in bulk using fiber coupled UV-Vis and FT-NIR spectroscopy in real-time with millisecond resolution.

Specific aim 3: Determine if and how the monomer structure, namely that of hydroxylated methacrylates, affects the propagation and termination kinetics of the bulk polymerization via supramolecular effects.

2.2 Roadmap of the thesis

Accordingly, the chapters of this thesis were structured as summarized in here:

Chapter 3

We present initial evidence for the latent production of primary radicals after the initial irradiation period. Connections between Methylene Blue (MB^+) photobleaching and polymerization kinetics and thermodynamics were established. We demonstrate that meta-stable intermediates from the reduction or semi-reduction of MB^+ can initiate polymerization beyond the spatial and temporal reach of the photons. Ultimately we present the first attempt to propose a photocatalysis mechanism that explains the prolonged latency and the initial experimental observations. This mechanism accounts for the existence of MB^+ only in its monomeric form.

Chapter 4

Next, we describe the design, troubleshooting and validation of a novel analytical apparatus to monitor UV-Vis and FT-NIR absorbance simultaneously in real-time with up to millisecond resolution and full spectral collection (250-2500 nm). This was required in order to correlate the consumption and regeneration of the MB^+ photocatalyst at different extents of the polymerization process under several conditions and irradiation regimes. This system was benchmarked with the camphorquinone/amine photoinitiating system typically used in dentistry. Furthermore, interesting mechanistic details were found on the photoreduction of camphorquinone by amine reductants. Finally, calculation of real-time quantum yields of initiation and polymerization for the entire extent of the reaction are showcased as some of the main advantages of successfully coupling these two spectroscopic techniques.

Chapter 5

Then, an iodonium salt was integrated into the CQ/amine formulations in order to assess the effect of oxidant addition to a conventional Type II photoinitiator. The regeneration of CQ, polymerization rate, final conversion, and extent of the latent polymerization were tested with the coupled UV-Vis/FT-NIR monitoring apparatus. This information provided a benchmark, to assess the role of the MB^+ photocatalyst in the unique primary radical production routes proposed in Chapter 3.

Chapter 6

Prove that the formation of a ground state electron donor-acceptor complex between photocatalysts, like MB^+ , and the Hünig's base explains the lack of polymerization seen during irradiation. The hypothesis is that when MB^+ or RUBY_3^{2+} forms a complex with such amines one of the alpha hydrogens is kept at a sufficiently close proximity for H^+ transfer to occur after an initial electron transfer from the lone pair of the nitrogen. If this happens, the amine is not going to form an alpha-amino alkyl radical, as expected from a single e^- transfer process, but rather closed shell species like iminium cations, enamines, and imines. Additionally, Leuco Methylene Blue will be readily formed as this reaction becomes highly feasible if the ground state complex is formed prior to irradiation. We intend to provide the first mechanistic explanation for the very unique way in which $i\text{Pr}_2\text{NEt}$, and other bulky amines, behave under certain experimental conditions, which has been identified to lead to high rates, yields and selectivity in organic chemistry, as well as interesting advantages in polymer chemistry.

Chapter 7

Finally, the supramolecular effect of intermolecular hydrogen bonding was determined by testing the partial irradiation of HEMA, and other monomers, with conventional Type I and Type II photoinitiators. By running the photopolymerizations of these monomers at different temperatures and analyzing the change in the mechanical properties after the light extinction we confirmed that a shorter latent vinyl polymerization is still present in the absence of the MB^+ /Hünig's base/iodonium salt photoinitiating system. The latter was then attributed primarily to the formation of collectively strong hydrogen bonds between the propagating polymer chains. By organizing in a random configuration as the propagation occurs these hydrogen-bonding interactions reduce the segmental and translational motion of the growing macromolecular construct (most likely a loosely crosslinked network). By doing so, the termination kinetics are significantly more reduced than what would be expected, essentially leading to a type of slow controlled polymerization reaction.

Chapter 3

Visible-light organic photocatalysis for latent radical-initiated polymerization via $2e^-/1H^+$ transfers: Initiation with parallels to photosynthesis¹

Abstract

We report the latent production of free radicals from energy stored in a redox potential through a $2e^-/1H^+$ transfer process, analogous to energy harvesting in photosynthesis, using visible-light organic photoredox catalysis (photocatalysis) of methylene blue chromophore with a sacrificial sterically-hindered amine reductant and an onium salt oxidant. This enables light-initiated free-radical polymerization to continue over extended time intervals (hours) in the dark after brief (seconds) low-intensity illumination, and beyond the spatial reach of light by diffusion of the meta-stable leuco-methylene blue photoproduct. The present organic photoredox catalysis system functions via a $2e^-/1H^+$ shuttle mechanism, as opposed to the $1e^-$ transfer process typical of organometallic-based and conventional organic multi-component photoinitiator formulations. This prevents immediate formation of open-shell (radical) intermediates from the amine upon light-absorption, and enables the ‘storage’ of light-energy without spontaneous initiation of the polymerization. Latent energy-release and radical production are then controlled by the subsequent light-independent reaction (analogous to the Calvin cycle) between leuco-methylene blue and the onium salt oxidant that is responsible for regeneration of the organic methylene blue photocatalyst. This robust approach for photocatalysis-based energy harvesting and extended release in the dark enables temporally-controlled redox initiation of polymer syntheses under low-intensity short exposure conditions, and permits visible-light-mediated synthesis of polymers at least one order of magnitude thicker than achievable with conventional photoinitiated formulations and irradiation regimes.

¹ This work was published in the Journal of the American Chemical Society (JACS): 10.1021/ja502441d.

3.1 Introduction

Free radicals (radicals) participate in a wide variety of organic synthetic¹ and polymerization reactions², e.g., vinyl homo- and co-polymerizations³, thiol-ene click chemistry⁴, Cu-catalyzed azide-alkyne cycloadditions⁵, Atom Transfer Radical Additions^{6,7}, and alcohol to halide conversions⁸. Radical production by light activation provides unique temporal control of reactions. However, radicals must be produced continuously by large irradiation doses to sustain the balance between competing creation and termination of radicals. As a result, radical-initiated reactions characteristically halt quickly due to efficient radical termination when the external energy supply (light) is extinguished. Persistent or trapped radicals in dense polymer networks allow a limited degree of polymerization after light-cessation.^{3,9} Whereas in Controlled or ‘Living’ Polymerization, the termination process is altered through an equilibrium that favors radicals in a dormant state so active radical concentrations remain low and essentially constant.^{10,11} However, living radical photopolymerization is usually slow and still requires continued irradiation.¹⁰ Furthermore, no scheme has yet been devised to sustain radical production after the energy supply is extinguished without altering the radical termination process. Here, we report the first use of organic photoredox catalysis to continue radical production for extended time intervals in the dark after a brief initial low-intensity light-exposure, opening new opportunities in photo-activated polymer and possibly organic synthesis¹².

Conventionally, light-activated radical-based polymer synthesis entails radical production via photolytic bond-cleavage, e.g. phosphine oxides or acetophenones¹³, or by light-mediated electron transfer or exchange between a chromophore, such as camphorquinone, and either a reductant or an oxidant¹⁴. In principle, radical generation in both of these approaches is restricted to where the excited molecules reside, i.e. within the imprint and penetration depth of photons. Examples of applications that rely on spatiotemporal controlled processing include the creation of patterned materials for nano- and micro-scale devices, metamaterials, laser imaging and holography.¹⁵⁻¹⁸ However, in optically thick materials, light absorption, scattering and reflection limit light penetration and thus polymerization to

mere millimeters, or often, to just tens to hundreds of micrometers from the irradiated surface while requiring high irradiation intensities or extended photocuring intervals.^{19,20} As a result, through-plane polymerization is severely limited, which is detrimental in applications such as dental and orthopedic composites, irregular surface coatings, photolithographic resists, and cell-encapsulation hydrogels^{17,21-23}, where unintentional property gradients and residual monomer beyond the light penetration depth limit is generally unacceptable. Ultimately, layer-by-layer polymerization is thus required if conventional free-radical photopolymer initiators are to be used for optically thick materials.

In contrast, radical generation through chemically-activated redox initiation, such as with peroxide/amine combinations, allows synthesis of thick polymeric materials under ambient conditions upon *in-situ* mixing of two-part formulations, as in bone cements.²⁴ However, this redox approach lacks temporal control of the initiation reaction beyond the mixing process. In other instances ‘dual-cure’ systems require post-irradiation heating or moisture cure²⁵. ‘Dual-cure’ systems, in which photo- and redox-activated chemistries work more or less simultaneously, introduce some temporal control. However, the two initiation modes work relatively independently and mixing immediately prior to use is still required; thus, imposing similar temporal control limitations as redox systems.²⁶

Frontal polymerization has been reported to allow deep shadow cure in free-radically and cationically initiated thick (centimeter scale) or opaque samples upon UV exposure.²⁷ Despite its attractive simplicity, limited storage stability of the peroxides-containing formulations and its inherent dependence on the self-propagated (by polymerization exothermicity) temperature wave front (over 100 °C) have precluded the use of this technique in most applications.²⁸⁻³⁰ No reports were found of free-radical photopolymerization of (meth)acrylates in which initiation extends beyond the irradiation space and time under ambient conditions without depending on the polymerization exotherm to sustain initiation in the dark.

In this contribution, we introduce the concept of organic photoredox catalysis as a novel approach to combine the temporal onset control of conventional photo-activation with the spatial reach of redox-

activated radical production. We demonstrate that the combination of these phenomena extends the capabilities of prevailing photoinitiated processes and enables the practical synthesis of initially optically thick, centimeter-scale vinyl photopolymers at ambient conditions.

In recent years, photoredox catalysis has gained attention as an alternative to achieve faster rates of radical-initiated polymerization upon low-intensity visible-light irradiation.³¹ Almost all of the reported mechanisms, including those for similar methylene blue (MB^+)/amine/onium salt formulations, rely on sequential $1e^-$ transfers to and from the photocatalyst, as is characteristic of ruthenium and iridium complexes.³¹⁻³⁸ In these mechanisms, transfer of a single electron allows production of (open-shell) radicals from the photo-induced electron transfer (PET) step and essentially initiates the polymerization process immediately after the light-absorption event. Then, the consecutive $1e^-$ transfer step(s), responsible for the regeneration of the photocatalyst, occur(s) so fast that light-energy ‘stored’ in the photocatalyst as chemical energy is used shortly (less than a few seconds) after the PET step; thus these radical production approaches are incapable of sustaining the polymer synthesis for prolonged periods (hours) following light cessation.^{10,33}

To the best of our knowledge, we report the first energy-harvesting approach using organic photocatalysis for latent light-induced radical-initiated polymer synthesis that relies on a two-electron/one-proton ($2e^-/1H^+$) transfer mechanism. Using a sterically-hindered amine (N,N-diisopropylethylamine, DIPEA) as a sacrificial donor that induces a $2e^-/1H^+$ transfer to the organic photocatalyst MB^+ in a 1-to-1 fashion, we prevent immediate free-radical initiation of polymer synthesis of (meth)acrylate monomers upon light absorption, and enable visible-light energy storage as chemical energy in a metastable closed-shell species: leuco-methylene blue (LMB). The stored energy is subsequently utilized to generate two initiating phenyl radicals per photocatalytic cycle from the ground-state redox reaction between the metastable LMB and the oxidizer (diphenyliodonium, DPI^+) for extended time intervals (hours) after short, low-intensity irradiation.

Using photocatalysis to store light-energy in a metastable species (via a $2e^-/1H^+$ transfer mechanism) in order to sustain ground-state reactions (e.g. radical generation that initiates polymer synthesis) for extended periods (hours) after a brief light-activation is the basis of the approach presented herein. Similar PET-based mechanisms have been envisioned as the basis for ‘molecular circuits’ and ‘molecular computing devices’^{39,40}, but we present the first example of a PET-based scheme for light harvesting analogous to photosynthesis that allows photopolymerization be extended well beyond irradiation. In this paper, we: 1) describe coupled experimental and quantum chemical studies that support the photo-induced redox radical formation via the $2e^-/1H^+$ transfer mechanism and 2) demonstrate the capabilities of this new radical production approach within the scope of radical chain-growth polymer synthesis.

3.2 Experimental section

3.2.1 Materials

Methylene blue (MB^+), N,N-diisopropylethylamine (DIPEA), and diphenyliodonium chloride salt (DPI-Cl) were used as received. 2-Hydroxyethyl methacrylate (HEMA) and glycerol dimethacrylate (GDMA) were selected as monomer because it readily dissolves $MB^+/DIPEA/DPI^+$. Homogeneous samples were prepared by vortex mixing. Methanol (MeOH), acetonitrile (ACN) and DI-water were used as solvents (spectro grade). All materials were commercially obtained from Aldrich (Milwaukee, WI), and used as received.

3.2.2 Light source

A halogen dental curing light (Max, DENTSPLY/Caulk, Milford, DE) modified to deliver broadband 500-800 nm light was used in the $MB^+/DIPEA/DPI^+$ photopolymerization experiments. Incident irradiance was measured with a radiometer (6253, International Light Technologies, Peabody, MA) within the 400-700 nm range, i.e. not all of which is absorbed by MB^+ . For all the CQ/EDMAB-

initiated formulations, the 400-500 nm output of an unaltered halogen lamp was applied with the incident irradiance verified by radiometer.

3.2.3 Fourier transform-infrared spectroscopy (FT-IR)

Bulk polymerizations of HEMA were monitored in real-time with a FT-near-IR spectrophotometer (Nicolet Magna-IR Series II, Thermo Scientific, West Palm Beach, FL) by following the peak area of the first overtone absorption band for the methacrylate =CH₂ group (6167 cm⁻¹). The spectrophotometer was equipped with a KBr beam splitter, a MCT/A detector, and an in-house fabricated horizontal stage adapted for *in-situ* photopolymerization experiments.⁴¹ The distance between the light source and the sample was ~7 cm to ensure uniform irradiation across the entire sample with controlled irradiance values. An 800 nm cut-off filter was used to eliminate the 633 nm HeNe reference beam within the NIR output signal. The sample holder for the *in-situ* polymerization, both in the dark and in the light, consisted of a 1 mm height, 1.6 cm diameter disc fabricated by interjecting a perforated silicone rubber shim in between two 1 mm thick glass slides. Rate of polymerization was calculated by numerically differentiating the peak area as a function of time. Concentrations used were as follows: [MB⁺] = 4 mM, [DIPEA] = 0.2 M, [DPI⁺] = 0.04 M, [CQ] = 0.02 M and [EDMAB] = 0.04 M. All FT-NIR-monitored polymerizations with MB⁺/DIPEA/DPI⁺ were performed with 12-13 mW/cm². For the CQ/EDMAB system the intensity used was 22-23 mW/cm². These intensities gave an approximate 3*10⁻⁸ Einsteins/s*cm² of photons absorbed in both systems based on differences in molar absorptivities and concentrations of the MB⁺ and CQ species.

3.2.4 Ultraviolet-visible (electronic) spectroscopy (UV-Vis)

A diode array spectrophotometer (Evolution 300, Thermo-Scientific, West Palm Beach, FL) was employed. Absorbance spectra were collected in quartz cuvettes with a 1 cm pathlength (l). FT-NIR samples were also employed to remotely monitor MB bleaching in real-time by UV-Vis in the same horizontal stage, but separately from the IR experiments. Concentrations used were as follows: [MB⁺] = 4 mM, [DIPEA] = 0.2 M and [DPI⁺] = 0.04 M. UV-Vis experiments were performed with an intensity of 60

mW/cm² to accelerate the bleaching rate of MB⁺ and avoid significant polymer diffusion constraints to the reoxidation reaction between LMB and DPI⁺.

3.2.5 Electrospray Ionization Mass Spectrometry (ESI-MS)

Identification of the intermediates and final products of the reaction was performed in a LC/MS/MS mass spectrometer system (ABI 4000 Q TRAP®, Life Technologies, Carlsbad, CA) equipped with a triple quadruple/linear ion trap analyzer, and electrospray ionization (ESI) detection.

3.2.6 Quantum chemical calculations

Excited state calculations were performed using time-dependent density functional theory (TD-DFT) with the uωB97XD⁴²/6-311G** level of theory where solvation in methanol was described using a polarizable continuum model (CPCM).⁴³ The reaction between an alpha amino-alkyl radical (derived from DIPEA) and HEMA monomer was determined to be barrierless, where the calculations were performed using uM06⁴⁴/6-311G**/CPCM-methanol. In predicting the thermochemistry in reaction 2, we employed uM06/6-311G**//uωB97XD/LANL2dz in CPCM described methanol solvent. To estimate the entropy contribution to the free energy, a frequency calculation was performed using uωB97XD/LANL2dz. All calculations were performed using the GAUSSIAN09⁴⁵ and GAMESS⁴⁶ computational chemistry software packages.

3.2.7 Lateral polymerization experiments

Experiments were performed in a J500 Mask Aligner from Optical Associates. Exposed monomer borders a 500 μm thick opaque rubber spacer on all sides such that photo-generated molecules can diffuse only in one direction. The exposed fringes were 2 x 18 mm and the total monomer samples were 8 x 18 mm. Light intensity was chosen so R_p is equal in the MB⁺/DIPEA/DPI⁺ and CQ/EDMAB initiating systems, hence achieving ~80 % conversion during the 10 min irradiance in both cases, i.e., diffusion restrictions are roughly equivalent. The use of a collimated light-beam and a non-reflective surface prevented light from reflecting into the masked region from the exposed region of the sample. A black mask was used as a substrate at the bottom of the samples to eliminate any reflectance of photons into the

masked region. A glass microscope slide was used as the top boundary to be able to obtain final polymer samples that adhered to the glass. Concentrations used were as follows: $[MB^+] = 0.4$ mM, $[DIPEA] = 0.2$ M, $[DPI^+] = 0.04$ M, $[CQ] = 0.02$ M and $[EDMAB] = 0.04$ M. Light intensity used was 12 mW/cm² for the $MB^+/DIPEA/DPI^+$ system and 23 mW/cm² for the $CQ/EDMAB$ system to obtain approximately equivalent amounts of absorbed photons.

3.2.8 Thick disc polymerization experiments

$MB^+/DIPEA/DPI^+$ and $CQ/EDMAB$ samples were prepared in HEMA. Monomer (1.5 ml) with each initiator in glass vials was irradiated for 1 min at 3.4 mW/cm² (>500 nm) for $MB^+/DIPEA/DPI^+$, and 6.6 mW/cm² (400-500 nm) for $CQ/EDMAB$ to achieve equivalent photon absorption. Samples were then stored in a closed container with no light access for over 30 min. The progression of the viscosity of the samples was periodically monitored in both cases qualitatively and photographed. Concentrations used in these experiments were as follows: $[MB^+] = 0.4$ mM, $[DIPEA] = 0.2$ M, $[DPI^+] = 0.04$ M, $[CQ] = 0.02$ M, $[EDMAB] = 0.04$ M. At these conditions the HEMA with $CQ/EDMAB$ remains liquid and cannot be sectioned for FT-NIR analysis. Thus, additional experiments with GDMA were performed using $9-10$ mW/cm² for $MB^+/DIPEA/DPI^+$ and $17-18$ mW/cm² for $CQ/EDMAB$. At these intensities, the ~ 1.2 cm thick samples were sectioned to ~ 1.5 mm slices, which were analyzed with FT-NIR after 60 s irradiation and 90-120 min in dark storage. To determine conversion means and standard deviations as a function of depth the experiments were repeated 3-4 times. All samples were purged with nitrogen for 5 minutes before irradiation at a pressure of 10-20 psi.

3.2.9 Methylene blue extraction from poly-HEMA gel

A 1.2×1.1 cm poly-HEMA disc was polymerized from bulk HEMA (97 %) with $MB^+/DIPEA/DPI^+$ using 5 min irradiation at 11 mW/cm² of a white LED lamp. The sample was left to react in the dark for 30 min. Then, the polymer gel was removed from the mold and introduced into 20 ml of water. UV-Vis absorbance of the water solution was monitored with time to track the change in the peak at ~ 660 nm, indicative of the MB^+ concentration in solution.

3.3 Results and discussion

3.3.1 Fast radical production in $MB^+/DIPEA/DPI^+$ formulations

Radical production was analyzed by monitoring the disappearance of the infrared absorption corresponding to the vinyl group ($=CH_2$) of the monomer with Fourier transform near-infrared spectroscopy (FT-NIR).⁴¹ The extent of vinyl group consumption indicates monomer conversion due to polymerization, which correlates with radical production. Under continuous, low-intensity visible-light irradiation, monomer solution (e.g. 2-hydroxyethyl methacrylate; HEMA) containing methylene blue (MB^+ , **1**), N,N-diisopropylethylamine (DIPEA, **2**), and diphenyliodonium cation (DPI^+ , **3**) reaches a vitrification-limited 85 % conversion in 500 s (Fig. 3.1a). Under the same conditions, formulations where either or both DIPEA and DPI^+ are absent ($MB^+/DIPEA$; MB^+/DPI^+ ; or MB^+) exhibit less than 2 % monomer consumption.

To further probe the initiation process, the concentration of MB^+ was analyzed via real-time ultraviolet-visible (UV-Vis) spectroscopy. MB^+ is consumed efficiently (Fig. 3.1b) in the presence of DIPEA with or without DPI^+ . However, the $MB^+/DIPEA$ formulation is ineffectual towards initiating polymerization, whereas the $MB^+/DIPEA/DPI^+$ formulation leads to a significant radical production rate, as demonstrated by HEMA conversion, that is comparable to the reaction kinetics and conversion achieved with a conventional visible-light initiator composed of camphorquinone (CQ) and ethyl 4-dimethylaminobenzoate (EDMAB), for which equivalent amounts of photons are absorbed (Fig. 3.1a- see experimental section). Hence, direct radical production from MB^+ consumption by DIPEA is negligible. This indicates that MB^+ consumption and radical production involve separate reaction steps (described in detail in Sections 2.2 and 2.3); while MB^+ consumption is primarily dependent on the presence of DIPEA; the oxidant (DPI^+) plays the main role in radical production.

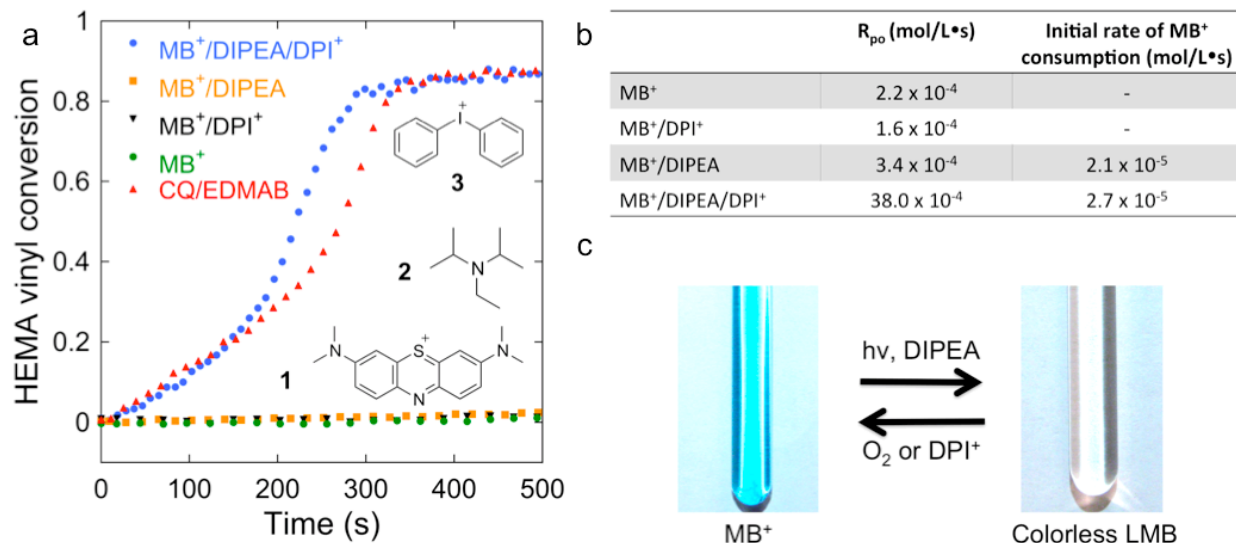
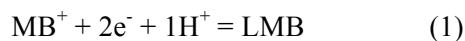


Figure 3.1 Evidence of radical production via photoredox catalysis of methylene blue (MB^+). **a**, Conversion of vinyl group (polymerization) of 2-hydroxyethyl methacrylate (HEMA) during continuous irradiation of 1 mm thick samples. MB^+ (1)/DIPEA (2)/DPI⁺ (3) are required for polymerization at a rate comparable to the conventional CQ/EDMAB formulation with the same amount of photons absorbed (~ 13 and 22 mW/cm², respectively). **b**, Initial rates of polymerization (R_{p0} from numerical differentiation of FT-IR data- see SI section 4) and initial rates of MB^+ bleaching (with UV-Vis spectroscopy at ~ 60 mW/cm²). $MB^+/DIPEA$ leads to efficient consumption of MB^+ (2.1×10^{-5} M/s) but no radical production (which correlates to the vinyl group conversion and R_{p0}), whereas $MB^+/DIPEA/DPI^+$ increases radical production rate dramatically (~ 100 -fold based on R_{p0}) with no significant improvement on MB^+ consumption rate (2.7×10^{-5} M/s). Rates of bleaching without DIPEA are negligible. This indicates that DIPEA does not produce radicals efficiently (shows negligible polymerization). Thus, DPI⁺ should play the main role in term of radical production. **c**, Photoredox cycle in methanol with DIPEA and O₂ or DPI⁺. MB^+ in methanol is bleached, photoreduced to colorless LMB, and regenerated by an oxidant. The process can be repeated as MB^+ is regenerated after each cycle, i.e. photocatalysis cycle.

3.3.2 PET reaction of $MB^+/DIPEA$ generates the colorless LMB

Now, we reevaluate the $MB^+/DIPEA$ system to establish the connection between photoreduction of MB^+ and the subsequent radical generation that necessitates the presence of DPI⁺. In general, the reduction of MB^+ has been proposed to proceed via a $2e^-/1H^+$ process to produce the leuco product LMB in a reducing environment,^{47,48} as represented in reaction (1).



Under irradiation, the $2e^-/1H^+$ transfer process (1) is driven by light and is referred to as photo-induced electron transfer (PET)^{49,50}. The PET of specific interest here is the reduction of MB^+ to the

colorless LMB in the presence of DIPEA (reductant). For example, in Figure 3.1b, we see that the rates of MB^+ consumption for the MB^+/DIPEA and $\text{MB}^+/\text{DIPEA}/\text{DPI}^+$ formulations are 2.1×10^{-5} and 2.7×10^{-5} M/s, respectively. Reduction of MB^+ to LMB is identified by the decrease of the ~ 650 nm-centered peak and appearance of a ~ 250 nm-centered peak (Fig. 3.1b- see SI section 7). This process is commonly known as ‘photo-bleaching’, where the signature blue color of MB^+ ($\lambda_{\text{max}} = \sim 650$ nm) disappears and the mixture turns colorless (Fig. 3.1c).

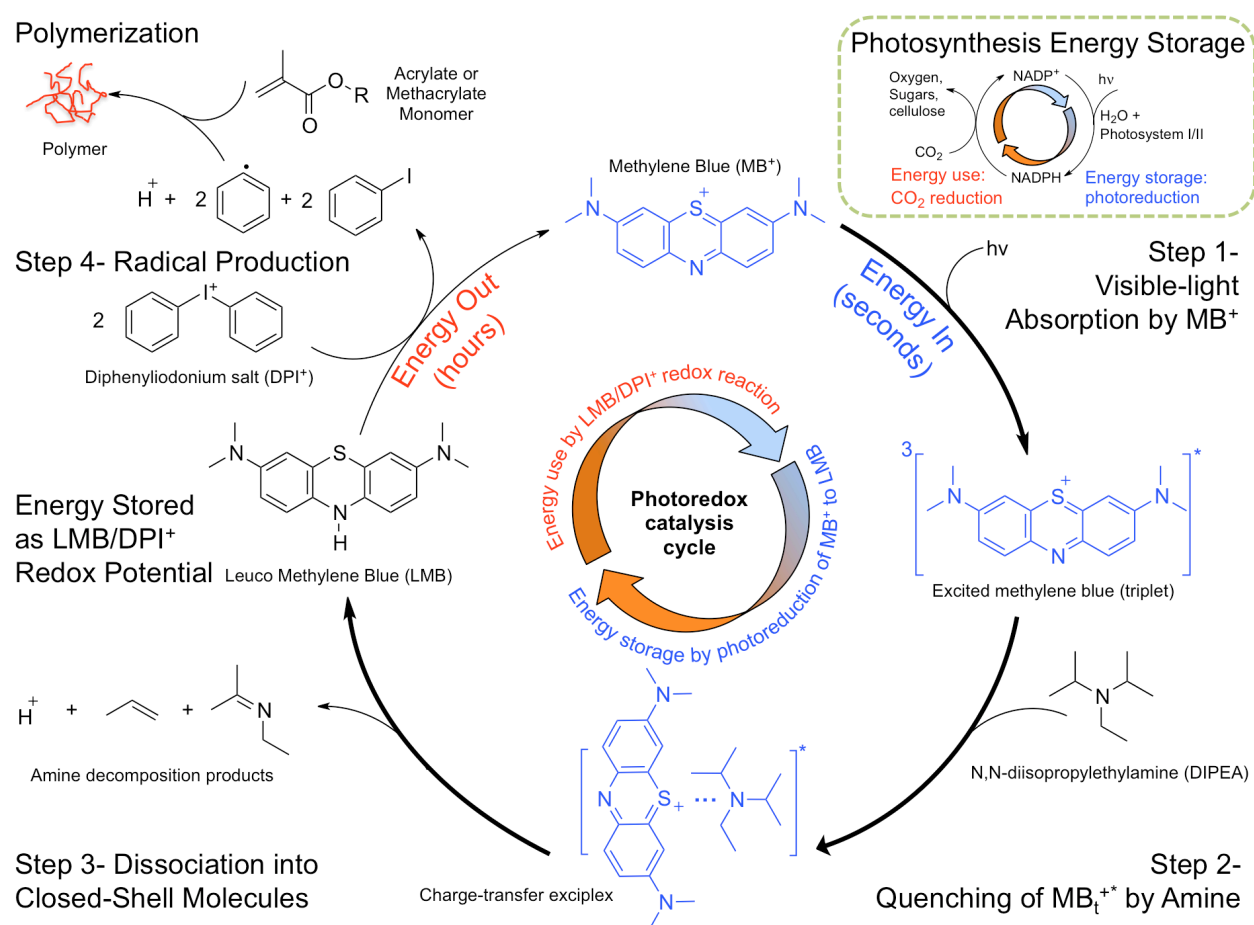


Figure 3.2 Free radical initiated polymer synthesis with light energy harvesting cycle. Step 1: Visible-light ($h\nu$) excitation of MB^+ to the singlet state (not shown), which quickly decays to the longer-lived triplet state (MB_t^{+*}) via intersystem crossing. Step 2: excess DIPEA quenches MB_t^{+*} to colorless LMB via transfer of two electrons and one proton (reaction 1) through formation of a charge-transfer excited state complex (exciplex). Step 3: after a $2e^-/1\text{H}^+$ transfer, the exciplex separates into LMB and DIPEA-decomposition products. DIPEA decomposes to closed-shell molecules, and does not initiate polymerization. Step 4: LMB is oxidized back to MB^+ by DPI^+ to produce two phenyl radicals per LMB. Phenyl radicals are responsible for the fast initiation of chain-growth polymerization of HEMA. Faster

(thicker arrows) MB^+ reduction and slower (thinner arrows) reoxidation steps allow LMB to accumulate, and also create a lag time between light absorption and radical generation. Thus, energy is stored as an electrochemical potential between LMB and DPI^+ , which produces radicals beyond light absorption. This is analogous to the $\text{NADP}^+/\text{NADPH}$ cycle (inset) known in photosynthesis in which the transfer of $2\text{e}^-/1\text{H}^+$ in the photoredox cycle stores light-energy in the form of a chemical potential that is used to reduce carbon dioxide to higher molecular weight sugars and carbohydrates.

Next, we describe the PET process in greater detail, as illustrated in Fig. 3.2. In step 1, absorption of photons excites MB^+ , which undergoes intersystem crossing to ultimately produce the triplet excited-state MB_t^{+*} . Subsequently in step 2, an excited-state complex (exciplex) forms between DIPEA and MB_t^{+*} prior to the PET reaction⁵¹. It is important to note that in conventional PET reactions involving amines and chromophores, the amine reductant typically provides one electron (e^-) and one proton (H^+) to the photo-excited chromophore^{32-34,49,50,52}. For example, with the CQ chromophore and EDMAB reductant, transfer of $1\text{e}^-/1\text{H}^+$ results in the production of the alpha-aminoalkyl radical that is reactive towards vinyl monomers and thus initiates polymerization^{38,53}. If the analogous $1\text{e}^-/1\text{H}^+$ transfers occur in MB^+/DIPEA photoreduction, two DIPEA molecules would be required for each bleached MB^+ (reaction 1). As a result, each amine would result in an alpha-aminoalkyl radical that would be expected to cause fast polymerization of the methacrylate monomer. Quantum chemical simulations predict that creation of a monomer-based radical with the alpha-aminoalkyl radical, i.e. initiation of the polymerization, is barrierless and thus confirm that polymerization would be fast and diffusion-limited in solution if DIPEA-based radicals were produced. In Figure 3.3, we show the equilibrium structures of (a) reactant, (b) transition state (TS) and (c) product for the C-C bond formation reaction between the alpha-aminoalkyl radical and HEMA monomer.

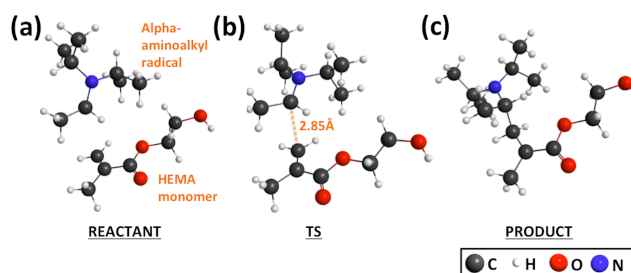


Figure 3.3 Reaction between alpha-aminoalkyl radical and HEMA monomer. Equilibrium structures of (a) Reactant, (b) Transition state (TS) and (c) Product are determined using unrestricted M06/6-311G(d,p)/CPCM-methanol. The enthalpic barrier for this reaction is determined to be $\Delta H_{\text{act}}^0 = -1.4$ kcal/mol, after zero-point-energy (ZPE) and thermal corrections to 298K. Note that although ΔE_{act}^0 is positive, thermal and zero-point corrections often produce a negative ΔH_{act}^0 for reactions that are essentially barrierless.

Despite the formation of LMB, we observed no significant polymerization with MB^+/DIPEA (Fig. 3.1a). This contrasts with other tertiary aliphatic amines that photoreduce MB^+ via $1e^-/1\text{H}^+$ transfers to produce alpha-aminoalkyl radicals that initiate polymerization efficiently, as previously reported^{37,54,55}, and confirmed by our FT-NIR spectroscopy measurements with other tertiary amines (SI, Section 2). This observation compelled us to propose that the strong and sterically-hindered DIPEA base plays a unique role in the MB^+ PET reaction examined here: it reacts rapidly with the photoexcited MB_t^{+*} in a 1-to-1 fashion, where DIPEA serves as a $2e^-/1\text{H}^+$ donor. Hence, closed-shell degradation products are produced from the PET reaction (Fig. 3.2, Step 3), but not DIPEA-based (alpha-aminoalkyl) radicals. Using electrospray ionization-mass spectrometry (ESI^+), we identified both 2-ethyliminopropane and propene as the by-products of the entropy-driven DIPEA decomposition via carbon-nitrogen σ -bond cleavage (SI, section 3).

To our knowledge, this is the first time a $2e^-/1\text{H}^+$ transfer mechanism has been demonstrated for the photoreduction of a photocatalyst (MB^+) with an amine (DIPEA) in 1:1 ratio that produces no alpha-aminoalkyl radicals during the PET reaction.

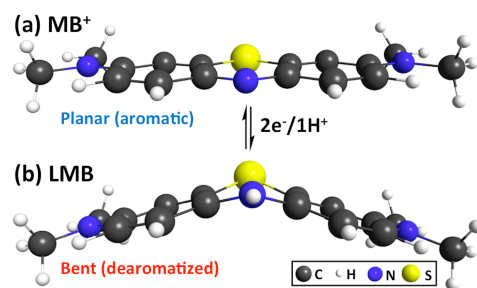


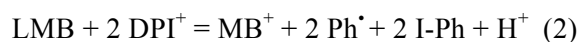
Figure 3.4 Dearomatization of MB⁺ after a 2e⁻/1H⁺ transfer. (a) MB⁺ is a planar aromatic molecule that absorbs strongly in the visible light spectrum ($\lambda_{\text{max}} = \sim 650\text{nm}$). (b) LMB is a photoproduct of a 2e⁻/1H⁺ transfer in MB⁺/DIPEA PET reaction. After a 2e⁻/1H⁺ transfer, the thiazine ring in LMB is dearomatized and is significantly bent from the original planar structure. Time-dependent DFT (TD-DFT, Methods) using $\omega\text{B97XD/LANL2dz/CPCM-methanol}$ predicts that LMB absorbs at $\lambda_{\text{max}} = \sim 300\text{ nm}$, which corroborates the observed blue-shift of λ_{max} to $\sim 250\text{ nm}$ and explains the bleaching of the solution to its colorless form.

Finally, the PET reaction in step 3 leads to the desired LMB product. Examination of the calculated LMB equilibrium structure (Fig. 3.4) suggests that a dearomatization process occurs after 2e⁻/1H⁺ transfer (1), where the thiazine ring distorts significantly from its original planar structure. Furthermore, excited state calculations using TD-DFT predict that the PET process significantly blue-shifts MB⁺ absorption, which is typical of a dearomatization process. LMB is predicted to absorb only in the near-UV region at $\sim 300\text{ nm}$ (compared to $\sim 650\text{ nm}$ for MB⁺), which agrees with the appearance of the $\sim 250\text{ nm}$ peak during PET. Next, we examine how LMB, a meta-stable closed-shell product from PET, participates in a ground-state reaction with the DPI⁺ oxidant to generate the radicals responsible for polymerization.

3.3.3 Radical production from LMB/DPI⁺ reaction

If photoreduction of MB⁺ by DIPEA produces LMB by (1) but generates no radicals, then the radicals responsible for the fast polymerization of the monomer with MB⁺/DIPEA/DPI⁺ must arise from the ground-state oxidation of LMB back to MB⁺ by DPI⁺. This proposal is based on the fact that LMB has been observed to oxidize to MB⁺ with O₂ as the oxidant, consistent with the observed gradual return of

MB⁺'s blue color (Fig. 3.1c). Furthermore, LMB is an efficient reducing agent^{37,56-58}. Herein we propose that radical production in MB⁺/DIPEA/DPI⁺ (Fig. 3.2, Step 4) occurs as follows:



DFT calculations performed at the uM06/6-311G**//uωB97XD/LANL2dz level of theory in CPCM implicit methanol solvent (see Methods) support reaction (2) with a predicted ΔG_{rxn}^0 of -5.2 kcal/mol. Furthermore, production of two highly reactive phenyl radicals per LMB accounts for the fast polymerization rate observed with MB⁺/DIPEA/DPI⁺ (Fig. 3.1a) under irradiation. ESI⁺ shows the production of iodobenzene-based products (SI, Section 3), which provides additional evidence for (2); the oxidation of LMB by DPI⁺ via (2) also explains the observed return of MB⁺'s blue color.

To further investigate the radical generation process described by reaction (2), we performed an Arrhenius analysis to determine that the activation barrier for the free radical production step in the polymerization of HEMA with MB⁺/DIPEA/DPI⁺ is $\Delta E_{\text{act}} = 6.6 \pm 1.0$ kcal/mol (Fig. 3.5a and SI, Section 3). Next, we used real-time UV-Vis to quantify the regeneration rate of MB⁺ at various temperatures after a 10 s irradiation (Fig. 3.5b). We observed that light-activated MB⁺ consumption is temperature independent (Fig. 3.3b, Light), as expected for a PET reaction where diffusion restrictions are mitigated by excess reductant (DIPEA). In contrast, MB⁺ regeneration is strongly temperature sensitive (Fig 3.5b, Shaded). From the UV-Vis results, we estimate that ΔE_{act} for MB⁺ regeneration is 7.2 ± 1.3 kcal/mol (SI, Section 4).

Statistical agreement in ΔE_{act} values from independent Arrhenius analyses of both monomer consumption and MB⁺ regeneration effectively confirms that the two observations are due to reoxidation of LMB by DPI⁺. Notably, there is an alternative radical production pathway based on direct redox reaction between DIPEA and DPI⁺; however, its ΔE_{act} is 13.1 ± 1.0 kcal/mol (SI, Section 4). From this we calculate that well over 90 % (depending on MB⁺/DIPEA/DPI⁺ concentrations) of the phenyl radicals originate from the LMB/DPI⁺ reaction once LMB is generated via MB⁺ photoreduction.

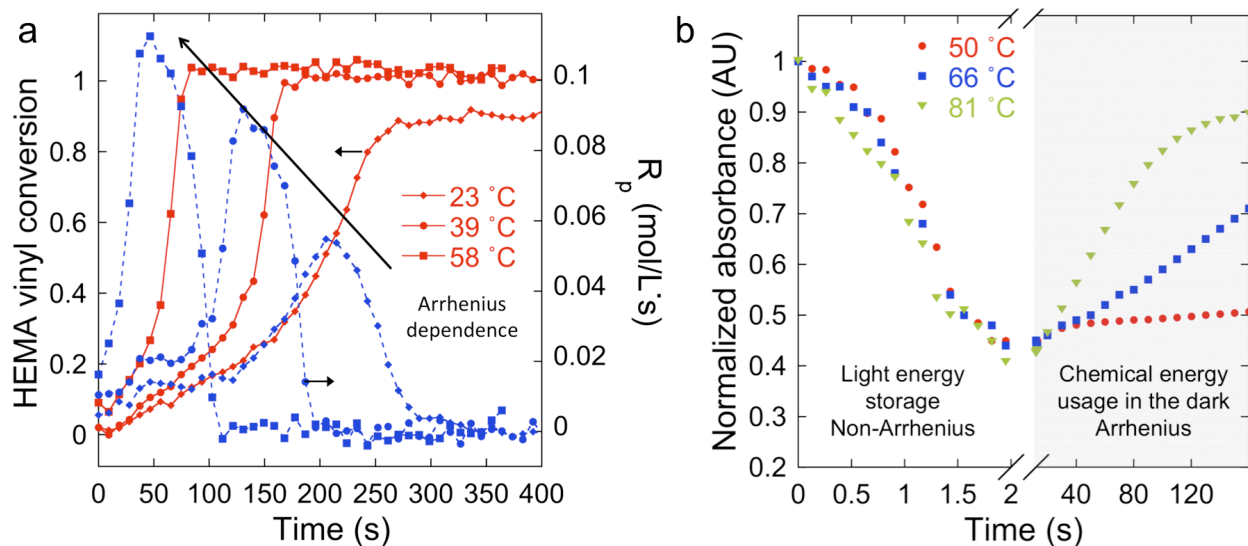


Figure 3.5 Activation energy for MB^+ regeneration matches initiation of polymerization. a, Vinyl conversion (red continuous line) and R_p (blue dashed line-obtained from numerical differentiation of FT-IR data) under illumination show Arrhenius (temperature) dependence. Activation energy for initiation of polymerization ($\Delta E_{act} = 6.6 \pm 1$ kcal/mol) is due to the redox reaction between LMB and DPI^+ (arrows indicate temperature increase). b, Absorbance monitoring (650 nm – MB^+ peak) proves temperature-insensitive (light-dependent) photoreduction of MB^+ by DIPEA, i.e. bleaching of the blue color. After 10 s of irradiation, MB^+ is regenerated in the absence of light. Activation energy for MB^+ regeneration ($\Delta E_{act} = 7.2 \pm 1.2$ kcal/mol) agrees with the estimated activation energy for the initiation of polymerization (from FT-NIR) because both are due to the LMB/ DPI^+ reaction.

3.3.4 Stored energy in LMB extends radical production after irradiation

Having demonstrated that this photocatalysis mechanism most likely proceeds via a $2e^-/1H^+$ transfer, we now show that $MB^+/DIPEA/DPI^+$ can be tuned so that the polymerization reaction continues for hours after light cessation. In Fig. 3.6a, we show that during a 1 min low-intensity light-exposure, the bulk polymerization of HEMA reached $\sim 8\%$ conversion for $MB^+/DIPEA/DPI^+$. Extinguishing the irradiation at this point led to the continued rise in conversion in the dark over the next 2 hours to reach 80%, with radical formation likely persisting over even longer timescales. This offers additional proof that the above-described radical production by LMB/ DPI^+ occurs via a ground-state “dark” reaction. Similar studies with additional irradiation times are provided in SI section 5 to confirm this unique behavior. The initial PET reaction ‘charges’ the photocatalytic cycle by quickly converting MB^+ into

LMB via steps 1-3 of Fig. 3.2, also demonstrated in Fig. 3.3b. The sample bleaches as LMB accumulates because step 4 (or equivalently reaction 2) is rate limiting. Light-energy is subsequently harvested as the chemical potential between MB^+ and LMB, and “dark” reaction with DPI^+ drives radical production and polymerization after the brief PET reaction. In contrast, polymerization did not continue in the dark for MB^+ /DIPEA or CQ/EDMAB in HEMA. It is noteworthy that the final ‘dark’ conversion achieved with MB^+ /DIPEA/ DPI^+ is nearly the same as that obtained with continuous light exposure (86 %, Fig. 3.1a), which indicates the final conversion is not significantly hampered by such a short initial light exposure period.

3.3.5 Photocatalysis cycle mimics photosynthesis

The photoredox catalysis here mimics nature’s photosynthesis where energy from visible-light is stored as the chemical potential in the MB^+ /LMB redox couple. This is analogous to photosynthesis, where visible-light absorbing proteins in Photosystem I and II undergo PET reactions to store energy in the NADP^+ /NADPH redox couple. Both redox couples store energy using a $2e^-/1\text{H}^+$ transfer reaction and participate in ground state (light-independent analogous to the Calvin cycle) reactions to release the stored energy. While the closed-shell NADPH energy carrier drives the synthesis of sugars and natural polymers in the absence of light^{59,60}; the system utilizes its stored energy, originally derived from light, in LMB to generate radicals (reaction 2) that initiate polymerization for the synthesis of macromolecules in the absence of light.

3.3.6 Spatial extension of radical production beyond the irradiation site

Next, we demonstrate that polymer synthesis with MB^+ /DIPEA/ DPI^+ not only extends temporally, but also spatially beyond the reach of photons (Fig. 3.6b). HEMA was polymerized on a glass substrate by exposing the unmasked 2 mm fringe of an 8 mm long monomer sample to continuous irradiation for 10 min. The lateral extent of photo-activated polymerization into the shadow region was determined by washing away unreacted monomer with acetone after 30 min of storage in the absence of light. CQ/EDMAB yielded a patterned polymer that extended only $170 \pm 190 \mu\text{m}$ into the masked region

(Fig. 3.6b, Islet). Notably, during this time, the $\text{MB}^+/\text{DIPEA}/\text{DPI}^+$ formulation shows 3.73 ± 0.73 mm of lateral polymerization into the dark area. This is due to relatively stable LMB produced in the irradiated region (reaction 2) diffusing into the masked region and reacting with DPI^+ ; thus, generating radicals and initiating polymerization ‘far’ (millimeters) from the LMB-formation site. Using embedded thermocouples, we verified that there is no thermal front involved in the extension of polymerization beyond the direct light activation⁶¹. While many photopolymer applications rely on the intrinsic spatial control associated with conventional photoinitiating systems, this approach uniquely decouples spatial restrictions from the photo-activation process. It is certainly advantageous in instances where radical generation around corners and into shadowed regions is desirable, such as in automotive and aerospace coatings of irregular surfaces and polymers for *in-situ* biomedical applications.

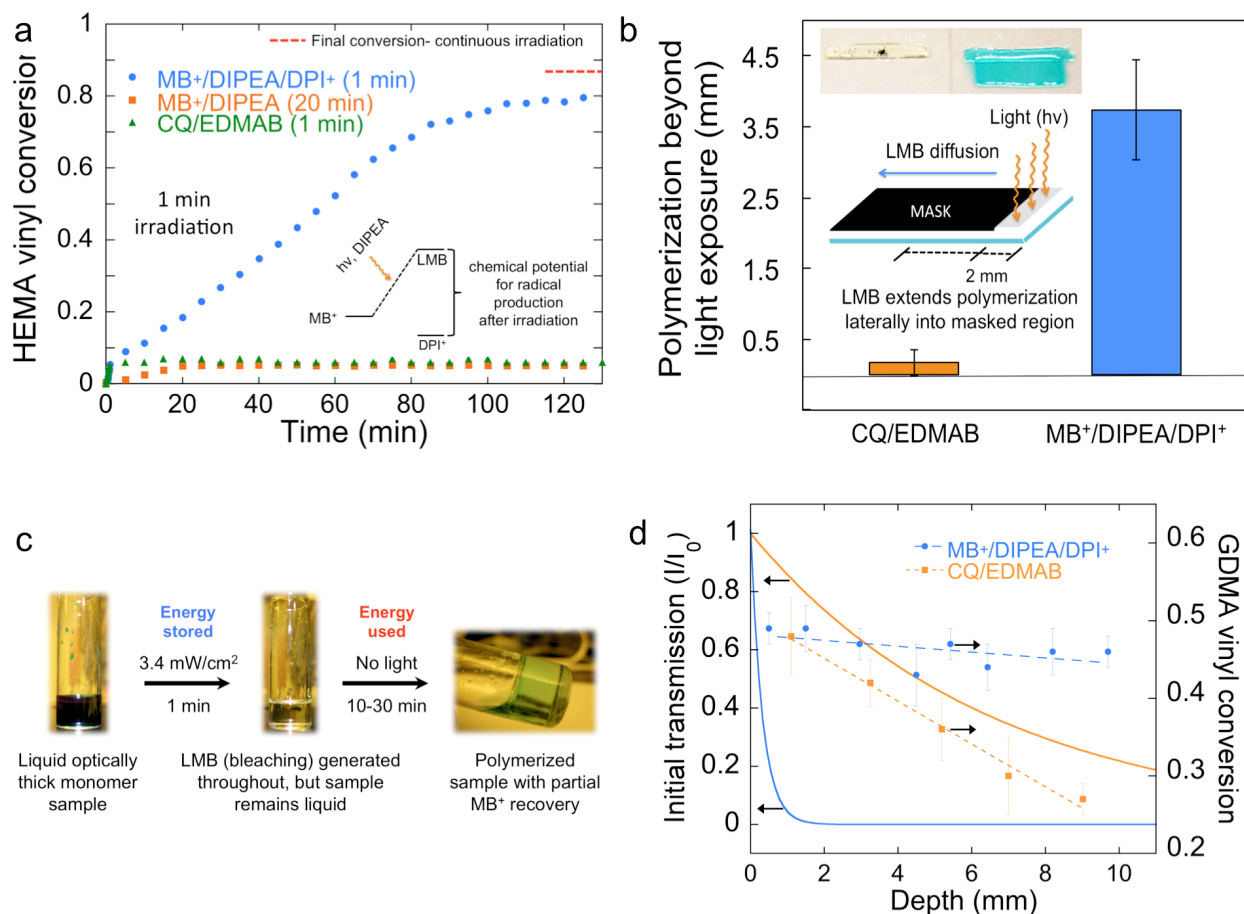


Figure 3.6 Radical generation in the dark from stored energy in LMB. **a**, HEMA with MB⁺/DIPEA/DPI⁺ reaches 80 % conversion with 60 s of illumination after having achieved only 8 % conversion during active illumination. MB⁺/DIPEA and CQ/EDMAB show no energy-harvesting capability. **b**, Stable LMB diffuses and extends radical production beyond the light absorption site. Polymerization is initiated into a masked region 3.7 ± 0.7 mm (standard deviation, $n=3$) away from the illuminated region (2 mm in width) with MB⁺/DIPEA/DPI⁺. Statistically negligible extension of polymerization was observed in the masked region with CQ/EDMAB at equivalent conditions. **c**, Polymerization of optically thick 1.2 cm (height) HEMA and GDMA. Poly-HEMA discs were made with 1 min irradiation (from the top). An analogous sample with CQ/EDMAB was irradiated with an equivalent number of absorbed photons showing negligible polymerization and remained liquid (SI section 5). **d**, Vinyl conversion by FT-NIR (with standard deviation, $n= 3$) is more uniform throughout the depth in a 10 times more optically opaque MB⁺/DIPEA/DPI⁺ sample than in a conventional CQ/EDMAB sample. Dashed lines indicate the linear regression of the final conversion profile, and solid lines indicate the local light transmission profile at the start of irradiation (based on the respective active wavelengths and molar absorptivities of CQ and MB⁺ in GDMA).

3.3.7 Photo-activated synthesis of thicker polymers

The aforementioned temporal and spatial extension of radical generation is utilized to achieve light-mediated synthesis of polymers at least an order of magnitude thicker than the millimeter-scale of conventional photoinitiated formulations under low-intensity and short exposure conditions. The full depth of ~1.2 cm thick HEMA polymer specimens (Fig. 3.6c) was photocured with a 1 min exposure to 3.4 mW/cm² light. Under these very mild conditions, the photoreduction of MB⁺ to LMB initially occurs near the top surface, close to the irradiation source, where photon flux is highest. As MB⁺ is transformed into LMB, bleaching occurs in a gradient fashion allowing the light to penetrate deeper into the originally optically thick sample. Within one minute of illumination the sample is entirely colorless, but not yet polymerized. HEMA polymerization then continued in the dark using the radicals from the LMB/DPI⁺ reaction. After 30 min, the sample was gelled throughout with polymerization continuing to completion in the dark over several hours.

Due to diffusion constraints in the polymer, the blue color in the polymer does not fully regenerate, as not all LMB is able to oxidize to MB⁺. The multi-millimeter diffusion of the relatively stable high-energy close-shell LMB (Fig. 3.4b) can aid in achieving centimeter plus-scale polymerization even if MB⁺ photobleaching were not complete throughout the entire depth of the sample. For instance, CQ transmits more light through the 1.2 cm samples and can be bleached efficiently with EDMAB allowing for progressive light penetration in the same sample geometry; however, CQ/EDMAB specimens show noticeably less polymerization at equivalent photon absorption, i.e. essentially no polymerization of HEMA at these mild conditions (SI section 6).

These capabilities can also be exploited with other monomers, such as the crosslinking photopolymerization of glycerol dimethacrylate (GDMA) or triethylene glycol di(meth)acrylate. The higher modulus GDMA polymer was used to prepare similarly thick samples, which were then sectioned (~ 1 mm slices) to reveal a much more uniform conversion profile to a depth of at least 1 cm, than what is achieved with the analogous CQ/EDMAB sample, which has an initially 10-fold greater optical

transparency (Fig. 3.6d). The limiting GDMA conversion (~65 %) is achieved in the top layer with either initiator system with an equivalent amount of photons absorbed. However, it is remarkable that conversion in the $\text{MB}^+/\text{DIPEA}/\text{DPI}^+$ system reduces only marginally (~5%) at a depth of 1 cm under such mild irradiation conditions, while conversion in the CQ/EDMAB formulation drops precipitously to zero, as is typical for conventional radical-initiated photopolymerizations. In general, much higher intensities and/or longer exposures are needed to achieve this same outcome with conventional photoinitiators as demonstrated using CQ/EDMAB.

Such a small variation in monomer vinyl conversion with depth permits the design of photo-activated initiation systems for synthesis of optically thick polymers under milder, highly energy-efficient irradiation regimes and within a timescale comparable to conventional redox initiators⁶², but with unprecedented temporal activation control. We contend that this is the first photoredox catalysis employed to design a temporally-controlled redox initiation system where the active radicals are not generated directly by the light-dependent reaction, and in which the rates of photo-reduction and oxidation in the photoredox cycle can be tuned to achieve energy storage that extends polymerization well beyond the time and distance associated with the light absorption process.

3.4 Conclusions

The key to extend initiation beyond irradiation with photoredox catalysis concept is achieving a fast, efficient photochemical storage step (photobleaching), in which light-energy is converted into chemical energy and later released in a much longer time interval based on the chemical potential of the redox pair (e.g. LMB/ DPI^+). The energy utilization on much longer timescales than that of light-absorption is tuned by the kinetics of the ground-state redox reaction. Thus, the primary reason for the use of DIPEA as the reductant in the presented system is its fast bleaching 'rate' with MB^+ and the lack of alpha-aminoalkyl radical formation. This approach unlocks new opportunities for the application of other chemistries that enable energy storage in bulk and solution polymer and possibly organic synthesis¹.

The concentration of MB^+ , and the associated LMB, will affect the rate (kinetics) and duration (thermodynamics) of the polymerization after the short light-pulse. The experimental parameters used herein were not optimized and we expect that this concept can be improved to synthesize even thicker polymers. This work serves only as proof of concept for the novel initiation scheme, and can be extended to a range of polymer applications and likely organic synthesis as well.

Ruthenium and iridium complexes produce photo-excited states that are a more powerful source of electrochemical potential¹², which may allow for greater potential, however different sacrificial reductants or oxidants would be required to allow analogous storage of energy derived from light and to avoid initiation shortly after the light-absorption event. Ultimately we propose that additional organic and organometallic photocatalysis schemes can be engineered to delay light-energy utilization to hours after light-absorption by appropriate formulation design. Photoredox organocatalysis is an attractive alternative for any synthetic applications in which expensive photocatalysts (i.e. organometallic) cannot be recovered, as would be the case in bulk polymerizations. Additionally, organic photocatalysts are more versatile, lower-cost and usually less toxic alternatives.

This concept could provide significant advantages, including photopolymerization of optically thick UV-absorbing monomer formulations, in wide ranging industrial and biomedical applications, such as: cell encapsulation, orthopedic and dental cements, tumor phototherapy, adhesives and high-throughput polymer films. The final blue tone of the polymer films and discs varied with irradiation dose and initial concentrations. However, if desired, the reformed MB^+ and the blue color can be partially or completely removed from most polymers by swelling, as seen in SI section 7, depending on cross-linked density of the polymer network.

3.5 References

1. Shih, H.-W., Vander Wal, M. N., Grange, R. L. & MacMillan, D. W. C. Enantioselective α -Benzoylation of Aldehydes via Photoredox Organocatalysis. *J. Am. Chem. Soc.* **132**, 13600–13603 (2010).
2. Hawker, C. J. & Wooley, K. L. The Convergence of Synthetic Organic and Polymer Chemistries. *Science* **309**, 1200–1205 (2005).
3. Kilambi, H., Reddy, S. K., Schneidewind, L., Stansbury, J. W. & Bowman, C. N. Copolymerization and dark polymerization studies for photopolymerization of novel acrylic monomers. *Polymer* **48**, 2014–2021 (2007).
4. Hoyle, C. E. & Bowman, C. N. Thiol-Ene Click Chemistry. *Angew. Chem. Int. Ed.* **49**, 1540–1573 (2010).
5. Adzima, B. J. *et al.* Spatial and temporal control of the alkyne-azide cycloaddition by photoinitiated Cu(II) reduction. *Nature Chemistry* **3**, 256–259 (2011).
6. Xuan, J. & Xiao, W.-J. Visible-Light Photoredox Catalysis. *Angew. Chem. Int. Ed.* **51**, 6828–6838 (2012).
7. Narayanam, J. M. R. & Stephenson, C. R. J. Visible light photoredox catalysis: applications in organic synthesis. *Chem. Soc. Rev.* **40**, 102 (2010).
8. Dai, C., Narayanam, J. M. R. & Stephenson, C. R. J. Visible-light-mediated conversion of alcohols to halides. *Nature Chemistry* **3**, 140–145 (2011).
9. Lee, T. Y., Roper, T. M., Jonsson, E. S., Guymon, C. A. & Hoyle, C. E. Influence of Hydrogen Bonding on Photopolymerization Rate of Hydroxyalkyl Acrylates. *Macromolecules* **37**, 3659–3665 (2004).
10. Fors, B. P. & Hawker, C. J. Control of a Living Radical Polymerization of Methacrylates by Light. *Angew. Chem. Int. Ed.* **51**, 8850–8853 (2012).
11. Wang, J.-S. & Matyjaszewski, K. Controlled/‘ living’ radical polymerization. Atom transfer radical polymerization in the presence of transition-metal complexes. *J. Am. Chem. Soc.* **117**, 5614–5615 (1995).
12. Yoon, T. P., Ischay, M. A. & Du, J. Visible light photocatalysis as a greener approach to photochemical synthesis. *Nature Chemistry* **2**, 527–532 (2010).
13. Allonas, X., Lalevée, J. & Fouassier, J.-P. Investigation of cleavage processes in photoinitiators: from experiments to molecular modeling. *Journal of Photochemistry & Photobiology, A: Chemistry* **159**, 127–133 (2003).
14. Fouassier, J. P. & Lalevée, J. *Photoinitiators for Polymer Synthesis: Scope, Reactivity, and Efficiency*. (Wiley-VCH, 2012).
15. Fouassier, J.-P. & Morlet-Savary, F. Photopolymers for laser imaging and holographic recording:

- design and reactivity of photosensitizers. *Optical engineering* **35**, 304–312 (1996).
16. EATON, D. Nonlinear optical materials. *Science* **253**, 281–287 (1991).
 17. Scott, T. F., Kowalski, B. A., Sullivan, A. C., Bowman, C. N. & McLeod, R. R. Two-Color Single-Photon Photoinitiation and Photoinhibition for Subdiffraction Photolithography. *Science* **324**, 913–917 (2009).
 18. Liu, N., Liu, H., Zhu, S. & Giessen, H. Stereometamaterials. *Nature Photon* **3**, 157–162 (2009).
 19. Goodner, M. D. & Bowman, C. N. Development of a comprehensive free radical photopolymerization model incorporating heat and mass transfer effects in thick films. *Chemical Engineering Science* **57**, 887–900 (2002).
 20. Catilaz Simonin, L. & Fouassier, J. P. Investigation of a system capable of photoinitiating radical polymerizations in thick pigmented media. *J. Appl. Polym. Sci.* **79**, 1911–1923 (2001).
 21. Stansbury, J. W. Curing dental resins and composites by photopolymerization. *J Esthet Dent* **12**, 300–308 (2000).
 22. Fisher, J. P. J., Dean, D. D. & Mikos, A. G. A. Photocrosslinking characteristics and mechanical properties of diethyl fumarate/poly(propylene fumarate) biomaterials. *Biomaterials* **23**, 4333–4343 (2002).
 23. DeForest, C. A., Polizzotti, B. D. & Anseth, K. S. Sequential click reactions for synthesizing and patterning three-dimensional cell microenvironments. *Nature Materials* **8**, 659–664 (2009).
 24. Hasenwinkel, J. M., Lautenschlager, E. P., Wixson, R. L. & Gilbert, J. L. A novel high-viscosity, two-solution acrylic bone cement: effect of chemical composition on properties. *J. Biomed. Mater. Res.* **47**, 36–45 (1999).
 25. Loctite Corporation. Dual curing coating method for substrates with shadow areas. (1985).
 26. Kwon, T.-Y., Bagheri, R., Kim, Y. K., Kim, K.-H. & Burrow, M. F. Cure mechanisms in materials for use in esthetic dentistry. *Journal of Investigative and Clinical Dentistry* **3**, 3–16 (2012).
 27. Nason, C., Roper, T., Hoyle, C. & Pojman, J. A. UV-Induced Frontal Polymerization of Multifunctional (Meth)acrylates. *Macromolecules* **38**, 5506–5512 (2005).
 28. Gregory, S. Ultraviolet curable resin compositions having enhanced shadow cure properties. (2001).
 29. Gugg, A., Gorsche, C., Moszner, N. & Liska, R. Frontal Polymerization: Polymerization Induced Destabilization of Peracrylates. *Macromol. Rapid Commun.* **32**, 1096–1100 (2011).
 30. Crivello, J. V. Hybrid free radical/cationic frontal photopolymerizations. *J. Polym. Sci. A Polym. Chem.* **45**, 4331–4340 (2007).
 31. *CHIMIA International Journal for Chemistry*.
 32. Tehfe, M.-A. *et al.* Organic Photocatalyst for Polymerization Reactions: 9,10-Bis[(triisopropylsilyl)ethynyl]anthracene. *ACS Macro Lett.* **1**, 198–203 (2012).

33. Zhang, G., Song, I. Y., Ahn, K. H., Park, T. & Choi, W. Free Radical Polymerization Initiated and Controlled by Visible Light Photocatalysis at Ambient Temperature. *Macromolecules* **44**, 7594–7599 (2011).
34. Padon, K. S. & Scranton, A. B. A mechanistic investigation of a three-component radical photoinitiator system comprising methylene blue, N-methyldiethanolamine, and diphenyliodonium chloride. *J. Polym. Sci. A Polym. Chem.* **38**, 2057–2066 (2000).
35. Kim, D. & Stansbury, J. W. A photo-oxidizable kinetic pathway of three-component photoinitiator systems containing porphyrin dye (Zn-tpp), an electron donor and diphenyl iodonium salt. *J. Polym. Sci. A Polym. Chem.* **47**, 3131–3141 (2009).
36. Kim, D. & Stansbury, J. W. Kinetic pathway investigations of three-component photoinitiator systems for visible-light activated free radical polymerizations. *J. Polym. Sci. A Polym. Chem.* **47**, 887–898 (2009).
37. Kim, D. & Scranton, A. The role of diphenyl iodonium salt (DPI) in three-component photoinitiator systems containing methylene blue (MB) and an electron donor. *J. Polym. Sci. A Polym. Chem.* **42**, 5863–5871 (2004).
38. Pierre Fouassier, J. & Lalevée, J. Three-component photoinitiating systems: towards innovative tailor made high performance combinations. *RSC Adv.* **2**, 2621 (2012).
39. Scholes, G. D., Fleming, G. R., Olaya-Castro, A. & van Grondelle, R. Lessons from nature about solar light harvesting. *Nature Chemistry* **3**, 763–774 (2011).
40. Kavarnos, G. J. in *Photoinduced Electron Transfer I* 21–58 (Springer, 1990).
41. Stansbury, J. W. & Dickens, S. H. Determination of double bond conversion in dental resins by near infrared spectroscopy. *Dental Materials* **17**, 71–79 (2001).
42. Chai, J.-D. & Head-Gordon, M. Long-range corrected hybrid density functionals with damped atom–atom dispersion corrections. *Phys. Chem. Chem. Phys.* **10**, 6615 (2008).
43. Li, H. & Jensen, J. H. Improving the efficiency and convergence of geometry optimization with the polarizable continuum model: New energy gradients and molecular surface tessellation. *J. Comput. Chem.* **25**, 1449–1462 (2004).
44. Zhao, Y. & Truhlar, D. G. The M06 suite of density functionals for main group thermochemistry, thermochemical kinetics, noncovalent interactions, excited states, and transition elements: two new functionals and systematic testing of four M06-class functionals and 12 other functionals. *Theor Chem Account* **120**, 215–241 (2007).
45. Shao, Y. *et al.* Advances in methods and algorithms in a modern quantum chemistry program package. *Phys. Chem. Chem. Phys.* **8**, 3172 (2006).
46. Schmidt, M. W. *et al.* General atomic and molecular electronic structure system. *J. Comput. Chem.* **14**, 1347–1363 (1993).
47. Mills, A., Lawrie, K. & McFarlane, M. Blue bottle light: lecture demonstrations of homogeneous and heterogeneous photo-induced electron transfer reactions. *Photochem. Photobiol. Sci.* **8**, 421

- (2009).
48. Galagan, Y., Hsu, S.-H. & Su, W.-F. Monitoring time and temperature by methylene blue containing polyacrylate film. *Sensors and Actuators B: Chemical* **144**, 49–55 (2010).
 49. Goodspeed, F. C., Scott, B. L. & Burr, J. G. Photooxidation of tertiary nitrogen compounds by methylene blue. *J. Phys. Chem.* **69**, 1149–1153 (1965).
 50. Kavarnos, G. J. & Turro, N. J. Photosensitization by reversible electron transfer: theories, experimental evidence, and examples. *Chem. Rev.* **86**, 401–449 (2001).
 51. Kim, D., Scranton, A. B. & Stansbury, J. W. Analysis of association constant for ground-state dye-electron acceptor complex of photoinitiator systems and the association constant effect on the kinetics of visible-light-induced polymerizations. *J. Polym. Sci. A Polym. Chem.* **47**, 1429–1439 (2009).
 52. Sirovatka Padon, K. & Scranton, A. B. The effect of oxygen on the three-component radical photoinitiator system: Methylene blue, N-methyldiethanolamine, and diphenyliodonium chloride. *J. Polym. Sci. A Polym. Chem.* **38**, 3336–3346 (2000).
 53. Asmusen, S., Arenas, G., Cook, W. D. & Vallo, C. Photobleaching of camphorquinone during polymerization of dimethacrylate-based resins. *Dental Materials* **25**, 1603–1611 (2009).
 54. Eaton, D. F. *Dye Sensitized Photopolymerization. Advances in Photochemistry* **13**, 427–487 (John Wiley & Sons, Inc., 1986).
 55. Kim, D., Scranton, A. B. & Stansbury, J. W. Effect of the electron donor structure on the shelf-lifetime of visible-light activated three-component initiator systems. *J. Appl. Polym. Sci.* **114**, 1535–1542 (2009).
 56. Galagan, Y. & Su, W.-F. Reversible photoreduction of methylene blue in acrylate media containing benzyl dimethyl ketal. *Journal of Photochemistry & Photobiology, A: Chemistry* **195**, 378–383 (2008).
 57. Impert, O. *et al.* Kinetics and mechanism of a fast leuco-Methylene Blue oxidation by copper (II)-halide species in acidic aqueous media. *Dalton Transactions* 348–353 (2003).
 58. Dektar, J. L. & Hacker, N. P. Photochemistry of diaryliodonium salts. *J. Org. Chem.* **55**, 639–647 (1990).
 59. Munekage, Y. *et al.* Cyclic electron flow around photosystem I is essential for photosynthesis. *Nature* **429**, 579–582 (2004).
 60. Hertle, A. P. *et al.* PGRL1 Is the Elusive Ferredoxin-Plastoquinone Reductase in Photosynthetic Cyclic Electron Flow. *Molecular Cell* **49**, 511–523 (2013).
 61. Datta, P., Efimenko, K. & Genzer, J. The effect of confinement on thermal frontal polymerization. *Polym. Chem.* **3**, 3243 (2012).
 62. Mathew, J. & Mahadevan, V. Redox polymerization of 2-hydroxyethyl methacrylate, 2. Kinetics,

mechanism and solvent effect using manganese triacetate/cyanoacetic acid as the redox system. *Macromol. Chem. Phys.* **197**, 367–374 (1996).

3.6 Supplemental Information

Reaction of alpha-amino radical (derived from DIPEA) and a HEMA monomer

In Figure S1, we calculate the enthalpic barrier (ΔH_{0act}) for the reaction between an amino-alkyl radical (product of one electron and one proton transfer of DIPEA) and a HEMA monomer. Stationary geometries (transition state and minima) were obtained at uWB97XD/LANL2dz/CPCM-methanol level of theory. ΔH_{0act} calculated at this level of theory was 0.1 kcal/mol. Single point energy calculations were then performed at uM06/6-311G(d,p) level of theory, where we obtained $\Delta H_{0act} = -1.4$ kcal/mol (barrierless). The M06 functional was designed to yield accurate thermochemical predictions; and when combined with 6-311G(d,p) basis sets, should yield reasonable predictions to the enthalpic barrier.

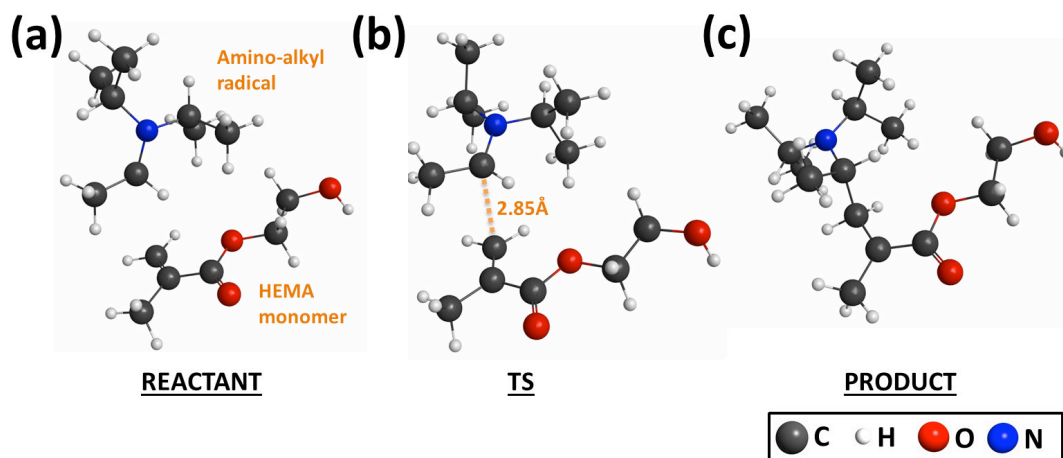


Figure S1 | Reaction between amino-alkyl radical and HEMA monomer, calculated at uM06/6-311G(d,p)//uWB97XD/LANL2dz/CPCM-methanol. (a) Reactant, (b) TS structure and (c) Product
Coordinates of Molecular Structures

All coordinates are reported as XYZ Cartesian coordinates. 0 K energies (not ZPE corrected) reported are calculated using uM06/6-311G(d,p)//uWB97XD/LANL2dz/CPCM-methanol in Hartrees.

LMB (-1183.1852140093)

S	1.38084	0.00392	1.14593
N	-0.23269	4.95441	0.61194
N	-0.23107	-4.94657	0.60705
C	0.75678	1.39691	0.12754
C	0.75723	-1.38828	0.12617
C	0.66865	1.24177	-1.26554
C	0.66904	-1.23179	-1.26676
C	0.05714	3.74027	-0.00242
C	0.05834	-3.73173	-0.00613
C	0.43851	2.60392	0.75741
C	0.43935	-2.59602	0.75484
C	0.26737	2.35837	-2.01910

C	0.26812	-2.34776	-2.02143
C	-0.01464	3.58585	-1.41223
C	-0.01351	-3.57593	-1.41579
C	-0.64309	6.09831	-0.19834
C	-0.18303	5.06489	2.06709
C	-0.64079	-6.08990	-0.20439
C	-0.18136	-5.05848	2.06208
H	0.50609	2.66117	1.83725
H	0.50698	-2.65433	1.83461
H	0.17776	2.26725	-3.09760
H	0.17847	-2.25560	-3.09984
H	-0.30620	4.41653	-2.04273
H	-0.30484	-4.40607	-2.04710
H	-0.81903	6.95765	0.45013
H	-1.57171	5.89750	-0.75101
H	0.13091	6.37994	-0.92498
H	-0.44767	6.08077	2.36346
H	-0.88883	4.37717	2.55418
H	0.82184	4.85360	2.45790
H	-0.81608	-6.95005	0.44318
H	-1.56961	-5.88915	-0.75677
H	0.13332	-6.37024	-0.93140
H	-0.44573	-6.07473	2.35743
H	-0.88735	-4.37144	2.54985
H	0.82345	-4.84729	2.45309
N	0.97519	0.00535	-1.88365
H	0.98131	0.00585	-2.89448

MB+ (-1182.4175828153)

S	0.00000	0.00000	1.42134
N	0.00000	5.07128	0.53149
N	0.00000	-5.07128	0.53149
N	0.00000	0.00000	-1.75698
C	0.00000	1.39897	0.29303
C	0.00000	-1.39897	0.29303
C	0.00000	1.19352	-1.13345
C	0.00000	-1.19352	-1.13345
C	0.00000	3.82498	0.00284
C	0.00000	-3.82498	0.00284
C	0.00000	2.66694	0.84297
C	0.00000	-2.66694	0.84297
C	0.00000	2.36833	-1.96001
C	0.00000	-2.36833	-1.96001
C	0.00000	3.62907	-1.42969
C	0.00000	-3.62907	-1.42969
C	0.00000	6.25956	-0.33974
C	0.00000	5.26487	1.99040
C	0.00000	-6.25956	-0.33974

C	0.00000	-5.26487	1.99040
H	0.00000	2.77932	1.91918
H	0.00000	-2.77932	1.91918
H	0.00000	2.21465	-3.03265
H	0.00000	-2.21465	-3.03265
H	0.00000	4.48139	-2.09438
H	0.00000	-4.48139	-2.09438
H	0.00000	7.15477	0.27927
H	-0.89205	6.28325	-0.97338
H	0.89205	6.28325	-0.97338
H	0.00000	6.33052	2.21088
H	-0.89193	4.82186	2.44522
H	0.89193	4.82186	2.44522
H	0.00000	-7.15477	0.27927
H	-0.89205	-6.28325	-0.97338
H	0.89205	-6.28325	-0.97338
H	0.00000	-6.33052	2.21088
H	-0.89193	-4.82186	2.44522
H	0.89193	-4.82186	2.44522

DPI+ (-7382.0962246181)

I	-0.00001	-1.44433	-0.00001
C	1.60172	-0.02727	-0.00001
C	2.09335	0.41606	1.23306
C	2.09320	0.41620	-1.23310
C	3.13139	1.36151	1.21884
H	1.69597	0.05257	2.17264
C	3.13122	1.36167	-1.21890
H	1.69571	0.05282	-2.17268
C	3.64553	1.83160	-0.00003
H	3.53095	1.72413	2.15806
H	3.53065	1.72442	-2.15812
H	4.44597	2.56206	-0.00004
C	-1.60174	-0.02729	0.00002
C	-2.09322	0.41618	1.23310
C	-2.09335	0.41606	-1.23305
C	-3.13121	1.36167	1.21890
H	-1.69575	0.05276	2.17268
C	-3.13136	1.36154	-1.21883
H	-1.69597	0.05257	-2.17264
C	-3.64549	1.83163	0.00004
H	-3.53064	1.72442	2.15813
H	-3.53090	1.72419	-2.15805
H	-4.44591	2.56213	0.00005

Phenyl radical (-231.4319744629)

C	0.64415	-3.03630	0.00271
C	2.05118	-3.04578	0.00316
C	2.77024	-1.82983	0.00250
C	2.01607	-0.66040	0.00153

C	0.62626	-0.59196	0.00112
C	-0.06749	-1.82261	0.00166
H	0.10222	-3.97572	0.00318
H	2.58997	-3.98766	0.00397
H	3.85466	-1.82159	0.00284
H	0.09138	0.35138	0.00030
H	-1.15260	-1.82648	0.00132

Iodobenzene (-7150.8087915277)

I	-1.52282	2.77274	0.53421
C	-2.37412	0.82403	0.72516
C	-2.27342	-0.07724	-0.34551
C	-3.02515	0.46939	1.91627
C	-2.83774	-1.35751	-0.21546
H	-1.76961	0.20110	-1.26368
C	-3.58499	-0.81434	2.03226
H	-3.10057	1.16936	2.74013
C	-3.49286	-1.72762	0.96993
H	-2.76275	-2.05760	-1.03992
H	-4.08929	-1.09296	2.95070
H	-3.92752	-2.71635	1.06476

DIPEA (-370.8458178021)

N	0.00413	0.26562	0.17904
C	1.03138	-0.80346	0.20464
C	2.13949	-0.45481	1.21684
C	1.65594	-1.15095	-1.17085
H	0.52985	-1.70717	0.56892
H	1.71213	-0.32724	2.21651
H	2.89713	-1.24665	1.25433
H	2.64187	0.47975	0.93751
H	0.88785	-1.36017	-1.92067
H	2.28385	-0.33244	-1.54155
H	2.29156	-2.03879	-1.07359
C	-1.40961	-0.16450	0.06773
C	-1.89053	-0.85967	1.35478
C	-1.72827	-1.03429	-1.17343
H	-1.99158	0.75957	-0.02985
H	-1.70196	-0.22116	2.22361
H	-2.96572	-1.06461	1.29495
H	-1.37945	-1.81687	1.51293
H	-1.38290	-0.55090	-2.09444
H	-1.25075	-2.01829	-1.09729
H	-2.81008	-1.19019	-1.25599
C	-0.18379	2.76356	0.02615
C	0.34174	1.46517	-0.60702
H	0.09683	3.62761	-0.58794
H	-1.27534	2.76035	0.11862
H	0.24273	2.89166	1.02667

H	-0.02499	1.38972	-1.64730
H	1.43192	1.54017	-0.67178

DIPEA-H+ (-371.3005826892)

N	0.04215	0.30794	0.30429
C	1.06395	-0.85398	0.22025
C	2.17525	-0.59749	1.24688
C	1.62765	-1.06803	-1.19015
H	0.50754	-1.74351	0.51888
H	1.77728	-0.52889	2.26441
H	2.88043	-1.43157	1.21938
H	2.73245	0.31730	1.01933
H	0.85098	-1.17061	-1.94968
H	2.30999	-0.26723	-1.48603
H	2.19954	-1.99977	-1.17461
C	-1.43132	-0.13184	0.16773
C	-1.85277	-0.91829	1.41619
C	-1.70204	-0.89781	-1.12898
H	-1.99178	0.80449	0.15182
H	-1.63913	-0.36463	2.33625
H	-2.93260	-1.07965	1.36973
H	-1.37534	-1.90029	1.47496
H	-1.40232	-0.33802	-2.01878
H	-1.21429	-1.87620	-1.13650
H	-2.77996	-1.06588	-1.19697
C	-0.34065	2.76705	-0.21877
C	0.40657	1.48528	-0.59155
H	0.09808	3.59111	-0.78683
H	-1.40314	2.72696	-0.46781
H	-0.23338	3.00199	0.84499
H	0.20797	1.19481	-1.62249
H	1.48053	1.63913	-0.47693
H	0.11790	0.66083	1.26546

N(C3H7)2C2H4_radical + HEMA (reactant) (-830.34789677)

N	-0.19714	-2.33973	-0.37374
C	1.22021	-1.98936	-0.13169
C	1.46717	-1.43660	1.28887
C	1.73178	-1.01367	-1.20880
H	1.79514	-2.91559	-0.22509
H	1.08063	-2.12780	2.04460
H	2.54265	-1.30470	1.45574
H	0.97625	-0.46662	1.42537
H	1.62258	-1.45430	-2.20484
H	1.15982	-0.07928	-1.18311
H	2.78904	-0.77585	-1.04410
C	-0.56128	-3.76871	-0.45254
C	-0.33810	-4.50310	0.88780
C	0.15821	-4.47950	-1.61473

H	-1.63123	-3.80167	-0.67418
H	-0.87397	-3.99266	1.69544
H	-0.70390	-5.53389	0.82197
H	0.72717	-4.53790	1.14539
H	-0.00702	-3.94027	-2.55295
H	1.23789	-4.55606	-1.44431
H	-0.23242	-5.49720	-1.72353
C	-2.62216	-1.57448	-0.42283
C	-1.16915	-1.36955	-0.08659
H	-3.16648	-0.65043	-0.20344
H	-2.79252	-1.81699	-1.48625
H	-3.09272	-2.37540	0.16551
H	-0.79492	-0.35339	-0.02011
O	0.36384	2.21959	0.38884
O	4.01266	2.54635	-0.01002
O	-0.89676	3.12593	-1.28694
C	1.59065	2.66748	-0.28115
C	2.74346	2.21078	0.61021
C	-2.02531	2.08990	0.58502
C	-0.83448	2.52803	-0.19694
C	-3.35919	2.33792	-0.07781
C	-1.87884	1.51290	1.79478
H	4.18581	3.50304	0.04437
H	1.56472	3.75623	-0.38871
H	1.65583	2.21297	-1.27337
H	2.65385	2.65911	1.60582
H	2.73492	1.12531	0.70827
H	-3.51320	3.40641	-0.26084
H	-3.41215	1.83202	-1.04792
H	-4.17359	1.97090	0.55145
H	-2.74516	1.18962	2.36328
H	-0.90104	1.35113	2.23421

N(C3H7)2C2H4_radical + HEMA (TS) (-830.34938384)

N	-4.32431	-2.98054	1.98016
C	-2.88477	-2.77699	2.26135
C	-2.63259	-1.89745	3.50416
C	-2.15564	-2.21385	1.02606
H	-2.46449	-3.76542	2.46822
H	-3.15129	-2.30265	4.37905
H	-1.55886	-1.85915	3.72075
H	-2.98306	-0.87462	3.33500
H	-2.28912	-2.87912	0.16698
H	-2.54258	-1.22382	0.75796
H	-1.08381	-2.11450	1.23058
C	-4.91829	-4.29902	2.28614
C	-4.93544	-4.58569	3.80295
C	-4.23782	-5.43542	1.50003
H	-5.95540	-4.25486	1.94481
H	-5.43916	-3.77255	4.33713
H	-5.46735	-5.52156	4.00693

H	-3.91708	-4.68251	4.19756
H	-4.21883	-5.20305	0.43050
H	-3.20993	-5.61123	1.83567
H	-4.79542	-6.36699	1.64505
C	-6.55526	-1.97157	1.32643
C	-5.13653	-1.85669	1.82099
H	-6.96228	-0.96585	1.18912
H	-6.62948	-2.49982	0.36104
H	-7.21520	-2.49357	2.03247
H	-4.60384	-0.93223	1.62088
O	-3.88636	1.49733	2.99276
O	-0.35418	2.37009	2.38982
O	-5.40142	3.02657	2.21517
C	-2.79245	2.35479	2.52901
C	-1.50233	1.58200	2.80210
C	-6.21672	1.01456	3.27406
C	-5.17518	1.93787	2.78642
C	-7.63939	1.39429	2.93163
C	-5.88183	-0.11664	3.94562
H	-0.19650	3.10604	3.00780
H	-2.81768	3.30155	3.07827
H	-2.91215	2.55888	1.46189
H	-1.44033	1.31035	3.86213
H	-1.46951	0.67159	2.20293
H	-7.90851	2.35908	3.37555
H	-7.77471	1.48932	1.84807
H	-8.33557	0.63666	3.30118
H	-6.64774	-0.80428	4.29044
H	-4.85822	-0.33997	4.21323

N(C3H7)2C2H4_radical + HEMA (Product) (-830.38246071)

N	-0.12611	-2.09632	-0.40924
C	1.33638	-2.14454	-0.22588
C	1.86262	-1.26325	0.93261
C	2.07663	-1.80493	-1.53624
H	1.58067	-3.18521	0.01744
H	1.40088	-1.54697	1.88386
H	2.94914	-1.37382	1.02937
H	1.64305	-0.20646	0.74484
H	1.74217	-2.46714	-2.34130
H	1.88836	-0.76861	-1.84242
H	3.15900	-1.92354	-1.40812
C	-0.93864	-3.19531	0.14221
C	-0.71503	-3.45651	1.65215
C	-0.74446	-4.49689	-0.66280
H	-1.98674	-2.89896	0.01718
H	-0.87663	-2.54564	2.23738
H	-1.41041	-4.22522	2.00881
H	0.30459	-3.81164	1.84348
H	-0.96879	-4.32338	-1.72012
H	0.28759	-4.86027	-0.58572

H	-1.40624	-5.28595	-0.28633
C	-1.81273	-0.83887	-1.74125
C	-0.75623	-0.79398	-0.62054
H	-2.17109	0.16994	-1.97899
H	-1.36979	-1.27148	-2.64331
H	-2.68185	-1.44529	-1.45857
H	0.03154	-0.10465	-0.93971
O	0.27727	2.02215	0.35059
O	3.64330	3.44416	-0.11434
O	-1.45134	3.51937	0.09411
C	1.23518	3.10393	0.12414
C	2.61804	2.45515	0.16764
C	-1.93555	1.19455	0.49906
C	-1.06997	2.33685	0.29763
C	-3.42006	1.39939	0.49005
C	-1.36794	-0.17669	0.69781
H	3.76200	4.04770	0.64057
H	1.12070	3.86325	0.90459
H	1.05017	3.56463	-0.85023
H	2.78356	1.97761	1.14007
H	2.70465	1.70083	-0.61564
H	-3.83962	1.16098	1.47700
H	-3.69242	2.42490	0.23436
H	-3.89487	0.71305	-0.22261
H	-2.16079	-0.84089	1.06006
H	-0.56799	-0.15364	1.44422

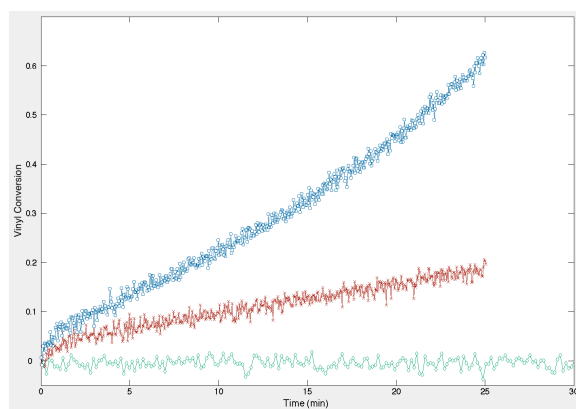


Figure S2 | Vinyl conversion of HEMA with MB⁺/DIPEA, MB⁺/MDEA and MB⁺/TEA. Vinyl conversion of HEMA in solution with MB⁺/DIPEA (green squares), MB⁺/MDEA (red crosses), and MB⁺/TEA (blue dots) at equivalent irradiation conditions and stoichiometric amount of amine.

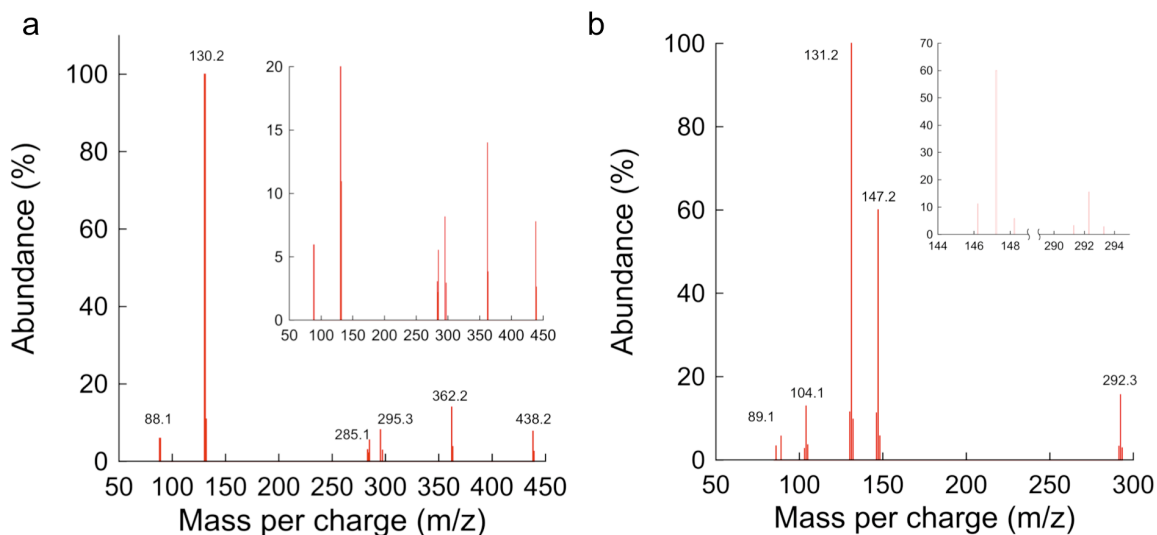
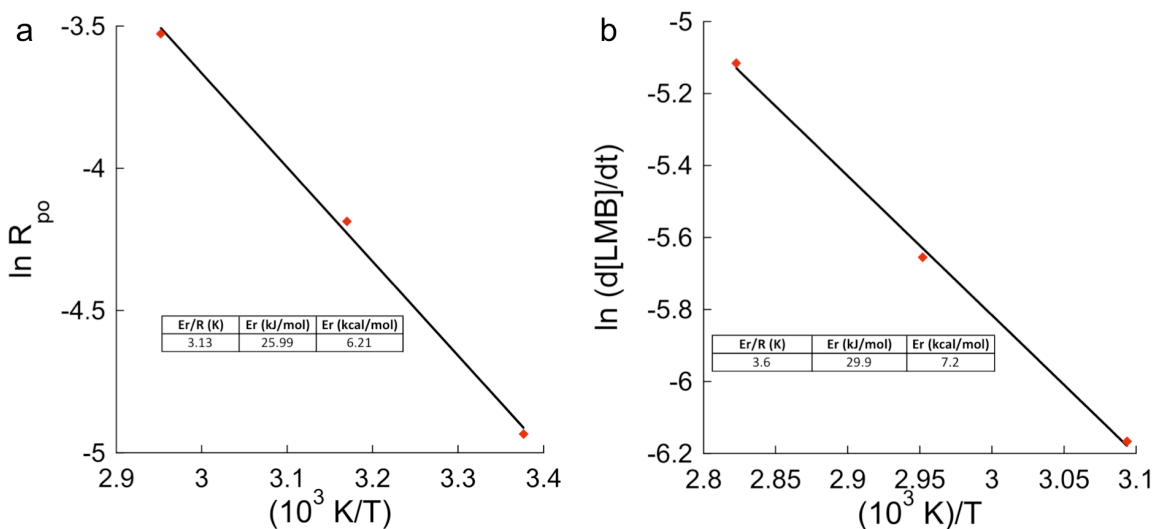
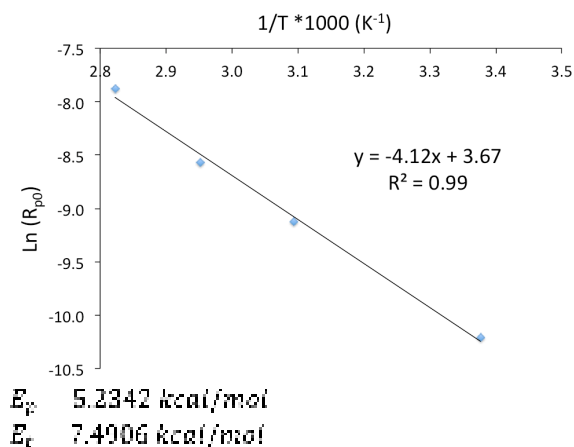


Figure S3 | ESI+- MS monitoring of the photoreaction with MB+/DIPEA and MB+/DIPEA/DPI+. a, Photoreduction of MB+ by DIPEA in the presence of DPI+ in methanol. Evidence of iodobenzene is the formation of the molecules with masses 285.1, 295.3, 362.2 and 438.2 m/z as iodobenzene is not very stable. b, Photoreduction of MB+ with DIPEA in the absence of DPI+. Peaks at 89.1, 104.1, 147.2 and 292.3 m/z are different decomposition products based on 2-ethyliminopropane. Evidence of the formation of DIPEA-H due to extensive photoredox cycling is the formation of a higher abundance at 131.2 m/z than in Figure S2 a. [MB] = 0.004 M, [DIPEA] = 0.2 M, [DPI+] = 0.04 M. Irradiation intensity equal to 37 mW/cm². DIPEA-H (131.2 m/z), MB+ and DPI+ abundances are less than 1 % abundance, thus not giving reliable signals. This peaks were assigned based on mass balances on the original reagents used and correlated to abundances detected to find iodine-containing molecules.



c

$$R_p = [M]_0 \frac{(A_{6165})_{t_1} - (A_{6165})_{t_2}}{(A_{6165})_{t_0} \times (t_2 - t_1)}$$



where A_{6165} is the FT-NIR peak area centered at 6165 cm^{-1} correlated to (meth)acrylates

$$\ln R_p = \ln \left[A_p \left(\frac{A_d}{A_t} \right)^{1/2} \right] + \ln \left[(fI) \right]^{1/2} - \frac{E_p}{RT}$$

first two terms on the right treated as constant for linearization

$$E_p = E_p + \frac{E_d}{2} + \frac{E_t}{2}$$

Figure S4 | Activation energy (ΔE_{act}) for reaction between LMB and DPI^+ , which generates both radicals and MB^+ . a, Activation energy for consumption of HEMA. If we subtract the activation energies for propagation and termination, calculated to be 1.5 kcal/mol with DMPA, we obtain an ΔE_{act} for initiation of 6.6 kcal/mol. Intensity equal to 13 mW/cm². b, Activation energy for the production of MB^+ after 10 s irradiation. Intensity equal to 60 mW/cm². $[MB] = 0.004$ M, $[DIPEA] = 0.2$ M, $[DPI^+] = 0.04$ M. Irradiation intensity equal to 12 mW/cm². c, Activation energy for the radical initiation of HEMA with DIPEA and $DPI+Cl^-$ without light exposure. The same procedure was used to calculate the activation of initiation after adjusting for propagation and termination. E_p from Goodner et al. (in references), and E_t from the photopolymerization of HEMA with DMPA.

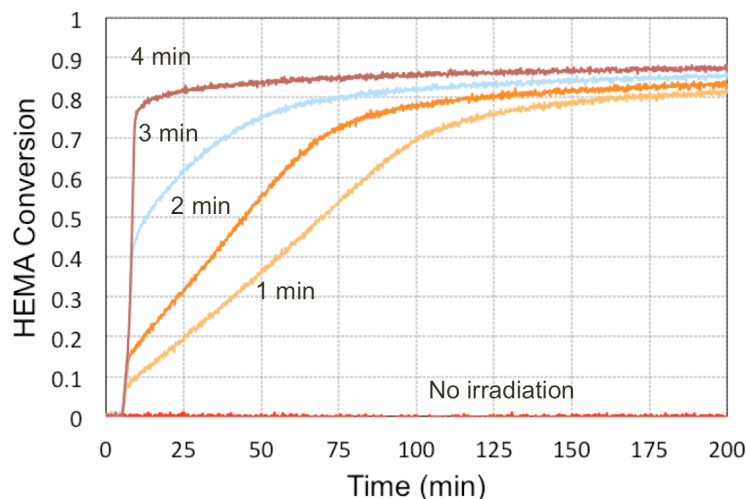


Figure S5 | Polymerization with increasing irradiation times. This shows the final plateau conversion is nearly the same in all cases, and as compared to the result with continuous irradiation. $[MB] = 0.004$ M, $[DIPEA] = 0.2$ M, $[DPI^+] = 0.04$ M. Irradiation intensity equal to 12 mW/cm².

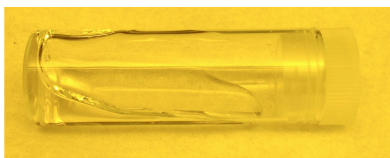


Figure S6 | CQ/EDMAB in HEMA after exposure to 60 s irradiation at equivalent amount of photons absorbed as MB^+ /DIPEA/DPI⁺ in Fig. 4c. Picture shows low degree of monomer conversion resulting in a liquid-like material after irradiation. Concentrations and exposure were as described in the methods section.

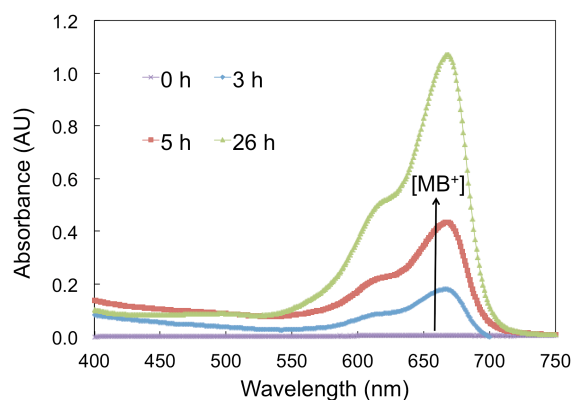


Figure S7 | Methylene blue extraction from poly-HEMA gel into a water solution by swelling of the loosely cross-linked network. $[\text{MB}^+]$ was monitored in time by observing the increase in light absorption around 660 nm. As the material swelled at room temperature, MB^+ diffuses into the solvent. Thus, some of the final blue color of the polymer films can be washed out of the polymer network.

Chapter 4

Coupled UV-Vis/FT-NIR Spectroscopy for Kinetic Analysis of Multiple Reaction Steps in Polymerizations

Abstract

We report the coupling of UV-Vis and FT-NIR spectroscopy for the real-time monitoring of polymerization reactions, allowing the simultaneous tracking of the rates of light absorption, and initiator and monomer consumption, from which dynamic and previously difficult-to-measure parameters are calculated, such as the quantum yields of initiator consumption, initiation, and polymerization, as well as the energy efficiency and residual content of leachable initiator(s). Determining these parameters from the same set of experiments is not possible with other probing techniques. We demonstrate the potential of our millisecond-resolved analytical tool using the free radical initiator system composed of camphorquinone (CQ) as photoreducible chromophore and amine(s) as reductant(s) for the visible-light-triggered bulk polymerization of methacrylate monomers, important for dental and bio-materials. Photoinitiation by CQ/amine pairs in different monomers demonstrates the importance of obtaining quantum yields in the polymerizing medium instead of the inert solvents previously used. Additionally, the often-intricate interactions between initiation reactions and the developing macromolecular architectures can be elucidated. For instance, we present the first quantification of the changes in the quantum yield of initiator consumption as a function of polymerization. This robust analytical tool opens opportunities in the rational design of macromolecular syntheses, fundamental to a broad array of materials.

4.1 Introduction

Polymerization reactions are receiving considerable attention because polymers provide unparalleled versatility and promise precise control of materials properties¹. As a result, there has been a rise in the number of routes to macromolecular synthesis, including Atom Transfer Radical Polymerization (ATRP)², Reversible Addition Fragmentation Chain-Transfer (RAFT)³, Copper-Catalyzed Azide-Alkyne Cycloadditions (CuAAC)⁴, and thiol-Michael reactions⁵. However, understanding of the mechanisms thereof has struggled to keep up because most of these polymer syntheses involve multiple reactions that are interwoven and difficult to characterize with current analytical techniques. Furthermore, the dynamic changes in the medium (e.g. viscosity, refractive index, and light scattering) impose practical restrictions on the analysis of these reactions, which can be dependent on the extent of the polymerization and the particular architecture of the macromolecules formed. Hence, the number of available analytical tools for in-situ characterization of the rapidly growing polymer chemistry toolbox is relatively limited⁶⁻⁹. Herein, we report the coupling of Ultraviolet-Visible (UV-Vis: 250-800 nm) and Fourier Transform-Near Infrared (FT-NIR: 800-2500 nm) spectroscopy to incorporate analysis of initiators and catalysts to that of the monomer(s) consumption with the goal of providing a better alternative to elucidate the intricate mechanisms of the growing plethora of polymerization reactions.

Most often, the consumption of monomers and/or production of polymer is exclusively evaluated¹⁰⁻¹⁵. Common discrete techniques are infrared, photoacoustic, raman, or nuclear magnetic resonance spectroscopy. Other continuous analytical methods¹⁶ typically used include calorimetry¹⁷⁻¹⁹, dilatometry, photothermal²⁰, IR radiometry, optical pyrometry^{21,22}, or interferometry²³. Limitations with most of these alternatives are that data acquisition is often too slow to analyze the fast reaction rates of many polymerizations¹⁶ and that quantification of residual monomer functional groups is impossible, which is becoming critical in many applications. Only real-time FT-IR allows direct determination of residual functional groups, conversion, and rate of polymerization (R_p) with millisecond resolution

without the need to know the enthalpy of the polymerization, as in calorimetry^{16,24,25}. Hence, and due to its ease of use, accessibility, and robustness, FT-IR is now vital for polymerization kinetics^{16,25-30}.

FT-IR analysis relies on the quantification of the light absorbed by the monomer in either the Near-Infrared (NIR, 800-2500 nm) or the mid-Infrared (Mid-IR, 2500-50,000 nm). Mid-IR has received more attention than NIR²⁴. However, the former is restricted to thin films or surface analysis because of its high absorptivities and diffraction limits, and requires the use of salt substrates, like KBr, because glass absorbs in the Mid-IR. This precludes the use of glass-based fiber optics for remote probing with Mid-IR. In contrast, NIR permits fiber-optic coupled nondestructive probing with less expensive substrates (e.g. glass or polymers), and more practical sample dimensions^{24,31}. Both NIR and Mid-IR can be used in transmission, transfection or reflection mode. But while the first two allow quantification of the average bulk monomer content, reflection FT-IR is surface-limited. Similarly, Raman spectroscopy, scattering-based, is restricted to a relatively thin layer of the sample due to fluorescence emission. Consequently, FT-NIR in transmission mode seemed like the most practical candidate for fiber-coupled integration of initiator/catalyst monitoring to the in-situ probing of bulk monomer consumption.

Real-time *in-situ* probing of initiators and catalysts during polymerization remains scarce^{20,32,33}. This is mainly due to the fact that these components are not detectable by most analytical instruments at the relatively low concentrations at which they are used. Hence, a lag is still present in mechanistic understanding of the initiation/catalysis pathways, and their dependence on the monomer and polymer chemistry. Moreover, new initiators and catalysts are constantly being developed for the wide library of monomers³⁴⁻⁴⁰. This is important because the rational design of initiators and catalysts is becoming a hurdle in the development of polymer syntheses^{41,42}. Recently, new insights and theories have been reported on the mechanisms of metal-⁴³, organic-⁴¹, and photo-catalysis⁴⁴. However, these often require expensive and laborious analytical methods, like isotope labeling⁴⁵, kinetic isotope effects, discrete NMR for light-induced ATRP in solution, or detection of reactive centers with Electron Paramagnetic

Resonance Spectroscopy (EPR). Hence, a need exists for robust and practical tools to deduce initiation and catalysis mechanisms from kinetic data obtained in-situ during polymerization reactions.

UV-Vis spectroscopy has been seldom employed to analyze initiation or catalysis^{32,33,46-49}. The use of UV-Vis to monitor these reactions is non-trivial because polymerization causes changes in light scattering and refractive index that often lead to artifacts in the results, which can preclude acquisition of useful data altogether. Thus, previously reported UV-Vis analyses were limited to reactions in solvent or very dilute monomer solutions, where such problems are mitigated⁴⁹⁻⁵². Furthermore, UV-Vis radiation has enough energy per photon to trigger undesired photochemical reactions. Hence, a single light beam for both probing and inducing polymerization has been used to avoid premature activation of the reaction. However, this approach restricts the analysis to the, usually narrow, wavelength range of the light sources that are used to initiate the polymerization. These light sources are also known for having an unstable emission^{32,33,47,53}. Additionally, UV-Vis analysis has been restricted to fixed-wavelength or wavelength-scanning approaches. This type of data acquisition leads to uncertainty in the acquisition times.

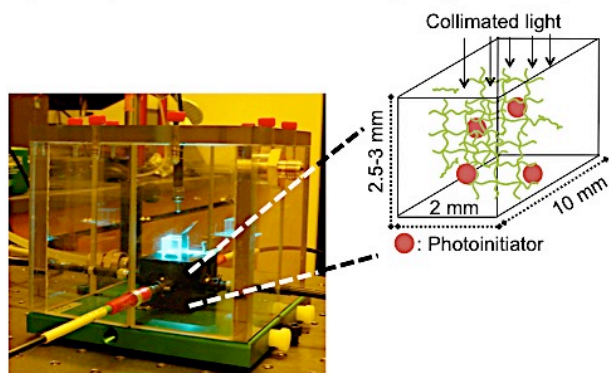
Herein we present the orthogonal coupling of UV-Vis to FT-NIR spectroscopy with fiber optics in the same plane, perpendicular to the direction of the independent polymerization-inducing irradiation, without premature activation of polymerization by the UV-Vis probing light, as shown in Figures 4.1a and 4.2. Our simultaneous full-spectrum UV-Vis acquisition (250-1100 nm) allows tracking of multiple absorption peaks (Fig. 4.1c) at precise acquisition time intervals; thus expanding the applicability of real-time UV-Vis probing for polymerization reactions. Data can be gathered with up to millisecond resolution in both UV-Vis and FT-NIR. This allows direct correlation of both initiation and polymerization kinetics. We can successfully obtain useful kinetic data from bulk polymerizations where changes in light scattering and refractive index are greatest. This is the first time that UV-Vis/FT-IR are coupled for polymerization analysis^{25,54,55}, but no other method exists for simultaneous probing of initiation/catalysis and polymerization reactions.

UV-Vis and Mid-IR spectroscopy were utilized separately in the only report of initiation and polymerization kinetics⁵⁴. Separate UV-Vis and FT-MIR acquisition complicates the direct overlap of the independent results on the same time scale because of the challenge of replicating irradiation conditions and specimen orientations between experiments in different instruments. In contrast, our simultaneous UV-Vis/FT-NIR approach eliminates these uncertainties by the concurrent acquisition of initiation/polymerization kinetics data from a single experiment under the same conditions (Fig. 4.1c).

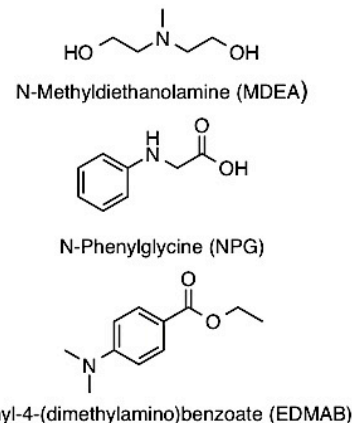
While thermal, redox, or light-induced initiation can be analyzed in our UV-Vis/FT-NIR device, we selected a visible-light initiated free radical polymerization. Figures 4.1b & 4.1c contain the structures of the initiator system: camphorquinone (CQ) chromophore and different amines as reductants. We analyzed the polymerizations of two methacrylate monomers and mixtures thereof, used in dental and biomaterials^{56,57} (Fig. 4.1c). These formulations are useful to introduce our apparatus and showcase its potential elucidation of new mechanistic insights. We present results for bulk polymerization, but solution reactions can also be analyzed. Studies of initiator consumption were performed with CQ/amine in similar monomers and, thus serve as a reference to validate the data output from our device^{32,33,47}. Most importantly, analysis of these reactions highlights the advantages of the UV-Vis/FT-NIR tool for the determination of real-time rates of initiator consumption ($d[\text{CQ}]/dt$), polymerization (R_p), and light absorption (I_{abs}), i.e. while the first two rates can be determined with other techniques (e.g. Raman), I_{abs} can only be directly obtained from UV-Vis data. Concurrent evaluation of these three rates permits the calculation of the propagation (k_p) and termination (k_t) kinetic constants, and the quantum yields of CQ reduction (Φ_{red}), initiation (Φ_i), and polymerization (Φ_p) from the same experiments, as described in the Results and Discussion section. This allows the assessment of reaction efficiencies for the multiple reaction steps, and deduction of complex interwoven mechanisms involved in the polymerization processes. For instance, we show previously unreported decreases in Φ_{red} associated with reduced mobility of the bulk polymer networks formed by the methacrylates. Not only can these insights aid in the mechanistic understanding of more recent light-induced polymer syntheses (e.g. ATRP, RAFT, CuAAC),

but it can also expedite the rational design of well-established polymerization reactions, as introduced here. Thus, opening new opportunities in the general field of polymer materials.

a) Analytical device and sample geometry



b) Selected amine reductants



c) Full spectrum acquired simultaneously

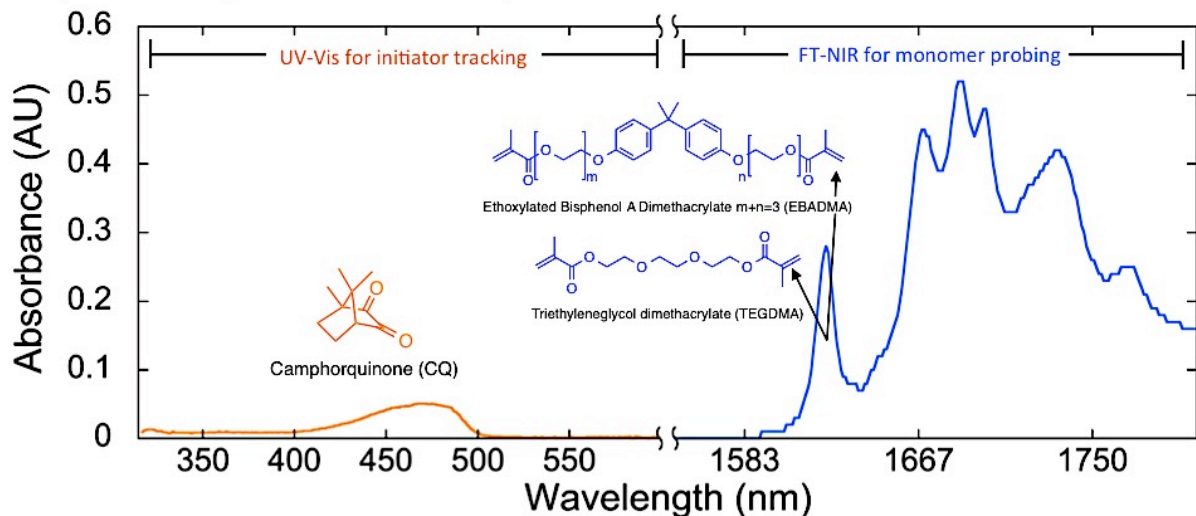


Figure 4.1. Coupled UV-Vis/FT-NIR spectroscopy for polymerization analysis. **a**, Picture of the UV-Vis/FT-NIR analytical device where the sample is contained in a PMMA cuvette inside an in-house modified cuvette holder that allows UV-Vis and FT-NIR light beams to run orthogonal to each other and perpendicular to the polymerization-inducing irradiation (from the top of the sample), as depicted in the schematic of the sample. An in-house-built purging chamber covers the sample holder. **b**, The amine reductants ethyl 4-N,N-dimethylamino benzoate (EDMAB), methyldiethanolamine (MDEA), and N-phenylglycine (NPG) were chosen because they are known to undergo proton-coupled electron transfer to the excited triplet state of the camphorquinone (CQ) chromophore. This photoreduction of CQ produces one ketyl radical that does not initiate and readily protonates, and an alpha aminoalkyl radical from the amine, which initiates polymerization of the methacrylate monomers (Fig. 4.3a,b). **c**, Snapshot of the simultaneous acquisition of the UV-Vis/FT-NIR spectrum (300-1900 nm), which covers the CQ absorption centered at 470 nm due to the $n \rightarrow \pi^*$ transition from the carbonyls, and the absorption caused by the 1st overtone of $=\text{CH}_2$ bond vibration (around 1620 nm) in the methacrylate monomers: ethoxylated bisphenol-A-dimethacrylate (EBADMA) and triethylene glycol dimethacrylate (TEGDMA). The

disappearance of the CQ (Fig. 4.3b) and =CH₂ peaks is simultaneously monitored *in-situ* during bulk polymerization triggered by a 480 nm LED.

4.2 Experimental section

4.2.1 Materials

Camphorquinone (CQ), ethyl-4-dimethylamine benzoate (EDMAB), methyl diethanolamine (MDEA), and N-phenylglycine (PG) were used as received from Sigma-Aldrich (Milwaukee, WI). The monomers: ethoxylated bisphenol-A-dimethacrylate (EBADMA) with an average degree of ethoxylation of three from Esstech (Essington, PA), and triethylene glycol dimethacrylate (TEGDMA) from Sigma-Aldrich were used without purification.

4.2.2 Polymerization-inducing irradiation

An eight-wavelength light emitting diode (LED) unit containing a blue (480 nm; 20 nm FWHM) chip (FC8-LED, Prizmatix, Southfield, MI) was used to induce the photoreduction of CQ by the amines (Fig. 4.3a). Irradiation intensity was controlled with an internal potentiometer and measured with a radiometer (6253, International Light Technologies, Peabody, MA) designed for the 400-700 nm range. The LED was connected via 1500 μm (inside diameter) fiber optics, collimated with a SMA-adapted lens from Thorlabs Inc., (Newton, NJ) and placed directly over the PMMA cuvettes. The pathlength in the direction of the curing irradiation was ~ 2.5 mm (Fig. 4.1a).

4.2.3 Coupling UV-Vis to FT-NIR

The UV-Vis and FT-NIR beams were coupled into a SMA-fitted cuvette holder (CUV-ALL-UV 4-Way Cuvette Holder, Ocean Optics, Dunedin, FL) that holds a dual-pathlength PMMA cuvette (UVette, Eppendorf, Hauppauge, NY). The sample volume used was 50-60 μL with dimensions of 2 mm x 10 mm x 2.5 mm. The longer pathlength was used for UV-Vis to prevent saturation of the NIR signal. UV-Vis/FT-NIR beams were transmitted orthogonally within a matched horizontal plane through the center of the sample at an approximate depth of 1.25 mm. The aperture of the UV-Vis probing beam was reduced

with a ~ 0.5 mm pinhole at the center of the sample to reduce the artifacts created by the light scattering of both the probing and the polymerization-inducing beams.

Monomer conversion was monitored with a FT-IR spectrophotometer (Nicolet Magna-IR Series II, Thermo Scientific, West Palm Beach, FL) by following the peak area of the first overtone absorption band of the $=\text{CH}_2$ bonds ($\sim 6167 \text{ cm}^{-1} = 1621 \text{ nm}$). Monomer absorbance was confirmed to fall within the linear Beer-Lambert region within the concentrations used here. The spectrophotometer is equipped with an extended range KBr beam splitter and an InGaAs detector. The NIR signal was transmitted to/from the remote specimen via matched $1000 \mu\text{m}$ fiber optic cables. The FT-IR settings were set to 8-16 scans, a resolution of 8, an optical gain of 1, and an optical aperture of 3-5. The velocity of the interferometer was adjusted according to the desired acquisition time.

Fiber optic coupled UV-Vis detectors USB2000-UV-VIS and USB4000-FL (Miniature Fiber Optic Spectrometers, Ocean Optics, Dunedin, FL) were employed to measure the change in the absorbance between 400 nm and 510 nm related to the $n \rightarrow \pi^*$ transition of the carbonyl groups in CQ, which decays as a function of CQ concentration. The CQ absorbance was calibrated against concentration to confirm that it follows Beer-Lambert's linearity. The spectrometers use Charge-coupled Device (CCD) detectors that allow full-spectrum acquisition. The high sensitivity USB4000-FL permits the use of low intensity UV-Vis light in continuous or pulsed mode to probe samples without initiating the polymerization. Integration time was set to < 1 s (Fig. 4.3). Negligible polymerization occurred from exposure to the UV-Vis probing beams from a low intensity halogen lamp from Oriel Instruments (Irvine, CA) with an emission spectrum in the range of 400-700 nm (Fig. 4.3c).

4.2.4 Spectral analysis

The FT-NIR results were obtained directly from the OMNIC Software (Thermo Scientific, West Palm Beach, FL) and processed in Excel according to the method reported by Decker¹⁶. The UV-Vis output was collected with the SpectraSuite Software (Ocean Optics, Dunedin, FL). A FORTRAN code

was written to merge the data into a single text file. Then a MATLAB script was written to process the full-spectrum absorbance, remove any baseline shifts from light scattering of the UV-Vis probing beam (see SI), and extract the absorbance maximum λ_{\max} (~ 470 nm), i.e. maximum absorbance was found for every spectrum and plotted against time. At least three replicates were performed for each experiment. Averaged data was then fitted to exponential equations using MATLAB curve fitting tool. R^2 values for all fittings were at least 0.95.

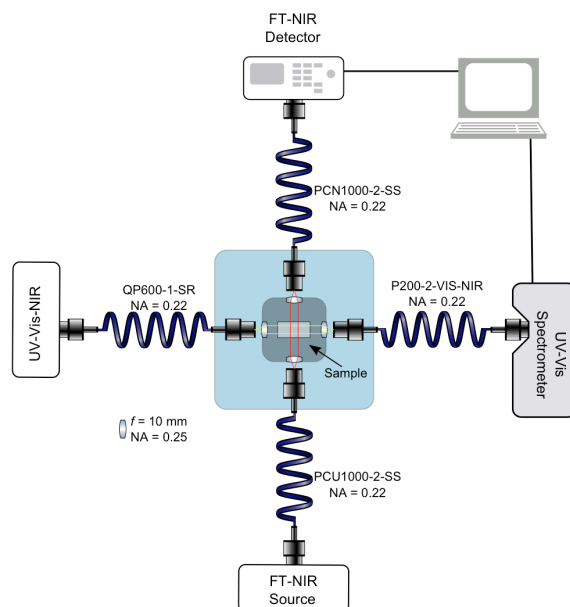


Figure 4.2. Top view of the analytical set-up. Fiber optic cables couple the UV-Vis and Infrared light sources and detectors to and from our modified cuvette holder. Fibers were connected with SMA fittings into focusing lenses and aligned to obtain the maximum signal in each detector. Probing beams run through the center of the sample (from top to bottom). The UV-Vis light source was connected to a computer to control the shutter and pulsation rate of the probing UV-Vis beam. The light intensity and pulsing of the monitoring UV-Vis light were set to prevent premature polymerization of the light sensitive samples. The aperture in the direction of the UV-Vis was reduced to ~ 0.5 mm diameter to minimize the noise in the UV-Vis signal caused by the polymerization-inducing 480 nm LED light that is reflected and scattered into the UV-Vis detector from the top.

4.3 Results and discussion

4.3.1 Validity of UV-Vis/FT-NIR data output

Figure 4.3a shows key reaction steps of the light-induced chain growth polymerizations selected for this introductory work: 1) absorption of light between 400-500 nm to convert ground-state CQ into an excited state singlet, 2) intersystem crossing from an excited singlet into a triplet state CQ, 3) reduction of the excited triplet CQ by the ground-state amine, 4) initiation of the methacrylate monomer by the alpha aminoalkyl radical formed, and 5) lumped propagation/termination steps involving the monomer-based radicals. The blue-labeled steps are those for which information can be deduced with our UV-Vis/FT-NIR device. The photophysical transitions: e.g. fluorescence and intersystem crossing (Step 2) require more expensive transient laser, pump-probe spectroscopy or flash photolysis, which are typically performed in inert solvents and under a narrow set of conditions because these photophysical steps involve significantly shorter lived intermediates, and their detection can be affected by a polymerizing medium. Nevertheless, simultaneous analysis of the blue-labeled reaction steps is presented here for the first time, and provides more information than previously possible with any other instrument.

The CQ absorbance spectrum (λ_{\max} at around 470 nm) correlates linearly with CQ concentration within the concentrations ($[CQ]$) used here. The slope of this correlation is the molar extinction coefficient, and was determined to be $\sim 35 \pm 1$ ($M^{-1} \cdot cm^{-1}$) in bulk TEGDMA and EBADMA monomers. Figure 4.3b shows a 3D plot of the light absorbance between 400 and 520 nm as a function of time (s) and wavelength (nm). The spectra shown have been adjusted to eliminate the shift in the baseline that we observed for all samples. The latter is due to changes in light scattering and refraction associated with fluctuations in density and materials properties during polymerization. These affect the amount of light transmitted through the samples into the UV-Vis detector, thus causing artificial fluctuations in the absorbance data. We include the uncorrected 3D spectra plot in Figure S1 (Supplemental Information). This baseline correction is routinely performed in the real-time IR analysis of polymerization reactions by

the software provided with the IR spectrophotometers, as used herein. Despite these baseline shifts, all UV-Vis and FT-NIR absorbance raw data remained under the saturation limits of the detectors during the reaction.

CQ photoreduction rates were fit to the expected single-exponential kinetic expressions ($R^2 \geq 0.94$) derived from the well-established mechanism (SI Section 2)⁵⁸⁻⁶⁰. The half-lives of CQ were in reasonable agreement with those reported by others^{32,33}. Then, scaling factors were determined for the effects of irradiance and initial concentrations. Figure 4.3c confirms that the rate of CQ photoreduction by EDMAB reductant scales linearly with incident irradiation intensity ($d[\text{CQ}]/dt \propto I_0^{0.95}$; $R_2=0.98$)⁵⁹, whereas the initial rate of polymerization (R_{p0}) for EBADMA was found to have the expected $\frac{1}{2}$ order dependence on I_0 ($R_p \propto I_0^{0.54}$; $R_2=0.96$). Additionally, Figure 4.3c shows that no CQ consumption or polymerization was observed in the absence of the polymerization-inducing LED irradiation, i.e. the UV-Vis probing beam does not activate the reaction.

Then, we confirmed the first order dependence of $d[\text{CQ}]/dt$ on the initial $[\text{CQ}]_0$ at 22 mW/cm^2 in EBADMA (Fig. 4.3d), while R_p increased until a certain threshold value with increasing $[\text{CQ}]_0$, as reported by Cook and Pyszka et al.^{57,61,62}. Within the concentrations used for this study $d[\text{CQ}]/dt$ was observed to be independent of $[\text{EDMAB}]_0$, as observed when the amine reductant is used in excess. R_{p0} for EBADMA also remained roughly constant with increase in $[\text{EDMAB}]_0$.

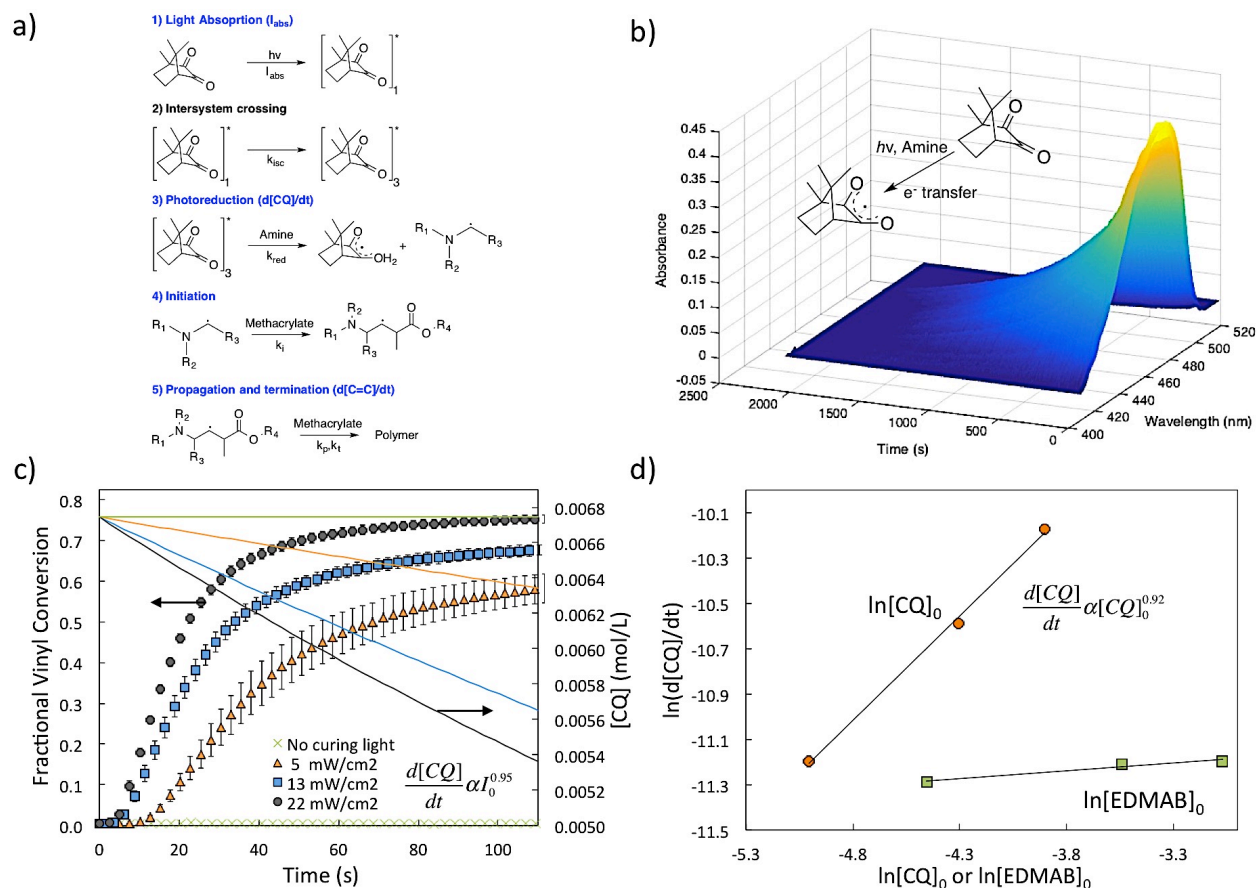


Figure 4.3. Data output for the kinetic analysis of multiple reaction steps during polymerization. **a**, Scheme of key reaction steps during the example chain growth polymerization of methacrylate monomers initiated by the light-triggered photoreduction of CQ by amine reductants. Blue-labeled steps can be analyzed with our UV-Vis/FT-NIR device via determination of the rates of light absorption (I_{abs}), initiator consumption (e.g. $d[\text{CQ}]/dt$), and polymerization ($R_p = -d[\text{C}=\text{C}]/dt$). **b**, 3D plot of UV-Vis absorbance (AU) vs Wavelength (nm) vs Time (s) showing the decay of the peak associated with CQ upon irradiation with a 480 nm LED in the presence of EDMAB reductant. These spectra have been spectrally processed to remove the shift in the baseline caused by the inherent changes in scattering and refraction as the bulk samples polymerize. **c**, Plot of the fractional vinyl conversion of EBADMA monomer and $[\text{CQ}]$ (mol/L) as a function of irradiation time (s) at different intensities with $[\text{CQ}] = 0.006(7)$ M and $[\text{EDMAB}] = 0.046(4)$ M. No polymerization was detected within this time from exposure to the UV-Vis probing beam, and the expected first order ($d[\text{CQ}]/dt \propto I_0^{0.95}$) and half dependence ($R_p \propto I_0^{0.54}$) on incident irradiation intensity were confirmed. **d**, Dependence of $d[\text{CQ}]/dt$ on the initial concentrations of CQ and EDMAB reductant. The expected first order scaling on $[\text{CQ}]_0$ was confirmed, as well as the independence of the photoreduction rate on $[\text{EDMAB}]_0$ when this reductant is used in excess. Photoreduction results were fit to a single-term exponential derived from the kinetic analysis of the proposed mechanism (SI Section 2).

4.3.2 Calculation of quantum yields

The quantum yields of initiator consumption (Φ_d), primary radical (e.g. alpha aminoalkyl) production (Φ_r), monomer initiation (Φ_i), and polymerization (Φ_p) are defined as the ratio of the rates of either initiator consumption (Fig. 4.3a- Step 3), primary radical production (Fig. 3a-Step 3), production of monomer-based radicals (Fig. 4.3a-Step 4), or polymerization of functional groups (Fig. 4.3a-Step 5), over the rate of photon absorption I_{abs} (Fig. 4.3a-Step 1). Hence, knowledge of I_{abs} is absolutely required and can only be obtained with UV-Vis spectroscopy. To quantify I_{abs} , i.e. the overlap between the absorbance spectrum of the initiator (CQ) and of the emission spectrum of the polymerization-inducing light (LED), as detailed in the Experimental Section and shown in Figure 4.4a. We recently used this method for the calculation of quantum yields of photolysis of photobase generators⁶³. I_{abs} is not normally determined this way because it requires full-spectrum acquisition in the UV-Vis region where the initiator absorbs. Thus, I_{abs} determination has been mostly limited to cases in which one-wavelength laser irradiation is used to trigger the polymerization reaction, because one-wavelength activation solely requires knowledge of initial concentration of the light-absorbing initiator, molar absorptivity at the emission wavelength (ϵ), and the pathlength of the sample. Then, the absorption is assumed to be constant throughout the polymerization on the grounds that the initiator concentration varies only slightly during the polymerization^{64,65}. In contrast, we can determine I_{abs} for any broad-spectrum irradiation light-source and without assuming a constant initiator concentration.

Furthermore, our UV-Vis/FT-NIR apparatus provides the advantage of determining I_{abs} in the actual monomer/polymer as opposed to previous analysis of the photochemical reactions in inert solvents^{46,66}. It is well known that absorbance spectra, and thus I_{abs} , depend on the electronic and resonance characteristics of the solvent (SI Section 3). Hence, obtaining I_{abs} in the actual polymerizing medium provides an unparalleled advantage over other analytical methods.

Initial I_{abs} for solutions with EDMAB, MDEA, and NPG were: 3.53×10^{-8} , 4.17×10^{-8} , and 4.51×10^{-8} Einsteins/cm³*s, respectively. These equate to 10, 12, and 13 % absorption of the incident irradiation ($I_0 = 3.53 \times 10^{-7}$ Einsteins/cm³*s), which allows us to assume that the concentration of photons is uniform with depth. Light emission from the LED has a Gaussian distribution, but the samples were centered relative to the light beam to ensure a homogeneously exposed sample cross-section.

Here, for example, we show that the amine reductant affects the absorbance spectrum of CQ (Fig. 4.4a). We observed that methyldiethanolamine (MDEA) shifts the absorbance spectrum to slightly a higher absorbance value as compared to the solutions with EDMAB. On the other hand, the absorbance spectrum with NPG not only increases, but is also blue-shifted by roughly 20 nm. The latter is most likely due to the formation of some ground-state complexes, as indicated by the fact that NPG also absorbs light in the 400-500 nm region, but the spectrum of CQ/NPG solutions is not the addition of the CQ and NPG individual spectra (SI Section 4). These differences in I_{abs} are frequently ignored in the analysis of light-induced polymerization reactions, but can now be readily addressed with our UV-Vis/FT-NIR technique.

Accounting for these differences in I_{abs} , we calculated the quantum yield of CQ photoreduction (Φ_{red}) as $d[\text{CQ}]/dt$ over I_{abs} as a function of reaction time (Fig. 4.4b) in TEGDMA. Initial Φ_{red} values for EDMAB, MDEA, and NPG (0.26 ± 0.02 , 0.27 ± 0.02 and 0.29 ± 0.01 , respectively) are in reasonable agreement with the quantum yields reported in inert solvents (e.g. ethyl acetate)⁶⁶. These values correlate linearly with the oxidation potentials of the amine reductants: 1.1 (EDMAB), 0.9 (MDEA), and 0.4 (NPG) eV, as would be expected. However, more experiments are needed to verify if Φ_{red} correlates primarily to the oxidation potentials of the amines or if there is also a significant contribution of the proton (H⁺) donation capability. A systematic study of a broader range of amine reductants can address this question, but here we want to introduce the UV-Vis/FT-NIR device and its potential to investigate these differences in efficiencies of photoreduction of CQ.

Despite the reasonable agreement in the initial Φ_{red} , the results in Fig. 4.4b show for the first time that Φ_{red} does not remain constant throughout the polymerization, as previously proposed⁴⁶. EDMAB reductant gave a negligible decrease in Φ_{red} as a function of conversion. However, MDEA shows a noticeable decrease in the photoreduction quantum yield, which appears to decrease linearly with vinyl fractional conversion. However, NPG was the most interesting case. While the initial Φ_{red} with NPG was the highest at the very beginning of the reaction, it drops dramatically from 0.29 to 0.20 by the time the gel-effect or Autoacceleration region (~ 4-5 % conversion) is reached in the poly-TEGDMA. Then, as the bulk polymer starts to vitrify at around 62 % vinyl conversion (Fig. 4.4b-c), Φ_{red} decays more steeply to a value of only 0.08-0.06. Ultimately Φ_{red} decreased by almost four times by the time the final vinyl conversion is reached. We labeled these transitions (I, II, and II) with the black dashed lines in Figures 4.4b and 4.4c, and propose that these are more drastic in the case of the NPG reductant because of its higher polarity relative to the MDEA and EDMAB. TEGDMA monomer has a very low polarity, and which decreases with polymerization. Hence the solubility, and thus, homogeneity, will be poorer for NPG during the polymerization. In fact, we observed that a longer isothermal sonication was required to get equimolar amounts of NPG into the TEGDMA solutions before polymerization.

Based on these results, we hypothesized that Φ_{red} with reductants other than NPG should also be affected by mobility with more viscous monomers. Figure 4.5c shows that while Φ_{red} remains fairly constant during the polymerization of rubbery poly-TEGDMA ($T_g = -85 \text{ }^\circ\text{C}^{67}$), it actually decreases slightly towards the end of the polymerization of the higher T_g poly-EBADMA ($T_g = -42 \text{ }^\circ\text{C}^{67}$). Cook reported that $d[\text{CQ}]/dt$ with N,N-3,5-tetramethylaniline remains constant despite changes in initial viscosity and final mechanical properties⁵⁹. However, our results indicate for the first time that the initiation by the bimolecular photoreduction reaction can be affected by the mobility of the developing macromolecular structure depending on the initiator and monomer used.

Additionally, if the photoreduction of CQ can be assumed to be the only reaction leading to the disappearance of the CQ UV-Vis peak (Step 3 in Fig. 4.4a), and we know the amount of primary radicals

produced per photoreduced CQ (n), then the quantum yield of primary radical production Φ_r can be determined as $\Phi_{red} * n$, i.e. for the reactions studied here we know that we can assume that every CQ that's is photoreduced leads to two primary radicals (a ketyl and an alpha aminoalkyl). Hence, in this case we could multiply $\Phi_{red} * 2$ to obtain the quantum yields of primary radical production with values of 0.52, 0.54, and 0.58 for EDMAB, MDEA, and NPG, respectively. In this example, this quantum yield is not important because the ketyl radical does not initiate the polymerization. Nevertheless, there are numerous cases in which the initiator actually produces multiple initiating primary radicals, which should be accounted for.

Direct determination of the quantum yield of monomer initiation (Φ_i) remains scarce because quantification of the short-lived monomer-based radical concentration requires expensive and sophisticated instrumentation (e.g. pulsed laser polymerization- size exclusion chromatography PLP-SEC) performed under a very narrow set of conditions, and limited to low monomer conversions⁶⁸⁻⁷⁰. Hence, relative Φ_i/Φ_{i-ref} ratios have been proposed to circumvent these issues. However, even determination of Φ_i/Φ_{i-ref} is limited because it requires knowledge of R_p and I_{abs} , which can only be obtained simultaneously with our UV-Vis/FT-NIR tool. We show that we can readily determine Φ_i/Φ_{i-ref} values with our UV-Vis/FT-NIR analytical apparatus (Fig. 4.4d) to assess the relative efficiency of the primary radicals produced (Fig. 4.3a-Step 3) in initiating the polymerization of the monomer by radical attack (Fig. 4.3a-Step 4). We found that the relative trend is EDMAB>NPG>MDEA, which agrees with previous reports of relative reactivities that were based on R_p analysis. It is important to acknowledge that NPG has been reported to initiate polymerization more efficiently in other monomers, which can be related to the fact that NPG is more compatible with higher polarity monomers or water-based polymerizations. Also, it is worth noting that Φ_i/Φ_{i-ref} is calculated from initial R_p (R_{p0}) and I_{abs} because the equation for Φ_i/Φ_{i-ref} depends on the assumption of equivalent propagation and termination kinetic constants.

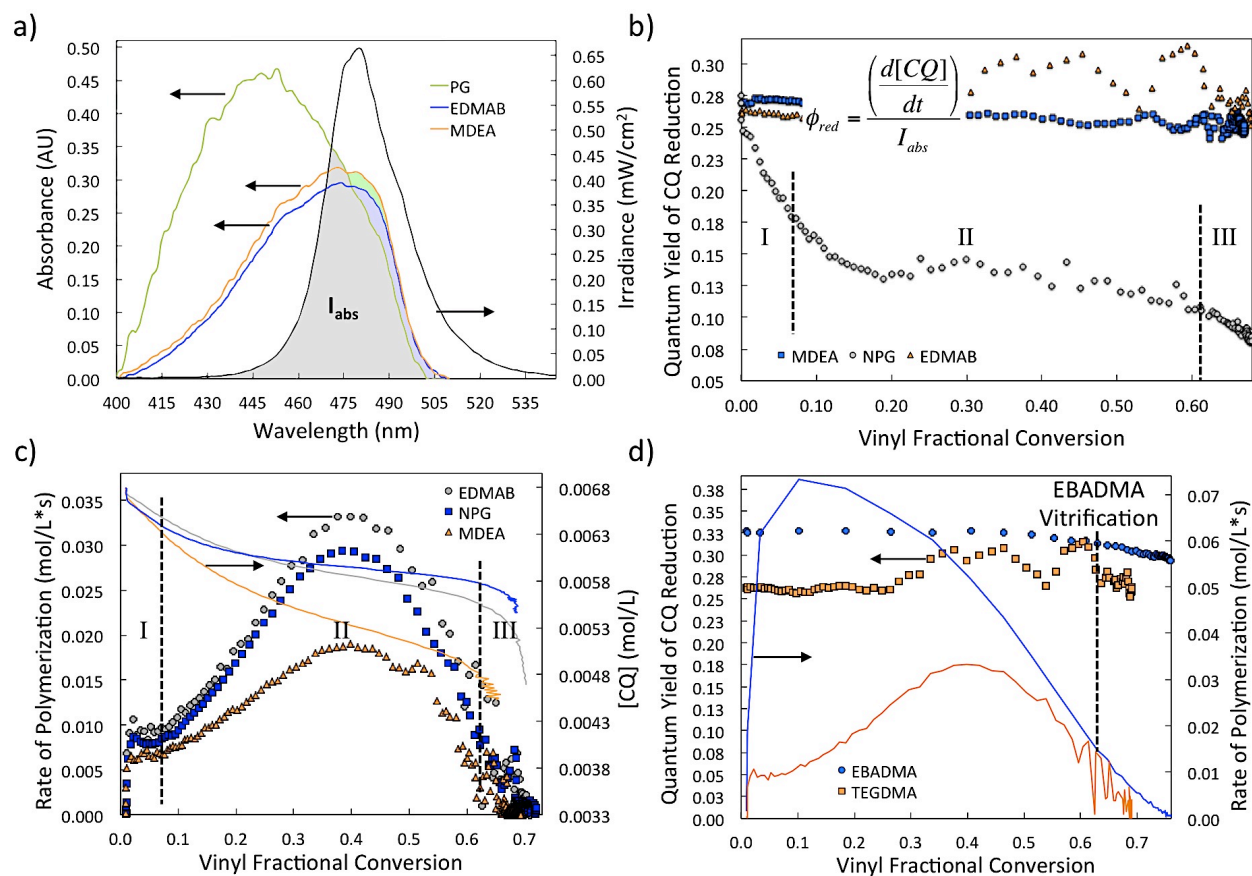


Figure 4.4. Simultaneous determination of light absorption rate, initiator consumption, polymerization, and relative initiation quantum yields during polymerization. **a**, Initial absorbance spectra before irradiation for CQ/amine formulations containing $[CQ]_0 = 0.00674$ M and $[Amine]_0 = 0.0464$ M. The secondary y-axis corresponds to the emission spectrum of the 480 nm LED. Shaded areas represent the amount of photons absorbed by CQ (I_{abs}). Ground-state association of CQ with the reductants changes the absorbance spectrum and, thus, the light absorption efficiency. **b**, Quantum yield of CQ reduction (Φ_{red}) as a function of vinyl fractional conversion with MDEA, EDMAB and NPG. Quantum yields with MDEA and EDMAB show that Φ_{red} decreases slightly as the mobility of the medium decrease during the bulk polymerization. This effect was significantly more drastic with NPG as reductant. **c**, The rate of polymerization (R_p) of TEGDMA and $[CQ]_t$ (mol/L*s) as a function of irradiation time (s). The rate of CQ photoreduction was slightly faster with NPG and roughly equivalent with MDEA and EDMAB up to 50 s. However, $d[CQ]/dt$ with NPG decreases significantly as the poly-TEGDMA starts to gel, whereas $d[CQ]/dt$ with the MDEA and EDMAB was not noticeably affected by the changes in the mobility of the poly-TEGDMA. This is most likely related to the higher polarity of NPG as compared to MDEA and EDMAB. **d**, Quantum yield of CQ reduction (Φ_{red}) and R_p as a function of vinyl fractional conversion for TEGDMA and EBADMA with $[CQ]_0 = 0.00674$ M and $[EDMAB]_0 = 0.0464$ M at 22 mW/cm². Φ_{red} decays negligibly in TEGDMA, but decreases noticeably the glassier poly-EBADMA at the point where the polymer starts vitrifying, i.e. mobility is reduced.

Additionally, the quantum yield of polymerization (Φ_p) can be obtained as R_p/I_{abs} (Fig. 4.5a). Φ_p values with the three amine reductants in TEGDMA at 22 mW/cm^2 were found to be in the low-end of the typical range for photopolymerizations performed under air (200-13,000), i.e. without inert gas purging⁷¹. Using these values to assess the reactivity of the amines tested, they rank EDMAB>NPG>MDEA, where EDMAB reached 1200, NPG reached a maximum of Φ_p 900, and MDEA only got to 600. It is worth noting that Φ_p varies only slightly before the polymerization hits the gel effect ($\sim 12.5 \text{ s}$ and $<4\text{-}5 \%$ conversion). These differences in Φ_p with amine should be associated with higher crosslinking densities due to higher initial concentration of primary radicals (with EDMAB), which leads to an enhanced effect of mobility in the termination constant (reaction-diffusion-controlled)^{64,65,72}.

While the reactivity trends of Φ_p and $\Phi_i/\Phi_{i\text{-ref}}$ were confirmed to be EDMAB>NPG>MDEA, we show that NPG>MDEA \geq EDMAB in terms of initial Φ_{red} (Fig. 4.4b). This difference could be attributed to alternate decomposition pathways, such as hydrogen abstraction from the alcohol or the carboxylic groups and N-H bonds in MDEA and NPG, respectively. These alternate hydrogen abstraction routes could lead to a faster photoreduction rates, but the primary radicals produced therefrom can have a significantly lower efficiency in initiating polymerization than the alpha aminoalkyl radicals that are typically produced. Alternatively, it is also likely that the concentration of primary radicals produced by the amine reductants is roughly equivalent, but that the alpha aminoalkyl radicals from EDMAB are more reactive towards the vinyl groups than those from MDEA and NPG. Herein, we emphasize the potential of our UV-Vis/FT-NIR technique for attaining more detailed analysis of these subtle differences in reactivity that can change as a function of reaction time, and cannot be elucidated with other instruments.

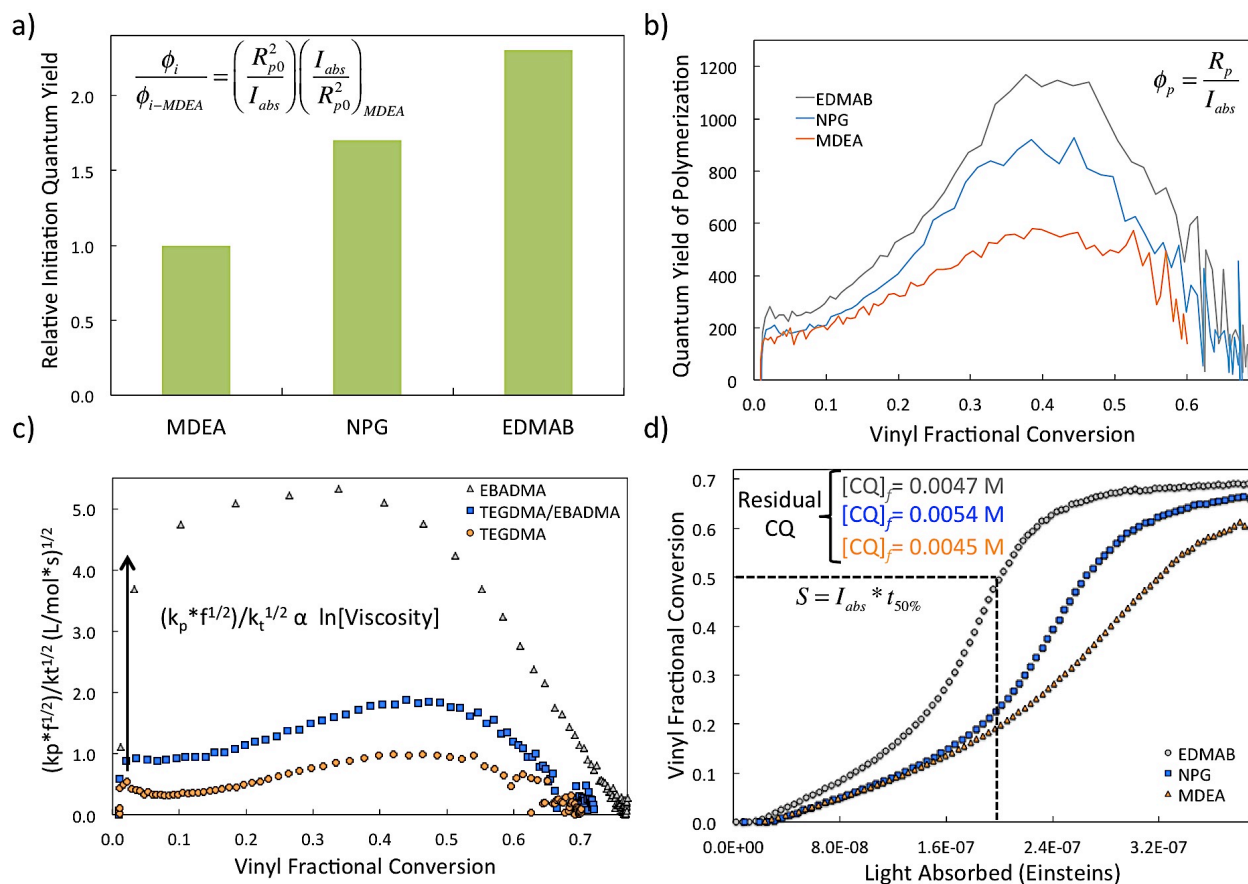


Figure 4.5. Analysis of quantum yield of polymerization, polymerization kinetic constants, CQ photoreduction, and photosensitivity from a single experiment set. **a**, Relative quantum yields of monomer initiation (Φ_i / Φ_{i-ref}) by the alpha-aminoalkyl radicals formed (Fig. 4.3a-Step 4). NPG and EDMAB are more efficient at initiating the radical polymerization of the methacrylate monomers. **b**, Quantum yield of polymerization (Φ_p) of TEGDMA monomer as a function of vinyl fractional conversion with three amine reductants: MDEA, NPG, and EDMAB ($[Amine]_0 = 0.0464 \text{ M}$) in the presence of $[CQ]_0 = 0.00674 \text{ M}$ and irradiated with a 22 mW/cm^2 at 480 nm . Maximum Φ_p is achieved at $\sim 40\%$ conversion of vinyl groups, where R_p reaches a maximum due to the transition to diffusion-controlled propagation. **c**, Ratio of the propagation (k_p) and termination ($k_t^{1/2}$) kinetic constants (multiplied times the initiation efficiency factor f) as a function of vinyl fractional conversion assuming steady state concentration of propagating radicals. Changes in $(k_p * f^{1/2}) / k_t^{1/2}$ scale linearly with the logarithm of the initial monomer(s): TEGDMA, TEGDMA/EBADMA 50:50 volume ratio, and EBADMA. **d**, Vinyl fractional conversion as a function of the total amount of light absorbed (Einsteins = moles of photons/L) with MDEA, NPG, and EDMAB in TEGDMA. Light absorbed at 50% vinyl conversion is referred to as photosensitivity (S) and used to evaluate the efficiency of light-induced polymerizations in stereolithography, coatings, and imaging, among other applications. The amount of residual camphorquinone is included as $[CQ]_f$ to show how we can better evaluate and compare photopolymerization formulations accounting for the amount of leftover mutagenic compounds.

4.3.3 Polymerization kinetics accounting for difference in I_{abs}

Assuming that the pseudo steady-state approximation is valid and that primary radical termination is negligible, a standard model for R_p has been well-established^{64,65,73,74}. This model was utilized by Anseth et al. to determine the propagation (k_p) and termination (k_t) constants using a combination of steady-state and non-steady-state experiments with photo-DSC. These experiments were performed under the assumption that the rate of monomer initiation (R_i) remains constant. This assumption is most often only valid at the very early stages of the reaction, and thus could lead to inaccuracies. Our UV-Vis-FT-NIR device allows the determination of the steady-state parameter $(k_p * f^{1/2})/k_t^{1/2}$ without assuming constant R_i , thus permitting a more accurate determination of k_p and k_t for a broader set of irradiation conditions (Fig. 4.5b).

$$R_p = \left(\frac{k_p}{k_t^{1/2}} \right) [M] * R_i^{1/2}, \text{ where } R_i = f * \phi_{red} * I_{abs}$$

$$\frac{R_p}{[M](I_{abs} * \phi_{red})^{1/2}} = \left(\frac{k_p}{k_t^{1/2}} \right) * f^{1/2}$$

where, f is the fraction of primary radicals that lead to propagating monomer-based radicals and $[M]$ is the concentration of vinyl groups. Here, R_p , I_{abs} , Φ_{red} , and $[M]$ are time-dependent variables determined from the same experiment. Higher initial viscosity of the monomer(s) leads to higher R_p 's due to diffusion-controlled and reaction-diffusion-controlled termination. Our results confirm that $(k_p * f^{1/2})/k_t^{1/2}$ correlates linearly with $\ln(\text{Viscosity})$, where initial viscosities are 0.0175, 0.0356, and 0.7750 Pa*s for 0, 50, 100% volume EBADMA^{67,73}. Non-steady kinetic experiments can be done in the UV-Vis/FT-NIR apparatus, but are beyond this introductory study.

4.3.4 Residual initiator and photosensitivity

A photosensitivity (S) term is utilized to compare light-activated polymerizations based on the amount of light energy absorbed during the time it takes to polymerize half of the functional groups ($t^{1/2}$)

for coatings, stereolithography, imaging, and electronics applications⁷⁵. However, S is a function of I_{abs} , and thus its calculation has been limited to the early stages of the polymerization. In contrast, we can easily calculate the amount of moles of photons (Einsteins) absorbed by the initiator at any reaction time with our coupled UV-Vis/FT-NIR tool (Fig. 4.5d). Hence, S can be calculated without assuming a constant absorption rate (I_{abs}); where I_{abs} depends on initiator concentration, irradiation intensity and emission spectrum (Fig. 4.3a). Fig. 4.5d shows that EDMAB reductant uses photons more efficiently towards the polymerization of TEGDMA than NPG and MDEA, which is in agreement with the results for $\Phi_i/\Phi_{i\text{-ref}}$, and Φ_p . Real-time determination of S accounting for changes in I_{abs} is important for many applications, where light-induced polymerizations are currently evaluated by their R_p 's, without standardizing for their differences in I_{abs} .

Lastly, both the residual amount of polymerizable groups, as well as initiator or catalyst can be simultaneously determined (Fig. 4.5d) with the UV-Vis/FT-NIR tool. This is important because there is increasing attention in the bio- and dental materials fields on reducing the cytotoxicity of polymer materials. For instance, residual CQ, MDEA, NPG, and EDMAB are known to be mutagenic leachable compounds that reduce the stability of dental restorative and adhesive materials^{56,76,77}. Quantification of these residues is normally done ex-situ and requires laborious extraction of the small molecules. Our technique permits immediate correlation of these values to the initiation and polymerization kinetics, and can thus expedite formulation design and optimization.

4.4 Conclusions

Rates of light absorption, initiator and monomer consumption were simultaneously tracked via coupled UV-Vis/FT-NIR spectroscopy for the first time. To permit the kinetic analysis of multiple reaction steps in the polymerization process from a single set of experiments carried out in the polymerizing medium under the same conditions. We confirmed well-established trends and values for the effects of light intensity, initial concentrations, viscosity, and amine reductant chemistry. Then, we

calculated key parameters that are impractical or impossible to determine with other analytical tools: the quantum yields of CQ photoreduction, initiation, and polymerization. We proved that the quantum yield of initiator consumption could be significantly affected by the mobility of the forming macromolecular architecture. This UV-Vis/FT-NIR device can also extract the kinetic constants of propagation and termination without assuming a constant rate of initiation, as well as the photosensitivity term used in many applications. Lastly, the residual initiator can be easily determined to evaluate the potential toxicity of a given formulation. This opens interesting possibilities for faster elucidation of the mechanisms involved in a wide range of polymer syntheses including ATRP, RAFT, CuAAC, thiol-Michael, and thiol-ene, for which new and complex light-activated initiators and catalysts are currently being developed.

4.5 References

1. Hawker, C. J. & Wooley, K. L. The Convergence of Synthetic Organic and Polymer Chemistries. *Science* **309**, 1200–1205 (2005).
2. Wang, J.-S. & Matyjaszewski, K. Controlled/‘ living’ radical polymerization. Atom transfer radical polymerization in the presence of transition-metal complexes. *J. Am. Chem. Soc.* **117**, 5614–5615 (1995).
3. Barner-Kowollik, C., Lutz, J. F. & Perrier, S. New methods of polymer synthesis. *Polym. Chem.* (2012). doi:10.1039/c1py00443c
4. Gong, T., Adzima, B. J. & Bowman, C. N. A novel copper containing photoinitiator, copper(ii) acylphosphinate, and its application in both the photomediated CuAAC reaction and in atom transfer radical polymerization. *Chem. Commun. (Camb.)* **49**, 7950–7952 (2013).
5. Hoyle, C. E. & Bowman, C. N. Thiol-Ene Click Chemistry. *Angew. Chem. Int. Ed.* **49**, 1540–1573 (2010).
6. Patterson, G. D. Light scattering from bulk polymers. *Annual Review of Materials Science* **13**, 219–245 (1983).
7. Boiko, Y. B., Granchak, V. M., Dilung, I. I. & Tikhonov, E. A. Light scattering in photopolymerizing layers under laser irradiation. *J Appl Spectrosc* **52**, 149–153 (2004).
8. Drenski, M. F., Mignard, E., Alb, A. M. & Reed, W. F. Simultaneous in-Situ Monitoring of Parallel Polymerization Reactions Using Light Scattering; A New Tool for High-Throughput Screening. *J. Comb. Chem.* **6**, 710–716 (2004).
9. Désilles, N., Gautrelet, C., Lecamp, L., Lebaudy, P. & Bunel, C. Effect of UV light scattering during photopolymerization on UV spectroscopy measurements. *European Polymer Journal* **41**, 1296–1303 (2005).

10. Mignard, E. *et al.* Kinetics and Molar Mass Evolution during Atom Transfer Radical Polymerization of n-Butyl Acrylate Using Automatic Continuous Online Monitoring. *Macromolecules* **38**, 9556–9563 (2005).
11. Chang, S. Y., Chang, S. Y., Wang, N. S. & Wang, N. S. *9. Monitoring Polymerization Reactions by Near-IR Spectroscopy*. (ACS Symposium Series, 1995). doi:10.1021/bk-1995-0598.ch009
12. Florenzano, F. H., Strelitzki, R. & Reed, W. F. Absolute, On-Line Monitoring of Molar Mass during Polymerization Reactions. **31**, 7226–7238 (1998).
13. Reed, W. F. A Method for Online Monitoring of Polydispersity during Polymerization Reactions. *Macromolecules* **33**, 7165–7172 (2000).
14. Alb, A. M., Mignard, E., Drenski, M. F. & Reed, W. F. In Situ Time-Dependent Signatures of Light Scattered from Solutions undergoing Polymerization Reactions. *Macromolecules* **37**, 2578–2587 (2004).
15. Alb, A. M., Serelis, A. K. & Reed, W. F. Kinetic Trends in RAFT Homopolymerization from Online Monitoring. *Macromolecules* **41**, 332–338 (2008).
16. Decker, C. & Moussa, K. A new method for monitoring ultra-fast photopolymerizations by real-time infra-red (RTIR) spectroscopy. *Die Makromolekulare Chemie* **189**, 2381–2394 (1988).
17. Esen, D. S., Karasu, F. & Arsu, N. The investigation of photoinitiated polymerization of multifunctional acrylates with TX-BT by Photo-DSC and RT-FTIR. *Progress in Organic Coatings* **70**, 102–107 (2010).
18. Cherdoud-Chihani, A., Mouzali, M. & Abadie, M. Étude pas dsc de la reticulation de systèmes dgeba/polyacides. *European Polymer Journal* **33**, 969–975 (1997).
19. Kloosterboer_1996_Monitoring of polymerization-induced phase separation photo-DSC_turbidity measurements. 1–6 (2003).
20. Allonas, X., Lalevée, J. & Fouassier, J.-P. in *Polymerization Reactors and Processes* **847**, 140–151 (American Chemical Society, 2009).
21. Roper, T. M., Guymon, C. A. & Hoyle, C. E. Design and performance of a thin-film calorimeter for quantitative characterization of photopolymerizable systems. *Rev. Sci. Instrum.* **76**, 054102 (2005).
22. Crivello, J. V. A new visible light sensitive photoinitiator system for the cationic polymerization of epoxides. *J. Polym. Sci. A Polym. Chem.* **47**, 866–875 (2009).
23. Fonseca, G. E., Dubé, M. A. & Penlidis, A. A Critical Overview of Sensors for Monitoring Polymerizations. *Macromol. React. Eng.* **3**, 327–373 (2009).
24. Stansbury, J. W. & Dickens, S. H. Determination of double bond conversion in dental resins by near infrared spectroscopy. *Dental Materials* **17**, 71–79 (2001).
25. Decker, C. & Moussa, K. Real-time kinetic study of laser-induced polymerization. *Macromolecules* **22**, 4455–4462 (1989).
26. Darcos, V., Monge, S. & Haddleton, D. M. In situ Fourier transform near infrared spectroscopy monitoring of copper mediated living radical polymerization. *J. Polym. Sci. A Polym. Chem.* **42**, 4933–4940 (2004).
27. Decker, C. & Moussa, K. A new class of highly reactive acrylic monomers, 1. Light-induced polymerization. *Die Makromolekulare Chemie, Rapid Communications* **11**, 159–167 (1990).

28. Decker, C. *UV-curing chemistry: past, present, and future*. (JCT, 1987).
29. Moussa, K. & Decker, C. Light-induced polymerization of new highly reactive acrylic monomers. *J. Polym. Sci. A Polym. Chem.* **31**, 2197–2203 (1993).
30. Decker, C. Photoinitiated crosslinking polymerisation. *Progress in Polymer Science* **21**, 593–650 (1996).
31. Mark, H. & Campbell, B. *An introduction to near infrared spectroscopy and associated chemometrics*. (The Near Infrared Research Corporation, 2008).
32. Asmusen, S., Arenas, G., Cook, W. D. & Vallo, C. Photobleaching of camphorquinone during polymerization of dimethacrylate-based resins. *Dental Materials* **25**, 1603–1611 (2009).
33. Asmusen, S., Arenas, G., Cook, W. D. & Vallo, C. Photoinitiation rate profiles during polymerization of a dimethacrylate-based resin photoinitiated with camphorquinone/amine. Influence of initiator photobleaching rate. *European Polymer Journal* **45**, 515–522 (2009).
34. Fouassier, J.-P., Morlet-Savary, F., Lalevée, J., Allonas, X. & Ley, C. Dyes as Photoinitiators or Photosensitizers of Polymerization Reactions. *Materials* **3**, 5130–5142 (2010).
35. Lalevée, J. *et al.* A Novel Photopolymerization Initiating System Based on an Iridium Complex Photocatalyst. *Macromol. Rapid Commun.* **32**, 917–920 (2011).
36. Timpe, H.-J., Kronfeld, K.-P., Lammel, U., Fouassier, J. P. & Lougnot, D.-J. Excited states of ketones as electron donors—ketone—iodonium salt systems as photoinitiators for radical polymerization. *Journal of Photochemistry & Photobiology, A: Chemistry* **52**, 111–122 (1990).
37. Allonas, X., Lalevée, J. & Fouassier, J.-P. Influence of the S₀–T₁ structural changes on the triplet–triplet sensitization of dienes. *Chemical Physics* **290**, 257–266 (2003).
38. Tehfe, M.-A. *et al.* Iridium complexes incorporating coumarin moiety as catalyst photoinitiators: Towards household green LED bulb and halogen lamp irradiation. *Polymer* **1–6** (2012).
39. Lalevée, J. *et al.* New Photoinitiators Based on the Silyl Radical Chemistry: Polymerization Ability, ESR Spin Trapping, and Laser Flash Photolysis Investigation. *Macromolecules* **41**, 4180–4186 (2008).
40. Allonas, X., Lalevée, J. & Fouassier, J.-P. Investigation of cleavage processes in photoinitiators: from experiments to molecular modeling. *Journal of Photochemistry & Photobiology, A: Chemistry* **159**, 127–133 (2003).
41. Treat, N. J. *et al.* Metal-Free Atom Transfer Radical Polymerization. *J. Am. Chem. Soc.* **136**, 16096–16101 (2014).
42. Tehfe, M.-A. *et al.* Organic Photocatalyst for Polymerization Reactions: 9,10-Bis[(triisopropylsilyl)ethynyl]anthracene. *ACS Macro Lett.* **1**, 198–203 (2012).
43. Worrell, B. T., Malik, J. A. & Fokin, V. V. Direct evidence of a dinuclear copper intermediate in Cu(I)-catalyzed azide-alkyne cycloadditions. *Science* **340**, 457–460 (2013).
44. Aguirre-Soto, A., Lim, C.-H., Hwang, A. T., Musgrave, C. B. & Stansbury, J. W. Visible-Light Organic Photocatalysis for Latent Radical-Initiated Polymerization via 2e⁻/1H⁺ Transfers: Initiation with Parallels to Photosynthesis. *J. Am. Chem. Soc.* **136**, 7418–7427 (2014).
45. Long, M., Rogers, S. H., Thornthwaite, D. W., Livens, F. R. & Rannard, S. P. Monitoring Atom Transfer Radical Polymerisation using ¹⁴C-radiolabelled initiators. *Polym. Chem.* **2**, 581–589 (2011).

46. Chen, Y.-C., Ferracane, J. L. & Prah, S. A. Quantum yield of conversion of the photoinitiator camphorquinone. *Dental Materials* **23**, 655–664 (2007).
47. Schmitt, M. New Method for Real-time Monitoring of Photopolymerization by UV-Vis Spectroscopy. *Macromol. Chem. Phys.* **212**, 1276–1283 (2011).
48. Alakhras, F. & Holze, R. In situ UV-vis- and FT-IR-spectroscopy of electrochemically synthesized furan–thiophene copolymers. *Synthetic Metals* **157**, 109–119 (2007).
49. Lamps, J. P. & Catala, J. M. Kinetic Study, by UV–Vis Spectroscopy, on the Strong Effect of LiCl on the Controlled Polymerization of 2-Bromo-3-hexyl-5-iodothiophene and 2-Iodo-3-hexyl-5-bromothiophene: Determination of the Propagation Rate Constants, Application to the Synthesis of High Molecular Weight Polydodecylthiophene. *Macromolecules* **44**, 7962–7968 (2011).
50. Meinwald, J., Meinwald, J., Klingele, H. O. & Klingele, H. O. Photochemical Reactions of Camphorquinone. *Journal of the American Chemical Society* **88**, 1000–1001 (1966). doi:10.1021/ja00961a056
51. Monroe, B. M. & Weiner, S. A. Mechanisms of photochemical reactions in solution. LVIII. Photoreduction of camphorquinone. *Journal of the American Chemical Society* **91**, 450–456 (1969).
52. Monroe, B. M. & Weiner, S. A. Mechanisms of photochemical reactions in solution. LII. Photoreduction of camphorquinone. *Journal of the American Chemical Society* **90**, 1913–1914 (1968).
53. Neumann, M. G., Miranda, W. G., Jr., Schmitt, C. C., Rueggeberg, F. A. & Correa, I. C. Molar extinction coefficients and the photon absorption efficiency of dental photoinitiators and light curing units. *Journal of Dentistry* **33**, 525–532 (2005).
54. Decker, C. Kinetic study of light-induced polymerization by real-time UV and IR spectroscopy. *J. Polym. Sci. A Polym. Chem.* **30**, 913–928 (1992).
55. Pączkowski, J. & Neckers, D. C. Following polymerization kinetics of multifunctional acrylates in real time by fluorescence probe methodology. *Macromolecules* **25**, 548–553 (1992).
56. Ilie, N. & Hickel, R. Can CQ be completely replaced by alternative initiators in dental adhesives? *Dent Mater J* **27**, 221–228 (2008).
57. Stansbury, J. W. Curing dental resins and composites by photopolymerization. *J Esthet Dent* **12**, 300–308 (2000).
58. Cook, W. D. & Chen, F. Enhanced photopolymerization of dimethacrylates with ketones, amines, and iodonium salts: The CQ system. *J. Polym. Sci. A Polym. Chem.* **49**, 5030–5041 (2011).
59. Cook, W. D. Photopolymerization kinetics of dimethacrylates using the camphorquinone/amine initiator system. *Polymer* **33**, 600–609 (1992).
60. Jakubiak, J., Allonas, X., Fouassier, J. P. & Sionkowska, A. Camphorquinone–amines photoinitiating systems for the initiation of free radical polymerization. *Polymer* (2003). doi:10.1016/S0032-3861(03)00568-8
61. Ikemura, K. K., Ichizawa, K. K., Yoshida, M. M., Ito, S. S. & Endo, T. T. UV-VIS spectra and photoinitiation behaviors of acylphosphine oxide and bisacylphosphine oxide derivatives in unfilled, light-cured dental resins. *Dent Mater J* **27**, 765–774 (2008).
62. Pyszka, I., Kucyba, Z. A. & Pączkowski, J. Reinvestigation of the Mechanism of the Free Radical Polymerization Photoinitiation Process by Camphorquinone-Coinitiator Systems: New Results. *Macromol. Chem. Phys.* **205**, 2371–2375 (2004).
63. Xi, W. *et al.* Spatial and Temporal Control of Thiol-Michael Addition via Photocaged Superbase in Photopatterning and Two-Stage Polymer Networks Formation. *Macromolecules* **47**, 6159–6165

- (2014).
64. Anseth, K. S., Wang, C. M. & Bowman, C. N. Reaction behaviour and kinetic constants for photopolymerizations of multi (meth) acrylate monomers. *Polymer* (1994). doi:10.1016/0032-3861(94)90129-5
 65. Anseth, K. S., Kline, L. M., Walker, T. A. & Anderson, K. J. Reaction kinetics and volume relaxation during polymerizations of multiethylene glycol dimethacrylates. ... **28**, 2491–2499 (1995).
 66. Davidenko, N., García, O. & Sastre, R. Photopolymerization kinetics of dimethacrylate-based light-cured dental resins. *J. Appl. Polym. Sci.* **97**, 1016–1023 (2005).
 67. Dickens, S. H., Stansbury, J. W., Choi, K. M. & Floyd, C. J. E. Photopolymerization Kinetics of Methacrylate Dental Resins. *Macromolecules* **36**, 6043–6053 (2003).
 68. García, N., Tiemblo, P. & Guzmán, J. Nominal vs Real Reaction Temperature in PLP Experiments. A Likely Explanation of the Observed Variation in the Propagation Rate Coefficients with Pulse Repetition Rate. *Macromolecules* **40**, 4802–4808 (2007).
 69. García, N. *et al.* Persistent Radicals and Transfer Reactions in the Postpolymerization of Methyl Methacrylate. *Macromolecules* **40**, 8168–8177 (2007).
 70. Olaj, O. F. & Vana, P. Chain length-dependent termination in pulsed-laser polymerization. VIII. The temperature dependence of the rate coefficient of bimolecular termination in the bulk polymerization of styrene. *J. Polym. Sci. A Polym. Chem.* **38**, 697–705 (2000).
 71. Fouassier, J. P. & Lalevéé, J. *Photoinitiators for Polymer Synthesis: Scope, Reactivity, and Efficiency.* (Wiley-VCH, 2012).
 72. Anseth, K. S., Rothenberg, M. D. & Bowman, C. N. A photochromic technique to study polymer network volume distributions and microstructure during photopolymerizations. *Macromolecules* **27**, 2890–2892 (1994).
 73. Lovell, L. G., Stansbury, J. W., Syrpes, D. C. & Bowman, C. N. Effects of Composition and Reactivity on the Reaction Kinetics of Dimethacrylate/Dimethacrylate Copolymerizations. *Macromolecules* **32**, 3913–3921 (1999).
 74. Anseth, K. S., Wang, C. M. & Bowman, C. N. Kinetic evidence of reaction diffusion during the polymerization of multi (meth) acrylate monomers. *Macromolecules* **27**, 650–655 (1994).
 75. Sugawara, S. S., Murase, K. K. & Kitayama, T. T. Holographic recording by dye-sensitized photopolymerization of acrylamide. *Appl Opt* **14**, 378–382 (1975).
 76. Atsumi, T., Iwakura, I., Fujisawa, S. & Ueha, T. The production of reactive oxygen species by irradiated camphorquinone-related photosensitizers and their effect on cytotoxicity. *Arch. Oral Biol.* **46**, 391–401 (2001).
 77. Tseng, W.-Y. *et al.* Monomer conversion and cytotoxicity of dental composites irradiated with different modes of photoactivated curing. **83B**, 85–90 (2007).

Chapter 5

Effect of oxidant addition to the kinetics of camphorquinone/amine initiated photopolymerization of dental monomers

Abstract

We report the coupled monitoring of vinyl functional groups and camphorquinone (CQ) in order to provide additional evidence for the interactions of oxidants with the CQ/amine pair used for the production of free radicals to initiate polymerization reactions. This was achieved using fiber optic coupled UV-Vis and FT-NIR spectroscopy. Three oxidants, diphenyliodonium hexafluorophosphate (DPI-PF₆), triphenylsulfonium tetrafluoroborate (TS-BF₄), and 2-(4-methoxyphenyl)-4,6-bis(trichloromethyl)-1,3,5-triazine (TA) were separately added to CQ/amine formulations. It was confirmed that the addition of an oxidant generally enhances the rate of polymerization (R_p). However, it was found that with other amines, such as N-phenylglycine, a decrease in the R_p is observed upon oxidant addition. The production of ketyl radicals from the photoreduction of CQ by the amines was found to be limiting. The rate of CQ consumption reached a maximum and then decreased with increasing initial oxidant concentration. Most importantly, no evidence was found of significant CQ regeneration by the oxidants. Our results indicate that the oxidants primarily participate in a sequential reaction process. This means that after production of a ketyl radical and an alpha-amino alkyl radical upon the proton-coupled electron transfer from the amine to CQ, the oxidant reacts with the terminating ketyl radical irreversibly; as a result, a reactive initiating radical is generated from the oxidant as well as CQ-based close shell colorless products. Such a mechanism was only proposed recently proposed, but evidence to support the irreversibility of the oxidation of the CQ-based radical remained elusive. Herein, we simultaneously monitor CQ and monomer consumption *in-situ* during the light-activated polymerization of methacrylate monomers with various three-component initiating systems to provide additional evidence of how oxidants interact with CQ/amine pairs, which can be advantageous in applications such as dental materials and biomaterials.

5.1 Introduction

Photopolymerization offers many practical advantages such as rapid reaction rates, solvent-free conditions, and precise spatiotemporal control¹. Most typical photoinitiators (PI) produce free radicals that initiate polymerization of vinyl monomers upon exposure to ultraviolet light (UV). However, the use of visible-light sensitive photoinitiators has been of heightened interest because of the damaging effects of UV radiation, primarily for the use of these light-activated polymerization reactions in dentistry², orthopedics³, and tissue engineering^{4,5}, where live or photolabile specimens are involved. Furthermore, the advent of cheaper and more energy efficient light emitting diodes has stimulated the transition from conventional UV to visible-light activated polymer syntheses.

The energy of the photons in the visible-light region (400-700 nm) is not sufficient to directly cleave most bonds in typical organic molecules (based on their bond dissociation energy). Thus, visible-light sensitive PI's typically rely on reactions of an excited state of the light-absorbing molecule (chromophore) with a secondary ground state reactant (co-initiator); electron transfer and hydrogen abstraction being the most common. This requirement of the so-called Type II PI's makes them commonly less efficient than Type I PI's, which work via bond cleavage, in terms of the rates of polymerization (R_p) that can be achieved. Additionally, these PI's usually produce only one active radical per photon absorbed rather than the two radicals that are, at least, generated by most Type I (direct cleavage) initiators. However, addition of a third component to chromophore/co-initiator pairs has been documented to initiate polymerization at faster rates, even 10-fold, than in the absence of such third component.

Some common visible-light PI's are composed of a chromophore (or photosensitizer), such as a ketone, and a co-initiator, such as an amine reductant⁶⁻¹¹. However, over the past three decades, as the interest in developing better visible-light PI's increased, it was realized that the addition of an oxidant to this CQ/amine pair increases the rate of polymerization (R_p) significantly^{12,13}. In some cases R_p has been reported to increase in up to 5-10 times as compared to the analogous formulations without the oxidant molecules. Typical oxidants used are triazines¹⁴, iodonium salts¹⁵, sulfonium salts¹⁶, maleimides, and

bromo or iron complexes. The issue is that the three-component PI's produced by the addition of an oxidant to chromophore/co-initiator pairs are not well understood as compared to their two-component counterparts^{12,13}.

Mechanisms for the interaction of oxidants with chromophore/co-initiator combinations have been divided into two categories: parallel and sequential. In the parallel mechanism it is thought that the oxidants and co-initiators react concurrently with the excited state chromophore. Padon and Scranton reported an example of a three-component PI working via a parallel mechanism, where Eosin Y Spirit Soluble absorbs visible-light and then reacts with both N-methyldiethanolamine (MDEA) reductant, and Diphenyliodonium chloride (DPI-Cl) oxidant¹⁷. Another example of a similar behavior is that of Rose Bengal and fluorescein chromophores with amines and iodonium salts¹⁸. In contrast, the sequential mechanism involves an initial photochemical reaction between the excited state chromophore and the co-initiator and a secondary reaction in the ground state between the oxidant at least one of the products from the first photochemical step¹⁵. Two examples of sequential mechanisms are the three-component systems: thioxanthene ketone/N-phenylglycine (PG)/Diphenyliodonium tetrafluoroborate (DPI-BF₄) and Methylene blue (MB⁺)/MDEA/DPI-Cl^{19,20}. Based on the report of so many different mechanisms it is most likely that the interaction of the oxidants with a given chromophore/co-initiator pair is highly sensitive to the choice of chromophore, co-initiator, oxidant, monomer, and solvents that may be present.

Experimental results seem to indicate that the chromophore is key in determining whether a parallel or sequential mechanism is to be followed. For example, organic dyes (such as MB⁺ and eosin) have long been known to readily undergo reversible reduction/oxidation reactions, whereas ketones have been reported to irreversibly form degradation products upon reduction or oxidation²¹⁻²⁵. The reversibility of some of organic dyes could be related to the highly conjugated structure stabilizing the radical intermediates formed upon reduction or oxidation of the dyes. Moreover, if the excited state chromophore can function as both a reductant and an oxidant, based on its redox potential as compared with that of the reductant and oxidant components, then a parallel mechanism should be expected. If the excited state chromophore were thermodynamically driven to function only as either a reductant or an oxidant, then a

sequential mechanism would be more likely. The thermodynamic feasibility of such pathways can be estimated with the Rehm-Weller equation (eq1), where the Gibbs Free-Energy for electron transfer reactions from a ground state to an excited state molecule is calculated using the redox potentials (E_{ox} and E_{red}), triplet state energy (E_T), and Coulombic interactions (not included for neutral molecules). However, this equation relies on the assumption that the electron transfer (ET) is the rate-limiting step, and it is not indicative of the kinetic driving force for the ET process. It does not take into account the possibility of a Marcus-type inverted region for the ΔG_{ET} , i.e. ET processes have been documented to slow down or even be precluded when the thermodynamic driving force (ΔG_{ET}) becomes more negative than a certain threshold²⁶⁻²⁸. Hence, this equation should not be utilized without experimental evidence supporting the kinetic feasibility of either a parallel or a sequential mechanism, as in the form of polymerization initiated by the radicals produced from the ET.

$$\Delta G_{et} = F * [E_{ox}(D/D^{+}) - E_{red}(A/A^{-})] - E_T \quad \text{Equation 1}$$

There have only a few studies on the interaction of oxidants with CQ/amine pairs^{12,13,15,29-31}. Cook and Chen recently proposed a sequential mechanism for the interaction of an oxidant with the CQ/amine pair⁵. They analyzed CQ/amine/iodonium salt formulations with Differential Scanning Calorimetry (DSC) and UV-Vis. Their systematic approach in the analysis of the CQ system led to a better understanding of the mechanism with the addition of an oxidant. Their conclusion was that the terminating ketyl radical is partially regenerated into the original CQ by the iodonium salt, forming a phenyl radical as a result. This phenyl radical is more reactive than the terminating ketyl radical, thus promoting additional initiation of monomer, faster rates of polymerization and higher final conversions. Furthermore, it is thought that oxidation of terminating ketyl radicals can reduce competing rates of back electron transfer and radical recombination, ultimately leading to a more efficient production of initiating radicals^{15,18,32}. Nonetheless, their mechanism needs some refinement as they propose that the reaction between the alpha amino-alkyl radicals and the DPI-PF₆ competes efficiently with the reaction between the vinyl groups, which are present at significantly higher concentrations, and the amine-based radicals, which are very reactive towards the C=C bonds³³. Additionally, their UV-Vis analysis of CQ photobleaching was limited and not

performed simultaneously with the polymerization monitoring, whereas their DSC experiments for polymerization kinetics were carried at 50°C without acknowledgment of the redox production of radicals from the interaction between the amine reductants and the iodonium salt oxidant (DPI-PF₆). There still exists a need for more conclusive evidence to support the sequential mechanism via which the ketyl radical produced upon photoreduction of CQ by the amine is irreversibly oxidized to closed-shell by-products. Herein, we make use of unique coupled UV-Vis/FT-NIR spectroscopy to follow the decay of both the polymerizable vinyl functional groups from the methacrylate monomer (Triethylene glycol dimethacrylate) and of the camphorquinone chromophore. The amines used in this study were methyl diethanolamine (MDEA) and N-phenylglycine (PG).

Cook and Chen only analyzed the use of one oxidant (Diphenyliodonium hexafluorophosphate: DPI-PF₆). In the present study, the effects of the oxidant chemistry were also explored by the comparison of DPI-PF₆ with a triazine derivative (2-(4-methoxyphenyl)-4,6-bis(trichloromethyl)-1,3,5-triazine) (TA) and a sulfonium derivative (triphenylsulfonium tetrafluoroborate) (TS-BF₄), chosen based on their varied redox potentials. Such an analysis has not been reported, and can be advantageous to evaluate how to better design these three-component PI's to achieve faster rates of polymerizations and higher final vinyl conversions upon visible-light irradiation.

5.2 Experimental section

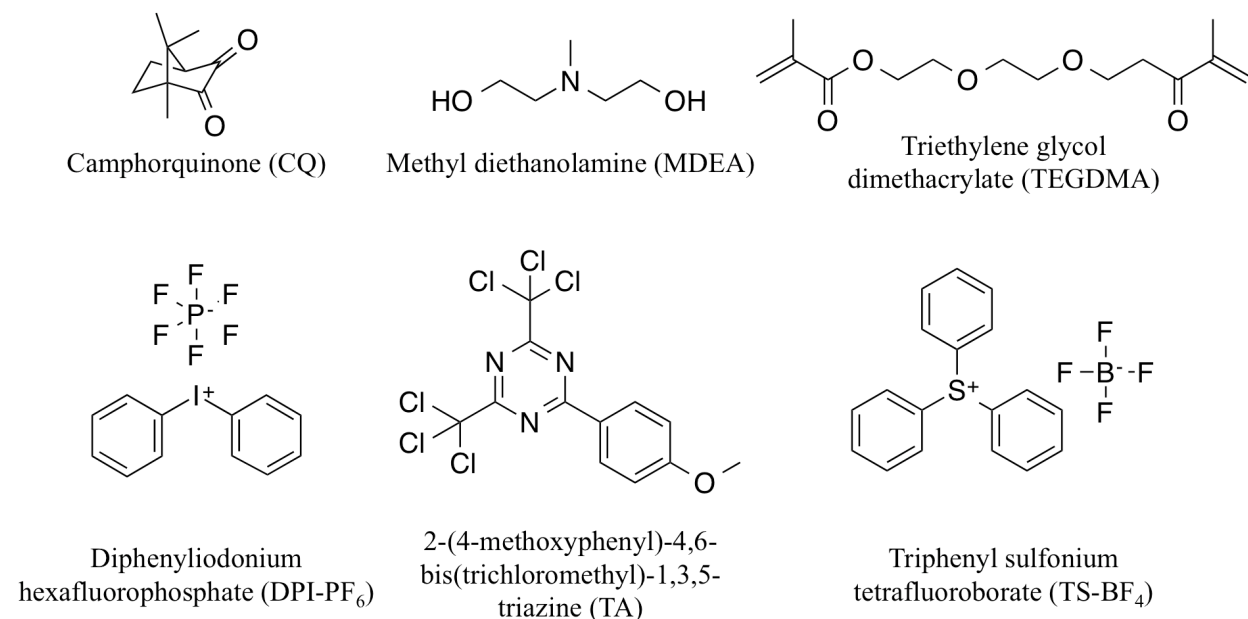


Figure 5.1 Components of the photopolymerizable formulations studied in this work. From top to bottom and left to right: Camphorquinone chromophore, amine co-initiator MDEA, methacrylate monomers (TEGDMA) and oxidants: DPI-PF₆, TA, and TS-BF₄.

5.2.1 Materials

Camphorquinone (CQ, Sigma Aldrich, Milwaukee, MI) was used as received. Methyl diethanolamine (MDEA) from Sigma Aldrich (Milwaukee, MI) was chosen as the main co-initiator reductant for the present study because we previously characterized that the rate of polymerization was lower than with other amines, thus making it a good candidate to show the improvement in R_p upon addition of the oxidants. N-phenylglycine (PG, Sigma Aldrich, Milwaukee, MI) was utilized for a few experiments included in here because it was observed that it reacts particularly as compared to other aromatic amines. The monomer Triethylene glycol dimethacrylate (TEGDMA, Sigma Aldrich, Milwaukee, MI) was used as received. The oxidants used in the study were diphenyliodonium hexafluorophosphate (DPI-PF₆, Sigma Aldrich, Milwaukee, WI), triphenylsulfonium tetrafluoroborate (TS-BF₄, Tokyo Chemical Industry, Tokyo, Japan), and 2-(4-methoxyphenyl)-4,6-bis(trichloromethyl)-1,3,5-triazine (TA, Tokyo Chemical Industry, Tokyo, Japan).

The initial camphorquinone loading used was 0.1 wt %, at which the absorbance at $\lambda_{\text{max}}=468$ nm did not exceed 0.5 AU through the experiment, thus facilitating the calculations and ensuring Beer-Lambert law validity. The oxidants were chosen based on their differences in oxidation potential (Fig. 5.2).

Oxidant	Reduction potential (eV vs SCE)
DPI-PF ₆	-0.2 ⁷
TA	-0.9 ⁸
TS-BF ₄	-1.2 V ⁹

Figure 5.2 Oxidation potentials of oxidants

5.2.2 Light source

A multi-wavelength light emitting diode (LED) unit containing a blue 480 nm LED chip (FC8-LED, Prizmatix, Southfield, MI) was used to excite camphorquinone to its singlet state. Irradiance or power density was controlled with a potentiometer and measured with a radiometer (6253, International Light Technologies, Peabody, MA) within the 400-700 nm range. The LED lamp was connected via fiber optic with an inner diameter of 1000 nm and the fiber optic was placed directly over the sample with a collimating lens (Thorlabs Inc., Newton, NJ) with the incident irradiant set at 22 mW/cm² Pathlength in the direction of the curing irradiation was 2.5 mm.

5.2.3 Coupling of FT-NIR and UV-Vis spectroscopy

Monomer conversion was monitored with a FT-IR spectrophotometer (Nicolet Magna-IR Series II, Thermo Scientific, West Palm Beach, FL) by following the peak area of the first overtone absorption band of the methacrylate =CH₂ group (~6167 cm⁻¹). The spectrophotometer is equipped with a KBr beam splitter and an InGaAs detector. The FT-IR settings were set to 18 scans, a resolution of 8, a gain of 1, and an optical aperture of 3-5.

A fiber optic coupled UV-VIS spectrometer (USB2000-UV-VIS Miniature Fiber Optic Spectrometer, Ocean Optics, Dunedin, FL) was employed to measure the photobleaching of CQ tracking the absorbance band between 400 nm and 510 nm due to the n → π* transition of the carbonyl group.

Integration time was set to under 1 s. A Matlab code was written to correlate the absorbance at λ_{\max} within the PI absorbance peak envelope. Negative controls were performed to ensure that no or negligible polymerization occurred due to exposure to the monitoring beam within the time of the experiments.

The coupling of the UV-Vis and FT-NIR beams was achieved with a cuvette holder (CUV-ALL-UV 4-Way Cuvette Holder, Ocean Optics, Dunedin, FL) that holds a dual-pathlength cuvette (UVette, Eppendorf, Hauppauge, NY) with a 10 mm and a 2 mm pathlength in its center. Sample volume was 60 μL . Fiber-optic coupled UV-Vis and FT-IR spectrophotometers were integrated via SMA connectors to remotely transmit orthogonal signals through the sample. The sample volume used in the two-pathlength cuvette was 50 μL with the sampler dimensions 2 mm x 10 mm x 2.5 mm.

5.2.4 Spectral analysis

The UV-Vis output was collected with the SpectraSuite Software (Ocean Optics, Dunedin, FL) and its output was processed using a MATLAB script to extract and plot the relevant data. The maximum absorbance close to 470 nm was found for every spectrum and plotted against time. Experiments were performed in sets of 3-5 replicates. The results were then fitted to a single exponential curve in MATLAB to extract the coefficients. All R^2 values were higher than 0.93. The coefficients were then averaged and the standard deviation and error determined to assess the significance of the differences identified.

The FT-NIR results were obtained directly from the OMNIC Software (Thermo Scientific, West Palm Beach, FL) and then processed with Excel.

5.3 Results and discussion

5.3.1 Effect of Oxidant Addition

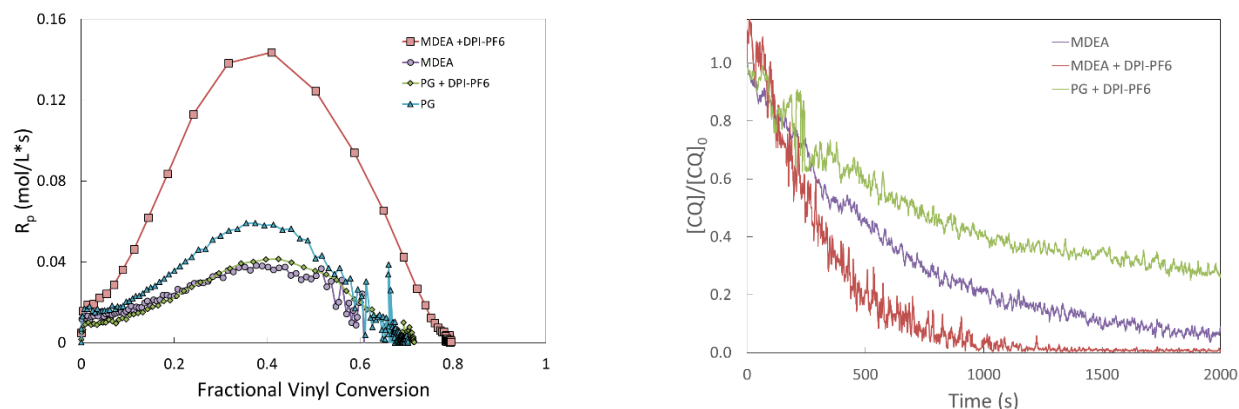


Figure 5.3 Changes in R_p and CQ consumption upon addition of DPI-PF₆ oxidant. Left- Rate of polymerization as a function of conversion with the addition of the DPI-PF₆ against different amines. Right- Bleaching of CQ with oxidant addition. $[\text{CQ}] = 0.1 \text{ wt } \%$, $[\text{MDEA}] = 0.5 \text{ wt } \%$, $[\text{DPI-PF}_6] = 0.7 \text{ wt } \%$, $I_0 = 22 \text{ mW/cm}^2$.

With the addition of an oxidant, an increase in R_p is expected. Results shown in Figure 5.3-Left demonstrate that with incorporation of the iodonium salt (DPI-PF₆) to the CQ/MDEA pair, there was a 3.5 times increase in the maximum rate of polymerization ($R_{p-\text{max}}$). It was confirmed that the R_p was negligible in the absence of MDEA at this conditions, indicating that initiating radicals are not efficiently produced from CQ alone or any interaction between CQ and TEGDMA. The combination of CQ and DPI-PF₆ was not tested since it has been confirmed that the photoreduction of CQ by DPI-PF₆ only increases the R_p slightly, indicating that CQ is more prone to be photoreduced^{12,13}. Additionally, it has been reported that CQ does not lead to initiating radicals upon oxidation^{21,22,24,34}. It was also observed that the conversion at $R_{p-\text{max}}$ was lowered. In the absence of DPI-PF₆ oxidant, the CQ/MDEA pair shows a relatively broad $R_{p-\text{max}}$ that extends from 40 to 50 % vinyl conversion. In contrast the CQ/MDEA/DPI-PF₆ PI seems to have a shorter $R_{p-\text{max}}$ region, which was not captured precisely due to the time resolution used for the FT-NIR analysis, but is expected to be below 40 % conversion. This indicates that in fact the

polymer network form gels faster and vitrifies at higher conversion than the network formed without DPI-PF₆³⁵⁻³⁷.

On the other hand, the rate of CQ photobleaching remained virtually unchanged or increased only slightly with the addition of DPI-PF₆ within the first 200 s. After roughly 200 s of irradiation, the CQ photobleaching rate is significantly lower for the CQ/MDEA system than for the CQ/MDEA/DPI-PF₆ formulation. Since we know that the polymerization reached the final conversion by 100 s it can be assumed that during the effective polymerization time the photobleaching rates were essentially the same. This supports that the regeneration of CQ from the oxidation of the ketyl radicals does not contribute significantly to the photoinitiation process, and that most likely, closed shell CQ-based by-products are produced (Figure 5.4)¹². In contrast, a significant reduction of the photobleaching rate was reported for the MB⁺/MDEA/DPI-Cl three-component PI studied by Padon and Scranton using fluorescence spectroscopy¹⁹. This supports that the refined mechanism proposed by Cook and Chen is most likely applicable when ketone-base chromophores are used, as opposed to highly conjugated dye molecules, where a very efficient initiating phenyl radical is formed by the irreversible oxidation of the terminating CQ-based ketyl radicals¹².

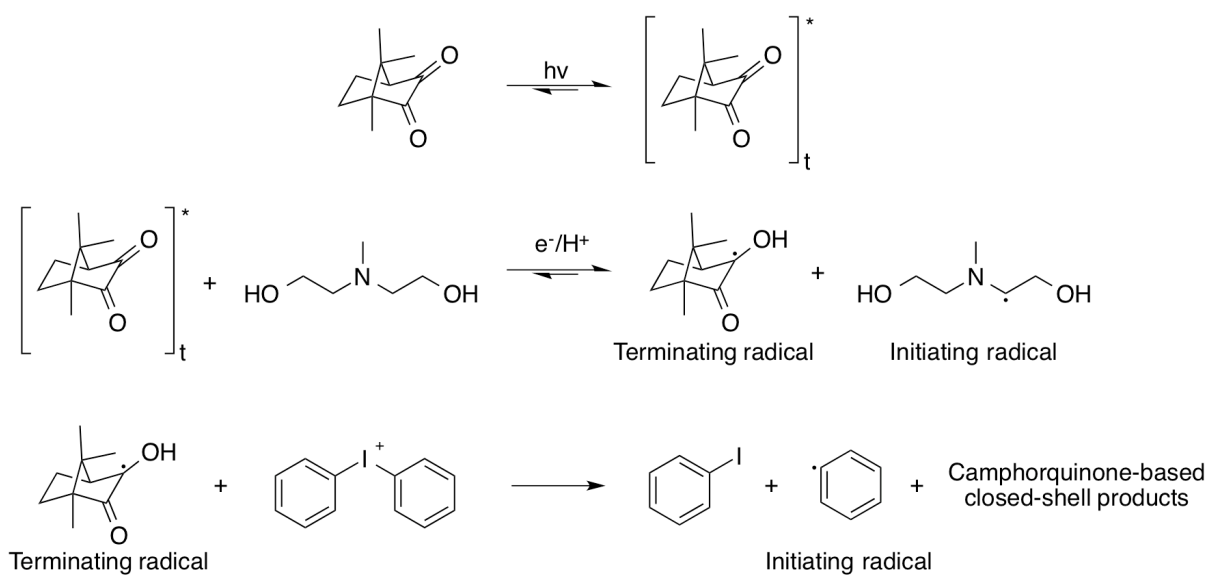


Figure 5.4 Refined mechanism for the interaction of DPI-PF₆ oxidant with the CQ-MDEA pair. As compared to the mechanism by Cook, we do not include the less feasible reaction between the CQ_t^* and the monomer (TEGDMA), which additionally is not expected to produce initiating radicals. Furthermore,

we do not include the reaction between the MDEA-based radical and DPI^+ as this seems to be kinetically less feasible than the reaction of the MDEA radical with the vinyl groups of the methacrylate, which are present at concentrations 2-3 orders of magnitude greater. This mechanism explains why the photobleaching rate of CQ is virtually unchanged with addition of DPI-PF₆ to CQ/MDEA, whereas R_p is increased 3.5 times i.e. by transformation of terminating radicals into initiating radicals.

The back electron transfer efficiency is most likely not affected since the proton transfer from the amine radical cation formed after single electron transfer essentially prevents back electron from occurring, in most cases³⁸. Note that the PG amino acid does not behave as the other aromatic or aliphatic amines used, as discussed in the next paragraph^{11,39,40}. This means that the feasibility of back electron or radical recombination is going to be primarily linked to the structure of the amine reductant rather than to the presence of the additional oxidant. If the proton transfer occurs, then back electron transfer and recombination reactions are no longer feasible and the effect of the oxidant on the fast a short distance electron transfers is going to be negligible.

However, contrary to the literature, the addition of the iodonium salt did not increase the rate of polymerization for PG. It is known that the reaction of excited state CQ with amino acids, like PG, involves decarboxylation after ET to camphorquinone³⁹. As a result of the entropical driving force related to the cleavage of the acid group it is likely that back electron transfer and recombination are going to happen less readily with PG in the initial stages of the polymerization. However, once the polymerization reaches the mobility restricted region, PG is most likely going to be prevented from reorganizing to allow for the decarboxylation process to occur and considering that PG is significantly more polar than MDEA. Hence, once the autoacceleration region is reached in the polymerization, the rate of CQ photobleaching with PG was significantly reduced as opposed to the case with ethyl 4-dimethylaminobenzoate (EDMAB), N,N-dimethylaniline (DMA), and MDEA. Furthermore, the possibility exists that the radicals produced by the oxidation of PG by the excited state of CQ react with DPI-PF₆ more readily than the alpha amino alkyl radicals formed from MDEA, EDMAB, or DMA.

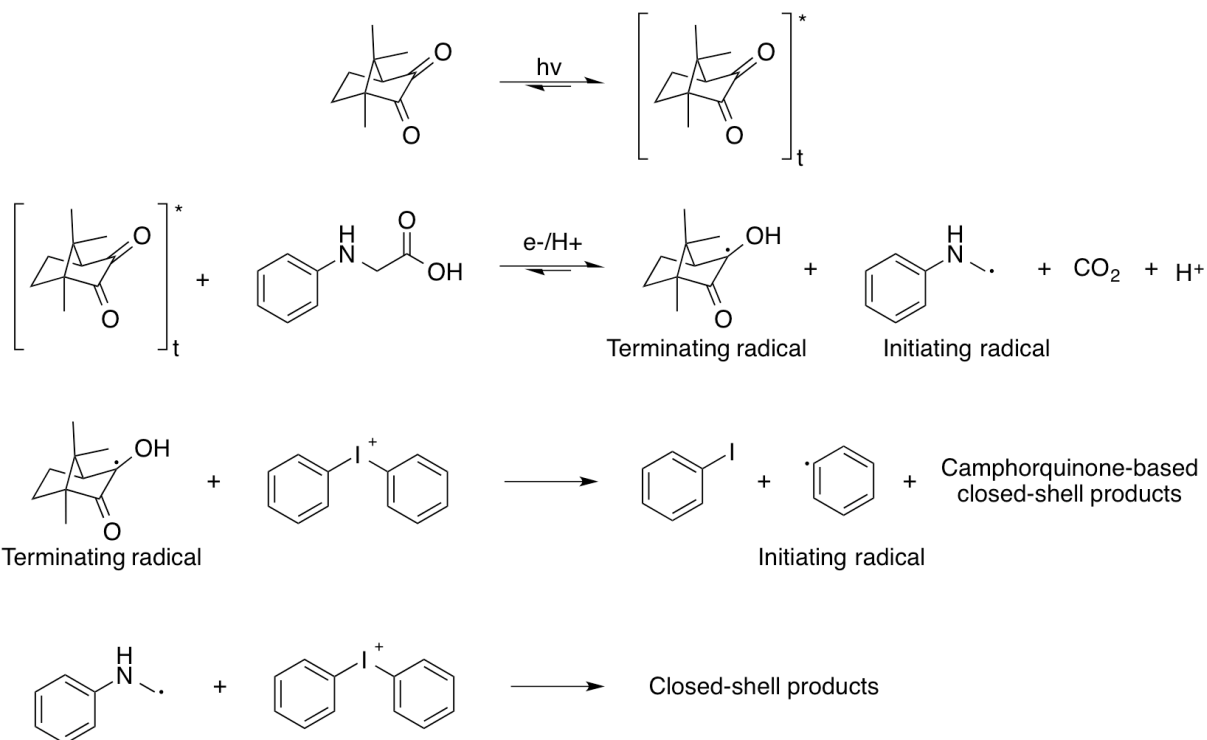


Figure 5.5 Refined mechanism for the interaction of DPI-PF₆ oxidant with the CQ/PG pair. This mechanism accounts for the possible oxidation of the PG-based radical produced by DPI-PF₆, which could explain the reduction in the rate of polymerization and the negligible change in CQ photobleaching.

5.3.2 Oxidant Concentration Effect

As presented in Figure 5.5, no statistically significant difference was observed in the rate of polymerization with MDEA at initial loadings of DPI-PF₆ between 0.3 and 4 wt%. While R_p -max and the breadth of the R_p vs. time curve seem to fluctuate for the different concentrations of DPI-PF₆ it appears that a threshold was reached even at 0.3 % DPI-PF₆. This agrees with our previous findings for the CQ/amine initiated polymerization of TEGDMA, which show that by the time the polymer reaches the final plateau conversion (within 60-100 s) the amount of CQ consumed is only 15-19 %. Thus, if DPI-PF₆ is reacting primarily with the terminating ketyl radical produced when CQ is consumed, then DPI-PF₆ will essentially always be in excess and no discernible effect of concentration should be expected.

With respect to photobleaching, the 0.3 wt% and 0.7 wt% DPI-PF₆ showed complete consumption of CQ, but when excess salt was added, residual camphorquinone remained after irradiation.

This observation may be attributed to some fluctuation in the mobility of the polymer network as more initiating radicals are produced. As we showed before in the study of CQ/amine initiated polymerizations of methacrylate monomers, the macromolecular structure and the mobility do affect the rate at which CQ is photobleached and are also correlated with the structure of the amine reductant used. If there is a mismatch in the polarity and electrostatics of the amine and the developing polymer network, as with PG and TEGDMA, the effect of mobility seems to be greater. This can also be stipulated since the rate of photobleaching up to 200 s is statistically the same regardless of the DPI-PF₆. Considering that the polymerization reached the final plateau conversion in approximately 60 s, it is fair to assume that there is no direct dependence of the photobleaching on [DPI-PF₆], as proven for the rate of polymerization. This is further proof that the ketyl radicals produced from the photoreduction of CQ by MDEA are the limiting reagent at these conditions.

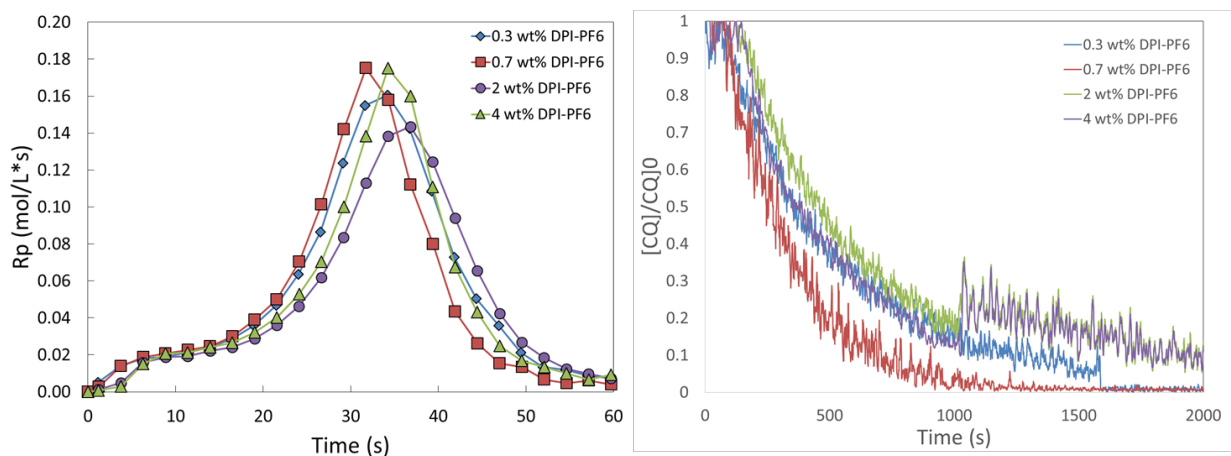


Figure 5.6 Left- Rate of polymerization of varying concentration of camphorquinone. Right- Camphorquinone bleaching of various salt concentrations. [CQ] = 0.1 wt %, [MDEA] = 0.5 wt % in TEGDMA at $I_0 = 22 \text{ mW/cm}^2$. It is important to note that the step changes observed in a couple of the results are most likely artifacts due to random scattering on some of the experiments.

5.3.3 Effect of Oxidant Chemistry

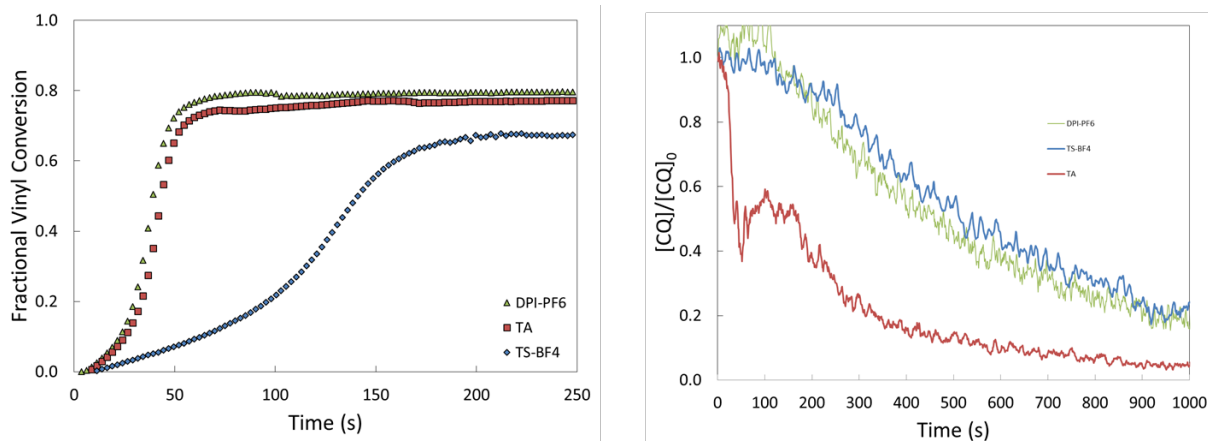


Figure 5.7 Left- Conversion versus time plot of different oxidant chemistries. Right- Bleaching of CQ as a function of salt chemistry. All experiments conducted in TEGDMA, $[CQ] = 0.1$ wt%, $[MDEA] = 0.5$ wt%, $[DPI-PF_6] = 0.7$ wt %, $[TA] = 1.9$ wt %, $[TS-BF_4] = 1.6$ wt %, $I_0 = 22$ mW/cm².

Finally, when we analyzed the effect of changing the oxidant structure we observed interesting variations in the photobleaching as compared to the effects in the vinyl conversion. Despite having the lowest reduction potential (or highest electron affinity) the sulfonium salt (TS-BF₄) had the lowest final conversion and rate of polymerization. This behavior may be attributed to steric hindrance or perhaps to a Marcus Inverted region which would reduce the kinetics of the electron transfer between this particular oxidant and the ketyl radicals. On the other hand, this behavior can also be attributed to a slower electron transfer despite a more negative ΔG_{ET} , as observed for Marcus-type electron transfer reactions. In contrast, DPI-PF₆ and TZ showed no significant difference in their polymerization profiles. The latter can potentially be explained by having a negligible difference in the oxidation rates at which these two react with the ketyl radical from camphorquinone, specially considering that CQ-based radical is rate limiting and that both DPI-PF₆ and TZ are in excess.

Most interestingly, we observed that CQ/MDEA/DPI-PF₆ and CQ/MDEA/TS-BF₄ essentially show the same CQ photobleaching rate. This further confirms that the increase in the rate of polymerization is not associated with CQ regeneration. Furthermore, TA significantly accelerated the rate of CQ photobleaching. This can be attributed to the presence of additional reductant functional groups in

the oxidant, namely the nitrogen in the triazine molecule. It seems likely that a simultaneous reaction between the excited state of CQ and TA might be present, thus leading to the dramatic increase in the amount of CQ consumed, but a negligible increase in the rate of polymerization.

5.4 Conclusions

The study presented herein examined aspects of the CQ/amine system with regards to the addition of an oxidant. There is a significant improvement on the rate of polymerization of CQ/MDEA with the addition of most oxidants (mainly iodonium salts and triazines). However, with PG amino acid, neither the rate of polymerization nor the photobleaching increase significantly with the addition of an oxidant. In fact the rate of polymerization decrease, most likely due to a different reaction between the primary form after decarboxylation, as opposed to the secondary radical formed from MDEA. We confirmed that small amounts of oxidant are needed because less than 20 % CQ is actually converted into ketyl radicals within the time it takes for the final conversion to be reached. Lastly, we observed that triazines might be able to react in multiple reactions, perhaps acting as reductants as well as oxidants. With all these observations and by being able to directly correlate CQ consumption to the extent of polymerization, we were able to provide stronger evidence to support a sequential mechanism in which first, CQ absorbs a photon and excites to the long lived triplet state via intersystem crossing, then the triplet state is reduced by the amine reductant to produce a terminating ketyl radical and an alpha amino alkyl radical. Subsequently, the terminating ketyl radicals are oxidized by DPI-PF₆, TS-BF₄, or TA; thus producing closed shell degradation products and a very reactive phenyl radical that further initiates polymerization. This refined mechanism can serve to develop novel three-component photoinitiators with potential advantages for dental materials, biomaterials, and tissue engineering, among other applications.

5.5 References

1. Bowman, C. N. & Kloxin, C. J. Toward an enhanced understanding and implementation of photopolymerization reactions. *AIChE J.* **54**, 2775–2795 (2008).
2. Stansbury, J. W. Curing dental resins and composites by photopolymerization. *J Esthet Dent* **12**, 300–308 (2000).
3. Shalaby, S. W. & Salz, U. *Polymers for Dental and Orthopedic Applications*. (CRC Press, 2006).
4. DeForest, C. A. & Anseth, K. S. Cytocompatible click-based hydrogels with dynamically tunable properties through orthogonal photoconjugation and photocleavage reactions. 1–7 (2011). doi:10.1038/nchem.1174
5. DeForest, C. A., Polizzotti, B. D. & Anseth, K. S. Sequential click reactions for synthesizing and patterning three-dimensional cell microenvironments. *Nature Materials* **8**, 659–664 (2009).
6. Jakubiak, J., Allonas, X., Fouassier, J. P. & Sionkowska, A. Camphorquinone–amines photoinitiating systems for the initiation of free radical polymerization. *Polymer* (2003). doi:10.1016/S0032-3861(03)00568-8
7. Kamoun, E. A., Winkel, A., Eisenburger, M. & Menzel, H. Carboxylated camphorquinone as visible-light photoinitiator for biomedical application: Synthesis, characterization, and application. *ARABIAN JOURNAL OF CHEMISTRY* 1–10 (2014). doi:10.1016/j.arabjc.2014.03.008
8. Schneider, L. F. J., Cavalcante, L. M., Prahl, S. A., Pfeifer, C. S. & Ferracane, J. L. Curing efficiency of dental resin composites formulated with camphorquinone or trimethylbenzoyl-diphenyl-phosphine oxide. *Dent Mater* **28**, 392–397 (2012).
9. Asmussen, S., Arenas, G., Cook, W. D. & Vallo, C. Photoinitiation rate profiles during polymerization of a dimethacrylate-based resin photoinitiated with camphorquinone/amine. Influence of initiator photobleaching rate. *European Polymer Journal* **45**, 515–522 (2009).
10. Nie, J. *et al.* A reappraisal of the photopolymerization kinetics of triethyleneglycol dimethacrylate initiated by camphorquinone-N,N-dimethyl-p-toluidine for dental purposes. *Acta Polymerica* **49**, 145–161 (1998).
11. Sionkowska, A., Kamińska, A., Linden, L.-A. & Rabek, J. F. Comparison of the photopolymerization kinetics of triethyleneglycol dimethacrylate initiated by camphorquinone/N-phenylglycine and camphorquinone/D,L- α -phenylglycine. *Polym. Bull.* **43**, 349–355 (1999).
12. Cook, W. D. & Chen, F. Enhanced photopolymerization of dimethacrylates with ketones, amines, and iodonium salts: The CQ system. *J. Polym. Sci. A Polym. Chem.* **49**, 5030–5041 (2011).
13. SCHROEDER, W. & VALLO, C. Effect of different photoinitiator systems on conversion profiles of a model unfilled light-cured resin. *Dental Materials* **23**, 1313–1321 (2007).
14. Grotzinger, C., Burget, D., Jacques, P. & Fouassier, J. P. Photopolymerization Reactions Initiated by a Visible Light Photoinitiating System: Dye/Amine/Bis (trichloromethyl)-Substituted-1, 3, 5-Triazine. *Macromol. Chem. Phys.* **202**, 3513–3522 (2001).

15. Kim, D. & Stansbury, J. W. A photo-oxidizable kinetic pathway of three-component photoinitiator systems containing porphyrin dye (Zn-tp), an electron donor and diphenyl iodonium salt. *J. Polym. Sci. A Polym. Chem.* **47**, 3131–3141 (2009).
16. Peter Pappas, S., Tilley, M. G. & Pappas, B. C. Anthracene-bound sulfonium salts: highly efficient photoinitiators for cationic polymerization. *Journal of Photochemistry & Photobiology, A: Chemistry* **159**, 161–171 (2003).
17. Padon, K. S. & Scranton, A. B. A mechanistic investigation of the three-component radical photoinitiator system Eosin Y spirit soluble, N-methyldiethanolamine, and diphenyliodonium chloride. *J. Polym. Sci. A Polym. Chem.* **39**, 715–723 (2001).
18. Kim, D. & Stansbury, J. W. Kinetic pathway investigations of three-component photoinitiator systems for visible-light activated free radical polymerizations. *J. Polym. Sci. A Polym. Chem.* **47**, 887–898 (2009).
19. Padon, K. S. & Scranton, A. B. A mechanistic investigation of a three-component radical photoinitiator system comprising methylene blue, N-methyldiethanolamine, and diphenyliodonium chloride. *J. Polym. Sci. A Polym. Chem.* **38**, 2057–2066 (2000).
20. Sirovatka Padon, K. & Scranton, A. B. The effect of oxygen on the three-component radical photoinitiator system: Methylene blue, N-methyldiethanolamine, and diphenyliodonium chloride. *J. Polym. Sci. A Polym. Chem.* **38**, 3336–3346 (2000).
21. Monroe, B. M. & Weiner, S. A. Mechanisms of photochemical reactions in solution. LII. Photoreduction of camphorquinone. *Journal of the American ...* **90**, 1913–1914 (1968).
22. Monroe, B. M. & Weiner, S. A. Mechanisms of photochemical reactions in solution. LVIII. Photoreduction of camphorquinone. *Journal of the American Chemical ...* **91**, 450–456 (1969).
23. Rubin, M. B. On the fate of initially formed radicals in photochemical hydrogen abstraction reactions. *Tetrahedron Letters* **10**, 3931–3934 (1969).
24. Rubin, M. B. & Ben-Bassat, J. M. A convenient new method for reduction of quinones and α -diketones. *Tetrahedron Letters* **12**, 3403–3406 (1971).
25. Rubin, M. B., Weiner, M. & Scharf, H. D. Photochemical reactions of cyclic, unsaturated diketones. *Journal of the American ...* **98**, 5699–5700 (1976).
26. Pączkowski, J. & Kucybala, Z. Generalization of the kinetic scheme for a dye-photosensitized free-radical polymerization initiating system via an intermolecular electron-transfer process. Application of Marcus theory. *Macromolecules* **28**, 269–273 (1995).
27. Paczkowski, J., Pietrzak, M. & Kucybala, Z. Generalization of the kinetic scheme for photoinduced polymerization via an intermolecular electron transfer process. 2. Application of the Marcus theory. *Macromolecules* **29**, 5057–5064 (1996).
28. Andrea, M. Marcus theory for electron transfer a short introduction. *MPIP Journal Club-Mainz* (2008).
29. Park, Y. J., Chae, K. H. & Rawls, H. R. Development of a new photoinitiation system for dental

- light-cure composite resins. *Dent Mater* **15**, 120–127 (1999).
30. Wang, Y., Spencer, P., Yao, X. & Ye, Q. Effect of coinitiator and water on the photoreactivity and photopolymerization of HEMA/camphoquinone-based reactant mixtures. *J. Biomed. Mater. Res.* **78A**, 721–728 (2006).
 31. Guo, X., Wang, Y., Spencer, P., Ye, Q. & Yao, X. Effects of water content and initiator composition on photopolymerization of a model BisGMA/HEMA resin. *Dental Materials* **24**, 824–831 (2008).
 32. Kim, D. & Scranton, A. The role of diphenyl iodonium salt (DPI) in three-component photoinitiator systems containing methylene blue (MB) and an electron donor. *J. Polym. Sci. A Polym. Chem.* **42**, 5863–5871 (2004).
 33. Aguirre-Soto, A., Lim, C.-H., Hwang, A. T., Musgrave, C. B. & Stansbury, J. W. Visible-Light Organic Photocatalysis for Latent Radical-Initiated Polymerization via $2e^-/1H^+$ Transfers: Initiation with Parallels to Photosynthesis. *J. Am. Chem. Soc.* **136**, 7418–7427 (2014).
 34. Meinwald, J., Meinwald, J., Klingele, H. O. & Klingele, H. O. Photochemical Reactions of Camphorquinone1. *Journal of the American Chemical ...* (1966). doi:10.1021/ja00961a056
 35. Anseth, K. S., Bowman, C. N. & Peppas, N. A. Dynamic mechanical studies of the glass transition temperature of photopolymerized multifunctional acrylates. *Polym. Bull.* **31**, 229–233 (1993).
 36. Anseth, K. S., Wang, C. M. & Bowman, C. N. Reaction behaviour and kinetic constants for photopolymerizations of multi (meth) acrylate monomers. *Polymer* (1994). doi:10.1016/0032-3861(94)90129-5
 37. Anseth, K. S., Kline, L. M., Walker, T. A. & Anderson, K. J. Reaction kinetics and volume relaxation during polymerizations of multiethylene glycol dimethacrylates. ... **28**, 2491–2499 (1995).
 38. Weinberg, D. R. *et al.* Proton-coupled electron transfer. *Chem. Rev.* **112**, 4016–4093 (2012).
 39. Ullrich, G., Burtscher, P., Salz, U., Moszner, N. & Liska, R. Phenylglycine derivatives as coinitiators for the radical photopolymerization of acidic aqueous formulations. *J. Polym. Sci. A Polym. Chem.* **44**, 115–125 (2005).
 40. Yamaoka, T., Zhang, Y. C. & Koseki, K. N-phenylglycine-(thio)xanthene dye photoinitiating system and application to photopolymer for visible laser exposure. *J. Appl. Polym. Sci.* **38**, 1271–1285 (1989).

Chapter 6

Ground state complex formation as tool for controlling photoredox catalysis (Photoredox catalysis also works via hydride transfer)

Abstract

Photoredox catalysis has become an important tool in both organic and polymer synthesis. It is widely accepted that photoredox catalysis most often operates via single electron (e^-) transfer steps, through which the light-absorbing photocatalyst is first consumed and then regenerated. Several reports have recently appeared in which *N,N*-diisopropylethylamine (*iPr*₂NEt) is used as reductant or electron donor with both organic and organometallic photocatalysts. These formulations have been used for many reactions, including cycloadditions, dehalogenations, alkylations, fluoromethylations, hydroxylations and chain growth polymerizations. High rates, yields, selectivity and unexpected reactions have been reported in all these cases, but an explanation of the link between *iPr*₂NEt and the exceptional performance remains elusive. In general aliphatic amines like *iPr*₂NEt are known to be good single e^- donors, but we propose herein for the first time that in numerous cases aliphatic amines undergo $e^-/H^+/e^-$ transfer instead of e^- . We show that such a change in the expected reaction pathway occurs whenever the aliphatic amines form a ground state complex with either the photocatalyst or a Lewis acid additive. Methylene blue (MB^+) and ruthenium bipyridine complexes were used as examples of photocatalyst that complexate with *iPr*₂NEt and other amines depending on the solvent polarity. The present work not only serves as the first mechanistic explanation of a broad set of unexpected results, but also provides guidelines for the rational selection of photocatalyst/amine/solvent/additive combinations to favor either $e^-/H^+/e^-$ or e^- transfer, depending on whether free radicals are desired or undesired. Thus, this opens new opportunities for the further development and application of photoredox catalysis for a broad range of fields within organic and polymer chemistry.

6.1 Introduction

Photoredox catalysis entails the use of light-absorption by organic or organometallic molecule (photocatalyst), to facilitate chemical reactions that would not otherwise occur, or that would be challenging to achieve without harnessing light as the driving energy. This has attracted attention in the last decade because it efficiently and selectively mediates a wide range of chemical transformations using low-energy visible light under mild conditions. Examples of some of these organic and macromolecular reactions are: alkylations¹, dehalogenations², [2+2] enone cycloadditions^{3,4}, atom transfer radical additions⁵, atom-transfer radical polymerization (ATRP)^{6,7}, and free radical and cationic chain growth polymerizations^{8,9}. The main advantages provided by the photoredox catalysis approach include: facilitating the synthesis of molecules not accessible via conventional high-energy UV radiation photochemistry^{3,4}, higher selectivity than UV-activated reactions because side reactions are suppressed by the exclusive light-absorption of the photocatalyst, lower toxicity, lower cost, environmentally benign, use of the entire visible spectrum, and sunlight-activation. In macromolecular chemistry, additionally, photoredox catalysis is paramount to the production of UV-sensitive polymer materials, such as holograms¹⁰, printing plates¹¹, photoresists, electrophoresis gels¹², dental adhesives and restoratives¹³⁻¹⁶, and 3D scaffolds¹⁷. Furthermore, it is useful in the controlled synthesis of a broad set of macromolecular architectures that employ light as spatial and temporal switch⁶.

Electron (e^-) transfer (reduction-oxidation or redox) steps are the most ubiquitous in photoredox catalysis. Hence, photocatalysts are most often utilized in conjunction with an electron donor and an electron acceptor. These two compounds allow the photocatalyst to first receive or donate an electron from its excited state, and to subsequently be regenerated by a secondary electron donation or acceptance step involving the intermediate formed from the initial reaction. Since 2008, exceptionally fast rates, high yields and high enantio- or chemoselectivity have been reported when using *N,N*-diisopropylethyl amine (Hünig's base, iPr_2NEt) as sacrificial electron donor with both organic (Methylene blue, MB^+) and organometallic ($Ru(bpy)_3^{2+}$) photocatalysts^{2-4,18-21}. For example, Yoon's [2+2] enone cycloadditions

achieved an impressive 94% yield of *cis*-dione even with 1 h of sunlight exposure with excellent diastereoselectivity⁴ using Ru(bpy)₃Cl₂, *i*Pr₂NEt, and LiBF₄ (as Lewis acid) in acetonitrile (MeCN). Stephenson demonstrated up to 95 % yield for tin-free reductive dehalogenation reactions using Ru(bpy)₃Cl₂, *i*Pr₂NEt, and HCO₂H (as Lewis acid) or Hantzsch ester in dimethyl formamide (DMF)². More recently, Scaiano showed that MB⁺ and *i*Pr₂NEt in 4:1 acetonitrile:water solution give 100 % conversion and 94 % yield in oxidative hydroxylation of arylboronic acids, and up to 83 % yield for trifluoromethylation reactions with several MB⁺/aliphatic amine combinations in DMF^{18,19}. In the field of polymer chemistry, we recently demonstrated that MB⁺, *i*Pr₂NEt and iodonium salt in acrylate or (meth)acrylate monomers allow light-energy storage and extension free radical photopolymerizations in space and time beyond the reach of the photons²¹. Furthermore, Zhang et al. showed that spatiotemporally controlled ATRP of several (meth)acrylate monomers can be achieved in DMF solution only when Ru(bpy)₃Cl₂, *i*Pr₂NEt, and ethyl-2-bromoisobutyrate are all present during irradiation²⁰.

However, the exceptional performance can be highly sensitive to variations in solvent, concentrations or amine structural features in most of these instances. Yoon and coworkers comment that no reaction occurs without LiBF₄, and that, unexpectedly, highly diastereoselective cycloadditions are only observed when both *i*Pr₂NEt and LiBF₄ are present in excess^{4,22}. These results were described as inconsistent with the typical mechanism involving direct triplet sensitization from the Ru(bpy)₃²⁺ complex, without further elaboration. Stephenson et al. mentioned that the yield of reductive dehalogenation increases from 25 % to > 90 % upon addition of formic acid (excess) or Hantzsch ester to their initial Ru(bpy)₃Cl₂/*i*Pr₂NEt formulation. Removal of any of the components or decrease in their concentrations afforded only trace amounts of their desired products, and substitution of *i*Pr₂NEt with triethylamine (Et₃N) decreased the yield to 25 %². Such observations strongly suggest that *i*Pr₂NEt has certain attributes that make it quite different than other reductants in general, even compared to other amines, in its role as the electron donor.

Despite these promising and intriguing developments, no conclusive theory exists to explain the phenomena displayed by *i*Pr₂NEt-containing photoredox systems, and to aid in the rational selection of other amine electron donors, photocatalysts and solvents that can afford equivalent or higher rates, yields and selectivity. One possibility is that *i*Pr₂NEt does not favor the typical single e⁻ transfer reactions observed with other, more conventional, formulations. In fact, Stephenson's group determined by isotope labeling studies that *i*Pr₂NEt rather functions as hydrogen atom source in their reductive dehalogenations. Recently, Kotani et al. showed that bulky aliphatic amines, including *i*Pr₂NEt, are good hydride donors for reduction of unsaturated ketones in the presence of trichlorosilyl triflate and for enantioselective reductive aldol reaction with excellent yields in the presence of Lewis acids^{23,24}. Singh et al. successfully coupled 2-chloroazoles with tertiary aliphatic amines via photoredox-mediated C-H functionalization using Ir(ppy)₃ photocatalyst in MeCN²⁵. Furthermore, we have previously shown that *i*Pr₂NEt can transfer e⁻/H⁺/e⁻ upon photo-oxidation by MB⁺ to produce closed shell decomposition by-products, as opposed to the typically expected alpha-amino radicals from single e⁻ transfer with other amines²¹. In spite of all this evidence, a mechanistic understanding remains elusive of what makes bulky aliphatic amines, like *i*Pr₂NEt, function as hydrogen or hydride donors instead of e⁻ donors, as other reductants normally do.

Herein, we propose that *i*Pr₂NEt favors hydride transfer (e⁻/H⁺/e⁻ transfer), as opposed to single e⁻ transfer, due to the formation of an electron-donor-acceptor (EDA) complex in the ground state with either the photocatalysts (MB⁺, Ru(bpy)₃²⁺) or an additional Lewis acids (Li⁺, HCO₂H). If such ground state complex is present before irradiation, then *i*Pr₂NEt undergoes sequential e⁻/H⁺/e⁻ because it is in close proximity to the molecule functioning as Lewis pair. As a result, no free radicals are produced from the photooxidation of the bulky aliphatic amines by the excited state of MB⁺ or Ru(bpy)₃²⁺ (Figure 6.1a), i.e. ionic, instead of radical, processes dominate as a result of the e⁻/H⁺/e⁻ transfer. While absence of free radicals is not ideal for conventional free radical polymerizations, it can be advantageous in organic synthesis where high yields and enantio-, chemo- or regio-selectivity are desired. The ability of MB⁺ and Ru(bpy)₃²⁺ to function as e⁻/H⁺/e⁻ acceptors has been discussed in the literature²⁶⁻²⁸, and will be analyzed

herein along with the dependence of complex formation on the solvent. In this way, the present work serves as the first mechanistic explanation of the uniqueness of bulky aliphatic amine reductants in photoredox catalysis, and to provide an initial set of guidelines of how to control whether photoredox catalysis operates by e^- or $e^-/H^+/e^-$ transfer through the rational selection of photocatalyst, amine, solvent and Lewis acid additives. McKay first mentioned the possibility of Lewis acid/base complexation between MB^+ and amines, but did not elaborate on such idea²⁹. More recently, Stephenson introduced the possibility of a hydrogen transfer occurring from a formic acid/*i*Pr₂NEt complex to Ru(bpy)₃²⁺. Nevertheless, a direct link between the formation of the complex, the $e^-/H^+/e^-$ transfer, and the excellent performance and selectivity of *i*Pr₂NEt-containing systems has not been addressed. Analysis of these correlations remains entirely absent. Thus, this work can be of great benefit and interest to a wide range of disciplines, fields, and applications ranging from synthetic organic chemistry to materials science and engineering in which photoredox catalysis is already a powerful tool.

6.2 Experimental section

6.2.1 Materials

Methylene blue (MB^+), N,N-diisopropylethylamine >99 % (*i*Pr₂NEt), triethylamine >99.5 %, tris(2,2'-bipyridyl)dichlororuthenium(II) hexahydrate 99.95 %, camphorquinone 97 %, N-methyldiethanolamine >99 %, and triethanolamine >99 % were obtained from Sigma-Aldrich (Milwaukee, WI) and used as received. 2-Hydroxyethyl (meth)acrylate (HEMA) was selected as monomer because it readily dissolves all photocatalysts and amines and has a relatively low polarity. Other acrylate and (meth)acrylate monomers are expected to behave very similarly if viscosity is equivalent. Samples were vortexed until complete dissolution. Components were always mixed immediately prior to experiments to avoid side reactions in the dark, unless otherwise stated. Methanol (MeOH), ethanol (EtOH), and acetonitrile (MeCN) were spectro grade from Sigma-Aldrich and used without additional purification. Distilled water was also used as solvent for UV-Vis analysis.

6.2.2 Crystallization of methylene blue (MB^+) and $[MB^+ \dots amine]$ complexes

Methylene blue (MB^+) crystals were first grown on a 5x5x1 mm microscope glass slide (as nucleation site) inside a glass vial by slow evaporation of ethanol using an initial concentration of $[MB^+] = 1 \times 10^{-5}$ M. Then, solutions were prepared with the same initial MB^+ concentration and 1000 equivalents of both Et_3N and iPr_2NEt in ethanol. Vials were left inside a hood with continuous airflow for 24 h until the ethanol solvent completely evaporated. All three glass slides were then taken to the microscope for analysis.

6.2.3 Polarized light microscopy for visualization of crystals

Images of the crystals were captured using a Nikon microscope directly from the glass slides with a 20x optical magnification lens using a polarization filter and an acquisition of 100-150 μs . The entire glass slide surface was captured and analyzed. Representative images are included in Figure 6.1b.

6.2.4 UV-Vis spectroscopy for determination of complex formation

Separate solutions of MB^+ , $Ru(bpy)_3^{2+}Cl_2$, and camphorquinone were prepared at concentrations of 1×10^{-5} M, 1×10^{-5} M, and 1×10^{-2} M, respectively, in 2-hydroxyethyl (meth)acrylate, ethanol, and acetonitrile. The UV-Vis spectra were collected with a Thermo-Scientific Evolution 300 spectrophotometer before addition of any amine reductant. Once the initial absorbance of each photocatalyst was measured, either Et_3N or iPr_2NEt were added drop by drop with a syringe. Each drop was determined to equate to a volume of approximately 100 μL . For each drop added another full UV-Vis spectrum was obtained until no change was observed in the absorbance of MB^+ and $Ru(bpy)_3^{2+}$. This process was repeated at least twice for each photocatalyst/amine/solvent combination.

The isosbestic point and the association constants were determined from the changes in the MB^+ , $Ru(bpy)_3^{2+}$ and CQ absorbance peaks. The evolution of the absorbance at the wavelength of highest absorbance for each photocatalyst was plotted against amine concentration based on the Ketelaar equation for a 1:1 EDA complex where the electron donor (amine) is used in excess and does not absorb in the

region where the acceptor (photocatalyst) absorbs³⁰. Linear fits were found for all cases analyzed with an R^2 greater than 0.94.

6.2.5 Coupled UV-Vis/FT-NIR full spectrum real-time monitoring

Coupling UV-Vis to FT-NIR. The UV-Vis and FT-NIR beams were coupled into a SMA-fitted cuvette holder (CUV-ALL-UV 4-Way Cuvette Holder, Ocean Optics, Dunedin, FL) that holds a dual-pathlength PMMA cuvette (UVette, Eppendorf, Hauppauge, NY). The sample volume used was 50-60 μL with dimensions of 2 mm x 10 mm x 2.5 mm. The longer pathlength was used for UV-Vis to prevent saturation of the NIR signal.

UV-Vis/FT-NIR beams were transmitted orthogonally within a matched horizontal plane through the center of the sample at an approximate depth of 1.25 mm. The aperture of the UV-Vis probing beam was reduced with a ~ 0.5 mm pinhole at the center of the sample to reduce the artifacts created by the light scattering of both the probing and the polymerization-inducing beams.

Monomer conversion was monitored with a FT-IR spectrophotometer (Nicolet Magna-IR Series II, Thermo Scientific, West Palm Beach, FL) by following the peak area of the first overtone absorption band of the $=\text{CH}_2$ bonds ($\sim 6167 \text{ cm}^{-1} = 1621 \text{ nm}$). Monomer absorbance was confirmed to fall within the linear Beer-Lambert region within the concentrations used here. The spectrophotometer is equipped with an extended range KBr beam splitter and an InGaAs detector. The NIR signal was transmitted to/from the remote specimen via matched 1000 μm fiber optic cables. The FT-IR settings were set to 8-16 scans, a resolution of 8, an optical gain of 1, and an optical aperture of 3-5. The velocity of the interferometer was adjusted according to the desired acquisition time.

Fiber optic coupled UV-Vis detectors USB2000-UV-VIS and USB4000-FL (Miniature Fiber Optic Spectrometers, Ocean Optics, Dunedin, FL) were employed to measure the change in the absorbance between 400 nm and 510 nm related to the $n \rightarrow \pi^*$ transition of the carbonyl groups in CQ, which decays as a function of CQ concentration. The CQ absorbance was calibrated against concentration to confirm that it follows Beer-Lambert's linearity. The spectrometers use Charge-coupled Device (CCD)

detectors that allow full-spectrum acquisition. The high sensitivity USB4000-FL permits the use of low intensity UV-Vis light in continuous or pulsed mode to probe samples without initiating the polymerization. Integration time was set to < 1 s (Fig. 6.3). Negligible polymerization occurred from exposure to the UV-Vis probing beams from a low intensity halogen lamp from Oriel Instruments (Irvine, CA) with an emission spectrum in the range of 400-700 nm (Fig. 6.3c).

The FT-NIR results were obtained directly from the OMNIC Software (Thermo Scientific, West Palm Beach, FL) and processed in Excel according to the method reported by Decker³¹. The UV-Vis output was collected with the SpectraSuite Software (Ocean Optics, Dunedin, FL). A FORTRAN code was written to merge the data into a single text file. Then a MATLAB script was written to process the full-spectrum absorbance, remove any baseline shifts from light scattering of the UV-Vis probing beam (see SI), and extract the absorbance maximum λ_{max} (~ 470 nm for CQ), i.e. maximum absorbance was found for every spectrum and plotted against time. At least three replicates were performed for each experiment. Averaged data was then fitted to exponential equations using MATLAB curve fitting tool. R^2 values for all fitted curves were at least 0.95.

6.2.6 *Quantum chemical calculations*

Complex formation calculations were performed using rM06/LANL2dz level of theory where solvation in methanol was described using a polarizable continuum model (CPCM). All calculations were performed using the GAUSSIAN 09 and computational chemistry software packages.

6.3 Results and discussion

6.3.1 MB^+ readily forms ground state complex with iPr_2NEt

First we demonstrate that MB^+ readily forms complexes in the ground state with aliphatic amines. Figure 6.1b shows images of both uncomplexated and complexated MB^+ using polarized light microscopy to analyze the differences in their morphology and color as a function of the degree of complexation. All crystals were grown on a microscope glass slide through slow evaporation of ethanol during 24 h under ambient conditions. MB^+ crystals have a particular needle-like morphology and a violet color that have been observed by others. Then, we added 1000 equivalents of triethylamine (Et_3N) to the same parent solution of MB^+ and let the ethanol slowly evaporate. The same process was employed for iPr_2NEt . If a Lewis acid (MB^+)/base type complex is formed it would be expected that Et_3N would complexate less than iPr_2NEt . In fact, we confirm that to be the case. The image in the left serves as a negative control and shows exclusively violet needle-like crystals with sizes over 50 μm corresponding to uncomplexated MB^+ . Then, the image in the center shows a combination of crystals corresponding to both uncomplexated MB^+ and the $[MB^+...Et_3N]$ complexes. Lastly, when iPr_2NEt was used, crystals associated with the $[MB^+...iPr_2NEt]$ complex were obtained almost exclusively. The crystals corresponding to the complexes with both amines are smaller in size, blue and green, and a different needle-like morphology. We believe the loss of the violet color, the change in morphology, and reduction in the crystals size are all associated with a disruption of the natural MB^+ crystal growth by the amines being in close proximity.

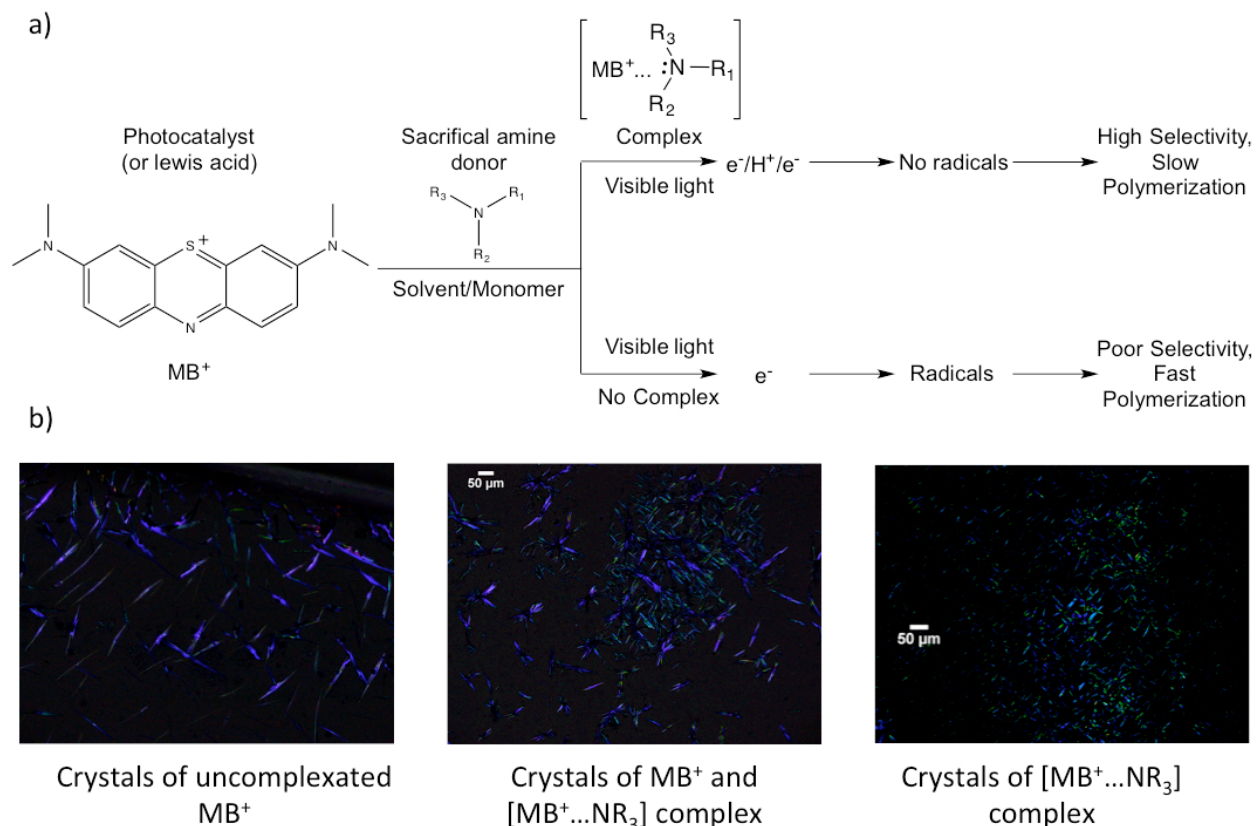


Figure 6.1 Aliphatic amines like N,N-diisopropylethylamine (*i*Pr₂NEt) form complexes with either the photocatalyst or a Lewis acid additive, and thus favor e⁻/H⁺/e⁻ transfer over single e⁻ transfer. **a**, Scheme of e⁻/H⁺/e⁻ vs e⁻ based on the formation of a ground state complex by the photocatalyst and the aliphatic amine donor. **b**, Morphology and color of crystals change as a function of the amount of Methylene blue (MB⁺)/amine complex (from left to right). Microscope image of crystals under polarized light at 20x magnification of uncomplexed methylene blue (MB⁺), complex of Methylene blue (MB⁺) and triethylamine (Et₃N), and MB⁺/N,N-diisopropylethylamine (*i*Pr₂NEt) complex. All crystals were grown by slow evaporation of ethanol solvent over a glass slide at ambient conditions. Et₃N and *i*Pr₂NEt were both present at 1000 equivalents to grow crystals from their complexes. Additional images are included in the SI Section 1.

In fact, the observed change in the color of the crystals can be explained by the changes in the UV-Vis absorbance of MB⁺ in solution upon addition of the aliphatic amines. Eaton reported that addition of triethylamine to New Methylene Blue lead to a decrease in the MB⁺ absorbance band at ~ 639 nm, and to the growth of a new peak centered at ~525 nm³². Concurrently, solutions change from blue to pink as the Et₃N concentration increases. The new absorbance band can be seen as a combination of blue and green under polarized light, as opposed to a violet color, which would correspond to original absorbance peak of MB⁺ in its uncomplexed state.

Similar results to Eaton's were obtained by monitoring the UV-Vis absorbance of MB^+ in solution as a function of amine concentration. We first analyzed the changes in MB^+ absorbance upon addition of $i\text{Pr}_2\text{NEt}$ in ethanol. Figure 6.2a shows the decrease in the characteristic MB^+ peak at 660 nm with increase in $i\text{Pr}_2\text{NEt}$ concentration, indicating formation of the $\text{MB}^+/i\text{Pr}_2\text{NEt}$ complex. We found an isosbestic point, typically associated with EDA complex formation, at 552 nm. Then, we used the Ketelaar equation (Figure 6.2b) to confirm that MB^+ and $i\text{Pr}_2\text{NEt}$ form a 1:1 complex with an association K constant of $72 \pm 2 \text{ M}^{-1} \cdot \text{cm}^{-1}$ ($R^2 = 0.99$)³⁰. Shown as an inset is the most stable configuration of the $\text{MB}^+/i\text{Pr}_2\text{NEt}$ complex was determined by DFT calculation with rM06/LANL2DZ level of theory with a $\Delta G = -6.4 \text{ kcal/mol}$ in methanol as continuum solvent model. Similar results were obtained in the 2-hydroxyethyl (meth)acrylate monomer, shown in Fig. 2b, but the association K constant was higher $320 \pm 5 \text{ M}^{-1} \cdot \text{cm}^{-1}$ ($R^2 = 0.94$) due to the lower polarity of the HEMA monomer as compared to ethanol (Fig. 6.2b). Formation of the $\text{MB}^+/i\text{Pr}_2\text{NEt}$ complex is expected to be stronger in polar aprotic MeCN and weaker in highly polar protic H_2O . In fact, we observed that addition of $i\text{Pr}_2\text{NEt}$ to MB^+ solutions in acetonitrile took only a few seconds to minutes to change in color from blue to pink. Methanol and ethanol solutions took weeks to months for the MB^+ blue color to transition to the pink color. Water solutions showed no disappearance of the blue color over months to years of storage in the dark. These observations are consistent with the UV-Vis results that show the disappearance of the MB^+ peak at 660 nm correlates with the appearance of a new peak centered at around 500 nm (Figure 6.2).

We also characterized the complex formation between MB^+ and triethylamine. We observed an isosbestic point at 580 nm and an association K constant of $67 \pm 1 \text{ M}^{-1} \cdot \text{cm}^{-1}$ ($R^2 = 0.98$) for the 1:1 complex. This agrees with our microscopy experiments, which show that $i\text{Pr}_2\text{NEt}$ complexates more than Et_3N with MB^+ and correlates with the higher basicity of $i\text{Pr}_2\text{NEt}$ (pKa 11.4-20 range depending on solvent) as compared to Et_3N (pKa 10-13), depending on the solvent. We confirmed that MB^+ does not form higher aggregates in ethanol, HEMA, methanol, or ethanol. It has been documented that MB^+ self-associates in water beginning at concentrations as low as $1 \cdot 10^{-6} \text{ M}$, which causes a decrease in the MB^+

absorbance³³. However, no aggregates were identified using UV-Vis absorbance analysis in the lower polarity solvents and concentrations used herein. As a negative control, we tested for the complexation of camphorquinone with both *i*Pr₂NEt and Et₃N, and confirmed that the CQ absorbance does not change upon addition of up to 1500 equivalents of either amine in ethanol or HEMA (SI Section 2).

Furthermore, we analyzed the fluorescence emission of ethanol solutions containing MB⁺ or MB⁺ and *i*Pr₂NEt at equivalent amounts of MB⁺ (1×10^{-5} M) and 1000 equivalents of *i*Pr₂NEt for the latter. A 660 nm LED was used for excitation. It was observed that when the MB⁺/*i*Pr₂NEt complex dominates, there appears to be a blue-shift in the fluorescence emission, which is most likely associated with changes in either the excited or the ground state singlet of uncomplexed Methylene Blue caused by *i*Pr₂NEt as the ground state complex is formed (Fig. 6.2c).

6.3.2 *Ru(bpy)₃²⁺ only forms complex with iPr₂NEt in polar aprotic solvents*

In contrast, Ru(bpy)₃²⁺ shows a lower tendency to complexate with *i*Pr₂NEt and Et₃N. We repeated the process used for the MB⁺/amine analysis, but substituted MB⁺ by Ru(bpy)₃²⁺ in ethanol, HEMA monomer, and MeCN. However, no changes in the photocatalyst absorbance were detected upon drop-wise addition of *i*Pr₂NEt to the Ru(bpy)₃²⁺ solutions in either EtOH or HEMA. On the other hand, the absorption band centered at around 290 nm changed significantly when adding as low as 50-100 equivalents of *i*Pr₂NEt in acetonitrile (Fig. 6.2d). No complex formation evidence was observed with Et₃N in ethanol, and minor changes in absorbance were seen in MeCN. Shown as an inset in Figure 6.2d is the most stable configuration of the Ru(bpy)₃²⁺/*i*Pr₂NEt complex, determined by DFT calculation with rM06/LANL2dz level of theory with a $\Delta G = -6.9$ kcal/mol for complexation in methanol as continuum solvent model.

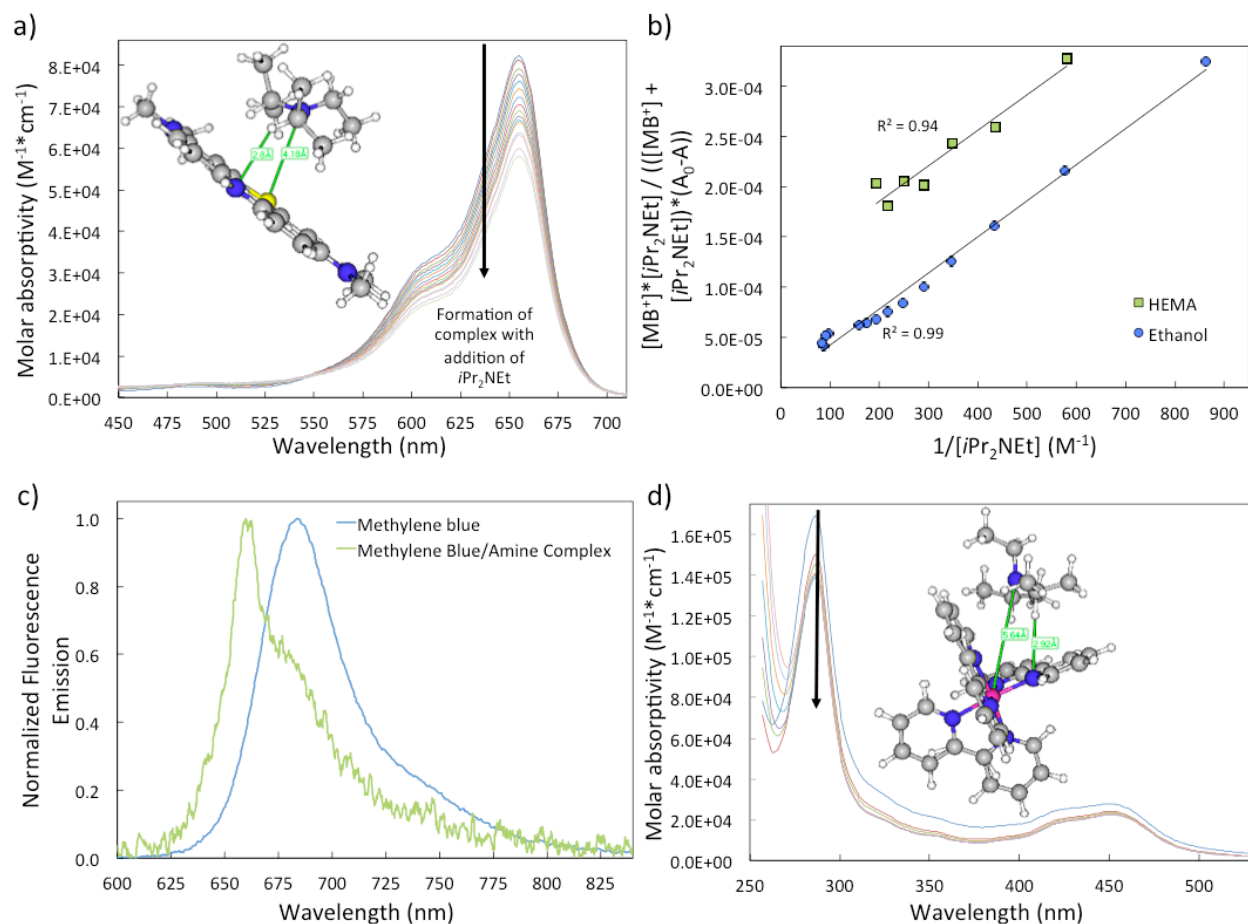


Figure 6.2 Photocatalyst form ground state complexes with aliphatic amines. **a**, Decrease in the UV-Vis absorbance of $[MB^+] = 1 \times 10^{-5}$ M ethanol solution upon drop-wise addition of iPr_2NEt due to the formation of the MB^+/iPr_2NEt complex. The inset shows the most stable configuration of the 1:1 complex obtained with DFT quantum chemical calculations with $\Delta G = -6.4$ kcal/mol in methanol. The distance between the α hydrogen from one of the isopropyl groups in iPr_2NEt is 2.8 Å, which is sufficient for the H^+/e^- transfer to occur after the initial e^- transfer from the iPr_2NEt lone pair. **b**, Plot of the Ketelaar equation for determination of the association constant of the MB^+/iPr_2NEt in ethanol and 2-hydroxyethyl (meth)acrylate monomer. $K_{EtOH} = 72 \pm 2 M^{-1} \cdot cm^{-1}$ ($R^2 = 0.99$) and $K_{HEMA} = 320 \pm 5 M^{-1} \cdot cm^{-1}$ ($R^2 = 0.94$). **c**, Change in the fluorescence emission upon addition of 1000 equivalents of iPr_2NEt to a $[MB^+] = 1 \times 10^{-5}$ M in ethanol. **d**, Changes in the UV-Vis absorbance spectrum of $[Ru(bpy)_3]^{2+} = 2 \times 10^{-5}$ M acetonitrile solution upon drop-wise addition of iPr_2NEt . Inset shows the most stable configuration of the 1:1 $Ru(bpy)_3^{2+}/iPr_2NEt$ complex determined with DFT calculations and having a $\Delta G = -6.9$ kcal/mol in methanol. The distance between the α hydrogen from one of the isopropyl groups in iPr_2NEt and one of the pyridinic nitrogens in $Ru(bpy)_3^{2+}$ is 2.9 Å.

6.3.3 Ground state complexes are close enough for hydrogen atom abstraction

Once we established that the formation of ground state complexes between MB^+ , or $\text{Ru}(\text{bpy})_3^{2+}$, and $i\text{Pr}_2\text{NEt}$ is thermodynamically and kinetically feasible, we investigated the mechanism via which such complexes might favor $e^-/\text{H}^+/e^-$ transfer over single e^- transfer. It is known that electron transfer can occur between centers separated by longer distances than those required for proton transfer^{34,35}. Hence, we searched for the most stable configurations of the 1:1 complexes using quantum chemical calculations (DFT) with rM06/LANL2dz level of theory. The goal was to determine whether the photocatalyst and amine were in close proximity for proton transfer to occur after the initial e^- transfer. Figure 6.2a and 6.2d contain the most stable configurations for both the $\text{MB}^+/i\text{Pr}_2\text{NEt}$ and the $\text{Ru}(\text{bpy})_3^{2+}/i\text{Pr}_2\text{NEt}$ complexes. In both cases, the results indicate that the nitrogen atom in $i\text{Pr}_2\text{NEt}$ is at distances of 4.18 and 5.64 Å from the sulfur atom in MB^+ and the ruthenium atom in $\text{Ru}(\text{bpy})_3^{2+}$, respectively. These distances are sufficient for the initial rate-limiting electron transfer. Most importantly, the alpha hydrogens from the isopropyl groups in $i\text{Pr}_2\text{NEt}$ were found at distances of 2.8 with MB^+ and 2.9 Å with $\text{Ru}(\text{bpy})_3^{2+}$. These smaller distances strongly imply that hydrogen atom transfer will be highly plausible if the complexes are formed before irradiation.

In general, it is widely accepted that amines readily lose one alpha proton after e^- transfer from the lone pair in the nitrogen atom because the bond dissociation energy of the C-H bonds weakens as a result of the initial e^- loss³⁶. Thus, abstraction of any of the isopropyl alpha hydrogens from $i\text{Pr}_2\text{NEt}$ after e^- loss from its lone pair is a highly probable outcome. Furthermore, we previously calculated using TDDFT methods that the basicity of MB^+ increases ($\text{pK}_a \sim 14$ in methanol) after the initial electron acceptance step²¹. This observation becomes important because it further supports the feasibility of the H^+ transfer from the weakened isopropyl alpha C-H bond to the basic thiazinic nitrogen in MB^+ after the initial e^- transfer. It has been shown experimentally and theoretically, that once the H^+ is transferred to MB^+ , the reduction potential of the semireduced protonated ($\text{MB}^{\cdot+}$) will favor the secondary e^- transfer,

allowing the fast formation of a stable iminium cation from iPr_2NEt , or the closed shell products that we reported earlier, if further oxidation of the iminium cation occurs, especially in basic solutions²¹.

Complete $e^-/H^+/e^-$ transfer would in turn readily produce the fully reduced version of MB^+ : Leuco Methylene Blue (LMB), which has no absorbance peaks in the visible region and has been identified by the appearance of an absorbance peak centered at 256 nm. In fact, MB^+ and the analogous thionine were documented to react via sequential $e^-/H^+/e^-$ transfer to readily form their leuco (colorless) intermediates in ethanol solution upon irradiation in the presence of Et_3N and leuco crystal violet²⁶⁻²⁸. We confirmed that LMB is almost exclusively produced by irradiation (660 nm) of all solutions that show evidence of complex formation, as seen by the loss of absorbance in the visible region (400-800 nm) and the appearance of a new peak centered at around 256 nm (SI Section 3). It is worth noting that Kayser and Young showed MB^+ reacted via single e^- transfer when irradiated in methanol solutions containing aryl amines, as evidenced by the formation of appearance of an absorbance peak at 420 nm associated with the semireduced MB^\bullet . In contrast, they were not able to detect the same accumulation of this intermediate with aliphatic amines, and had to rely on the recovery of the MB^+ absorbance peak for their kinetic analysis for these cases^{37,38}. This indicates that aliphatic amines might favor $e^-/H^+/e^-$, while aryl amines will primarily engage in e^- transfer when photo-oxidized by the excited state triplet of MB^+ . The latter might be a consequence of the lack of complex formation between MB^+ and aryl amines, as compared to aliphatic amines.

6.3.4 Free radical polymerization is absent when photocatalyst/amine complex is present

To further prove that aliphatic amines react via $e^-/H^+/e^-$ when complexed with the photocatalysts we used our previously reported coupled UV-Vis/FT-NIR characterization technique to directly correlate the consumption of the photocatalyst with the production of free radicals. If complexes are in fact favoring $e^-/H^+/e^-$ over single e^- , then we expected solutions containing acrylates or methacrylates to show no evidence of polymerization of the vinyl monomer. Whereas, solutions that don't display evidence of complex formation should show signs of efficient free radical production, relative the consumption of the

photocatalyst. As a matter of fact, we demonstrate here that $\text{MB}^+/\text{iPr}_2\text{NEt}$ solutions in methanol, ethanol or bulk HEMA all displayed an almost instant consumption of MB^+ , as seen by the fast disappearance of the absorbance peak at 660 nm. Figure 6.3 shows that when the maximum absorbance associated with MB^+ is plotted against irradiation time using a red LED centered at 660 nm with an intensity of 5 mW/cm^2 only 5% MB^+ remains unreacted within 60 s. In contrast, there is only a 1-2 % consumption of vinyl groups from the HEMA monomer at 1600 s irradiation as seen in Fig. 6.3, which is extracted from the Near-Infrared absorbance associated to the (meth)acrylate groups (see Experimental Section). This result clearly shows that the photoinduced reaction between MB^+ and iPr_2NEt does not efficiently lead to free radicals. As we previously mentioned, if the reaction proceeded via single e^- transfer, then an alpha amino alkyl radical from iPr_2NEt would be the most probable product. Such radical has a very high reactivity towards the vinyl groups in (meth)acrylates. Hence, the most reasonable explanation is that MB^+ and iPr_2NEt do not efficiently undergo single e^- transfer, but rather $e^-/\text{H}^+/e^-$ transfer. This observation agrees with the production of Leuco Methylene Blue, which requires $e^-/\text{H}^+/e^-$ to be formed. We also identified that the colorless product from the $\text{MB}^+/\text{iPr}_2\text{NEt}$ photoinduced reaction is long-lived and reacts very slowly with molecular oxygen. Colorless solutions were made upon irradiation of the $\text{MB}^+/\text{iPr}_2\text{NEt}$ ethanol and HEMA solutions. After no blue color remained, the solutions were left standing for hours with very minor recovery of the blue color. In contrast, Kayser and Young report that the semireduced $\text{MB}\bullet$ produced from single e^- transfer reacts for quickly with either molecular oxygen or the unreacted amine present in solution.

In contrast, the $\text{Ru}(\text{bpy})_3^{2+}/\text{iPr}_2\text{NEt}$ solution in ethanol that did not show evidence of complex formation displays a more typical efficiency towards free radical polymerization. Figure 6.3 shows that when the ruthenium complex is irradiated with a blue LED centered at 440 nm, the absorbance from the ruthenium decays slowly to about 80 % within 1600 s. However, over 25 % polymerization was observed within this irradiation. This rate of polymerization is slow as compared to conventional light-initiated polymerizations, but that is most likely because iPr_2NEt is known to be poor nucleophile. Thus, it is

reasonable to conclude that when $i\text{Pr}_2\text{NEt}$ does not form a complex with the photocatalyst, the production of free radicals will be significantly faster than when a ground state complex is formed, but generally slower as compared to other formulations with other amine reductants. We also tested the reaction of $\text{CQ}/i\text{Pr}_2\text{NEt}$ in bulk HEMA monomer with the same rate of photon absorption and the same conditions but using a blue LED centered at 480 nm. Results showed a similar free radical polymerization efficiency as compared to the $\text{Ru}(\text{bpy})_3^{2+}/i\text{Pr}_2\text{NEt}$ system (SI Section 4). Upon review of our results along with those from other groups on photoredox catalysis with $i\text{Pr}_2\text{NEt}$ we identified that when $\text{Ru}(\text{bpy})_3^{2+}$ was used with $i\text{Pr}_2\text{NEt}$ in polar aprotic solvent like DMF or MeCN the polymerization of methyl (meth)acrylate and several other monomers has been documented to be absent during irradiation (Figure 6.4-Entries 1-6)²⁰.

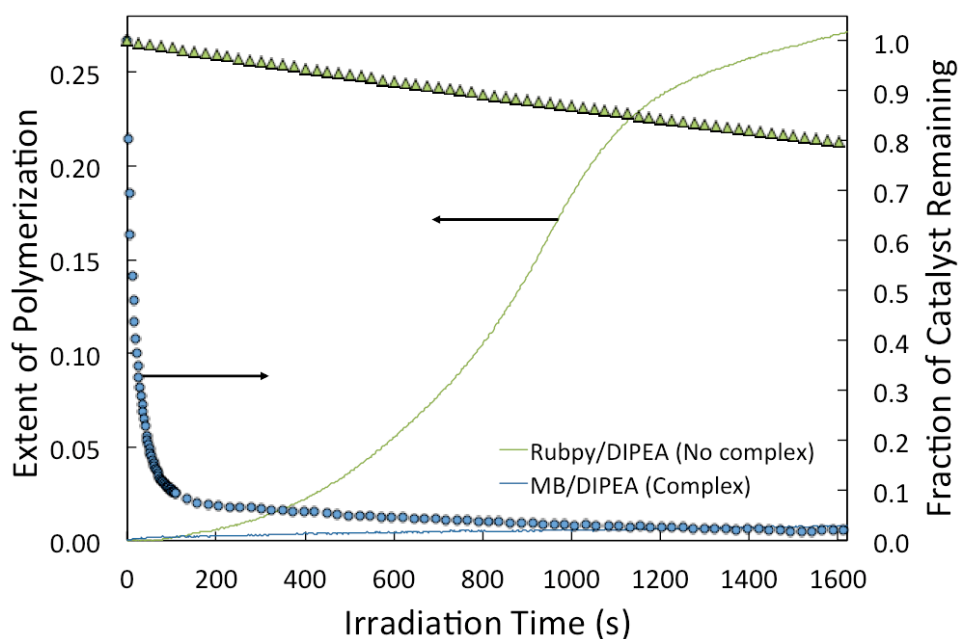


Figure 6.3 Formation of the photocatalyst/ $i\text{Pr}_2\text{NEt}$ leads to lack of free radical production. Coupled UV-Vis/FT-NIR was used to simultaneously monitor both photocatalyst and (meth)acrylate monomer consumption in real-time during irradiation. We show that whenever the photocatalyst forms a ground state complex with $i\text{Pr}_2\text{NEt}$ or Et_3N , a negligible extent of free radical polymerization was observed due to formation of closed shell species from the $e^-/\text{H}^+/e^-$ transfer. Whereas, when there is no or low tendency for the formation of the complex, the polymerization efficiency increases significantly as a result of the production of alpha amino alkyl radical from the single e^- transfer. $\text{MB}^+/\text{Et}_3\text{N}$ formulations behave similarly to $\text{MB}^+/i\text{Pr}_2\text{NEt}$, whereas $\text{CQ}/i\text{Pr}_2\text{NEt}$ formulations gave a similar result to $\text{Ru}(\text{bpy})_3^{2+}/i\text{Pr}_2\text{NEt}$

formulations. The lack of production of free radicals with such an efficient consumption of MB^+ clearly indicates that the reaction involved is an $e^-/\text{H}^+/e^-$ transfer and not a single e^- transfer process.

Our results are in agreement with the extensive literature on dye-sensitized polymerizations, which has shown that formulations containing thiazine dyes, such as MB^+ , thionine, new methylene blue, and methylene green, in combination with aliphatic amines leads to an inefficient polymerization process in most cases (Figure 6.4)^{39,40}. Higher rates of polymerization were seen with triethanolamine in polyethylene glycol, whereas lower rates were obtained in water⁴¹⁻⁴³. More importantly, when MB^+ and amine combinations are used in bulk acrylate or methacrylate monomers, the extent of polymerization is ineffectual and higher temperatures are needed to obtain observable rates of polymerization (Figure 6.4-Entry 10 & 12)^{15,16}. Higher temperatures might potentially be dissociating the ground state complex and thus leading to more efficient radical production, as well as affecting the polymerization process. Because of this issue, research has been targeted towards the addition of an oxidant, typically an onium salt, to the inefficient MB^+ /amine combinations. As we showed recently, there is two to three order magnitude in the rate of radical production upon addition of the an onium salt to $\text{MB}^+/\text{iPr}_2\text{NEt}$ because the oxidant is significantly more reactive towards LMB than molecular oxygen and because it produces free radicals from the reduction by LMB.

6.4 Conclusions

6.4.1 Guidelines to favor $e^-/\text{H}^+/e^-$ over e^- transfer in photoredox catalysis

Based on these results we propose that either production of free radicals can be favored or disfavored by rational selection of the photocatalyst/amine/solvent combination. In many instances, it has been observed that highly selective organic reactions occur only in the present of Lewis acid additive likes LiBF_4 and HCO_2H . We propose that in these cases, these Lewis acids have a higher tendency to complexate with iPr_2NEt than does the $\text{Ru}(\text{bpy})_3^{2+}$ itself, even in MeCN solvent. Thus, Stephenson's proposed mechanism including reaction from a formic acid/ iPr_2NEt complex leading to the production of an iminium cation appears to be correct, but most importantly is the main reason why slight variations in

the concentrations of the Lewis acids, or change in the amine used as the reductant can dramatically lower the yield and the selectivity.

Entry	Photocatalyst (Lewis acid)	Amine Donor	Solvent/Monomer	Complex	Radicals	Selectivity	Ref.
1	Rubpy (LiBF ₄)	iPr ₂ NEt	MeCN	Yes*	No	High	Yoon
2	Rubpy (HCO ₂ H)	iPr ₂ NEt	DMF	Yes*	No	High	Stephenson
3	Rubpy	iPr ₂ NEt	DMF	Yes	No	High	Zhang
4	Rubpy	iPr ₂ NEt	EtOH/HEMA	No	Yes	Poor	This work
5	Rubpy	Et ₃ N	MeCN	No	Yes	Poor	This work
6	Rubpy	Et ₃ N	MeCN	Yes	No	High	This work
7	MB ⁺	iPr ₂ NEt	EtOH/HEMA	Yes	No	-	This work
8	MB ⁺	iPr ₂ NEt	MeCN	Yes	No	-	This work
9	MB ⁺	Et ₃ N	HEMA	Yes	No	-	This work
10	MB ⁺	Et ₃ N	HEMA (50 °C)	No	Yes	-	Scranton
11	MB ⁺	MeN(EtOH) ₂	HEMA	Yes	No	-	This work
12	MB ⁺	MeN(EtOH) ₂	HEMA (50 °C)	No	Yes	-	Scranton
13	MB ⁺	iPr ₂ NEt	MeCN:H ₂ O (4:1)	Yes	No	High	Scaiano
14	MB ⁺	TMEDA	MeCN	Yes*	No*	-	Scaiano
15	MB ⁺	amines	H ₂ O/C ₃ H ₅ NO	No	Low	-	Eaton
16	MB ⁺	PR ₃ ,AsR ₃	H ₂ O/C ₃ H ₅ NO	No	High	-	Rust
17	MB ⁺	PR ₃ ,AsR ₃	H ₂ O/C ₅ H ₁₀ O ₂	No	High	-	Rust
18	CQ	iPr ₂ NEt	HEMA	No	Yes	-	This work

Figure 6.4 Correlation of complex formation with radical production and selectivity. Polar aprotic solvents favor complexation in general. Aliphatic amines tend to form ground state complexes for readily than aromatic amines. Bulky aliphatic amines like those analyzed by Kotani are particularly efficient at doing e⁻/H⁺/e⁻ transfer when complexated with a photocatalyst²³. Thiazine dyes, such as MB⁺, have a higher tendency to form complexes with aliphatic amines than ruthenium complexes.

This analysis suggests that it is quite possible to tune the mechanism via which a particular photoredox catalysis system operates, and thus to rationally control whether open or closed shell intermediates are formed. For instance, all of Konti's bulky aliphatic amines should behave similarly or better than iPr₂NEt in terms of lack of production of free radicals, fast rates of MB⁺ photobleaching, production of LMB, and high selectivity and yields for Yoon's cycloadditions, Stephenson's

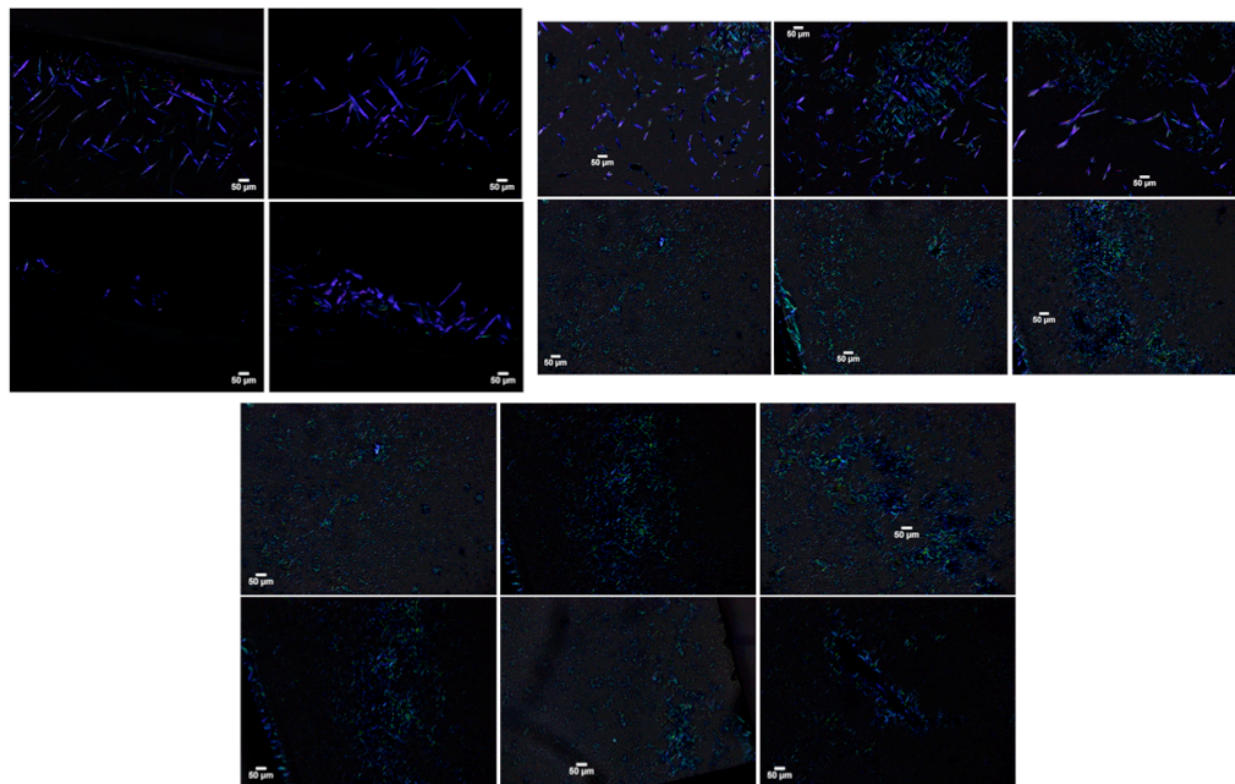
dehalogenation's, or Scaiano's hydroxylation.

6.5 References

1. Yoon, T. P., Ischay, M. A. & Du, J. Visible light photocatalysis as a greener approach to photochemical synthesis. *Nature Chemistry* **2**, 527–532 (2010).
2. Narayanam, J. M. R., Tucker, J. W. & Stephenson, C. R. J. Electron-Transfer Photoredox Catalysis: Development of a Tin-Free Reductive Dehalogenation Reaction. *J. Am. Chem. Soc.* **131**, 8756–8757 (2009).
3. Ischay, M. A., Lu, Z. & Yoon, T. P. [2+2] Cycloadditions by Oxidative Visible Light Photocatalysis. *J. Am. Chem. Soc.* **132**, 8572–8574 (2010).
4. Ischay, M. A., Anzovino, M. E., Du, J. & Yoon, T. P. Efficient Visible Light Photocatalysis of [2+2] Enone Cycloadditions. *J. Am. Chem. Soc.* **130**, 12886–12887 (2008).
5. Wallentin, C.-J., Nguyen, J. D., Finkbeiner, P. & Stephenson, C. R. J. Visible Light-Mediated Atom Transfer Radical Addition via Oxidative and Reductive Quenching of Photocatalysts. *J. Am. Chem. Soc.* **134**, 8875–8884 (2012).
6. Fors, B. P. & Hawker, C. J. Control of a Living Radical Polymerization of Methacrylates by Light. *Angew. Chem. Int. Ed.* **51**, 8850–8853 (2012).
7. Treat, N. J. *et al.* Metal-Free Atom Transfer Radical Polymerization. *J. Am. Chem. Soc.* **136**, 16096–16101 (2014).
8. Tehfe, M.-A. *et al.* Polyaromatic Structures as Organo-Photoinitiator Catalysts for Efficient Visible Light Induced Dual Radical/Cationic Photopolymerization and Interpenetrated Polymer Networks Synthesis. *Macromolecules* **45**, 4454–4460 (2012).
9. Tehfe, M.-A. *et al.* Iridium complexes incorporating coumarin moiety as catalyst photoinitiators: Towards household green LED bulb and halogen lamp irradiation. *Polymer* 1–6 (2012).
10. Eaton, D. F. in *Photoinduced Electron Transfer I* **156**, 199–225 (Springer Berlin Heidelberg, 1990).
11. EATON, D. Nonlinear optical materials. *Science* **253**, 281–287 (1991).
12. Lyubimova, T., Caglio, S., Gelfi, C., Righetti, P. G. & Rabilloud, T. Photopolymerization of polyacrylamide gels with methylene blue. *ELECTROPHORESIS* **14**, 40–50 (1993).
13. Kim, D. & Stansbury, J. W. A photo-oxidizable kinetic pathway of three-component photoinitiator systems containing porphyrin dye (Zn-tp), an electron donor and diphenyl iodonium salt. *J. Polym. Sci. A Polym. Chem.* **47**, 3131–3141 (2009).
14. Kim, D. & Stansbury, J. W. Kinetic pathway investigations of three-component photoinitiator systems for visible-light activated free radical polymerizations. *J. Polym. Sci. A Polym. Chem.* **47**, 887–898 (2009).

15. Padon, K. S. & Scranton, A. B. A mechanistic investigation of a three-component radical photoinitiator system comprising methylene blue, N-methyldiethanolamine, and diphenyliodonium chloride. *J. Polym. Sci. A Polym. Chem.* **38**, 2057–2066 (2000).
16. Padon, K. S. & Scranton, A. B. A mechanistic investigation of the three-component radical photoinitiator system Eosin Y spirit soluble, N-methyldiethanolamine, and diphenyliodonium chloride. *J. Polym. Sci. A Polym. Chem.* **39**, 715–723 (2001).
17. DeForest, C. A. & Anseth, K. S. Cytocompatible click-based hydrogels with dynamically tunable properties through orthogonal photoconjugation and photocleavage reactions. 1–7 (2011). doi:10.1038/nchem.1174
18. Pitre, S. P., McTiernan, C. D., Ismaili, H. & Scaiano, J. C. Metal-Free Photocatalytic Radical Trifluoromethylation Utilizing Methylene Blue and Visible Light Irradiation. *ACS Catal.* (2014). doi:10.1021/cs5005823
19. Pitre, S. P., McTiernan, C. D., Ismaili, H. & Scaiano, J. C. Mechanistic Insights and Kinetic Analysis for the Oxidative Hydroxylation of Arylboronic Acids by Visible Light Photoredox Catalysis: A Metal-Free Alternative. *J. Am. Chem. Soc.* **135**, 13286–13289 (2013).
20. Zhang, G., Song, I. Y., Ahn, K. H., Park, T. & Choi, W. Free Radical Polymerization Initiated and Controlled by Visible Light Photocatalysis at Ambient Temperature. *Macromolecules* **44**, 7594–7599 (2011).
21. Aguirre-Soto, A., Lim, C.-H., Hwang, A. T., Musgrave, C. B. & Stansbury, J. W. Visible-Light Organic Photocatalysis for Latent Radical-Initiated Polymerization via $2e^-/1H^+$ Transfers: Initiation with Parallels to Photosynthesis. *J. Am. Chem. Soc.* **136**, 7418–7427 (2014).
22. Du, J. & Yoon, T. P. Crossed Intermolecular [2+2] Cycloadditions of Acyclic Enones via Visible Light Photocatalysis. *J. Am. Chem. Soc.* **131**, 14604–14605 (2009).
23. Kotani, S., Osakama, K., Sugiura, M. & Nakajima, M. A Tertiary Amine as A Hydride Donor: Trichlorosilyl Triflate-mediated Conjugate Reduction of Unsaturated Ketones. *Org. Lett.* **13**, 3968–3971 (2011).
24. Osakama, K., Sugiura, M., Nakajima, M. & Kotani, S. Enantioselective reductive aldol reaction using tertiary amine as hydride donor. *Tetrahedron Letters* **53**, 4199–4201 (2012).
25. Singh, A., Arora, A. & Weaver, J. D. Photoredox-Mediated C–H Functionalization and Coupling of Tertiary Aliphatic Amines with 2-Chloroazoles. *Org. Lett.* **15**, 5390–5393 (2013).
26. Liu, Y., Yamamoto, S., Fujiyama, Y. & Sueishi, Y. Kinetic study on the reversible hydride transfer between methylene blue and thionine. *Phys. Chem. Chem. Phys.* **2**, 2367–2371 (2000).
27. Liu, Y., Yamamoto, S. & Sueishi, Y. Photoinduced hydride transfer reaction between methylene blue and leuco crystal violet. *Journal of Photochemistry and ...* (2001). doi:10.1016/S1010-6030(01)00530-5
28. Yamamoto, S., Fujiyama, Y., Shiozaki, M., Sueishi, Y. & Nishimura, N. Hydride transfer reactions of leuco methylene blue and leuco thionine with some p-benzoquinones. *Journal of*

- Physical Organic Chemistry* **8**, 805–809 (1995).
29. McKay, R. B. Red Forms of Methylene Blue. *Nature* **210**, 296–297 (1966).
 30. Seal, B. K., Sil, H. & Mukherjee, D. C. Independent determination of equilibrium constant and molar extinction coefficient of molecular complexes from spectrophotometric data by a graphical method. *Spectrochimica Acta Part A: Molecular Spectroscopy* **38**, 289–292 (1982).
 31. Decker, C. & Moussa, K. A new method for monitoring ultra-fast photopolymerizations by real-time infra-red (RTIR) spectroscopy. *Die Makromolekulare Chemie* **189**, 2381–2394 (1988).
 32. Eaton, D. F. *Dye Sensitized Photopolymerization*. 427–487 (John Wiley & Sons, Inc., 1986). doi:10.1002/9780470133439.ch6
 33. RABINOWITCH, E. & Epstein, L. F. Polymerization of dyestuffs in solution. thionine and methylene blue1. *Journal of the American Chemical ...* (1941). doi:10.1021/ja01846a011
 34. Hammes-Schiffer, S. Comparison of hydride, hydrogen atom, and proton-coupled electron transfer reactions. *Chemphyschem* **3**, 33–42 (2002).
 35. Deno, N. C., Peterson, H. J. & Saines, G. S. The Hydride-Transfer Reaction. *Chem. Rev.* (1960).
 36. Lalevée, J., Allonas, X. & Fouassier, J.-P. N–H and α (C–H) Bond Dissociation Enthalpies of Aliphatic Amines. *J. Am. Chem. Soc.* **124**, 9613–9621 (2002).
 37. Kayser, R. H. & Young, R. H. THE PHOTOREDUCTION OF METHYLENE BLUE BY AMINES—I. A FLASH PHOTOLYSIS STUDY OF THE REACTION BETWEEN TRIPLET METHYLENE BLUE AND *Photochem Photobiol* (1976).
 38. Kayser, R. H. & Young, R. H. The photoreduction of methylene blue by amines—II. An investigation of the decay of semireduced methylene blue. *Photochem Photobiol* (1976).
 39. Chen, C. S. H. Dye-sensitized photopolymerization. I. Polymerization of acrylamide in aqueous solution sensitized by methylene blue–triethanolamine system. *Journal of Polymer Science Part A: General Papers* **3**, 1107–1125 (1965).
 40. Chen, C. S. H. Dye-sensitized photopolymerization. II. Enhanced sensitization by combination of a cationic and an anionic dye. *Journal of Polymer Science Part A: General Papers* **3**, 1127–1136 (1965).
 41. Chen, C. S. H. Dye-sensitized photopolymerization. III. Structural effects of thiazine dyes. *Journal of Polymer Science Part A: General Papers* **3**, 1137–1154 (1965).
 42. Chen, C. S. H. Dye-sensitized photopolymerization. IV. Enhanced rates of polymerization of acrylamide in ethylene glycol, sensitized by thiazine dyes with triethanolamine. *Journal of Polymer Science Part A: General Papers* **3**, 1155–1170 (1965).
 43. Chen, C. S. H. Dye-sensitized photopolymerization. V. Polymerization of acrylamide in deaerated systems. *Journal of Polymer Science Part A: General Papers* **3**, 1807–1823 (1965).



6.S1. Microscope images of MB^+ and ground state complex crystals grown from ethanol solutions, from top to bottom, left to right: MB^+ , $\text{MB}^+/\text{Et}_3\text{N}$ and $\text{MB}^+/\text{iPr}_2\text{NEt}$.

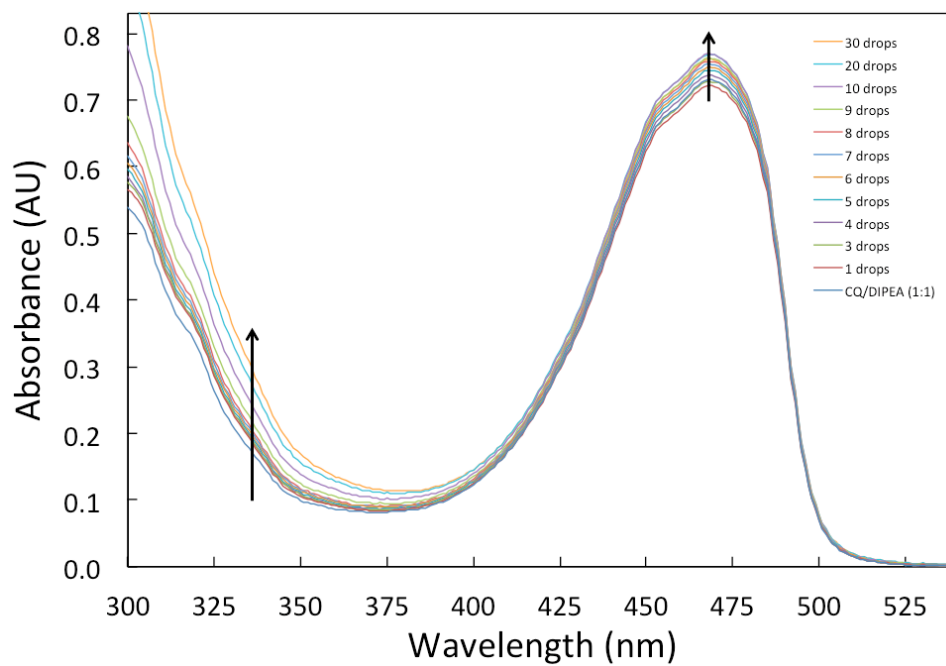


Figure 6.S2. Changes in UV-Vis absorbance of CQ upon drop-wise addition of iPr_2NEt in ethanol.

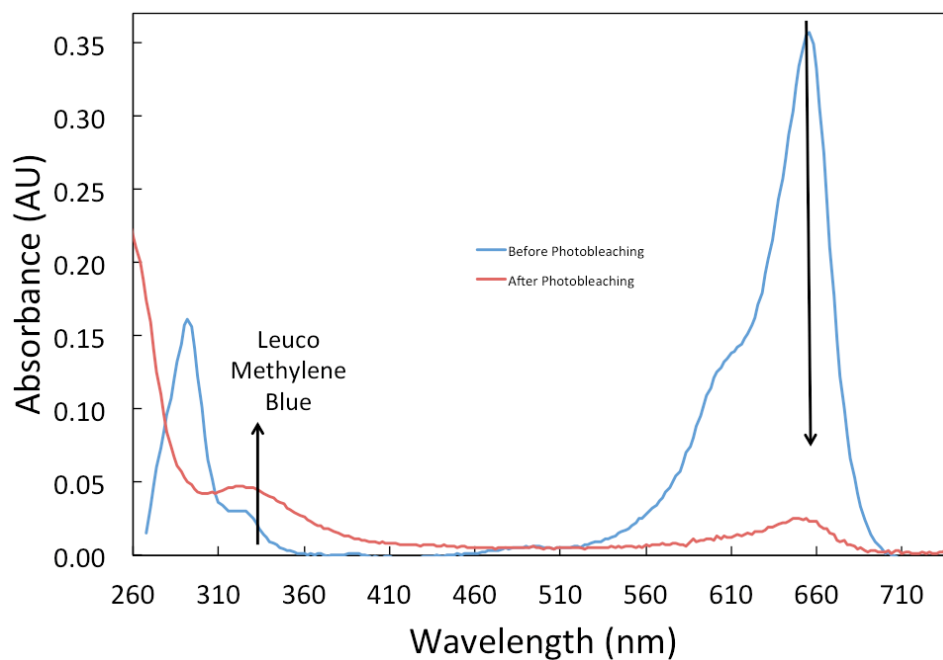


Figure 6.S3. Formation of Leuco Methylene Blue from UV-Vis analysis of MB^+ /amine solution in ethanol during irradiation with 660 nm red LED.

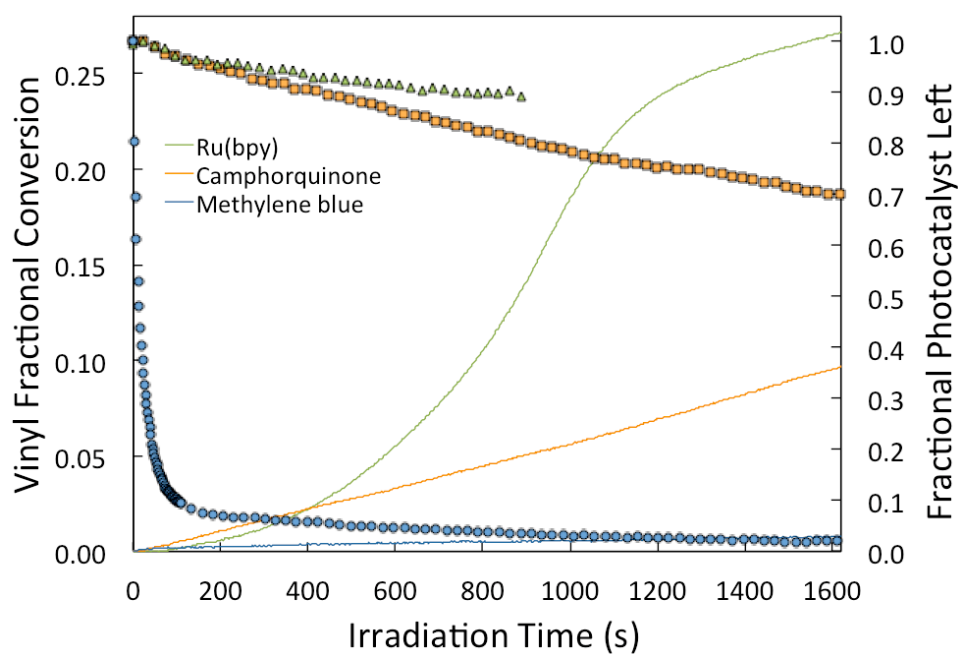


Figure 6.S4. Photocatalyst and monomer consumption vs. time for CQ/ $i\text{Pr}_2\text{NEt}$ and MB^+ / $i\text{Pr}_2\text{NEt}$ solutions in HEMA.

Chapter 7

Long-lived macroradicals stabilized by supramolecular interactions: Self-organization and the Trommsdorff-Norrish effect

Abstract

We report the prolonged persistence of methacrylate-based macroradicals stabilized by self-organization via hydrogen bonding interactions that leads to hindered bimolecular termination and, as a result, unusually extended vinyl polymerization after brief initial irradiation periods. We analyzed the polymerization of a hydroxylated mono-vinyl methacrylate, 2-hydroxyethyl methacrylate (HEMA), using conventional photoinitiators to produce free radicals that initiate the polymerization upon irradiation. It was found that the free radical initiated polymerization of the vinyl groups from the methacrylate continues in the dark for unusually prolonged periods in the order of thousands of seconds after the production of radicals has ceased, i.e. when the irradiation is extinguished. Such an unusual behavior is explained in this work by intermolecular hydrogen bonding interactions between the loosely crosslinked poly-HEMA networks. These supramolecular interactions can significantly reduced the mobility of the developing macromolecular structure. Multiple hydrogen bonding sites can then self-organize by forming hydrogen bridges between the oxygen atoms from the carbonyl and the alcohol and the hydrogen atoms from the pendant alcohol groups. As this self-organization reduces the mobility of the network it leads to an enhanced Trommsdorff-Norrish effect by which the propagation and termination kinetics are reduced as a function of the extent of the polymerization. We confirmed using EPR spectroscopy that the addition of the alcohol group leads to long-lived propagating radicals and that such radicals are found in a lower mobility environment. The extent of the latent vinyl polymerization was also sensitive to physical mobility restrictions imposed on the polymerizing samples. Furthermore, the temperature dependence of the polymerization that occurs in the dark indicates that chain-transfer is not responsible for such an unusual behavior. These findings are important for the rational design of novel monomers for free radical light-triggered polymer syntheses where high rates of polymerization and high final conversions are required, as in most applications of polymer materials.

7.1 Introduction

Methacrylate and acrylate monomers are important precursors for the free radical initiated synthesis of polymers utilized in a broad range of applications: stereolithography¹, holography², orthopedic implants³, dental restorative materials⁴, printed circuits⁵, tissue engineering⁶, among many others. The single most important property of a (meth)acrylic monomer is arguably the rate of polymerization (R_p). Typically, acrylates are more reactive than their methacrylate counterparts^{7,8}. Furthermore, monomers containing multiple vinyl groups have been documented to react significantly than mono-vinyl monomers^{9,10} in most instances. Additionally, moderate to high viscosity monomers (although not excessively high) are known to generally polymerize at high rates than low viscosity monomers primarily due to mobility restricted termination⁸. However, using highly viscous monomers is often not practical. Hence, diluents are required to allow the monomer formulation to be more easily handled before the polymerization occurs, and typically increase the final vinyl conversion attainable, i.e. reducing the amount of residual functional groups as well as extractable free monomer. Nonetheless, inert diluents often decrease the rate of polymerization. One of the biggest challenges in the development of (meth)acrylic monomer formulations has been the synthesis of reactive diluents that lower the viscosity of the initial liquid monomer composition, as well as the amount of residual vinyl groups, without compromising the rate of polymerization^{7,11-13}. Mono-vinyl acrylates and methacrylates can be used as reactive diluents. Nevertheless, since they tend to contribute to lower reactivity than their multi-vinyl counterparts, attention has been focused on finding or synthesizing mono-vinyl monomers than can polymerize at faster rates than what is normally expected. It has been observed that the secondary functionality of mono-vinyl acrylate and methacrylate monomers, defined as the non-polymerizable functional group covalently attached to the vinyl ester moiety, is key in determining their rates of polymerization^{11,14-17}. Despite the proposal of several theories to explain the connection between the chemistry of the secondary functionality and the R_p 's, a conclusive explanation for such correlation has remained elusive. In this work, we study the polymerization of a widely used mono-vinyl methacrylate

monomer, namely 2-hydroxyethylmethacrylate (HEMA), which contains an alcohol group as the secondary functionality, and it is used as reactive diluent due to its unusually high rate of polymerization.

Secondary functional groups that have been studied thus far include carbonates^{13,17}, carbamates¹⁸⁻²⁰, oxazolidones²¹, alcohol^{22,23}, and urethanes²⁴. With some of these monomers, the rates of polymerization are equivalent or even higher than multi-vinyl analog monomers, while achieving a higher final conversion of vinyl groups¹⁴. Proposed theories about the explanation of how certain secondary functional groups lead to high rates of photopolymerization include: 1) creation of covalently linked polymer networks by hydrogen abstraction (from labile atoms in the secondary functional group), 2) formation of covalent crosslinks from di-vinyl impurities in the monomer, and 3) supramolecular interactions altering the kinetics of the termination reactions (e.g. radical-radical quenching). The key aspect to note with these three theories is that ultimately they all attempt to explain the unexpectedly fast rates of polymerization by the effect that reduced mobility (either by formation of covalent crosslinks or by supramolecular interactions between the pendant groups) has on the termination kinetics. This concept is traditionally referred to as the Trommsdorff-Norrish or gel effect, which states that: “a marked increase in rate of vinyl consumption is observed toward the end of the polymerization, mainly in bulk or concentrated monomer solutions, as a result of the increase in viscosity of the medium as a function of the extent of polymerization and associated to a loss in the steady state kinetics.” In other words, the increase in viscosity, i.e. reduction in mobility, leads to the well-established diffusion-controlled termination kinetics of the propagating macroradicals, which results in more radicals being generated than those being terminated. In consequence, the concentration of radicals increases if the rate of initiation is sustained (e.g. as when irradiation is continuously used to produce radicals). The connections between these theories with the Trommsdorff-Norrish effect have been previously discussed. For example, increasing the initial concentration of crosslinking agent(s), i.e. reducing the mobility of the polymer network, leads to an earlier onset of the Autoacceleration (gel) effect, but does not change the initial rate of the polymerization²⁵. On the other hand, addition of a hydroxyl group to N-Butyl acrylate, making it

hydroxybutyl acrylate, led to a dramatic increase in the initial rate of polymerization as well as a considerably earlier onset of Autoacceleration. The same observation was made when comparing HEMA against 2-methoxyethylmethacrylate (MEMA). Despite the greater similarities in dipole-dipole interactions between these two monomers, HEMA showed a dramatic increase in the rate of polymerization from the very early stages of the reaction. Chain-transfer reactions between methacrylate monomers have been documented to be limited or absent, and hence these are not expected to contribute to such a large acceleration of the vinyl group consumption. These monomers were purified to remove any esterification products that can act as crosslinking agents making it difficult to assume that any leftover di-vinyl molecules could generate such large differences in the polymerization kinetics²⁵. As a result of these observations, the most likely explanation for the dramatic increases in R_p seen in hydrogen bonding mono-vinyl monomers was proposed as being related to a certain “organization” of the developing macromolecular architecture. Nevertheless, no conclusive evidence or analysis was presented to explain how such an organization occurs.

A theory on the pre-organization of the monomer molecules before polymerization has been proposed as follows: supramolecular interactions (hydrogen bonding, dipole-dipole, or π - π interactions) facilitated by the secondary functional groups may align and place the reactive vinyl groups (C=C bonds) in closer proximity to one another²⁴⁻²⁶. If this were the case, such alignment could increase the effective monomer concentration around the propagating radicals, facilitating the propagation of the macroradicals. This theory has been exclusively analyzed for the polymerization of mono-vinyl acrylates and not for methacrylates, which we study in this work. Jansen and coworkers reported that the maximum rate of polymerization of the acrylates that were tested is strongly dependent on the ability to form hydrogen bonds by the secondary functionality²⁶. Three main observations were made to support this theory: first, there seems to be a correlation of the distance between the hydrogen bonding site and the C=C bond in the monomer molecules with the rate of polymerization achieved; second, the polymerization of hydrogen bonded mono-acrylates displays an Anti-Arrhenius temperature dependence; lastly, the fraction of

isotactic polymer sections increased with increasing hydrogen bonding contributions from the secondary functional groups. However, in these few reports, the requirement for the organization of the hydrogen bonding sites to occur “before” (pre-) the polymerization was not assessed. It is likely that self-organization both before and during the reaction is equally important. Furthermore, differences in initial viscosity were not considered²⁷. Herein, we present evidence supporting the importance of organization of the hydrogen bonding pendant groups during the light-induced polymerization for methacrylate monomers. The role of such organization both before (preorganization) and during the polymerization is discussed. Furthermore, we expand the organization theory by incorporating the analysis of the effect that such supramolecular organization has on the stability of the propagating macromolecular radicals. We propose that whilst an alignment of the reactive C=C bonds could accelerate the polymerization rate, the reduction in segmental and translational motion of the propagating radicals caused by the aligned pendant groups may as well be the most important mechanism via which the high rates are achieved. This refinement of the pre-organization would not oppose to any of the previous observation, but would explain them based upon the reduction of termination²² (Trommsdorff-Norrish effect) as opposed to the acceleration of the propagation kinetics due to C=C bond alignment.

The analysis of highly reactive mono-vinyl acrylate and methacrylate monomers has almost exclusively involved continuous irradiation^{12,14,22,23}. Under such reaction condition, the production of radicals is sustained throughout the polymerization process. However, experiments with these atypical monomers where the samples are partially irradiated are relatively scarce^{22,28-30}. If irradiation were ceased at a particular point in time (and vinyl conversion) before the end of the reaction, no more radicals would be produced. By doing so, the stability or lifetime of the macroradicals could be evaluated, as well as the effect of hydrogen bonding on the termination kinetics. This can provide additional information on the mechanism(s) by which macromolecular organization, due to interactions between pendant functional groups, influences the termination of the propagating radicals, and as a result the overall rate of polymerization. In turn, this analysis can, not only, aid in the more comprehensive understanding of

polymerization reactions in general, but also provide further evidence of the often complex structure-kinetics-property relationships that can facilitate a rational design of polymer materials.

7.2 Experimental section

7.2.1 Materials

Ethylmethacrylate (EMA), 2-Hydroxyethyl methacrylate (HEMA) and 2-hydroxypropylmethacrylate (HPMA) were used as monomer. Camphorquinone (CQ) and ethyl-4-dimethylaminobenzoate (EDMAB) as well as Methylene blue (MB^+), N,N-diisopropylethylamine (DIPEA), and diphenyliodonium chloride salt (DPI-Cl) were used as photoinitiator systems. All materials were commercially obtained from Aldrich (Milwaukee, WI), and were used as received. 2,2-Dimethoxy-2-phenylacetophenone (DMPA) was received from Ciba and also used without purification.

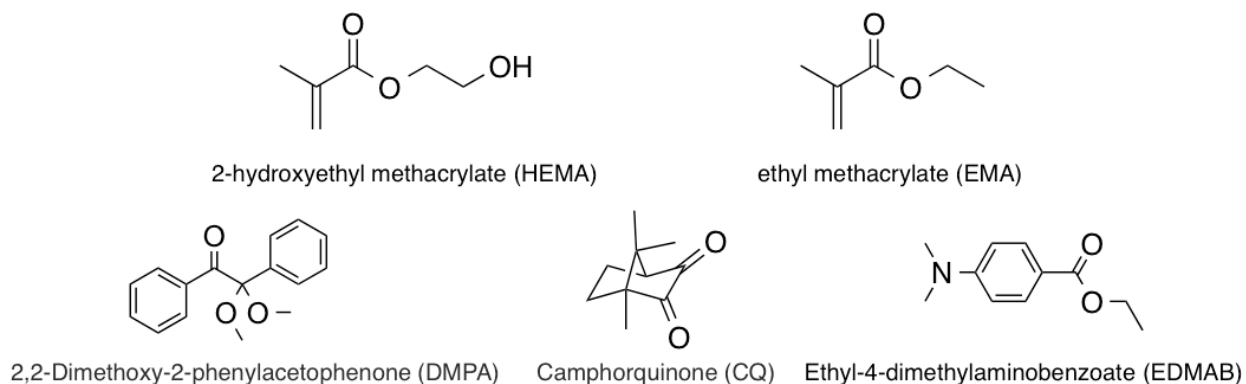


Figure 7.1 Structures of the monomers and photoinitiators used. HEMA and EMA are the methacrylate monomers. DMPA is a Type I photoinitiator and the CQ/EDMAB combination functions as a Type II photoinitiator.

7.2.2 Light source

Incident irradiance was measured with a radiometer (6253, International Light Technologies, Peabody, MA) within two probes, one for the 290-400 nm range and the other for the 400-700 nm range. For all the CQ/EDMAB-initiated formulations, the 400-500 nm output of a mercury lamp (EFOS Acticure)

was used with the incident irradiance verified by radiometer. For formulations containing DMPA the mercury lamp emission was restricted to 365 nm light with a narrow pass band filter.

7.2.3 Fourier transform-infrared spectroscopy (FT-IR)

Bulk polymerizations of HEMA were monitored in real-time with a FT-IR spectrophotometer (Nicolet Magna-IR Series II, Thermo Scientific, West Palm Beach, FL) by following either the peak area of the first overtone absorption band for the methacrylate =CH₂ group (6167 cm⁻¹) or the peak associated with the C=C stretching vibration from the methacrylate at around 1637 cm⁻¹. The spectrophotometer was equipped with a KBr beam splitter, a MCT/A detector, and an in-house fabricated horizontal stage adapted for *in-situ* photopolymerization experiments.²⁷ The distance between the light source and the sample was ~7 cm to ensure uniform irradiation across the entire sample with controlled irradiance values. An 800 nm cut-off filter was used to eliminate the 633 nm HeNe reference beam within the NIR output signal when red-light (633 nm) sensitive photoinitiator were used.

The sample holder for the *in-situ* polymerization, both in the dark and in the light, consisted of a 1 mm height, 1.6 cm diameter disc fabricated by interjecting a perforated silicone rubber shim in between two 1 mm thick glass slides. Rate of polymerization was calculated by numerically differentiating the peak area as a function of time. Concentrations used were as follows: [DMPA]= 0.5 wt %, [CQ] = 0.02 M and [EDMAB] = 0.04 M, [MB⁺] = 4 mM, [DIPEA] = 0.2 M, [DPI⁺] = 0.04 M. Irradiation intensity for the DMPA formulations was 4 mW/cm². For the CQ/EDMAB system the intensity used was 22-23 mW/cm² of light from the mercury lamp with long band pass filter between 400-500. All FT-NIR-monitored polymerizations with MB⁺/DIPEA/DPI⁺ were performed with 12-13 mW/cm². The intensities of the CQ/EDMAB and MB⁺/DIPEA/DPI⁺ were chosen to equate to approximately the same rate of photons absorbed per time per volume taking into account the absorbance spectrum of both photoinitiators.

7.2.4 Electron paramagnetic resonance spectroscopy (EPR)

A Bruker X-band EPR spectrometer was used for the real-time photopolymerization experiments. A custom-built support was integrated to allow for irradiation through the cavity.

7.3 Results and discussion

7.3.1 Dependence of the latent polymerization on the radical production rate

Recently we reported the latent polymerization observed in formulations containing Methylene Blue (MB^+)/Hünig's base/Diphenyliodonium salt as a visible light photoinitiator system that produces free radicals by a unique photocatalysis mechanism. Due to the particular radical production scheme of this photoinitiator combination, a prolonged latent polymerization was observed to follow the rapid MB^+ photobleaching after the curing light was shuttered. However, in doing so we also noticed that even with conventional photoinitiators, 2-hydroxyethyl methacrylate and 2-hydroxypropyl methacrylate (not shown) still exhibit an extended consumption of vinyl groups after the irradiation has ceased (Figure 7.2-Left). This observation led us to analyze the polymerization of this monomer in order to elucidate the reason for such an unusually prolonged reactivity that extends beyond the initial irradiation period. In Figure 7.2-Left, we show the fractional vinyl conversion of HEMA with MB^+ /DIPEA/ DPI^+ , CQ/EDMAB, and MB^+ /DIPEA. It was previously identified that the MB^+ /DIPEA produces radicals very inefficiently³⁰. It was observed that regardless of the vinyl conversion at which the irradiation was extinguished, no latent polymerization was observed with this photoinitiator combination. However, when we use conventional photoinitiators, namely CQ/EDMAB and DMPA (Figure 7.3- Left), or the MB^+ /DIPEA/ DPI^+ combination, a significantly prolonged extent of vinyl consumption was present. We propose that such differences are due to the amount of radicals produced during the irradiation for the conventional single and dual component initiators. As we pointed out in another report, the MB^+ /DIPEA/ DPI^+ system is able to produce radicals via a redox process after brief initial exposure to light. Furthermore, this photoinitiator produces two very reactive phenyl radicals per every photon absorbed, based on the photocatalysis mechanism presented elsewhere³⁰. In contrast, the CQ/EDMAB combination produces only one amine-based radical per photon absorbed. However, we showed that the rate of polymerization with these photoinitiator systems is comparable at equivalent amounts of photons absorbed. Ultimately, this initial

observation indicates that the extent of the latent polymerization may be dependent upon the structure of the polymer network that is formed, which depends on the amounts of radicals produced.

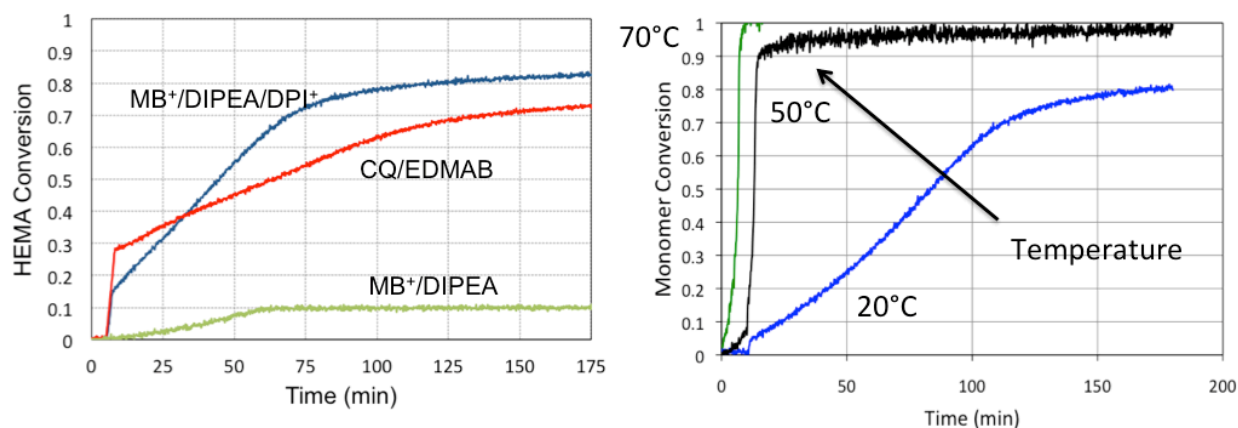


Figure 7.2 Latent polymerization of 2-hydroxyethyl methacrylate (HEMA) with three photoinitiators and at different temperatures. Left- Plot of the vinyl fractional conversion of HEMA with Methylene Blue (MB^+) and *N,N*-diisopropylethylamine (DIPEA), Camphorquinone (CQ) and ethyl 4-dimethylaminobenzoate (EDMAB), and MB^+ /DIPEA/Diphenyliodonium chloride (DPI^+). MB^+ /DIPEA combination shows no latent polymerization, CQ/EDMAB shows a little over 40% vinyl conversion after light extinction, and MB^+ /DIPEA/ DPI^+ shows over 65% vinyl polymerization in the dark. Also see SI Section 1 for change in mechanical properties (G' and G'') in the dark as a confirmation of the latent polymerization in HEMA. Right- Plot shows the Arrhenius behavior of the polymerization of HEMA with the MB^+ /DIPEA/ DPI^+ combination. Since radicals are produced from the redox reactions between MB-intermediates and DPI^+ , as well as between DIPEA and DPI^+ .

It can be observed in Figure 7.2-Right that when MB^+ /DIPEA/ DPI^+ formulations in bulk HEMA are heated to higher temperatures during the photopolymerization, the rate of polymerization increases, as well as the final vinyl conversion. As we reported before, this photoinitiator is characterized by a radical production primarily from a ground state redox reaction³⁰. Initiation of polymer synthesis using redox reactions that produce free radicals is expected to be temperature dependent, as opposed to reactions where radicals are produced photochemically³¹. Typically an Arrhenius dependence on temperature is observed for such systems, as the one presented here for the polymerization of HEMA with MB^+ /DIPEA/ DPI^+ . In contrast, when we increased the temperature during the photopolymerization of HEMA with conventional photoinitiators (DMPA and CQ/EDMAB) an Anti-Arrhenius behavior was observed (Figure 7.3- Right). It is important to note that at the elevated temperature, polymerization is observed even before irradiation; while on the timescale of the experiments here, no spontaneous

polymerization is noted under ambient conditions. During irradiation the rates remain relatively level until the point at which we stop the light exposure. This further confirms that temperature dependent radical production leads to an Arrhenius dependence in the consumption of vinyl groups. The latter is meant to serve as a reference for the evaluation of the temperature dependence observed in the polymerization of HEMA with conventional photochemical initiators, as discussed in the next section.

7.3.2 Latent polymerization as a function of the conversion-at-light shut-off and temperature

Next, we studied the extent of the consumption of vinyl groups after several irradiation times (20, 30, 35, and 45 s) in the presence of DMPA under 365 nm light from a mercury lamp. It was observed that the extent of the consumption of vinyl groups in the dark decreases with increasing conversion at light shut-off, where stopping the irradiation at around 37 % (45 s) conversion achieved 43 % conversion after light cessation as opposed to slightly over 55 % ‘dark’ conversion achieved when shutting the light at around 8 % (20 s) conversion. In these experiments it is important to note that, after the irradiation is ceased, the rate of polymerization remains constant for a few seconds before the noticeable change in slope shown in Figure 7.3-Right is observed. This is indicative of two different regions that are present after light exposure: the first, where the slope in the conversion vs. time curves is virtually unchanged, and the second, where a slower but non-zero slope (R_p) is identified. When we performed a similar set of partial irradiations for multi-vinyl methacrylates (data not shown), namely the dental formulation of BisGMA/TEGDMA 70:30, we did not observe these two regions after irradiation. With these other monomers we only observed a few seconds of vinyl consumption after the irradiation was stopped; then the polymerization stopped completely (the slope became zero). It appears like the timescale of both regions seen for HEMA are dependent on the conversion at which the irradiation ceases. For example, when the light was shuttered at 8 % conversion, the inflection point (change in slope) occurs at ~10 % conversion, whereas when exposure to light continued up to 37 %, the inflection point is seen at around 50 % conversion. Such a quick jump in conversion at approximately the same rate (before the inflection point) was observed by Decker and coworkers²⁸. In their reports, Decker proposed that the post-

irradiation conversion could constitute a significant fraction of the overall final conversion when photopolymerizing multi-vinyl acrylate monomers. The latter has been interpreted as being due to mobility restrictions delaying slightly the termination of most of the radicals that were present at the time when irradiation is stopped. We observed the exact same evolution of conversion for the BisGMA/TEGDMA formulations with same amount of DMPA and light intensity as the ones used with HEMA. Ultimately, this can be interpreted herein as occurring as well in the partial exposure experiments with HEMA, i.e. mobility restrictions sustain the rate of vinyl consumption for a few seconds before the termination of most of the propagation radicals becomes significant.

However, the slower but non-zero rate of polymerization observed in HEMA (after the inflection point) seems to indicate that the effective concentration of propagating radicals that was present just before the exposure was terminated remains higher than with typical monomers, such as with BisGMA/TEGDMA. This could be explained if the termination of the propagating radicals in HEMA is somewhat lower than in conventional monomers. Furthermore, a correlation between the extent and duration of this second slower region with the conversion at light shut-off can be made. For example, the fraction of vinyl groups consumed after the inflection varied as follows: 55, 55, 50, 30 %, for the increasing exposure times. Such a decrease in the vinyl consumption after the inflection points may also be linked to a reduction in the mobility of the polymer network at the moment when then the photochemical initiation is no longer present.

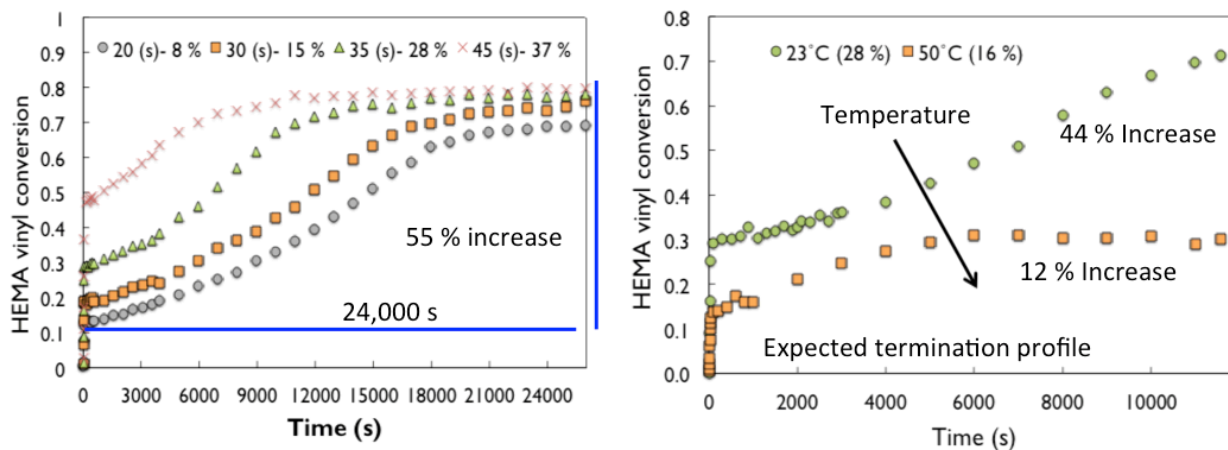


Figure 7.3 Latent polymerization of 2-hydroxyethyl methacrylate (HEMA) with 2,2-Dimethoxy-2-phenylacetophenone (DMPA) photoinitiator after several irradiation times and different temperatures. Left- Plot shows the latent vinyl consumption of HEMA upon 20, 30, 35 and 45 s of irradiation with a mercury lamp filtered to 365 nm light. Up to 55 % vinyl consumption is observed after the light has ceased. The latent polymerization lasted up to 24,000 s. Right- Anti-Arrhenius temperature dependence indicates significant effect from hydrogen bonding the propagation kinetics. Decrease of the extent of latent polymerization upon heating of the HEMA samples. At 50°C most of the hydrogen bonds are broken and this leads an approximate 4-fold decrease in the latent polymerization in terms of vinyl conversion after light cessation.

Additionally we tested the response of the latent vinyl conversion to temperature. In Figure 7.3- Right we show an inverse dependence on temperature for the rate of vinyl consumption in all the different stages of the polymerization: irradiation, fast dark polymerization, and slow dark polymerization. For these experiments we used the same initial DMPA concentration, irradiation intensity and exposure time. However, it can be observed that approximately 28 % conversion was reached at the moment when the light was extinguished at 23 °C as opposed to only about 16 % at 50 °C. An increase in conversion of the vinyl groups of 2-3 % was seen at 23 °C, whereas at 50 °C there was no noticeable fast jump in conversion after light cessation. In other words, at 50 °C we observed only one dark polymerization rate regime which was slower but non-zero up to about 30 % conversion.

At 50 °C, the polymerization was completely quenched at about 6000 s, whereas at 23 °C the plateau conversion was reached only after 15,000 s. This is an amazingly long lifetime for free radical persistence particularly considering that polyHEMA forms a loosely crosslinked network that should

support relatively high mobility below vitrification. Hence, we used typical the rate of termination and for usual concentrations of propagating radicals to determine that a common timescale for reaching a final plateau conversion is roughly 0.1-17 s after irradiation^{22,28,31}. This means that the extent of the latent polymerization of HEMA is two to three orders of magnitude greater than with conventional monomers. Decker reported values on the order of 0.6-1 s of post-irradiation polymerization with increases of up to 10 % with multi-vinyl acrylates. Lee and coworkers on the other hand reported 2-5 s to reach the plateau conversion after light was ceased at between 10 and 39 % conversion of mono-vinyl hydroxylated acrylates. However, García et al. reported the consumption of vinyl groups after an initial irradiation for durations between 10,000 and 25,000 s using mono-vinyl methacrylates with varying sizes of secondary functional groups³²⁻³⁴, which included: butyl, dodecyl and silyloxy. Their results for the bulk photopolymerization of these methacrylates by FT-IR, PLP-SEC and EPR spectroscopy confirmed that even at low monomer conversions at light shut-off, a certain non-negligible macroradical concentration remains. They also observed that conversion continued in the dark after the initial irradiation up to 70 % conversion in some cases and for timescales ranging from 600 to 28,000 s.

7.3.3 Effect of physical mobility restrictions on the extent of the latent vinyl consumption

For all the results presented up to this point Near-Infrared spectroscopy was utilized to monitor the concentration of the vinyl groups in the bulk specimens. For such FT-NIR experiments, samples were contained in between two glass slides with a rubber spacer of a thickness of either 0.5 or 1 mm. Hence, the samples that were contained within the perforated rubber gasket were not compressed by the metal clamps used to hold the glass slides in place. However, we wanted to study the extent of the post-irradiation consumption of vinyl groups in Mid-Infrared region because Lee et al. reported their shorter dark conversion periods for hydroxylated mono-vinyl acrylates using thinner films monitored by FT-MIR. Hence, we replicated their experimental conditions for the partial irradiation of HEMA with DMPA using several exposure times: 15, 50, 60 s and continuous irradiation (Figure 7.4). This would allow us as well to rule out any effects that might have been present in the thicker FT-NIR samples related to light

attenuation and temperature gradients forming in the samples. It is expected that all samples analyzed here are optically clear and that heat dissipation based on the thinner aspect ratio would prevent any heterogeneous temperature distributions.

First, it was proven that if we expose the non-hydroxylated analog of HEMA, ethyl methacrylate (EMA), to the same irradiation intensity with the same initial DMPA loading a 12-fold longer exposure time is required to achieved the same conversion of $\sim 5\%$ conversion at which point the light was switched off. Moreover, with EMA, the vinyl consumption is almost immediately quenched as would be expected for a traditional monomer. On the other hand, with HEMA we observed the same two regimes in the rate of polymerization post-irradiation that were seen with FT-NIR (Figures 7.2 and 7.3): first, there is a quick jump in conversion from 5 to 13 % at about the same rate as that during the light exposure. Subsequently the slope of the conversion vs. time curve drops but remains non-zero. The latter indicates that the macroradical concentration drops sharply just after the light is shut-off, but that a non-negligible concentration of persistent macroradicals continues the polymerization for long periods of time. In their analysis, García et al. included the estimation of the rate constants for termination based on the partial irradiation experiments. They confirmed that even at low conversions the rate constant for termination (k_t) can be dramatically affected by the chain-length of the macromolecular chains formed during the initial light exposure.

Furthermore, it can be observed that the rate of polymerization seems to be slightly slower for the FT-MIR analysis than in the FT-NIR results during the exposure time, e.g. 21 % conversion in 50 s and 37 % conversion in 45 s, respectively. We hypothesized that this is related to the compression of the samples in between the salt plates by the metal clamps used to keep the specimen construct in place. The thin films in the FT-MIR samples were under 10 μm thick. But, most importantly a significant mechanical force was applied on the sample, which can be thought of as restricting the segmental and translational motion of the developing polymer structure. Additionally, the HEMA thin films where the light was switched off at 5 % conversion in the FT-MIR experiments behave more similarly to what would be

expected from conventional monomers, as opposed to the thicker HEMA samples used for the FT-NIR where the irradiation was stopped at about 8 %. However, the samples in the compressed thin films actually achieved a higher extent of vinyl consumption within the regime associated with the slower rate of polymerization, i.e. after the inflection point. For example, the samples with an inflection point around 21 % conversion displayed an increase in conversion within 3000 s of 29 % in the compressed thin film specimens, as opposed to the ~ 5% increase in conversion within 3000 s in the thicker FT-NIR specimens. This seems to support the idea that the mobility of the medium is the main reason behind the latent vinyl consumption post-irradiation. In other words, if we applied a certain compression force to the developing macromolecular structure it is analogous to lower the temperature of the sample and thus reducing the relaxation of the macromolecules. Hence, it would be expected that we should see an acceleration of the rate at which the vinyl groups are consumed after the inflection point, as opposed to what happens when we increase the temperature during the polymerization experiments (Figure 7.3-Right).

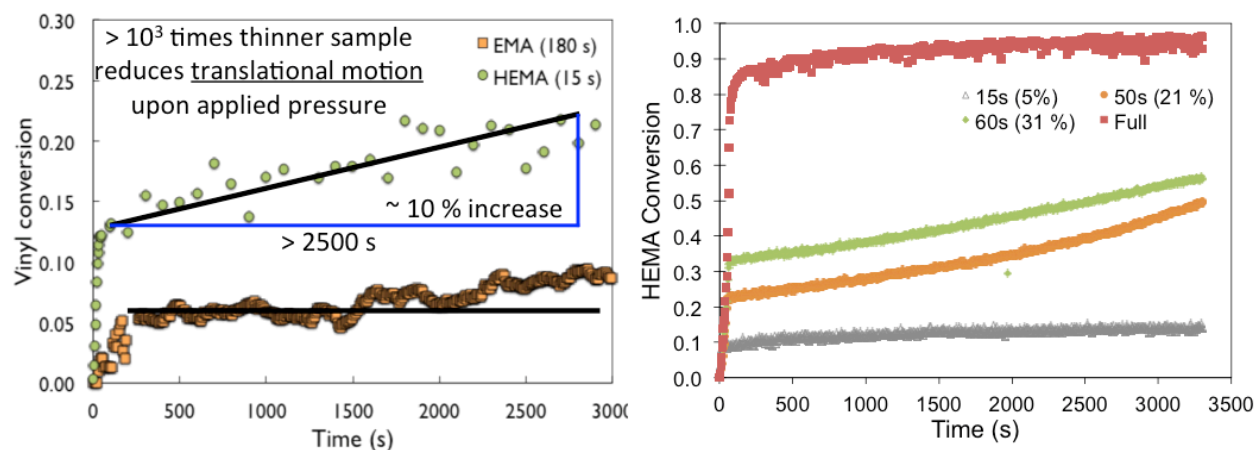


Figure 7.4 Latent polymerization of HEMA and ethyl methacrylate (EMA) in $<10\ \mu\text{m}$ thick films. Left-HEMA and EMA samples containing DMPA photoinitiator were placed in between NaCl plates and sandwiched with metal binders to reduce the sample thickness to a minimum. Samples were exposed to a mercury lamp with a 365 nm filter for different times to achieve the same conversion at the moment of light shut-off. Then the peak corresponding to the C=C from the methacrylates was monitored after the extinction of irradiation. EMA shows absence of latent polymerization, whereas HEMA shows

approximately 10% vinyl conversion in the dark lasting for 3000 s. Right- Partial irradiation of HEMA with DMPA with different exposure times.

7.3.4 Long-lived propagating radicals formed in monomers with alcohol group

In order to get additional evidence confirming the presence of a non-negligible concentration of persistent macroradicals, we utilized EPR spectroscopy to analyze the production and lifetime of the signal associated with the carbon-centered radicals formed during polymerization of the methacrylate monomers. First it was observed that a 9 to 11 lines peak appeared in the region of the EPR spectrum where the signal for propagating radicals has been reported³⁵. Furthermore, it was identified that the lines in the case of the HEMA were broader than the lines in the case of the non-hydroxylated EMA monomer. This has been previously associated with immobilization of the paramagnetic species. We propose that the anisotropy in the lines is due to longer relaxation times of the macroradical, i.e. lower mobility. Additionally, when we track the highest point in the EPR signal with time during several partial irradiation cycles we observed that regardless of the time of exposure of the EMA samples the peak associated with the macroradicals dropped down to zero almost immediately after light cessation. In contrast, when the same was performed with HEMA it was noticeable that the signal decayed more slowly, and lasted for over 3500 s depending on the exposure time and intensity. These observations seem to support the theory that supramolecular organization of the pendant groups in the polymer backbone due to hydrogen bonding can provide enough energy (~23 kJ/mol) to prolong the relaxation time of the polymer chains, and as a result limit the segmental and translational motion of the macroradicals, effectively stabilizing them for a lot longer times than what would be expected.

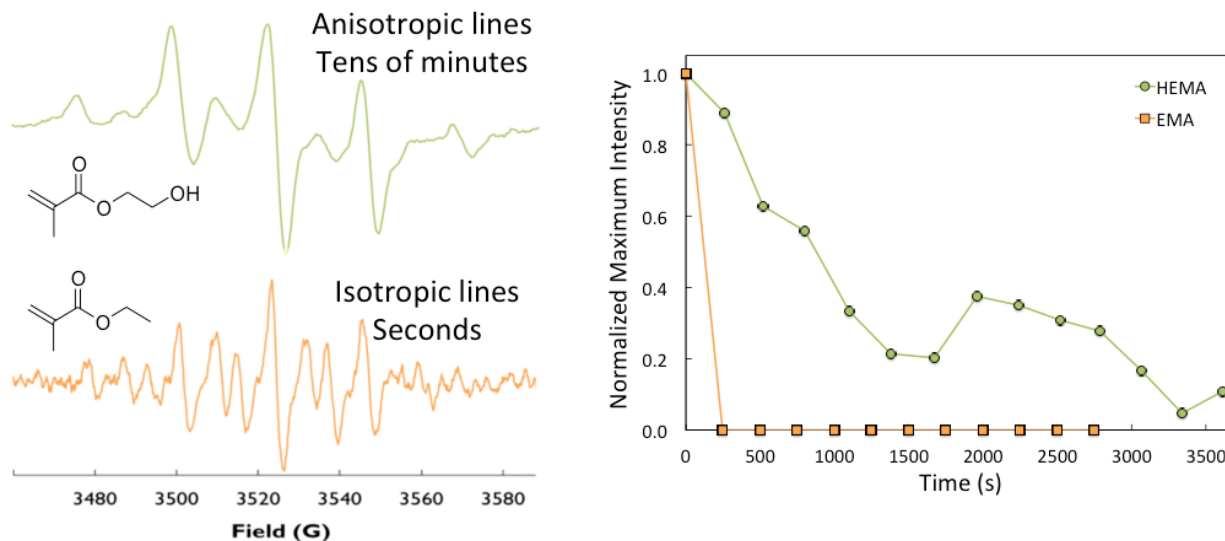


Figure 7.5 EPR signals for the propagating radicals produced by irradiating HEMA and EMA samples containing DMPA photoinitiator. Left- EPR signals correspond to the carbon-centered radical formed on the methacrylate monomers. Samples were briefly irradiated with a mercury lamp filtered to 365 nm at a low intensity to avoid drastic polymerization within the EPR cavity. In the case of the HEMA the EPR peaks show anisotropic lines that are typically related with immobilized radicals. In contrast, the signal observed for EMA, centered at the same magnetic field (~ 3522 G), showed no line broadening which is indicative of a freely mobile carbon-centered radical. Right- Additionally, the signal in HEMA lasted for tens of minutes after light cessation, whereas that of EMA quickly disappeared within a few seconds, as expected for a freely moving reactive radical.

7.3.5 Importance of methyl group in the methacrylate monomers

The choice of methacrylates for this study was important because chain-transfer reactions due to hydrogen abstraction from these monomer structures are widely accepted to be limited or nearly absent. Hydrogen abstraction from the secondary functional groups would lead to branching and/or crosslinking of the polymer chains that are expected to be linear as the monomers only have one vinyl group. This essentially eliminates the need to consider the formation of covalent crosslinks forming from abstraction reactions since if this were to happen it would occur so slowly that it would not account for such dramatic effects presented here and by others. The bond dissociation energy of the O-H (~ 91 kcal/mol) bond is not that different from that of the C-H (~ 98 kcal/mol) bonds in the HEMA structure. These values were based on the literature and confirmed using calculations with Marvin Software. Furthermore, if chain-transfer was responsible for the high rates and extensive persistence of

macroradicals post-irradiation, then an Arrhenius temperature dependence would have been observed. Secondly, as mentioned in the Introduction section, HEMA has been documented to display high rates of polymerization during light exposure with or without a purification process to remove the by-products from the esterification reaction that is used to synthesize this monomer. If these impurities were present they would amount to an extremely low number of covalent crosslinks that cannot be expected to reduce the mobility of the polymer network so much to cause the highly unique phenomena presented here. As a result, it is safe to propose that the most likely explanation for both the unusually high rate of polymerization and extensive vinyl consumption observed with HEMA are caused by hydrogen bonding interactions between the alcohol functional groups that are pendant to the carbon backbone structure.

However, considering the results presented here and those reported by others on the reactivity of mono-vinyl acrylates and methacrylates and the extent of the of vinyl consumption post-irradiation associated with them, a plausible mechanistic conclusion is that: mono-vinyl methacrylate monomers display by far the longest vinyl consumption post-irradiation that has been documented. From this assessment, we propose that there may be a significant contribution from the bulky methyl group that will be also pendant to the polymer backbone. It is important to acknowledge then that the alignment of both the hydroxyethyl and the methyl groups may contribute synergistically to fight the naturally entropical driving force that would otherwise lead to a more random arrangement of the macromolecular structure. This becomes important, because it could explain why the significantly shorter durations of post-irradiation vinyl consumption have been reported for mono-vinyl acrylates, including HEMA's acrylate analog HEA (2-hydroxyethyl acrylate)²². Acrylate mono-vinyl monomers might, for example, be able to relax faster due the significantly smaller hydrogen atom that resides adjacent to the secondary functionality. Ultimately, methacrylate monomers seem to be better suited for the analysis of structure-kinetics-property relationships since they are less prone to side reactions.

It is important to note that poly-HEMA samples have been documented to have a very limited solubility in non-polar organic solvents such as hexane. Poly-HEMA is often used to make hydrogels that

are swollen polymer constructs with a high loading of water. When we submerged poly-HEMA in DI-water, we identified a noticeable swelling but the polymers did not dissolve or acquire more than 100 % of their volume via swelling even after days. We also, attempted to dissolve poly-HEMA samples in THF after polymerizing purified HEMA with conventional photoinitiators. These polymer samples did not dissolve in THF and thus did not allow for GPC analysis of the molecular weight. These observations may also be explained by the theory of hydrogen bonding (H-bonding) reduced relaxation. If the amount of covalent crosslinks is in fact negligible after purification with hexane, then the inability of poly-HEMA samples to dissolve in most solvents points to very strong interactions between the H-bonding pendant groups which can ultimately serve as supramolecular crosslinking sites between the entangled polymer linear sections. If the macromolecular structure is relatively entangled and with limited free volume, then it would be difficult more the solvents to provide enough force to dissociate the multiple H-bonding sites that were produced during the bulk polymerization.

7.3.6 Pre-organization (C=C templating) theory vs mobility theory

The results presented herein are not aimed at elucidating the reason for the unusually high rate of polymerization of HEMA, which has been the focus of some of the references cited through this contribution. In contrast, we attempt to provide additional evidence of the effect that supramolecular interactions have on the mobility of the polymers formed, and as a result on the rate and extent of macroradical termination. It is clear now that both the high R_p 's and the non-negligible amount of persistent radicals post-irradiation are due to an alignment or organization of the hydrogen bonding pendant groups. This self-organization is not required to in these cases to form perfectly uniform structures, as those that have been the topic of many recent contributions in polymer science. In the case of bulk polymerization of mono-vinyl methacrylates with hydrogen bonding secondary functional groups the organization only has to allow for the adoption of a relatively random, but yet constrained macromolecular network, whose relaxation is going to be hindered by the strong hydrogen bonds that are

promoted to align as the polymer grows and more hydrogen bonding sites are forced to be adjacent to one another.

From this analysis, it seems possible then to provide a potential link between these two phenomena. On one side, the theory of pre-organization devised by Jansen et al. proposes that the alignment of the pendant hydrogen bonding groups accelerates the vinyl consumption rate of acrylates during irradiation because it leads to an alignment of the C=C bonds. As a result, the effective or local concentration of polymerizable vinyl groups around the macroradical increase based upon some sort of ‘templating’ feature which could reduce the energy barrier for propagation and make it kinetically more favorable for more monomer to add to the growing polymer. On other hand, we have confirmed in this work that the alignment of hydrogen bonding groups most likely leads to longer relaxation times, i.e. reduced mobility, which in turn hinders the bimolecular termination reactions that are expected to be the dominant if not the only source of radical occlusion. In consequence, a non-negligible amount of persistent macroradicals remains after irradiation has ceased for even tens of thousands of seconds. Despite the fact that both these interpretations rely on hydrogen bonding alignment, the ‘templating’ theory depends on propagation being increased, while our theory on H-bonding enhanced Trommsdorff-Norrish effects is based on reduced termination. The reduction in termination kinetics will lead to polymerization kinetics that are clearly outside of a steady-state regime. As a result, macroradicals can quickly accumulate while irradiation is present. In turn, the consumption of vinyl groups could be accelerated by the significant increase in the limiting reagent, namely the radical species. While more evidence is needed to assess the precise contributions of both: 1) accumulation of radicals due to hindered termination and 2) virtual increase in effective or local concentration of vinyl groups around the radicals through templating or alignment, it seems reasonable to expect that these two mechanisms are working synergistically to both accelerate the polymerization rate during light exposure and also extend the consumption of vinyl groups for considerably longer times beyond irradiation than what would normally be expected.

7.4 Conclusions

In this contribution, we experimentally analyzed the effects of hydrogen bonding on the persistence of macroradicals after an initial exposure to radiation. We focused our attention on comparing the polymerization profiles of HEMA and EMA using different photoinitiators, temperatures, and mechanical loads during the polymerization process. The extent and profile of the vinyl consumption post-irradiation seems to vary as a function of the conversion at which the irradiation was extinguished, the temperature of the experiment and amount of radicals produced during irradiation. The results included in this contribution were discussed as compared to those from others in order to determine that the most plausible explanation for the long-lived macroradicals is the stabilization of the macromolecular radicals by the mobility restrictions imposed by the alignment of multiple hydrogen bonding sites. Formation of these supramolecular bonds can be then thought as being correlated with the extent of the polymerization and the particular macromolecular structure form thereof. In conclusion, preference of the pendant groups to interact amongst themselves may fight against the entropical driving force that normally would favor relaxation or motion of the linear polymer sections found between whatever minimal amount of covalent crosslinks present. These findings provide additional evidence of the contribution of supramolecular bonding on the polymerization kinetics, and can thus permit the elucidation of refined structure-kinetics-property relationships useful for the rational design of better polymer syntheses and materials.

7.5 References

1. Jariwala, A. S. *et al.* Modeling effects of oxygen inhibition in mask-based stereolithography. *Rapid Prototyping Journal* **17**, 168–175 (2011).
2. EATON, D. Nonlinear optical materials. *Science* **253**, 281–287 (1991).
3. Young, J. S. J., Gonzales, K. D. K. & Anseth, K. S. K. Photopolymers in orthopedics: characterization of novel crosslinked polyanhydrides. *Biomaterials* **21**, 1181–1188 (2000).
4. Stansbury, J. W. Curing dental resins and composites by photopolymerization. *J Esthet Dent* **12**, 300–308 (2000).
5. Eaton, D. F. in *Photoinduced Electron Transfer I* **156**, 199–225 (Springer Berlin Heidelberg, 1990).
6. Ifkovits, J. L. & Burdick, J. A. Review: Photopolymerizable and Degradable Biomaterials for Tissue Engineering Applications. *Tissue Engineering* **13**, 2369–2385 (2007).
7. Moussa, K. & Decker, C. Light-induced polymerization of new highly reactive acrylic monomers. *J. Polym. Sci. A Polym. Chem.* **31**, 2197–2203 (1993).
8. Anseth, K. S., Wang, C. M. & Bowman, C. N. Reaction behaviour and kinetic constants for photopolymerizations of multi (meth) acrylate monomers. *Polymer* (1994). doi:10.1016/0032-3861(94)90129-5
9. Bowman, C. N. & Kloxin, C. J. Toward an enhanced understanding and implementation of photopolymerization reactions. *AIChE J.* **54**, 2775–2795 (2008).
10. Anseth, K. S., Bowman, C. N. & Peppas, N. A. Dynamic mechanical studies of the glass transition temperature of photopolymerized multifunctional acrylates. *Polym. Bull.* **31**, 229–233 (1993).
11. Kilambi, H. *et al.* Design, Development, and Evaluation of Monovinyl Acrylates Characterized by Secondary Functionalities as Reactive Diluents to Diacrylates. *Macromolecules* **40**, 6112–6118 (2007).
12. KILAMBI, H. *et al.* Evaluation of highly reactive mono-methacrylates as reactive diluents for BisGMA-based dental composites. *Dental Materials* **25**, 33–38 (2009).
13. Berchtold, K. A., Nie, J., Stansbury, J. W. & Bowman, C. N. Reactivity of Monovinyl (Meth)acrylates Containing Cyclic Carbonates. *Macromolecules* **41**, 9035–9043 (2008).
14. Kilambi, H., Stansbury, J. W. & Bowman, C. N. Enhanced reactivity of monovinyl acrylates characterized by secondary functionalities toward photopolymerization and Michael addition: Contribution of intramolecular effects. *J. Polym. Sci. A Polym. Chem.* **46**, 3452–3458 (2008).
15. Kilambi, H., Konopka, D., Stansbury, J. W. & Bowman, C. N. Factors affecting the sensitivity to acid inhibition in novel acrylates characterized by secondary functionalities. *J. Polym. Sci. A Polym. Chem.* **45**, 1287–1295 (2007).

16. Kilambi, H., Reddy, S. K., Schneidewind, L., Stansbury, J. W. & Bowman, C. N. Influence of the secondary functionality on the radical-vinyl chemistry of highly reactive monoacrylates. *J. Polym. Sci. A Polym. Chem.* **47**, 4859–4870 (2009).
17. Berchtold, K. A. *et al.* Novel monovinyl methacrylic monomers containing secondary functionality for ultrarapid polymerization: steady-state evaluation. *Macromolecules* **37**, 3165–3179 (2004).
18. Beckel, E. R., Stansbury, J. W. & Bowman, C. N. Effect of Aliphatic Spacer Substitution on the Reactivity of Phenyl Carbamate Acrylate Monomers. *Macromolecules* **38**, 3093–3098 (2005).
19. Beckel, E. R., Nie, J., Stansbury, J. W. & Bowman, C. N. Effect of Aryl Substituents on the Reactivity of Phenyl Carbamate Acrylate Monomers. *Macromolecules* **37**, 4062–4069 (2004).
20. Berchtold, K. A. *et al.* Rapid Solid-State Photopolymerization of Cyclic Acetal-Containing Acrylates. *Macromolecules* **42**, 2433–2437 (2009).
21. Kilambi, H., Stansbury, J. W. & Bowman, C. N. Deconvoluting the Impact of Intermolecular and Intramolecular Interactions on the Polymerization Kinetics of Ultrarapid Mono(meth)acrylates. *Macromolecules* **40**, 47–54 (2007).
22. Lee, T. Y., Roper, T. M., Jonsson, E. S., Guymon, C. A. & Hoyle, C. E. Influence of Hydrogen Bonding on Photopolymerization Rate of Hydroxyalkyl Acrylates. *Macromolecules* **37**, 3659–3665 (2004).
23. Lee, T. Y. *et al.* The kinetics of vinyl acrylate photopolymerization. *Polymer* **44**, 2859–2865 (2003).
24. Jansen, J. F. G. A., Dias, A. A., Dorsch, M. & Coussens, B. Fast Monomers: Factors Affecting the Inherent Reactivity of Acrylate Monomers in Photoinitiated Acrylate Polymerization. *Macromolecules* **36**, 3861–3873 (2003).
25. Berchtold, K. A. CHAPTER 4. 1–6 (2001).
26. *Kinetic Studies of Free Radical Photopolymerizations-II Effect of Preorganization Due to Hydrogen Bonding on the Rate of Photoinitiated Acrylate ...* (ACS ..., 2003). doi:10.1021/bk-2003-0847.ch011
27. Stansbury, J. W. & Dickens, S. H. Determination of double bond conversion in dental resins by near infrared spectroscopy. *Dental Materials* **17**, 71–79 (2001).
28. Decker, C. & Moussa, K. A new method for monitoring ultra-fast photopolymerizations by real-time infra-red (RTIR) spectroscopy. *Die Makromolekulare Chemie* **189**, 2381–2394 (1988).
29. Kilambi, H., Reddy, S. K., Schneidewind, L., Stansbury, J. W. & Bowman, C. N. Copolymerization and dark polymerization studies for photopolymerization of novel acrylic monomers. *Polymer* **48**, 2014–2021 (2007).
30. Aguirre-Soto, A., Lim, C.-H., Hwang, A. T., Musgrave, C. B. & Stansbury, J. W. Visible-Light Organic Photocatalysis for Latent Radical-Initiated Polymerization via $2e^-/1H^+$ Transfers: Initiation with Parallels to Photosynthesis. *J. Am. Chem. Soc.* **136**, 7418–7427 (2014).

31. Odian, G. *Principles of Polymerization*. 1–839 (Wiley Interscience, 2004).
32. García, N., Tiemblo, P., Hermosilla, L., Sieiro, C. & Guzmán, J. Long-Lived Radicals in the Postpolymerization of Methacrylic Monomers at Low Conversions. *Macromolecules* **38**, 7601–7609 (2005).
33. García, N., Tiemblo, P. & Guzmán, J. Nominal vs Real Reaction Temperature in PLP Experiments. A Likely Explanation of the Observed Variation in the Propagation Rate Coefficients with Pulse Repetition Rate. *Macromolecules* **40**, 4802–4808 (2007).
34. García, N. *et al.* Persistent Radicals and Transfer Reactions in the Postpolymerization of Methyl Methacrylate. *Macromolecules* **40**, 8168–8177 (2007).
35. Berchtold, K. A., Lovell, L. G., Nie, J. & Hacioğlu, B. The significance of chain length dependent termination in cross-linking polymerizations. *Polymer* (2001).

7.6 Supplemental Information

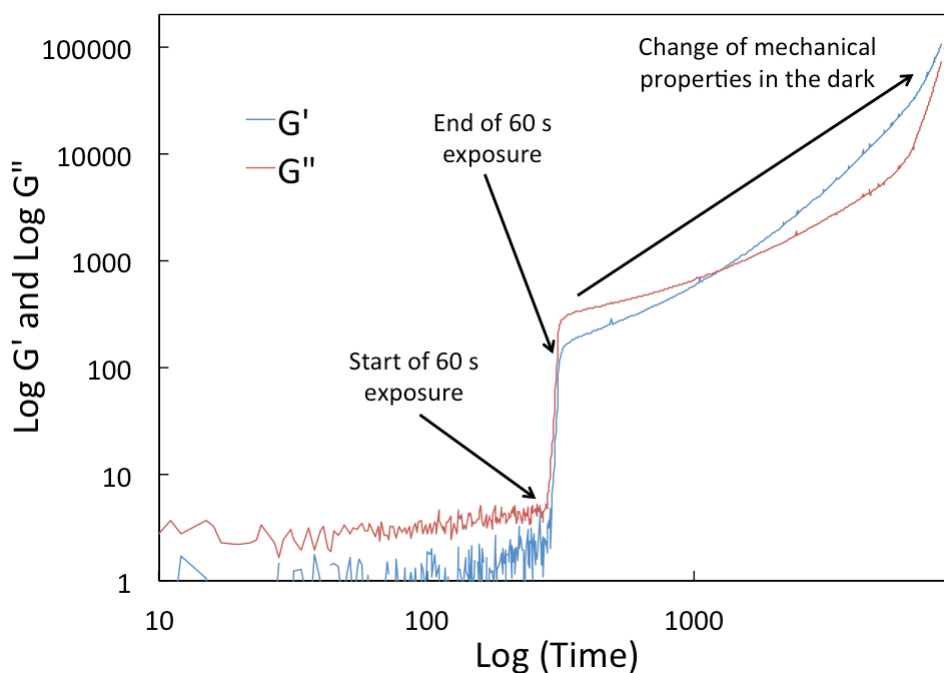


Figure 7.S1. Evolution of mechanical properties of a DMPA solution in HEMA exposed to 10 mW/cm^2 irradiation at 365 nm for 60 s and monitored during and after irradiation in the absence of atmospheric oxygen.

Chapter 8

Conclusions and future directions

8.1 Conclusions

8.1.1 Summary of the key points from each chapter

In this dissertation we focused our attention on answering the question: what are the causes for the unusually prolonged consumption of vinyl groups, i.e. polymerization, post-irradiation in the formulations containing Methylene Blue (MB^+)/N,N-Diisopropylethylamine(DIPEA)/Diphenyliodonium (DPI^+) cations in bulk mono-vinyl hydroxylated monomers, namely 2-hydroxyethyl methacrylate (HEMA)?

First we started by elucidating a novel mechanism via which the MB^+ /DIPEA/ DPI^+ combination produces free radicals that initiate the polymerization (consume the vinyl groups). We demonstrate in Chapter 3 that free radicals are almost exclusively produced from the redox reaction between metastable MB^+ intermediates and the DPI^+ cations. The latter prove to account for the dramatic increase in the rate of polymerization (R_p) that comes with the addition of DPI^+ , and for a significant production of initiating radicals after an initial brief exposure to light, which can also extend beyond the spatial reach of photons.

While investigating the mechanisms involved in the bulk light-induced polymerization of acrylates and methacrylates it became clear that one of the biggest challenges to better understanding these often-complex photochemical reactions and their connections to polymer development is the limited amount of characterization or analytical tools to quantify the rates at which the involved reactants are being consumed *in-situ* (Chapter 4). Hence, we decided to design and construct a novel apparatus for the coupling of real-time UV-Vis and FT-NIR spectroscopy in order to expand the amount of compounds that can be probed with millisecond resolution during the reaction. We validated the technique using the conventional camphorquinone/amine photoinitiator pair that is commonly used for the photopolymerization of dental materials. Additionally, the analysis of this system showcased the potential

of this device to aid in the elucidation of the photochemical reactions used for polymer synthesis, and how these are intricately dependent on the extent of the polymerization.

Next, we decided to analyze the effect of the addition of an oxidant to the CQ/amine photoinitiator system for the polymerization of methacrylate monomers to show further evidence of the advantages of the coupled UV-Vis and FT-NIR technique, as well as to provide a comparison between the CQ/amine/DPI⁺ and the MB⁺/DIPEA/DPI⁺ system in terms of the mechanisms for radical production (Chapter 5). From this study, we learned that evidence suggests the CQ-based intermediates produced after the photoreduction by the amine react with DPI⁺ as does the MB-based intermediates produced by photoreduction with DIPEA. In both cases, a dramatic increase in R_p is observed upon addition of DPI⁺. However, it appears that regeneration of the α -diketone (CQ) does not occur to any significant degree as opposed to the efficient regeneration of MB⁺ that is directly linked to the rate of polymerization. This may be interpreted as indicating that the main reason for the drastic increase in R_p with oxidant addition is the production of very efficient initiating radicals from the reduction of DPI⁺. However, the effect of the replenishment of the chromophore might be somewhat lesser, and most inherently connected with the different chemistries, namely thiazinic organic dyes and ketones.

Later in Chapter 6 provide a detailed mechanistic theory for the phenomena described in Chapter 3 with the aid of the coupled UV-Vis and FT-NIR monitoring device that we introduced in Chapter 4. These constructs have been recently found to exist in prevalent concentrations as compared to the purely monomeric form of MB⁺. Hence, it became obvious that our assumption that MB⁺ functions as a photocatalyst in its monomer state is not valid, especially when solutions in moderately polar monomers are involved. Despite the obviousness of such concept, this assertion had previously been absent in the literature of organic photocatalysis in general. In consequence, the mechanism proposed in Chapter 3 was refined to account for these changes while still explaining all the experimental and theoretical results included in both chapters.

Lastly, in Chapter 7 we investigate the contribution of the monomer, HEMA, to the extensive latent vinyl consumption that was originally observed. We determined here that the hydroxyl or alcohol functional group that is attached to the methacrylate leads to an alignment of the pendant groups via hydrogen bonding. The most likely explanation is then that when this alignment or self-organization of multiple hydrogen bonding sites occurs the mobility and free volume of macromolecular structure is restricted. As a result of the longer relaxation times, slower reptation, of the polymer chain segments between the very few covalent crosslinks, that might be formed, the macroradicals are to persist for time scales on the order of tens of thousands of seconds. In other words, hydrogen bonding hinders mobility and may lead to non-steady state kinetics which translate into both accumulation of a higher concentration of macroradicals during the polymerization, as well as a non-negligible concentration of these radicals post-irradiation, which would be trapped and consume more vinyl groups slowly in the dark.

8.1.2 Answer to the central question: role of each component on the latent vinyl polymerization

Based on these observations and analysis we can now provide an answer to the question postulated as central to this dissertation. Both the organic photocatalysis of MB⁺/Hünig's base/DPI⁺ and the monomer structure (HEMA) are responsible for the uniquely prolonged vinyl consumption observed post-irradiation. The role of each one of the components is as follows:

Methylene Blue photocatalyst

Methylene blue is responsible for the light absorption in the long-wavelength visible-light. It is a known redox indicator and organic dye that has been utilized in a variety of different photochemical reactions. When MB⁺ absorbs light it excites to an excited state singlet, which then undergoes a change in spin to form an excited state triplet with a yield higher than 50 %. Once the excited state triplet is formed it can readily be quenched by reductants, such as the Hünig's base (DIPEA) due to the longer lifetime of said triplet state. The key uniqueness of this photocatalyst is that when it is dissolved in slightly polar or apolar liquids (which represent most monomers) it exists primarily in its complexed form. Hence, the

excited states formed are those corresponding to the complex and not to the purely monomeric form. In turn, when the dimer excited state triplet is reduced by DIPEA forms a meta-stable radical. Then, these stabilized radicals are not able to either terminate or initiate the polymerization very efficiently. However, the inherent reversibility of MB^+ , most likely associated with its highly conjugated planar structure, allows for the semi-reduced MB dimer, which is colorless, to be regenerated into the original MB^+ dimer, which has a color. It is due to the meta-stability of the MB-dimer intermediate and to its feasible regeneration that, in the presence of DPI^+ , radicals can be produced long after irradiation has ceased.

Hünig's base (DIPEA)

The importance of the Hünig's in organic photocatalysis is slowly being discovered. Here, the role of DIPEA in the latent polymerization is primarily that this non-nucleophilic basic aliphatic amine does not produce free radicals after single electron transfer (SET), as most tertiary amines. Perhaps driven by its unique steric hindrance, DIPEA most likely donates a hydrogen atom after SET to the powerful oxidant that is the MB-dimer excited state triplet. As a result, a radical cation is formed, which further oxidizes to produce closed shell products, including enamines, and imines. Such a behavior prevents fast polymerization of the monomer immediately after the photochemical reaction between MB^+ and DIPEA, as would typically be expected. Hence, most of the energy from the light is essentially stored in the meta-stable semi-reduced MB-dimer intermediates and slowly utilized to produce radicals over a much longer timescale than that of the very rapid photochemical reaction.

Diphenyliodonium salt (DPI^+)

The main role of DPI^+ cations is to produce free radicals that efficiently initiate polymerization of the vinyl groups as a result of the reduction by the semi-reduced MB-dimer intermediates. Hence, the

higher the electron affinity and the higher the concentrated of DPI⁺ cations, the faster the polymerization will occur and less photobleaching will be observed. Non-nucleophilic counteranions were tested and found to have a negligible effect on the latent vinyl polymerization and the rates of polymerization.

2-Hydroxyethyl methacrylate (HEMA)

Finally, the monomer HEMA contributes to the latent free radical polymerization observed because the termination rate is hindered by the mobility restrictions due to supramolecular hydrogen bonding between the pendant hydroxylated secondary groups. This effect allows the persistence of a non-negligible amount of macroradicals for up to 24,000 s, in some cases, after irradiation (with conventional photoinitiators like DMPA and CQ/EDMAB). However, the radicals responsible for the prolonged but slow vinyl consumption with conventional photoinitiators are not enough to achieve a final plateau conversion within 2000-3000 s, which typically occur in the presence of MB⁺/DIPEA/DPI⁺. Furthermore, the temperature response and kinetic analysis was key in determining that the redox reaction between the semi-reduced MB-dimer intermediates and DPI⁺ generates a significant amount of radicals after light exposure. These radicals accelerate or accentuate the rate of polymerization in the dark, which inherently happens when HEMA is partially polymerized by a brief exposure to light in the presence of a free radical producing photoinitiator. The latter is dependent nevertheless on the efficiency of the radical production process that occurs during the irradiation period. We observed that a low amount of macroradical is formed, as with MB⁺/DIPEA, the concentration of persistent macroradicals at light shut-off becomes negligible and the vinyl consumption stops immediately.

8.1 Future directions

Along the time it took to complete this work several realizations were made that are worthy of proposing herein as short- and long-term paths to follow as continuation of the works that were selected to form part in the Chapters of the present dissertation. These ideas are listed below:

- 1) Utilization of a photobase generator to improve the thermal stability of MB^+ /base/ DPI^+ formulations in bulk monomer.
- 2) Design an analytical device to monitor rheological properties (Rheometer), photoinitiator concentration (UV-Vis) and monomer consumption (FT-NIR/FT-MIR) at the same time to achieve enhanced characterization capabilities.

8.2.1 Addition of photobase

First, from the very beginning of the present project, it was identified that when combining MB^+ , DIPEA, and salts of DPI^+ in bulk monomer solutions, spontaneous polymerization occurs. This was observed to occur slowly (within hours to days) as compared to the relatively fast (few minutes) polymerizations induced by light. However, we recognized that the limited thermal stability of these formulations is arguably the single most important reason why these three component photoinitiators are not widely utilized in practice. We studied this phenomenon and discovered that it is due to the reaction between DIPEA and DPI^+ . This redox reaction can be expected because DIPEA can readily function as a reductant, despite its low nucleophilicity, as in the reaction with the excited state triplet formed after light absorption by the MB^+ dimer aggregates. Ultimately, when DPI^+ is reduced, either by DIPEA or by LMB, phenyl radicals are produced, which efficiently initiate the polymerization of the methacrylate monomers. Furthermore, if DIPEA/ DPI^+ monomer solutions are prepared not only is a gradual spontaneous polymerization observed, but also the development of a brown-orange color in the solutions. Using ESI^+ /MS and UV-Vis we identified that the color is associated with the further oxidation of the Hünig's base and of its enamine and imine products created after the initial oxidation by DPI^+ . It was clear that the oxidation depended on the presence of oxygen, as the color was stronger at the top of the polymer

samples were the polymer density was lower due to the very slow polymerization process allowing for the flow of denser polymer to the bottom. It was found that upon further oxidation enamines and imines can oligomerize and result in brown-orange or copper colored higher molecular weight products, as identified with ESI⁺/MS.

We propose that addition of a photobase generator to the MB⁺/DPI⁺ formulations has the potential of significantly extending the stability of the formulations under ambient conditions. The latter originates from the fact that photobase generator inherently involve the light-triggered generation of a base with a high pKa from an initially low pKa molecule. Hence, if we make it thermodynamically less feasible for the reaction between the reductant (in this case it would be the photobase generator) and DPI⁺ to occur before light exposure we may be able to design formulations that exhibit little or no inadvertent polymerization until light of a particular wavelength is used to create a reactive reductant. In such a way, we could also generate formulations that would be more photochemically stable as well. The latter may occur since the photocatalytic formulation would require absorption of light at two different wavelengths at the same time, one for the MB⁺ dimers and the other for the photobase generator. As an example, if a blue-light (400-450 nm) sensitive photobase generator is incorporated with MB⁺ and DPI⁺, the polymerization would be expected to efficiently and quickly activated only in the presence or exposure to both blue and red light (~620 nm). We recognize that the combination of the photobase generator and DPI⁺ may be enough to efficiently polymerize the monomers. Nevertheless, this has to be tested in order to assess if there is an advantage in terms of rate of polymerization for having the three components: MB⁺/photobase generator/DPI⁺.

8.2.2 Simultaneous rheology/initiation/polymerization monitoring

The main problem we faced with the analytical device introduced in Chapter 4 is that polymerization inherently changes the refraction and scattering of the light as the solid polymer develops from a liquid monomer. This leads to two practical issues: 1) there is an inevitable loss in light

transmission as the polymer forms 2) the excitation light beam that is responsible for initiation of the polymerization runs perpendicularly to the UV-Vis and FT-NIR probing beams and can contaminate the UV-Vis signal as the changing in light scattering isotropically scatters the excitation beam as a function of the extent of polymerization. These two issues can create significant artifacts that in extreme cases can preclude the use of the data gathered by the UV-Vis spectrometer. The FT-NIR data is in general unaffected by these artifacts. We realized that removing the bubbles from the liquid monomer solutions before polymerization significantly reduced or eliminated the contamination of the UV-Vis probing signal by the excitation beam. However, a shift in the UV-Vis baseline as a function of polymerization was always present. The latter can be attributed to a changing refraction index and/or creation of small heterogeneities in the interface between the cuvettes and the developing polymer as the material shrinks.

We recognize this is most likely the main reason why the few previous studies that report on the real-time UV-Vis analysis of photopolymerization reactions were performed in thin film specimens contained within glass or quartz slides. By doing so, the effect of light scattering is reduced because it is dependent on a function of the pathlength of the sample. Furthermore, the samples are allowed to shrink more freely, thus delamination of the polymer from the substrates is reduced as well.

Considering the advantages of utilizing such a sample geometry we think there is significant potential for the integration of fiber coupled UV-Vis/FT-IR into a single beam combined with the excitation that permits the use of thin films where one dimension is lost given the aspect ratio of the samples. Additionally, this can be integrated to the current rheology/FT-IR concept that was developed previously in our lab. This is important because it not only would reduce the inherent problems associated with the present UV-Vis/FT-NIR device, but it would also incorporate real-time monitoring of the mechanical properties, and the possibility of using FT-MIR as well as FT-NIR since the thickness of the samples would be readily changed in the rheometer set-up.

References

1. FUJITA, K., TANIGUCHI, K. & OHNO, H. Dynamic analysis of aggregation of methylene blue with polarized optical waveguide spectroscopy. *Talanta* 65, 1066–1070 (2005).
2. Rodriguez-Serrano, A., Rai-Constapel, V., Daza, M. C., Doerr, M. & Marian, C. M. A theoretical study of thionine: spin–orbit coupling and intersystem crossing. *Photochem. Photobiol. Sci.* 11, 1860–1867 (2012).

Bibliography

Chapter 1

1. Hawker, C. J. & Wooley, K. L. The Convergence of Synthetic Organic and Polymer Chemistries. *Science* **309**, 1200–1205 (2005).
2. Barner-Kowollik, C., Lutz, J. F. & Perrier, S. New methods of polymer synthesis. *Polym. Chem.* (2012). doi:10.1039/c1py00443c
3. Decker, C. *UV-curing chemistry: past, present, and future*. (JCT, 1987).
4. Carothers, W. H. Studies on polymerization and ring formation. I. An introduction to the general theory of condensation polymers. *J. Am. Chem. Soc.* **51**, 2548–2559 (1929).
5. Flory, P. J. The Configuration of Real Polymer Chains. *J. Chem. Phys.* **17**, 303 (1949).
6. Odian, G. *Principles of Polymerization*. 1–839 (Wiley Interscience, 2004).
7. Cowie, J. M. G. *Polymers*. (CRC Press, 1991).
8. Hoyle, C. E. & Bowman, C. N. Thiol-Ene Click Chemistry. *Angew. Chem. Int. Ed.* **49**, 1540–1573 (2010).
9. Flory, P. J. *Principles of polymer chemistry*. (1953).
10. Cramer, N. B. *et al.* Investigation of thiol-ene and thiol-ene–methacrylate based resins as dental restorative materials. *Dental Materials* **26**, 21–28 (2010).
11. Cramer, N. B. *et al.* Properties of methacrylate-thiol-ene formulations as dental restorative materials. *Dental Materials* **26**, 799–806 (2010).
12. Goodner, M. D. & Bowman, C. N. *ACS Symposium Series*. **713**, 220–231 (American Chemical Society, 2009).
13. Goodner, M. D. & Bowman, C. N. Development of a comprehensive free radical photopolymerization model incorporating heat and mass transfer effects in thick films. *Chemical Engineering Science* **57**, 887–900 (2002).
14. Goodner, M. D. & Bowman, C. N. Modeling Primary Radical Termination and Its Effects on Autoacceleration in Photopolymerization Kinetics. *Macromolecules* **32**, 6552–6559 (1999).
15. Goodner, M. D., Lee, H. R. & Bowman, C. N. Method for determining the kinetic parameters in diffusion-controlled free-radical homopolymerizations. *Ind. Eng. Chem. Res.* **36**, 1247–1252 (1997).
16. Anseth, K. S., Kline, L. M., Walker, T. A. & Anderson, K. J. Reaction kinetics and volume relaxation during polymerizations of multiethylene glycol dimethacrylates. ... **28**,

- 2491–2499 (1995).
17. Maurin, V., Croutxé-Barghorn, C. & Allonas, X. Photopolymerization process of UV powders. Characterization of coating properties. *Progress in Organic Coatings* **73**, 250–256 (2011).
 18. Stansbury, J. W. Curing dental resins and composites by photopolymerization. *J Esthet Dent* **12**, 300–308 (2000).
 19. Scott, T. F., Kowalski, B. A., Sullivan, A. C., Bowman, C. N. & McLeod, R. R. Two-Color Single-Photon Photoinitiation and Photoinhibition for Subdiffraction Photolithography. *Science* **324**, 913–917 (2009).
 20. Rengier, F. *et al.* 3D printing based on imaging data: review of medical applications. *Int J CARS* **5**, 335–341 (2010).
 21. EATON, D. Nonlinear optical materials. *Science* **253**, 281–287 (1991).
 22. DeForest, C. A. & Anseth, K. S. Cytocompatible click-based hydrogels with dynamically tunable properties through orthogonal photoconjugation and photocleavage reactions. 1–7 (2011). doi:10.1038/nchem.1174
 23. DeForest, C. A., Polizzotti, B. D. & Anseth, K. S. Sequential click reactions for synthesizing and patterning three-dimensional cell microenvironments. *Nature Materials* **8**, 659–664 (2009).
 24. Yang, D. B., Wolf, D., Wakamatsu, T. & Holmes, M. Characterization of cure profiles of anaerobic adhesives by real-time FT-IR spectroscopy. Part II. Surface activation. *Journal of adhesion science and technology* **9**, 1369–1379 (1995).
 25. Lai, Y. C. Effect of crosslinkers on photocopolymerization of N-vinylpyrrolidone and methacrylates to give hydrogels. *J. Appl. Polym. Sci.* **66**, 1475–1484 (1997).
 26. Eaton, D. F. *Dye Sensitized Photopolymerization. Advances in Photochemistry* **13**, 427–487 (John Wiley & Sons, Inc., 1986).
 27. Kloosterboer, J. G. *Network formation by chain crosslinking photopolymerization and its applications in electronics.* 1–61 (Springer, 1988).
 28. Anseth, K. S., Wang, C. M. & Bowman, C. N. Reaction behaviour and kinetic constants for photopolymerizations of multi (meth) acrylate monomers. *Polymer* (1994). doi:10.1016/0032-3861(94)90129-5
 29. Stansbury, J. W. Difunctional and multifunctional monomers capable of cyclopolymerization. *Macromolecules* **24**, 2029–2035 (1991).
 30. Stansbury, J. W. & Dickens, S. H. Determination of double bond conversion in dental resins by near infrared spectroscopy. *Dental Materials* **17**, 71–79 (2001).
 31. Stansbury, J. W. Dimethacrylate network formation and polymer property evolution as determined by the selection of monomers and curing conditions. *Dental Materials* **28**, 13–

- 22 (2012).
32. Kilambi, H. *et al.* Design, Development, and Evaluation of Monovinyl Acrylates Characterized by Secondary Functionalities as Reactive Diluents to Diacrylates. *Macromolecules* **40**, 6112–6118 (2007).
 33. Shalaby, S. W. & Salz, U. *Polymers for Dental and Orthopedic Applications*. (CRC Press, 2006).
 34. Ramakrishna, S., Mayer, J., Wintermantel, E. & Leong, K. W. Biomedical applications of polymer-composite materials: a review. *Composites Science and Technology* **61**, 1189–1224 (2001).
 35. Ifkovits, J. L. & Burdick, J. A. Review: Photopolymerizable and Degradable Biomaterials for Tissue Engineering Applications. *Tissue Engineering* **13**, 2369–2385 (2007).
 36. Young, J. S. J., Gonzales, K. D. K. & Anseth, K. S. K. Photopolymers in orthopedics: characterization of novel crosslinked polyanhydrides. *Biomaterials* **21**, 1181–1188 (2000).
 37. Bowman, C. N. & Peppas, N. A. Coupling of kinetics and volume relaxation during polymerizations of multiacrylates and multimethacrylates. *Macromolecules* **24**, 1914–1920 (1991).
 38. Bowman, C. N. The Effects of Light Intensity, Temperature, and Comonomer Composition on the Polymerization Behavior of Dimethacrylate Dental Resins. **78**, 1469–1476 (1999).
 39. Decker, C. Photoinitiated crosslinking polymerisation. *Progress in Polymer Science* **21**, 593–650 (1996).
 40. Ibrahim, A. *et al.* Investigation of termination reactions in free radical photopolymerization of UV powder formulations. *European Polymer Journal* **48**, 1475–1484 (2012).
 41. Tian, Y., HAMIELEC, A. E. & Eaton, D. R. Termination of trapped radicals at elevated temperatures during copolymerization of MMA/EGDMA. *Polymer* **31**, 1726–1734 (1990).
 42. Berchtold, K. A., Lovell, L. G., Nie, J. & Hacıoğlu, B. The significance of chain length dependent termination in cross-linking polymerizations. *Polymer* (2001).
 43. Decker, C. & Jenkins, A. D. Kinetic approach of oxygen inhibition in ultraviolet-and laser-induced polymerizations. *Macromolecules* (1985).
 44. Decker, C. A novel method for consuming oxygen instantaneously in photopolymerizable films. *Die Makromolekulare Chemie* **180**, 2027–2030 (1979).
 45. Bowman, C. N. & Kloxin, C. J. Toward an enhanced understanding and implementation of photopolymerization reactions. *AIChE J.* **54**, 2775–2795 (2008).
 46. Kloxin, A. M., Tibbitt, M. W., Kasko, A. M., Fairbairn, J. A. & Anseth, K. S. Tunable Hydrogels for External Manipulation of Cellular Microenvironments through Controlled

- Photodegradation. *Adv. Mater.* **22**, 61–66 (2010).
47. Tibbitt, M. W. & Anseth, K. S. Hydrogels as extracellular matrix mimics for 3D cell culture. *Biotechnol. Bioeng.* **103**, 655–663 (2009).
 48. Fouassier, J. P., Lougnot, D.-J. & Pilot, T. Visible laser light in photoinduced polymerization. I. A quantitative comparison with UV laser irradiation. *Journal of Polymer Science: Polymer Chemistry Edition* **23**, 569–573 (1985).
 49. Valdes-Aguilera, O., Pathak, C. P., Shi, J. & Watson, D. Photopolymerization studies using visible light photoinitiators. ... **25**, 541–547 (1992).
 50. Avens, H. J., Randle, T. J. & Bowman, C. N. Polymerization behavior and polymer properties of eosin-mediated surface modification reactions. *Polymer* **49**, 4762–4768 (2008).
 51. Ilie, N. & Hickel, R. Can CQ be completely replaced by alternative initiators in dental adhesives? *Dent Mater J* **27**, 221–228 (2008).
 52. Shintani, H., Inoue, T. & Yamaki, M. Analysis of camphorquinone in visible light-cured composite resins. *Dental Materials* (1985). doi:10.1016/S0109-5641(85)80002-6
 53. Jakubiak, J., Allonas, X., Fouassier, J. P. & Sionkowska, A. Camphorquinone–amines photoinitiating systems for the initiation of free radical polymerization. *Polymer* (2003). doi:10.1016/S0032-3861(03)00568-8
 54. Nie, J. *et al.* A reappraisal of the photopolymerization kinetics of triethyleneglycol dimethacrylate initiated by camphorquinone–N,N-dimethyl-p-toluidine for dental purposes. *Acta Polymerica* **49**, 145–161 (1998).
 55. Cook, W. D. Photopolymerization kinetics of dimethacrylates using the camphorquinone/amine initiator system. *Polymer* **33**, 600–609 (1992).
 56. Oxman, J. D. & Jacobs, D. W. Ternary photoinitiator system for curing of epoxy/polyol resin composition. (2001).
 57. Oxman, J. D. *et al.* Evaluation of initiator systems for controlled and sequentially curable free-radical/cationic hybrid photopolymerizations. *J. Polym. Sci. A Polym. Chem.* **43**, 1747–1756 (2005).
 58. Lalevée, J. *et al.* Photoredox catalysis for polymerization reactions. *Chimia (Aarau)* **66**, 439–441 (2012).
 59. Decker, C. & Moussa, K. A new method for monitoring ultra-fast photopolymerizations by real-time infra-red (RTIR) spectroscopy. *Die Makromolekulare Chemie* **189**, 2381–2394 (1988).
 60. Lee, T. Y., Roper, T. M., Jonsson, E. S., Guymon, C. A. & Hoyle, C. E. Influence of Hydrogen Bonding on Photopolymerization Rate of Hydroxyalkyl Acrylates. *Macromolecules* **37**, 3659–3665 (2004).

61. Kim_Stansbury_Patent 1_2009. 1–25 (2010).
62. Kim_STansbury_Patent_2_2009. 1–51 (2010).
63. Padon, K. S. & Scranton, A. B. A mechanistic investigation of a three-component radical photoinitiator system comprising methylene blue, N-methyldiethanolamine, and diphenyliodonium chloride. *J. Polym. Sci. A Polym. Chem.* **38**, 2057–2066 (2000).
64. Sirovatka Padon, K. & Scranton, A. B. The effect of oxygen on the three-component radical photoinitiator system: Methylene blue, N-methyldiethanolamine, and diphenyliodonium chloride. *J. Polym. Sci. A Polym. Chem.* **38**, 3336–3346 (2000).
65. Kim, D. & Scranton, A. The role of diphenyl iodonium salt (DPI) in three-component photoinitiator systems containing methylene blue (MB) and an electron donor. *J. Polym. Sci. A Polym. Chem.* **42**, 5863–5871 (2004).
66. Kim, D., Scranton, A. B. & Stansbury, J. W. Effect of the electron donor structure on the shelf-lifetime of visible-light activated three-component initiator systems. *J. Appl. Polym. Sci.* **114**, 1535–1542 (2009).
67. WEIL, L. ON THE MECHANISM OF THE PHOTO-OXIDATION OF AMINO ACIDS SENSITIZED BY METHYLENE BLUE. *Arch. Biochem. Biophys.* **110**, 57–68 (1965).
68. Chaberek, S. & Allen, R. J. Dye-Sensitized Photopolymerization Processes. 1a II. A Comparison of the Photoactivities of Thionine and Methylene Blue. *J. Phys. Chem.* **69**, 647–656 (1965).
69. Nilsson, R., Merkel, P. B. & Kearns, D. R. Kinetic properties of the triplet states of methylene blue and other photosensitizing dyes. *Photochem Photobiol* **16**, 109–116 (1972).
70. Kilambi, H., Reddy, S. K., Schneidewind, L., Stansbury, J. W. & Bowman, C. N. Copolymerization and dark polymerization studies for photopolymerization of novel acrylic monomers. *Polymer* **48**, 2014–2021 (2007).

Chapter 3

1. Shih, H.-W., Vander Wal, M. N., Grange, R. L. & MacMillan, D. W. C. Enantioselective α -Benzoylation of Aldehydes via Photoredox Organocatalysis. *J. Am. Chem. Soc.* **132**, 13600–13603 (2010).
2. Hawker, C. J. & Wooley, K. L. The Convergence of Synthetic Organic and Polymer Chemistries. *Science* **309**, 1200–1205 (2005).
3. Kilambi, H., Reddy, S. K., Schneidewind, L., Stansbury, J. W. & Bowman, C. N. Copolymerization and dark polymerization studies for photopolymerization of novel

- acrylic monomers. *Polymer* **48**, 2014–2021 (2007).
4. Hoyle, C. E. & Bowman, C. N. Thiol-Ene Click Chemistry. *Angew. Chem. Int. Ed.* **49**, 1540–1573 (2010).
 5. Adzima, B. J. *et al.* Spatial and temporal control of the alkyne-azide cycloaddition by photoinitiated Cu(II) reduction. *Nature Chemistry* **3**, 256–259 (2011).
 6. Xuan, J. & Xiao, W.-J. Visible-Light Photoredox Catalysis. *Angew. Chem. Int. Ed.* **51**, 6828–6838 (2012).
 7. Narayanam, J. M. R. & Stephenson, C. R. J. Visible light photoredox catalysis: applications in organic synthesis. *Chem. Soc. Rev.* **40**, 102 (2010).
 8. Dai, C., Narayanam, J. M. R. & Stephenson, C. R. J. Visible-light-mediated conversion of alcohols to halides. *Nature Chemistry* **3**, 140–145 (2011).
 9. Lee, T. Y., Roper, T. M., Jonsson, E. S., Guymon, C. A. & Hoyle, C. E. Influence of Hydrogen Bonding on Photopolymerization Rate of Hydroxyalkyl Acrylates. *Macromolecules* **37**, 3659–3665 (2004).
 10. Fors, B. P. & Hawker, C. J. Control of a Living Radical Polymerization of Methacrylates by Light. *Angew. Chem. Int. Ed.* **51**, 8850–8853 (2012).
 11. Wang, J.-S. & Matyjaszewski, K. Controlled/‘ living’ radical polymerization. Atom transfer radical polymerization in the presence of transition-metal complexes. *J. Am. Chem. Soc.* **117**, 5614–5615 (1995).
 12. Yoon, T. P., Ischay, M. A. & Du, J. Visible light photocatalysis as a greener approach to photochemical synthesis. *Nature Chemistry* **2**, 527–532 (2010).
 13. Allonas, X., Lalevée, J. & Fouassier, J.-P. Investigation of cleavage processes in photoinitiators: from experiments to molecular modeling. *Journal of Photochemistry & Photobiology, A: Chemistry* **159**, 127–133 (2003).
 14. Fouassier, J. P. & Lalevée, J. *Photoinitiators for Polymer Synthesis: Scope, Reactivity, and Efficiency*. (Wiley-VCH, 2012).
 15. Fouassier, J.-P. & Morlet-Savary, F. Photopolymers for laser imaging and holographic recording: design and reactivity of photosensitizers. *Optical engineering* **35**, 304–312 (1996).
 16. EATON, D. Nonlinear optical materials. *Science* **253**, 281–287 (1991).
 17. Scott, T. F., Kowalski, B. A., Sullivan, A. C., Bowman, C. N. & McLeod, R. R. Two-Color Single-Photon Photoinitiation and Photoinhibition for Subdiffraction Photolithography. *Science* **324**, 913–917 (2009).
 18. Liu, N., Liu, H., Zhu, S. & Giessen, H. Stereometamaterials. *Nature Photon* **3**, 157–162 (2009).
 19. Goodner, M. D. & Bowman, C. N. Development of a comprehensive free radical

- photopolymerization model incorporating heat and mass transfer effects in thick films. *Chemical Engineering Science* **57**, 887–900 (2002).
20. Catilaz Simonin, L. & Fouassier, J. P. Investigation of a system capable of photoinitiating radical polymerizations in thick pigmented media. *J. Appl. Polym. Sci.* **79**, 1911–1923 (2001).
 21. Stansbury, J. W. Curing dental resins and composites by photopolymerization. *J Esthet Dent* **12**, 300–308 (2000).
 22. Fisher, J. P. J., Dean, D. D. & Mikos, A. G. A. Photocrosslinking characteristics and mechanical properties of diethyl fumarate/poly(propylene fumarate) biomaterials. *Biomaterials* **23**, 4333–4343 (2002).
 23. DeForest, C. A., Polizzotti, B. D. & Anseth, K. S. Sequential click reactions for synthesizing and patterning three-dimensional cell microenvironments. *Nature Materials* **8**, 659–664 (2009).
 24. Hasenwinkel, J. M., Lautenschlager, E. P., Wixson, R. L. & Gilbert, J. L. A novel high-viscosity, two-solution acrylic bone cement: effect of chemical composition on properties. *J. Biomed. Mater. Res.* **47**, 36–45 (1999).
 25. Loctite Corporation. Dual curing coating method for substrates with shadow areas. (1985).
 26. Kwon, T.-Y., Bagheri, R., Kim, Y. K., Kim, K.-H. & Burrow, M. F. Cure mechanisms in materials for use in esthetic dentistry. *Journal of Investigative and Clinical Dentistry* **3**, 3–16 (2012).
 27. Nason, C., Roper, T., Hoyle, C. & Pojman, J. A. UV-Induced Frontal Polymerization of Multifunctional (Meth)acrylates. *Macromolecules* **38**, 5506–5512 (2005).
 28. Gregory, S. Ultraviolet curable resin compositions having enhanced shadow cure properties. (2001).
 29. Gugg, A., Gorsche, C., Moszner, N. & Liska, R. Frontal Polymerization: Polymerization Induced Destabilization of Peracrylates. *Macromol. Rapid Commun.* **32**, 1096–1100 (2011).
 30. Crivello, J. V. Hybrid free radical/cationic frontal photopolymerizations. *J. Polym. Sci. A Polym. Chem.* **45**, 4331–4340 (2007).
 31. *CHIMIA International Journal for Chemistry.*
 32. Tehfe, M.-A. *et al.* Organic Photocatalyst for Polymerization Reactions: 9,10-Bis[(triisopropylsilyl)ethynyl]anthracene. *ACS Macro Lett.* **1**, 198–203 (2012).
 33. Zhang, G., Song, I. Y., Ahn, K. H., Park, T. & Choi, W. Free Radical Polymerization Initiated and Controlled by Visible Light Photocatalysis at Ambient Temperature. *Macromolecules* **44**, 7594–7599 (2011).
 34. Padon, K. S. & Scranton, A. B. A mechanistic investigation of a three-component radical

- photoinitiator system comprising methylene blue, N-methyldiethanolamine, and diphenyliodonium chloride. *J. Polym. Sci. A Polym. Chem.* **38**, 2057–2066 (2000).
35. Kim, D. & Stansbury, J. W. A photo-oxidizable kinetic pathway of three-component photoinitiator systems containing porphyrin dye (Zn-tpp), an electron donor and diphenyliodonium salt. *J. Polym. Sci. A Polym. Chem.* **47**, 3131–3141 (2009).
 36. Kim, D. & Stansbury, J. W. Kinetic pathway investigations of three-component photoinitiator systems for visible-light activated free radical polymerizations. *J. Polym. Sci. A Polym. Chem.* **47**, 887–898 (2009).
 37. Kim, D. & Scranton, A. The role of diphenyl iodonium salt (DPI) in three-component photoinitiator systems containing methylene blue (MB) and an electron donor. *J. Polym. Sci. A Polym. Chem.* **42**, 5863–5871 (2004).
 38. Pierre Fouassier, J. & Lalevée, J. Three-component photoinitiating systems: towards innovative tailor made high performance combinations. *RSC Adv.* **2**, 2621 (2012).
 39. Scholes, G. D., Fleming, G. R., Olaya-Castro, A. & van Grondelle, R. Lessons from nature about solar light harvesting. *Nature Chemistry* **3**, 763–774 (2011).
 40. Kavarnos, G. J. in *Photoinduced Electron Transfer I* 21–58 (Springer, 1990).
 41. Stansbury, J. W. & Dickens, S. H. Determination of double bond conversion in dental resins by near infrared spectroscopy. *Dental Materials* **17**, 71–79 (2001).
 42. Chai, J.-D. & Head-Gordon, M. Long-range corrected hybrid density functionals with damped atom–atom dispersion corrections. *Phys. Chem. Chem. Phys.* **10**, 6615 (2008).
 43. Li, H. & Jensen, J. H. Improving the efficiency and convergence of geometry optimization with the polarizable continuum model: New energy gradients and molecular surface tessellation. *J. Comput. Chem.* **25**, 1449–1462 (2004).
 44. Zhao, Y. & Truhlar, D. G. The M06 suite of density functionals for main group thermochemistry, thermochemical kinetics, noncovalent interactions, excited states, and transition elements: two new functionals and systematic testing of four M06-class functionals and 12 other functionals. *Theor Chem Account* **120**, 215–241 (2007).
 45. Shao, Y. *et al.* Advances in methods and algorithms in a modern quantum chemistry program package. *Phys. Chem. Chem. Phys.* **8**, 3172 (2006).
 46. Schmidt, M. W. *et al.* General atomic and molecular electronic structure system. *J. Comput. Chem.* **14**, 1347–1363 (1993).
 47. Mills, A., Lawrie, K. & McFarlane, M. Blue bottle light: lecture demonstrations of homogeneous and heterogeneous photo-induced electron transfer reactions. *Photochem. Photobiol. Sci.* **8**, 421 (2009).
 48. Galagan, Y., Hsu, S.-H. & Su, W.-F. Monitoring time and temperature by methylene blue containing polyacrylate film. *Sensors and Actuators B: Chemical* **144**, 49–55 (2010).

49. Goodspeed, F. C., Scott, B. L. & Burr, J. G. Photooxidation of tertiary nitrogen compounds by methylene blue. *J. Phys. Chem.* **69**, 1149–1153 (1965).
50. Kavarnos, G. J. & Turro, N. J. Photosensitization by reversible electron transfer: theories, experimental evidence, and examples. *Chem. Rev.* **86**, 401–449 (2001).
51. Kim, D., Scranton, A. B. & Stansbury, J. W. Analysis of association constant for ground-state dye-electron acceptor complex of photoinitiator systems and the association constant effect on the kinetics of visible-light-induced polymerizations. *J. Polym. Sci. A Polym. Chem.* **47**, 1429–1439 (2009).
52. Sirovatka Padon, K. & Scranton, A. B. The effect of oxygen on the three-component radical photoinitiator system: Methylene blue, N-methyldiethanolamine, and diphenyliodonium chloride. *J. Polym. Sci. A Polym. Chem.* **38**, 3336–3346 (2000).
53. Asmusen, S., Arenas, G., Cook, W. D. & Vallo, C. Photobleaching of camphorquinone during polymerization of dimethacrylate-based resins. *Dental Materials* **25**, 1603–1611 (2009).
54. Eaton, D. F. *Dye Sensitized Photopolymerization. Advances in Photochemistry* **13**, 427–487 (John Wiley & Sons, Inc., 1986).
55. Kim, D., Scranton, A. B. & Stansbury, J. W. Effect of the electron donor structure on the shelf-lifetime of visible-light activated three-component initiator systems. *J. Appl. Polym. Sci.* **114**, 1535–1542 (2009).
56. Galagan, Y. & Su, W.-F. Reversible photoreduction of methylene blue in acrylate media containing benzyl dimethyl ketal. *Journal of Photochemistry & Photobiology, A: Chemistry* **195**, 378–383 (2008).
57. Impert, O. *et al.* Kinetics and mechanism of a fast leuco-Methylene Blue oxidation by copper (II)-halide species in acidic aqueous media. *Dalton Transactions* 348–353 (2003).
58. Dektar, J. L. & Hacker, N. P. Photochemistry of diaryliodonium salts. *J. Org. Chem.* **55**, 639–647 (1990).
59. Munekage, Y. *et al.* Cyclic electron flow around photosystem I is essential for photosynthesis. *Nature* **429**, 579–582 (2004).
60. Hertle, A. P. *et al.* PGRL1 Is the Elusive Ferredoxin-Plastoquinone Reductase in Photosynthetic Cyclic Electron Flow. *Molecular Cell* **49**, 511–523 (2013).
61. Datta, P., Efimenko, K. & Genzer, J. The effect of confinement on thermal frontal polymerization. *Polym. Chem.* **3**, 3243 (2012).
62. Mathew, J. & Mahadevan, V. Redox polymerization of 2-hydroxyethyl methacrylate, 2. Kinetics, mechanism and solvent effect using manganese triacetate/cyanoacetic acid as the redox system. *Macromol. Chem. Phys.* **197**, 367–374 (1996).

Chapter 4

1. Hawker, C. J. & Wooley, K. L. The Convergence of Synthetic Organic and Polymer Chemistries. *Science* **309**, 1200–1205 (2005).
2. Wang, J.-S. & Matyjaszewski, K. Controlled/‘ living’ radical polymerization. Atom transfer radical polymerization in the presence of transition-metal complexes. *J. Am. Chem. Soc.* **117**, 5614–5615 (1995).
3. Barner-Kowollik, C., Lutz, J. F. & Perrier, S. New methods of polymer synthesis. *Polym. Chem.* (2012). doi:10.1039/c1py00443c
4. Gong, T., Adzima, B. J. & Bowman, C. N. A novel copper containing photoinitiator, copper(ii) acylphosphinate, and its application in both the photomediated CuAAC reaction and in atom transfer radical polymerization. *Chem. Commun. (Camb.)* **49**, 7950–7952 (2013).
5. Hoyle, C. E. & Bowman, C. N. Thiol-Ene Click Chemistry. *Angew. Chem. Int. Ed.* **49**, 1540–1573 (2010).
6. Patterson, G. D. Light scattering from bulk polymers. *Annual Review of Materials Science* **13**, 219–245 (1983).
7. LIGHT SCATTERING IN PHOTOPOLYMERIZING LAYERS UNDER LASER IRRADIATION. 1–5 (2004).
8. Drenski, M. F., Mignard, E., Alb, A. M. & Reed, W. F. Simultaneous in-Situ Monitoring of Parallel Polymerization Reactions Using Light Scattering; A New Tool for High-Throughput Screening. *J. Comb. Chem.* **6**, 710–716 (2004).
9. Désilles, N., Gautrelet, C., Lecamp, L., Lebaudy, P. & Bunel, C. Effect of UV light scattering during photopolymerization on UV spectroscopy measurements. *European Polymer Journal* **41**, 1296–1303 (2005).
10. Mignard, E. *et al.* Kinetics and Molar Mass Evolution during Atom Transfer Radical Polymerization of n-Butyl Acrylate Using Automatic Continuous Online Monitoring. *Macromolecules* **38**, 9556–9563 (2005).
11. Chang, S. Y., Chang, S. Y., Wang, N. S. & Wang, N. S. 9. *Monitoring Polymerization Reactions by Near-IR Spectroscopy*. (ACS Symposium Series, 1995). doi:10.1021/bk-1995-0598.ch009
12. Florenzano, F. H., Strelitzki, R. & Reed, W. F. Absolute, On-Line Monitoring of Molar Mass during Polymerization Reactions. **31**, 7226–7238 (1998).
13. Reed, W. F. A Method for Online Monitoring of Polydispersity during Polymerization Reactions. *Macromolecules* **33**, 7165–7172 (2000).
14. Alb, A. M., Mignard, E., Drenski, M. F. & Reed, W. F. In Situ Time-Dependent

- Signatures of Light Scattered from Solutions undergoing Polymerization Reactions. *Macromolecules* **37**, 2578–2587 (2004).
15. Alb, A. M., Serelis, A. K. & Reed, W. F. Kinetic Trends in RAFT Homopolymerization from Online Monitoring. *Macromolecules* **41**, 332–338 (2008).
 16. Asmusen, S., Arenas, G., Cook, W. D. & Vallo, C. Photobleaching of camphorquinone during polymerization of dimethacrylate-based resins. *Dental Materials* **25**, 1603–1611 (2009).
 17. Asmussen, S., Arenas, G., Cook, W. D. & Vallo, C. Photoinitiation rate profiles during polymerization of a dimethacrylate-based resin photoinitiated with camphorquinone/amine. Influence of initiator photobleaching rate. *European Polymer Journal* **45**, 515–522 (2009).
 18. Allonas, X., Lalevée, J. & Fouassier, J.-P. in *Polymerization Reactors and Processes* **847**, 140–151 (American Chemical Society, 2009).
 19. Long, K. N., Scott, T. F., Qi, H. J., Bowman, C. N. & Dunn, M. L. Photomechanics of light-activated polymers. *Journal of the Mechanics and Physics of Solids* **57**, 1103–1121 (2009).
 20. Decker, C. & Moussa, K. A new class of highly reactive acrylic monomers, 1. Light-induced polymerization. *Die Makromolekulare Chemie, Rapid Communications* **11**, 159–167 (1990).
 21. Fors, B. P. & Hawker, C. J. Control of a Living Radical Polymerization of Methacrylates by Light. *Angew. Chem. Int. Ed.* **51**, 8850–8853 (2012).
 22. Zhang, T., Chen, T., Amin, I. & Jordan, R. ATRP with a light switch: photoinduced ATRP using a household fluorescent lamp. *Polym. Chem.* **5**, 4790–4796 (2014).
 23. Hutchison, J. B. *et al.* Robust polymer microfluidic device fabrication via contact liquid photolithographic polymerization (CLiPP). *Lab Chip* **4**, 658 (2004).
 24. Scott, T. F., Kowalski, B. A., Sullivan, A. C., Bowman, C. N. & McLeod, R. R. Two-Color Single-Photon Photoinitiation and Photoinhibition for Subdiffraction Photolithography. *Science* **324**, 913–917 (2009).
 25. Stansbury, J. W. Curing dental resins and composites by photopolymerization. *J Esthet Dent* **12**, 300–308 (2000).
 26. Pfeifer, C. S. *et al.* Characterization of dimethacrylate polymeric networks: A study of the crosslinked structure formed by monomers used in dental composites. *European Polymer Journal* **47**, 162–170 (2011).
 27. Maurin, V., Croutxé-Barghorn, C. & Allonas, X. Photopolymerization process of UV powders. Characterization of coating properties. *Progress in Organic Coatings* **73**, 250–256 (2011).
 28. Czech, Z., Butwin, A. & Kabatc, J. Photoreactive UV-crosslinkable acrylic pressure-

- sensitive adhesives containing type-II photoinitiators. *European Polymer Journal* **47**, 225–229 (2011).
29. Ilie, N. & Hickel, R. Can CQ be completely replaced by alternative initiators in dental adhesives? *Dent Mater J* **27**, 221–228 (2008).
 30. Nair, C. Advances in addition-cure phenolic resins. *Progress in Polymer Science* **29**, 401–498 (2004).
 31. DeForest, C. A. & Anseth, K. S. Cytocompatible click-based hydrogels with dynamically tunable properties through orthogonal photoconjugation and photocleavage reactions. 1–7 (2011). doi:10.1038/nchem.1174
 32. Tibbitt, M. W. & Anseth, K. S. Hydrogels as extracellular matrix mimics for 3D cell culture. *Biotechnol. Bioeng.* **103**, 655–663 (2009).
 33. Ifkovits, J. L. & Burdick, J. A. Review: Photopolymerizable and Degradable Biomaterials for Tissue Engineering Applications. *Tissue Engineering* **13**, 2369–2385 (2007).
 34. Fouassier, J. P. & Lalevée, J. *Photoinitiators for Polymer Synthesis: Scope, Reactivity, and Efficiency*. (Wiley-VCH, 2012).
 35. Bowman, C. N. & Kloxin, C. J. Toward an enhanced understanding and implementation of photopolymerization reactions. *AIChE J.* **54**, 2775–2795 (2008).
 36. Decker, C. & Moussa, K. A new method for monitoring ultra-fast photopolymerizations by real-time infra-red (RTIR) spectroscopy. *Die Makromolekulare Chemie* **189**, 2381–2394 (1988).
 37. Esen, D. S., Karasu, F. & Arsu, N. The investigation of photoinitiated polymerization of multifunctional acrylates with TX-BT by Photo-DSC and RT-FTIR. *Progress in Organic Coatings* **70**, 102–107 (2010).
 38. Cherdoud-Chihani, A., Mouzali, M. & Abadie, M. Étude pas dsc de la reticulation de systèmes dgeba/polyacides. *European Polymer Journal* **33**, 969–975 (1997).
 39. Kloosterboer_1996_Monitoring of polymerization-induced phase separation photo-DSC_turbidity measurements. 1–6 (2003).
 40. Roper, T. M., Guymon, C. A. & Hoyle, C. E. Design and performance of a thin-film calorimeter for quantitative characterization of photopolymerizable systems. *Rev. Sci. Instrum.* **76**, 054102 (2005).
 41. Crivello, J. V. A new visible light sensitive photoinitiator system for the cationic polymerization of epoxides. *J. Polym. Sci. A Polym. Chem.* **47**, 866–875 (2009).
 42. Fonseca, G. E., Dubé, M. A. & Penlidis, A. A Critical Overview of Sensors for Monitoring Polymerizations. *Macromol. React. Eng.* **3**, 327–373 (2009).
 43. Decker, C. & Moussa, K. Real-time kinetic study of laser-induced polymerization. *Macromolecules* **22**, 4455–4462 (1989).

44. Stansbury, J. W. & Dickens, S. H. Determination of double bond conversion in dental resins by near infrared spectroscopy. *Dental Materials* **17**, 71–79 (2001).
45. Darcos, V., Monge, S. & Haddleton, D. M. In situ Fourier transform near infrared spectroscopy monitoring of copper mediated living radical polymerization. *J. Polym. Sci. A Polym. Chem.* **42**, 4933–4940 (2004).
46. Decker, C. *UV-curing chemistry: past, present, and future*. (JCT, 1987).
47. Moussa, K. & Decker, C. Light-induced polymerization of new highly reactive acrylic monomers. *J. Polym. Sci. A Polym. Chem.* **31**, 2197–2203 (1993).
48. Decker, C. Photoinitiated crosslinking polymerisation. *Progress in Polymer Science* **21**, 593–650 (1996).
49. Mark, H. & Campbell, B. *An introduction to near infrared spectroscopy and associated chemometrics*. (The Near Infrared Research Corporation, 2008).
50. Schmitt, M. New Method for Real-time Monitoring of Photopolymerization by UV-Vis Spectroscopy. *Macromol. Chem. Phys.* **212**, 1276–1283 (2011).
51. Alakhras, F. & Holze, R. In situ UV–vis- and FT-IR-spectroscopy of electrochemically synthesized furan–thiophene copolymers. *Synthetic Metals* **157**, 109–119 (2007).
52. Lamps, J. P. & Catala, J. M. Kinetic Study, by UV–Vis Spectroscopy, on the Strong Effect of LiCl on the Controlled Polymerization of 2-Bromo-3-hexyl-5-iodothiophene and 2-Iodo-3-hexyl-5-bromothiophene: Determination of the Propagation Rate Constants, Application to the Synthesis of High Molecular Weight Polydodecylthiophene. *Macromolecules* **44**, 7962–7968 (2011).
53. Chen, Y.-C., Ferracane, J. L. & Prael, S. A. Quantum yield of conversion of the photoinitiator camphorquinone. *Dental Materials* **23**, 655–664 (2007).
54. Meinwald, J., Meinwald, J., Klingele, H. O. & Klingele, H. O. Photochemical Reactions of Camphorquinone1. *Journal of the American Chemical ...* (1966). doi:10.1021/ja00961a056
55. Monroe, B. M. & Weiner, S. A. Mechanisms of photochemical reactions in solution. LVIII. Photoreduction of camphorquinone. *Journal of the American Chemical ...* **91**, 450–456 (1969).
56. Monroe, B. M. & Weiner, S. A. Mechanisms of photochemical reactions in solution. LII. Photoreduction of camphorquinone. *Journal of the American ...* **90**, 1913–1914 (1968).
57. Neumann, M. G., Miranda, W. G., Jr., Schmitt, C. C., Rueggeberg, F. A. & Correa, I. C. Molar extinction coefficients and the photon absorption efficiency of dental photoinitiators and light curing units. *Journal of Dentistry* **33**, 525–532 (2005).
58. Decker, C. Kinetic study of light-induced polymerization by real-time UV and IR spectroscopy. *J. Polym. Sci. A Polym. Chem.* **30**, 913–928 (1992).

59. Paćzkowski, J. & Neckers, D. C. Following polymerization kinetics of multifunctional acrylates in real time by fluorescence probe methodology. *Macromolecules* **25**, 548–553 (1992).
60. Fouassier, J.-P., Morlet-Savary, F., Lalevée, J., Allonas, X. & Ley, C. Dyes as Photoinitiators or Photosensitizers of Polymerization Reactions. *Materials* **3**, 5130–5142 (2010).
61. Lalevée, J. *et al.* A Novel Photopolymerization Initiating System Based on an Iridium Complex Photocatalyst. *Macromol. Rapid Commun.* **32**, 917–920 (2011).
62. Timpe, H.-J., Kronfeld, K.-P., Lammel, U., Fouassier, J. P. & Loughnot, D.-J. Excited states of ketones as electron donors—ketone—iodonium salt systems as photoinitiators for radical polymerization. *Journal of Photochemistry & Photobiology, A: Chemistry* **52**, 111–122 (1990).
63. Allonas, X., Lalevée, J. & Fouassier, J.-P. Influence of the S₀–T₁ structural changes on the triplet–triplet sensitization of dienes. *Chemical Physics* **290**, 257–266 (2003).
64. Tehfe, M.-A. *et al.* Iridium complexes incorporating coumarin moiety as catalyst photoinitiators: Towards household green LED bulb and halogen lamp irradiation. *Polymer* 1–6 (2012).
65. Lalevée, J. *et al.* New Photoinitiators Based on the Silyl Radical Chemistry: Polymerization Ability, ESR Spin Trapping, and Laser Flash Photolysis Investigation. *Macromolecules* **41**, 4180–4186 (2008).
66. Allonas, X., Lalevée, J. & Fouassier, J.-P. Investigation of cleavage processes in photoinitiators: from experiments to molecular modeling. *Journal of Photochemistry & Photobiology, A: Chemistry* **159**, 127–133 (2003).
67. García, N., Tiemblo, P. & Guzmán, J. Nominal vs Real Reaction Temperature in PLP Experiments. A Likely Explanation of the Observed Variation in the Propagation Rate Coefficients with Pulse Repetition Rate. *Macromolecules* **40**, 4802–4808 (2007).
68. García, N. *et al.* Persistent Radicals and Transfer Reactions in the Postpolymerization of Methyl Methacrylate. *Macromolecules* **40**, 8168–8177 (2007).
69. Olaj, O. F. & Vana, P. Chain length-dependent termination in pulsed-laser polymerization. VIII. The temperature dependence of the rate coefficient of bimolecular termination in the bulk polymerization of styrene. *J. Polym. Sci. A Polym. Chem.* **38**, 697–705 (2000).
70. Cook, W. D. Photopolymerization kinetics of dimethacrylates using the camphorquinone/amine initiator system. *Polymer* **33**, 600–609 (1992).
71. Cook, W. D. Curing efficiency and ocular hazards of dental photopolymerization sources. *Biomaterials* **7**, 449–454 (1986).
72. Terrones, G. & Pearlstein, A. J. Effects of Optical Attenuation and Consumption of a Photobleaching Initiator on Local Initiation Rates in Photopolymerizations. *Macromolecules* **34**, 3195–3204 (2001).

73. Anseth, K. S., Wang, C. M. & Bowman, C. N. Reaction behaviour and kinetic constants for photopolymerizations of multi (meth) acrylate monomers. *Polymer* (1994). doi:10.1016/0032-3861(94)90129-5
74. Ikemura, K. K., Ichizawa, K. K., Yoshida, M. M., Ito, S. S. & Endo, T. T. UV-VIS spectra and photoinitiation behaviors of acylphosphine oxide and bisacylphosphine oxide derivatives in unfilled, light-cured dental resins. *Dent Mater J* **27**, 765–774 (2008).
75. Jakubiak, J., Allonas, X., Fouassier, J. P. & Sionkowska, A. Camphorquinone–amines photoinitiating systems for the initiation of free radical polymerization. *Polymer* (2003). doi:10.1016/S0032-3861(03)00568-8
76. Jakubiak, J., Wrzyszczyński, A. & Linden, L. Å. The role of amines in the camphorquinone photoinitiated polymerization of multifunctional monomer. *Science* (2007). doi:10.1080/10601320601031440
77. Nie, J. *et al.* A reappraisal of the photopolymerization kinetics of triethyleneglycol dimethacrylate initiated by camphorquinone-N,N-dimethyl-p-toluidine for dental purposes. *Acta Polymerica* **49**, 145–161 (1998).
78. Pyszka, I., Kucyba a, Z. A. & P czkowski, J. Reinvestigation of the Mechanism of the Free Radical Polymerization Photoinitiation Process by Camphorquinone-Coinitiator Systems: New Results. *Macromol. Chem. Phys.* **205**, 2371–2375 (2004).
79. Lovell, L. G., Stansbury, J. W., Syrpes, D. C. & Bowman, C. N. Effects of Composition and Reactivity on the Reaction Kinetics of Dimethacrylate/Dimethacrylate Copolymerizations. *Macromolecules* **32**, 3913–3921 (1999).
80. Anseth, K. S., Kline, L. M., Walker, T. A. & Anderson, K. J. Reaction kinetics and volume relaxation during polymerizations of multiethylene glycol dimethacrylates. ... **28**, 2491–2499 (1995).
81. Anseth, K. S., Wang, C. M. & Bowman, C. N. Kinetic evidence of reaction diffusion during the polymerization of multi (meth) acrylate monomers. *Macromolecules* **27**, 650–655 (1994).
82. Dickens, S. H., Stansbury, J. W., Choi, K. M. & Floyd, C. J. E. Photopolymerization Kinetics of Methacrylate Dental Resins. *Macromolecules* **36**, 6043–6053 (2003).
83. Rosspeintner, A., Kattnig, D. R., Angulo, G., Landgraf, S. & Grampp, G. The Rehm–Weller Experiment in View of Distant Electron Transfer. *Chem. Eur. J.* **14**, 6213–6221 (2008).

Chapter 5

1. Bowman, C. N. & Kloxin, C. J. Toward an enhanced understanding and implementation of photopolymerization reactions. *AIChE J.* **54**, 2775–2795 (2008).
2. Stansbury, J. W. Curing dental resins and composites by photopolymerization. *J Esthet Dent* **12**, 300–308 (2000).
3. Shalaby, S. W. & Salz, U. *Polymers for Dental and Orthopedic Applications*. (CRC Press, 2006).
4. DeForest, C. A. & Anseth, K. S. Cytocompatible click-based hydrogels with dynamically tunable properties through orthogonal photoconjugation and photocleavage reactions. 1–7 (2011). doi:10.1038/nchem.1174
5. DeForest, C. A., Polizzotti, B. D. & Anseth, K. S. Sequential click reactions for synthesizing and patterning three-dimensional cell microenvironments. *Nature Materials* **8**, 659–664 (2009).
6. Jakubiak, J., Allonas, X., Fouassier, J. P. & Sionkowska, A. Camphorquinone–amines photoinitiating systems for the initiation of free radical polymerization. *Polymer* (2003). doi:10.1016/S0032-3861(03)00568-8
7. Kamoun, E. A., Winkel, A., Eisenburger, M. & Menzel, H. Carboxylated camphorquinone as visible-light photoinitiator for biomedical application: Synthesis, characterization, and application. *ARABIAN JOURNAL OF CHEMISTRY* 1–10 (2014). doi:10.1016/j.arabjc.2014.03.008
8. Schneider, L. F. J., Cavalcante, L. M., Prah, S. A., Pfeifer, C. S. & Ferracane, J. L. Curing efficiency of dental resin composites formulated with camphorquinone or trimethylbenzoyl-diphenyl-phosphine oxide. *Dent Mater* **28**, 392–397 (2012).
9. Asmussen, S., Arenas, G., Cook, W. D. & Vallo, C. Photoinitiation rate profiles during polymerization of a dimethacrylate-based resin photoinitiated with camphorquinone/amine. Influence of initiator photobleaching rate. *European Polymer Journal* **45**, 515–522 (2009).
10. Nie, J. *et al.* A reappraisal of the photopolymerization kinetics of triethyleneglycol dimethacrylate initiated by camphorquinone-N,N-dimethyl-p-toluidine for dental purposes. *Acta Polymerica* **49**, 145–161 (1998).
11. Sionkowska, A., Kamińska, A., Linden, L.-A. & Rabek, J. F. Comparison of the photopolymerization kinetics of triethyleneglycol dimethacrylate initiated by camphorquinone/N-phenylglycine and camphorquinone/D,L- α -phenylglycine. *Polym. Bull.* **43**, 349–355 (1999).
12. Cook, W. D. & Chen, F. Enhanced photopolymerization of dimethacrylates with ketones, amines, and iodonium salts: The CQ system. *J. Polym. Sci. A Polym. Chem.* **49**, 5030–5041 (2011).

13. SCHROEDER, W. & VALLO, C. Effect of different photoinitiator systems on conversion profiles of a model unfilled light-cured resin. *Dental Materials* **23**, 1313–1321 (2007).
14. Grotzinger, C., Burget, D., Jacques, P. & Fouassier, J. P. Photopolymerization Reactions Initiated by a Visible Light Photoinitiating System: Dye/Amine/Bis (trichloromethyl)-Substituted-1, 3, 5-Triazine. *Macromol. Chem. Phys.* **202**, 3513–3522 (2001).
15. Kim, D. & Stansbury, J. W. A photo-oxidizable kinetic pathway of three-component photoinitiator systems containing porphyrin dye (Zn-tp), an electron donor and diphenyl iodonium salt. *J. Polym. Sci. A Polym. Chem.* **47**, 3131–3141 (2009).
16. Peter Pappas, S., Tilley, M. G. & Pappas, B. C. Anthracene-bound sulfonium salts: highly efficient photoinitiators for cationic polymerization. *Journal of Photochemistry & Photobiology, A: Chemistry* **159**, 161–171 (2003).
17. Padon, K. S. & Scranton, A. B. A mechanistic investigation of the three-component radical photoinitiator system Eosin Y spirit soluble, N-methyldiethanolamine, and diphenyliodonium chloride. *J. Polym. Sci. A Polym. Chem.* **39**, 715–723 (2001).
18. Kim, D. & Stansbury, J. W. Kinetic pathway investigations of three-component photoinitiator systems for visible-light activated free radical polymerizations. *J. Polym. Sci. A Polym. Chem.* **47**, 887–898 (2009).
19. Padon, K. S. & Scranton, A. B. A mechanistic investigation of a three-component radical photoinitiator system comprising methylene blue, N-methyldiethanolamine, and diphenyliodonium chloride. *J. Polym. Sci. A Polym. Chem.* **38**, 2057–2066 (2000).
20. Sirovatka Padon, K. & Scranton, A. B. The effect of oxygen on the three-component radical photoinitiator system: Methylene blue, N-methyldiethanolamine, and diphenyliodonium chloride. *J. Polym. Sci. A Polym. Chem.* **38**, 3336–3346 (2000).
21. Monroe, B. M. & Weiner, S. A. Mechanisms of photochemical reactions in solution. LII. Photoreduction of camphorquinone. *Journal of the American ...* **90**, 1913–1914 (1968).
22. Monroe, B. M. & Weiner, S. A. Mechanisms of photochemical reactions in solution. LVIII. Photoreduction of camphorquinone. *Journal of the American Chemical ...* **91**, 450–456 (1969).
23. Rubin, M. B. On the fate of initially formed radicals in photochemical hydrogen abstraction reactions. *Tetrahedron Letters* **10**, 3931–3934 (1969).
24. Rubin, M. B. & Ben-Bassat, J. M. A convenient new method for reduction of quinones and α -diketones. *Tetrahedron Letters* **12**, 3403–3406 (1971).
25. Rubin, M. B., Weiner, M. & Scharf, H. D. Photochemical reactions of cyclic, unsaturated diketones. *Journal of the American ...* **98**, 5699–5700 (1976).
26. Pączkowski, J. & Kucybala, Z. Generalization of the kinetic scheme for a dye-photosensitized free-radical polymerization initiating system via an intermolecular electron-transfer process. Application of Marcus theory. *Macromolecules* **28**, 269–273 (1995).

27. Paczkowski, J., Pietrzak, M. & Kucybala, Z. Generalization of the kinetic scheme for photoinduced polymerization via an intermolecular electron transfer process. 2. Application of the Marcus theory. *Macromolecules* **29**, 5057–5064 (1996).
28. Andrea, M. Marcus theory for electron transfer a short introduction. *MPIP Journal Club-Mainz* (2008).
29. Park, Y. J., Chae, K. H. & Rawls, H. R. Development of a new photoinitiation system for dental light-cure composite resins. *Dent Mater* **15**, 120–127 (1999).
30. Wang, Y., Spencer, P., Yao, X. & Ye, Q. Effect of coinitiator and water on the photoreactivity and photopolymerization of HEMA/camphoquinone-based reactant mixtures. *J. Biomed. Mater. Res.* **78A**, 721–728 (2006).
31. Guo, X., Wang, Y., Spencer, P., Ye, Q. & Yao, X. Effects of water content and initiator composition on photopolymerization of a model BisGMA/HEMA resin. *Dental Materials* **24**, 824–831 (2008).
32. Kim, D. & Scranton, A. The role of diphenyl iodonium salt (DPI) in three-component photoinitiator systems containing methylene blue (MB) and an electron donor. *J. Polym. Sci. A Polym. Chem.* **42**, 5863–5871 (2004).
33. Aguirre-Soto, A., Lim, C.-H., Hwang, A. T., Musgrave, C. B. & Stansbury, J. W. Visible-Light Organic Photocatalysis for Latent Radical-Initiated Polymerization via $2e^-/1H^+$ Transfers: Initiation with Parallels to Photosynthesis. *J. Am. Chem. Soc.* **136**, 7418–7427 (2014).
34. Meinwald, J., Meinwald, J., Klingele, H. O. & Klingele, H. O. Photochemical Reactions of Camphorquinone1. *Journal of the American Chemical ...* (1966). doi:10.1021/ja00961a056
35. Anseth, K. S., Bowman, C. N. & Peppas, N. A. Dynamic mechanical studies of the glass transition temperature of photopolymerized multifunctional acrylates. *Polym. Bull.* **31**, 229–233 (1993).
36. Anseth, K. S., Wang, C. M. & Bowman, C. N. Reaction behaviour and kinetic constants for photopolymerizations of multi (meth) acrylate monomers. *Polymer* (1994). doi:10.1016/0032-3861(94)90129-5
37. Anseth, K. S., Kline, L. M., Walker, T. A. & Anderson, K. J. Reaction kinetics and volume relaxation during polymerizations of multiethylene glycol dimethacrylates. ... **28**, 2491–2499 (1995).
38. Weinberg, D. R. *et al.* Proton-coupled electron transfer. *Chem. Rev.* **112**, 4016–4093 (2012).
39. Ullrich, G., Burtscher, P., Salz, U., Moszner, N. & Liska, R. Phenylglycine derivatives as coinitiators for the radical photopolymerization of acidic aqueous formulations. *J. Polym. Sci. A Polym. Chem.* **44**, 115–125 (2005).
40. Yamaoka, T., Zhang, Y. C. & Koseki, K. N-phenylglycine-(thio)xanthene dye

photoinitiating system and application to photopolymer for visible laser exposure. *J. Appl. Polym. Sci.* **38**, 1271–1285 (1989).

Chapter 6

1. Yoon, T. P., Ischay, M. A. & Du, J. Visible light photocatalysis as a greener approach to photochemical synthesis. *Nature Chemistry* **2**, 527–532 (2010).
2. Narayanam, J. M. R., Tucker, J. W. & Stephenson, C. R. J. Electron-Transfer Photoredox Catalysis: Development of a Tin-Free Reductive Dehalogenation Reaction. *J. Am. Chem. Soc.* **131**, 8756–8757 (2009).
3. Ischay, M. A., Lu, Z. & Yoon, T. P. [2+2] Cycloadditions by Oxidative Visible Light Photocatalysis. *J. Am. Chem. Soc.* **132**, 8572–8574 (2010).
4. Ischay, M. A., Anzovino, M. E., Du, J. & Yoon, T. P. Efficient Visible Light Photocatalysis of [2+2] Enone Cycloadditions. *J. Am. Chem. Soc.* **130**, 12886–12887 (2008).
5. Wallentin, C.-J., Nguyen, J. D., Finkbeiner, P. & Stephenson, C. R. J. Visible Light-Mediated Atom Transfer Radical Addition via Oxidative and Reductive Quenching of Photocatalysts. *J. Am. Chem. Soc.* **134**, 8875–8884 (2012).
6. Fors, B. P. & Hawker, C. J. Control of a Living Radical Polymerization of Methacrylates by Light. *Angew. Chem. Int. Ed.* **51**, 8850–8853 (2012).
7. Treat, N. J. *et al.* Metal-Free Atom Transfer Radical Polymerization. *J. Am. Chem. Soc.* **136**, 16096–16101 (2014).
8. Tehfe, M.-A. *et al.* Polyaromatic Structures as Organo-Photoinitiator Catalysts for Efficient Visible Light Induced Dual Radical/Cationic Photopolymerization and Interpenetrated Polymer Networks Synthesis. *Macromolecules* **45**, 4454–4460 (2012).
9. Tehfe, M.-A. *et al.* Iridium complexes incorporating coumarin moiety as catalyst photoinitiators: Towards household green LED bulb and halogen lamp irradiation. *Polymer* 1–6 (2012).
10. Eaton, D. F. in *Photoinduced Electron Transfer I* **156**, 199–225 (Springer Berlin Heidelberg, 1990).
11. EATON, D. Nonlinear optical materials. *Science* **253**, 281–287 (1991).
12. Lyubimova, T., Caglio, S., Gelfi, C., Righetti, P. G. & Rabilloud, T. Photopolymerization of polyacrylamide gels with methylene blue. *ELECTROPHORESIS* **14**, 40–50 (1993).
13. Kim, D. & Stansbury, J. W. A photo-oxidizable kinetic pathway of three-component photoinitiator systems containing porphyrin dye (Zn-tpp), an electron donor and diphenyl

- iodonium salt. *J. Polym. Sci. A Polym. Chem.* **47**, 3131–3141 (2009).
14. Kim, D. & Stansbury, J. W. Kinetic pathway investigations of three-component photoinitiator systems for visible-light activated free radical polymerizations. *J. Polym. Sci. A Polym. Chem.* **47**, 887–898 (2009).
 15. Padon, K. S. & Scranton, A. B. A mechanistic investigation of a three-component radical photoinitiator system comprising methylene blue, N-methyldiethanolamine, and diphenyliodonium chloride. *J. Polym. Sci. A Polym. Chem.* **38**, 2057–2066 (2000).
 16. Padon, K. S. & Scranton, A. B. A mechanistic investigation of the three-component radical photoinitiator system Eosin Y spirit soluble, N-methyldiethanolamine, and diphenyliodonium chloride. *J. Polym. Sci. A Polym. Chem.* **39**, 715–723 (2001).
 17. DeForest, C. A. & Anseth, K. S. Cytocompatible click-based hydrogels with dynamically tunable properties through orthogonal photoconjugation and photocleavage reactions. 1–7 (2011). doi:10.1038/nchem.1174
 18. Pitre, S. P., McTiernan, C. D., Ismaili, H. & Scaiano, J. C. Metal-Free Photocatalytic Radical Trifluoromethylation Utilizing Methylene Blue and Visible Light Irradiation. *ACS Catal.* (2014). doi:10.1021/cs5005823
 19. Pitre, S. P., McTiernan, C. D., Ismaili, H. & Scaiano, J. C. Mechanistic Insights and Kinetic Analysis for the Oxidative Hydroxylation of Arylboronic Acids by Visible Light Photoredox Catalysis: A Metal-Free Alternative. *J. Am. Chem. Soc.* **135**, 13286–13289 (2013).
 20. Zhang, G., Song, I. Y., Ahn, K. H., Park, T. & Choi, W. Free Radical Polymerization Initiated and Controlled by Visible Light Photocatalysis at Ambient Temperature. *Macromolecules* **44**, 7594–7599 (2011).
 21. Aguirre-Soto, A., Lim, C.-H., Hwang, A. T., Musgrave, C. B. & Stansbury, J. W. Visible-Light Organic Photocatalysis for Latent Radical-Initiated Polymerization via $2e^-/1H^+$ Transfers: Initiation with Parallels to Photosynthesis. *J. Am. Chem. Soc.* **136**, 7418–7427 (2014).
 22. Du, J. & Yoon, T. P. Crossed Intermolecular [2+2] Cycloadditions of Acyclic Enones via Visible Light Photocatalysis. *J. Am. Chem. Soc.* **131**, 14604–14605 (2009).
 23. Kotani, S., Osakama, K., Sugiura, M. & Nakajima, M. A Tertiary Amine as A Hydride Donor: Trichlorosilyl Triflate-mediated Conjugate Reduction of Unsaturated Ketones. *Org. Lett.* **13**, 3968–3971 (2011).
 24. Osakama, K., Sugiura, M., Nakajima, M. & Kotani, S. Enantioselective reductive aldol reaction using tertiary amine as hydride donor. *Tetrahedron Letters* **53**, 4199–4201 (2012).
 25. Singh, A., Arora, A. & Weaver, J. D. Photoredox-Mediated C–H Functionalization and Coupling of Tertiary Aliphatic Amines with 2-Chloroazoles. *Org. Lett.* **15**, 5390–5393 (2013).

26. Liu, Y., Yamamoto, S., Fujiyama, Y. & Sueishi, Y. Kinetic study on the reversible hydride transfer between methylene blue and thionine. *Phys. Chem. Chem. Phys.* **2**, 2367–2371 (2000).
27. Liu, Y., Yamamoto, S. & Sueishi, Y. Photoinduced hydride transfer reaction between methylene blue and leuco crystal violet. *Journal of Photochemistry and ...* (2001). doi:10.1016/S1010-6030(01)00530-5
28. Yamamoto, S., Fujiyama, Y., Shiozaki, M., Sueishi, Y. & Nishimura, N. Hydride transfer reactions of leuco methylene blue and leuco thionine with some p-benzoquinones. *Journal of Physical Organic Chemistry* **8**, 805–809 (1995).
29. McKay, R. B. Red Forms of Methylene Blue. *Nature* **210**, 296–297 (1966).
30. Seal, B. K., Sil, H. & Mukherjee, D. C. Independent determination of equilibrium constant and molar extinction coefficient of molecular complexes from spectrophotometric data by a graphical method. *Spectrochimica Acta Part A: Molecular Spectroscopy* **38**, 289–292 (1982).
31. Decker, C. & Moussa, K. A new method for monitoring ultra-fast photopolymerizations by real-time infra-red (RTIR) spectroscopy. *Die Makromolekulare Chemie* **189**, 2381–2394 (1988).
32. Eaton, D. F. *Dye Sensitized Photopolymerization*. 427–487 (John Wiley & Sons, Inc., 1986). doi:10.1002/9780470133439.ch6
33. RABINOWITCH, E. & Epstein, L. F. Polymerization of dyestuffs in solution. thionine and methylene blue¹. *Journal of the American Chemical ...* (1941). doi:10.1021/ja01846a011
34. Hammes-Schiffer, S. Comparison of hydride, hydrogen atom, and proton-coupled electron transfer reactions. *Chemphyschem* **3**, 33–42 (2002).
35. Deno, N. C., Peterson, H. J. & Saines, G. S. The Hydride-Transfer Reaction. *Chem. Rev.* (1960).
36. Lalevée, J., Allonas, X. & Fouassier, J.-P. N–H and α (C–H) Bond Dissociation Enthalpies of Aliphatic Amines. *J. Am. Chem. Soc.* **124**, 9613–9621 (2002).
37. Kayser, R. H. & Young, R. H. THE PHOTOREDUCTION OF METHYLENE BLUE BY AMINES—I. A FLASH PHOTOLYSIS STUDY OF THE REACTION BETWEEN TRIPLET METHYLENE BLUE AND *Photochem Photobiol* (1976).
38. Kayser, R. H. & Young, R. H. The photoreduction of methylene blue by amines—II. An investigation of the decay of semireduced methylene blue. *Photochem Photobiol* (1976).
39. Chen, C. S. H. Dye-sensitized photopolymerization. I. Polymerization of acrylamide in aqueous solution sensitized by methylene blue–triethanolamine system. *Journal of Polymer Science Part A: General Papers* **3**, 1107–1125 (1965).
40. Chen, C. S. H. Dye-sensitized photopolymerization. II. Enhanced sensitization by

combination of a cationic and an anionic dye. *Journal of Polymer Science Part A: General Papers* **3**, 1127–1136 (1965).

41. Chen, C. S. H. Dye-sensitized photopolymerization. III. Structural effects of thiazine dyes. *Journal of Polymer Science Part A: General Papers* **3**, 1137–1154 (1965).
42. Chen, C. S. H. Dye-sensitized photopolymerization. IV. Enhanced rates of polymerization of acrylamide in ethylene glycol, sensitized by thiazine dyes with triethanolamine. *Journal of Polymer Science Part A: General Papers* **3**, 1155–1170 (1965).
43. Chen, C. S. H. Dye-sensitized photopolymerization. V. Polymerization of acrylamide in deaerated systems. *Journal of Polymer Science Part A: General Papers* **3**, 1807–1823 (1965).

Chapter 7

1. Jariwala, A. S. *et al.* Modeling effects of oxygen inhibition in mask-based stereolithography. *Rapid Prototyping Journal* **17**, 168–175 (2011).
2. EATON, D. Nonlinear optical materials. *Science* **253**, 281–287 (1991).
3. Young, J. S. J., Gonzales, K. D. K. & Anseth, K. S. K. Photopolymers in orthopedics: characterization of novel crosslinked polyanhydrides. *Biomaterials* **21**, 1181–1188 (2000).
4. Stansbury, J. W. Curing dental resins and composites by photopolymerization. *J Esthet Dent* **12**, 300–308 (2000).
5. Eaton, D. F. in *Photoinduced Electron Transfer I* **156**, 199–225 (Springer Berlin Heidelberg, 1990).
6. Ifkovits, J. L. & Burdick, J. A. Review: Photopolymerizable and Degradable Biomaterials for Tissue Engineering Applications. *Tissue Engineering* **13**, 2369–2385 (2007).
7. Moussa, K. & Decker, C. Light-induced polymerization of new highly reactive acrylic monomers. *J. Polym. Sci. A Polym. Chem.* **31**, 2197–2203 (1993).
8. Anseth, K. S., Wang, C. M. & Bowman, C. N. Reaction behaviour and kinetic constants for photopolymerizations of multi (meth) acrylate monomers. *Polymer* (1994). doi:10.1016/0032-3861(94)90129-5
9. Bowman, C. N. & Kloxin, C. J. Toward an enhanced understanding and implementation of photopolymerization reactions. *AIChE J.* **54**, 2775–2795 (2008).
10. Anseth, K. S., Bowman, C. N. & Peppas, N. A. Dynamic mechanical studies of the glass transition temperature of photopolymerized multifunctional acrylates. *Polym. Bull.* **31**, 229–233 (1993).

11. Kilambi, H. *et al.* Design, Development, and Evaluation of Monovinyl Acrylates Characterized by Secondary Functionalities as Reactive Diluents to Diacrylates. *Macromolecules* **40**, 6112–6118 (2007).
12. KILAMBI, H. *et al.* Evaluation of highly reactive mono-methacrylates as reactive diluents for BisGMA-based dental composites. *Dental Materials* **25**, 33–38 (2009).
13. Berchtold, K. A., Nie, J., Stansbury, J. W. & Bowman, C. N. Reactivity of Monovinyl (Meth)acrylates Containing Cyclic Carbonates. *Macromolecules* **41**, 9035–9043 (2008).
14. Kilambi, H., Stansbury, J. W. & Bowman, C. N. Enhanced reactivity of monovinyl acrylates characterized by secondary functionalities toward photopolymerization and Michael addition: Contribution of intramolecular effects. *J. Polym. Sci. A Polym. Chem.* **46**, 3452–3458 (2008).
15. Kilambi, H., Konopka, D., Stansbury, J. W. & Bowman, C. N. Factors affecting the sensitivity to acid inhibition in novel acrylates characterized by secondary functionalities. *J. Polym. Sci. A Polym. Chem.* **45**, 1287–1295 (2007).
16. Kilambi, H., Reddy, S. K., Schneidewind, L., Stansbury, J. W. & Bowman, C. N. Influence of the secondary functionality on the radical-vinyl chemistry of highly reactive monoacrylates. *J. Polym. Sci. A Polym. Chem.* **47**, 4859–4870 (2009).
17. Berchtold, K. A. *et al.* Novel monovinyl methacrylic monomers containing secondary functionality for ultrarapid polymerization: steady-state evaluation. *Macromolecules* **37**, 3165–3179 (2004).
18. Beckel, E. R., Stansbury, J. W. & Bowman, C. N. Effect of Aliphatic Spacer Substitution on the Reactivity of Phenyl Carbamate Acrylate Monomers. *Macromolecules* **38**, 3093–3098 (2005).
19. Beckel, E. R., Nie, J., Stansbury, J. W. & Bowman, C. N. Effect of Aryl Substituents on the Reactivity of Phenyl Carbamate Acrylate Monomers. *Macromolecules* **37**, 4062–4069 (2004).
20. Berchtold, K. A. *et al.* Rapid Solid-State Photopolymerization of Cyclic Acetal-Containing Acrylates. *Macromolecules* **42**, 2433–2437 (2009).
21. Kilambi, H., Stansbury, J. W. & Bowman, C. N. Deconvoluting the Impact of Intermolecular and Intramolecular Interactions on the Polymerization Kinetics of Ultrarapid Mono(meth)acrylates. *Macromolecules* **40**, 47–54 (2007).
22. Lee, T. Y., Roper, T. M., Jonsson, E. S., Guymon, C. A. & Hoyle, C. E. Influence of Hydrogen Bonding on Photopolymerization Rate of Hydroxyalkyl Acrylates. *Macromolecules* **37**, 3659–3665 (2004).
23. Lee, T. Y. *et al.* The kinetics of vinyl acrylate photopolymerization. *Polymer* **44**, 2859–2865 (2003).
24. Jansen, J. F. G. A., Dias, A. A., Dorsch, M. & Coussens, B. Fast Monomers: Factors Affecting the Inherent Reactivity of Acrylate Monomers in Photoinitiated Acrylate

- Polymerization. *Macromolecules* **36**, 3861–3873 (2003).
25. Berchtold, K. A. CHAPTER 4. 1–6 (2001).
 26. *Kinetic Studies of Free Radical Photopolymerizations-11 Effect of Preorganization Due to Hydrogen Bonding on the Rate of Photoinitiated Acrylate* (ACS ..., 2003). doi:10.1021/bk-2003-0847.ch011
 27. Stansbury, J. W. & Dickens, S. H. Determination of double bond conversion in dental resins by near infrared spectroscopy. *Dental Materials* **17**, 71–79 (2001).
 28. Decker, C. & Moussa, K. A new method for monitoring ultra-fast photopolymerizations by real-time infra-red (RTIR) spectroscopy. *Die Makromolekulare Chemie* **189**, 2381–2394 (1988).
 29. Kilambi, H., Reddy, S. K., Schneidewind, L., Stansbury, J. W. & Bowman, C. N. Copolymerization and dark polymerization studies for photopolymerization of novel acrylic monomers. *Polymer* **48**, 2014–2021 (2007).
 30. Aguirre-Soto, A., Lim, C.-H., Hwang, A. T., Musgrave, C. B. & Stansbury, J. W. Visible-Light Organic Photocatalysis for Latent Radical-Initiated Polymerization via $2e^-/1H^+$ Transfers: Initiation with Parallels to Photosynthesis. *J. Am. Chem. Soc.* **136**, 7418–7427 (2014).
 31. Odian, G. *Principles of Polymerization*. 1–839 (Wiley Interscience, 2004).
 32. García, N., Tiemblo, P., Hermosilla, L., Sieiro, C. & Guzmán, J. Long-Lived Radicals in the Postpolymerization of Methacrylic Monomers at Low Conversions. *Macromolecules* **38**, 7601–7609 (2005).
 33. García, N., Tiemblo, P. & Guzmán, J. Nominal vs Real Reaction Temperature in PLP Experiments. A Likely Explanation of the Observed Variation in the Propagation Rate Coefficients with Pulse Repetition Rate. *Macromolecules* **40**, 4802–4808 (2007).
 34. García, N. *et al.* Persistent Radicals and Transfer Reactions in the Postpolymerization of Methyl Methacrylate. *Macromolecules* **40**, 8168–8177 (2007).
 35. Berchtold, K. A., Lovell, L. G., Nie, J. & Hacıoğlu, B. The significance of chain length dependent termination in cross-linking polymerizations. *Polymer* (2001).

Conclusions and future directions

1. FUJITA, K., TANIGUCHI, K. & OHNO, H. Dynamic analysis of aggregation of methylene blue with polarized optical waveguide spectroscopy. *Talanta* **65**, 1066–1070 (2005).
2. Rodriguez-Serrano, A., Rai-Constapel, V., Daza, M. C., Doerr, M. & Marian, C. M. A theoretical study of thionine: spin–orbit coupling and intersystem crossing. *Photochem.*

Photobiol. Sci. 11, 1860–1867 (2012).

Appendix A

1. Meng, Y., Fenoli, C. R., Aguirre-Soto, A., Bowman, C. N. & Anthamatten, M. Photoinduced Diffusion Through Polymer Networks. *Adv. Mater.* **26**, 6497–6502 (2014).
2. Scott, T. F., Schneider, A. D., Cook, W. D. & Bowman, C. N. Photoinduced plasticity in cross-linked polymers. *Science* **308**, 1615–1617 (2005).
3. Xi, W. *et al.* Spatial and Temporal Control of Thiol-Michael Addition via Photocaged Superbase in Photopatterning and Two-Stage Polymer Networks Formation. *Macromolecules* **47**, 6159–6165 (2014).
4. Avens, H. J. & Bowman, C. N. Mechanism of cyclic dye regeneration during eosin-sensitized photoinitiation in the presence of polymerization inhibitors. *J. Polym. Sci. A Polym. Chem.* **47**, 6083–6094 (2009).
5. Avens, H. J., Randle, T. J. & Bowman, C. N. Polymerization behavior and polymer properties of eosin-mediated surface modification reactions. *Polymer* **49**, 4762–4768 (2008).
6. Kaastrup, K., Chan, L. & Sikes, H. D. Impact of Dissociation Constant on the Detection Sensitivity of Polymerization-Based Signal Amplification Reactions. *Anal. Chem.* **85**, 8055–8060 (2013).
7. Kaastrup, K. & Sikes, H. D. Polymerization-based signal amplification under ambient conditions with thirty-five second reaction times. *Lab Chip* **12**, 4055 (2012).
8. Lee, J. K., Heimer, B. W. & Sikes, H. D. Systematic Study of Fluorescein-Functionalized Macrophotoinitiators for Colorimetric Bioassays. *Biomacromolecules* **13**, 1136–1143 (2012).
9. Lee, J. K. & Sikes, H. D. Balancing the Initiation and Molecular Recognition Capabilities of Eosin Macroinitiators of Polymerization-Based Signal Amplification Reactions. *Macromol. Rapid Commun.* **35**, 981–986 (2014).

Appendix A

Applications of the coupled UV-Vis/FT-NIR monitoring device

A.1 Versatile applications of the analytical apparatus introduced in this dissertation

A.1.1 Real-time detection of fluorophore diffusing out of polymer films

In the early stages of the development of the analytical device for coupled UV-Vis and FT-NIR spectroscopy we experimented with the use of a modified Czerny-Turner spectrometer that has a higher sensitivity to light and thus allows to monitor fluorescence and phosphorescence. Since we identified that it worked well for the detection of light emitting (fluorescent) molecules we collaborated with the Anthamatten Group at Rochester University to adapt our probing system in order to monitor the release of the known fluorophore Fluorenylmethyloxycarbonyl chloride (FMOC-Cl), which is highly fluorescent because of the fluorenyl group. Our collaborators synthesized polymer networks with Radical Addition Fragmentation Chain-Transfer moieties, namely trithiocarboates, and tethered FMOC-Cl¹. When a UV light sensitive photoinitiator was present in the polymer films, the networks quickly rearranged their structure by the reversible cleaving of the trithiocarbonate groups, i.e. photoinduced plasticity². In consequence, when the polymer films were mechanically fixed to the bottom of a quartz cuvette containing spectroscopic grade THF solvent and exposed to 365 nm light from a mercury lamp the fluorescent moieties were expected to detached from the macromolecular network and be released into the solvent. Figure A.1-a shows a depiction of the probing set-up used for the quantification of FMOC-Cl release into solution.

We monitored the light emission from the solvent at 490 nm (where FMOC-Cl fluoresces) during several irradiation sequences and intensities. We confirmed that the fluorophore efficiently diffuses out of the relaxing polymer network in response to the UV light. Figure A.1-c shows the release profiles at 60 and 77 mW/cm² and the diffusivity constants that were calculated with the experimental data. In the case of the experiments at 77 mW/cm² we also showed that the fluorescence signal immediately disappears when the UV light is turned off. However, when the light is turned on back again the release profile

follows the same exponential trend confirming that there are artifacts on the fluorescence emission from the 365 nm light.

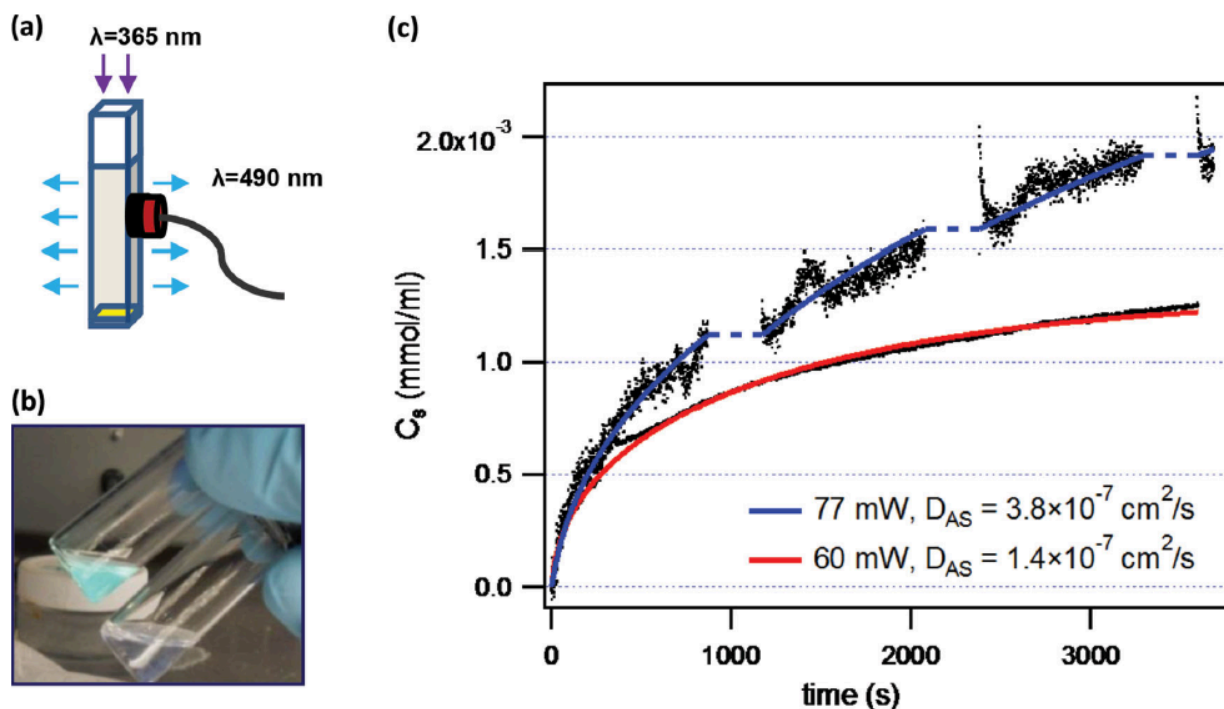


Figure A.1 Photo-induced extraction of a fluorophore from a solvent-swollen polymer film. a) Depiction of the analytical device used to monitor the fluorescence emission at 490 nm associated Fmoc-Cl being released from the polymer at the bottom of a quartz cuvette upon UV irradiation from the top. B) Photographs of THF solutions of Fmoc-Cl under UV-light with Fmoc-Cl (top vial) and with pure solvent. C) Plot of the Fmoc-Cl concentration released into the THF solution with time upon UV irradiation and fitted to least-squares fits using an equation for the diffusion out of the polymer network. Figure extracted from paper published in *Advanced Materials*¹.

A.1.2 Determination of quantum yields of base production from photobase generators

Then, we collaborated in a project where the full-spectrum monitoring (200-1000 nm) capabilities along with the millisecond resolution in the acquisition of spectral data was integral in estimating the quantum yield of base generation by several photobase generators: NVOC-HA,-DEA,-TMG and NPPOC-HA,-DEA,-TMG (structures shown in Figure A.2), which can be used to catalyze the thiol-Michael addition in the synthesis of polymer networks. The photolysis of these photobase generators is shown in Figure A.2.

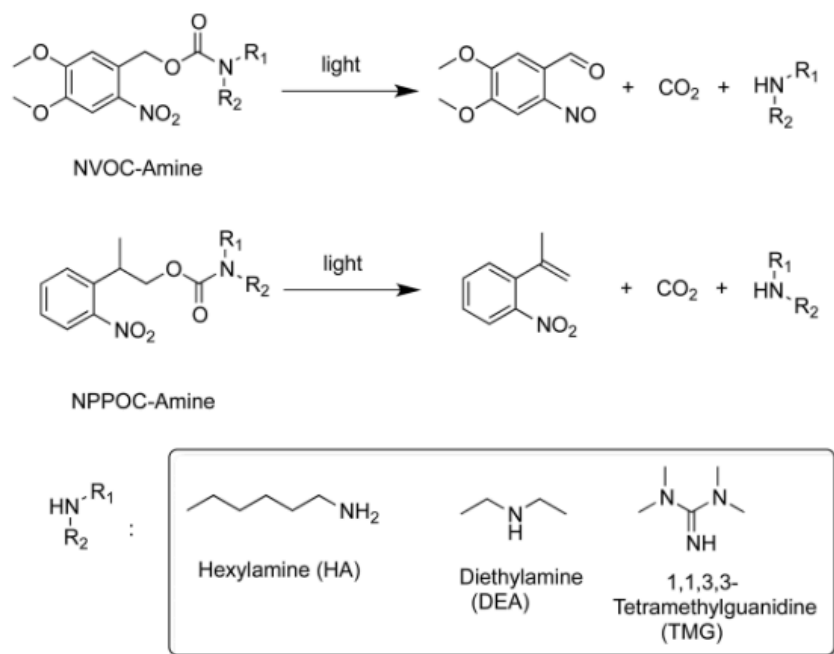


Figure A.2 Photolysis of photobase generators to produce superbases that catalyze thiol-Michael addition. Extracted from Xi et al³.

By doing an analysis of the molar absorptivity of each one of these photobase generators we were able to calculate the rate of photon absorption per time per volume (I_{abs}) after obtaining both the absorbance spectra during the photochemical reaction as well as the emission spectrum from the 320-290 nm light output obtained from a mercury lamp filtered with a narrow band pass filter. From these calculations we were able to determine the rate of photolysis of the photobase generators and the rate of photon absorption. From these two values we then determined the quantum yield for the photolysis of the photolabile bases by the ratio of [cleaved photobase]/[photons absorbed]. The values that we calculated are in decent agreement with those reported previously by others.

entry	compound	$\epsilon_{368}/\text{cm}^{-1} \text{ M}^{-1}$	Φ_{chem}
1	NVOC-HA	4780	0.0013
2	NVOC-DEA	1776	0.0085
3	NVOC-TMG	1988	0.0074
4	NPPOC-HA	4600	0.0010
5	NPPOC-DEA	196	0.2014
6	NPPOC-TMG	240	0.1497

Figure A.3 Photochemical properties of the photobase generators. Extracted from Xi et al.³.

A.1.3 Elucidation of the mechanism for photoreduction of eosin by amine

Another project that stem from both the work on photocatalysis and the development of the coupled UV-Vis and FT-NIR monitoring technique was the collaboration with the Sikes Group at MIT to elucidate the mechanism via which eosin is photoreduced by an tertiary aliphatic amine, namely triethanolamine (TEA) and then regenerated by oxygen. The combination of eosin/TEA has been reported to be an interesting photoinitiator for the free radical polymerization of acrylates and methacrylates. It seems like this system leads to the reduction of the inhibition by molecular oxygen^{4,5}. However, the mechanism to explain the unique behavior of this photoinitiator to oxygen has not been thoroughly addressed. Furthermore, the resilience of this photoinitiator to oxygen inhibition has been exploited for the Polymeriation Based Amplification (PBA) concept in which light-induced polymerization is used in assays to detect the presence of biologically relevant molecules⁶⁻⁹. The proposed mechanism thus far is that the semi-reduced eosin intermediate reacts with the peroxy radicals formed from the inhibition reaction between molecular oxygen and either the alpha aminoalkyl or carbon-centered monomer radicals via a peroxidation reaction. If this happens the eosin would be regenerated and the inhibiting radicals would be quenched. However, a few points have not been addressed: 1) is a semi-reduced eosin radical or a protonated eosin intermediate formed in the process, 2) is eosin regeneration by the peroxy radicals sufficient to explain the lack of short inhibition period, or could it be also explained by the regeneration of eosin directly by molecular oxygen, 3) is eosin triplet state interacting with molecular oxygen as well? As

part of our collaboration we addressed some of these questions. Here we present preliminary data on the regeneration of eosin by molecular oxygen and the appearance of a peak at ~ 410 nm, which is most likely associated with a semi-reduced eosin radical and not a protonated closed shell intermediate Figure A.4.

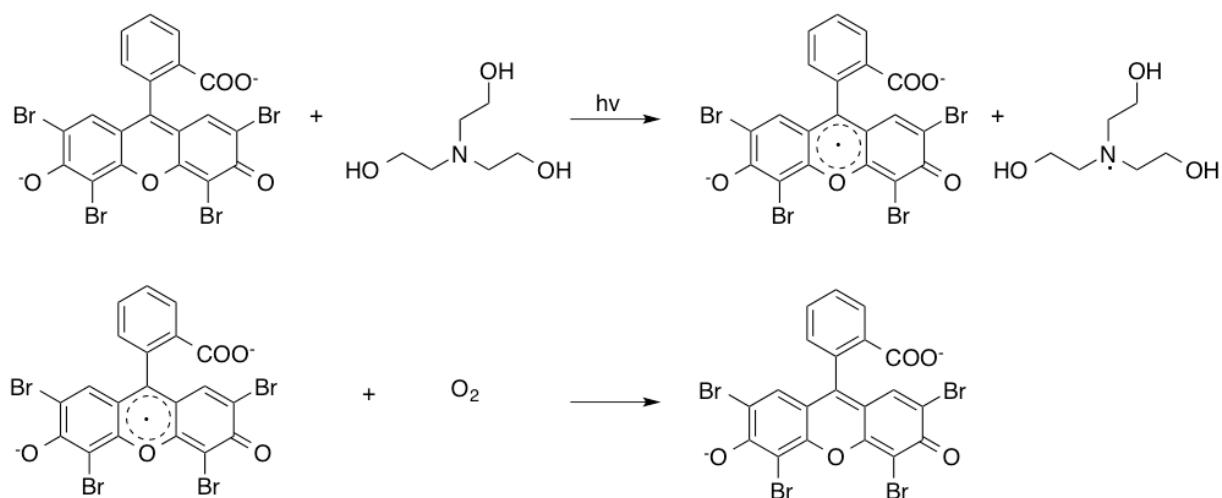


Figure A.4 Photoreduction of eosin by triethanolamine upon irradiation with 500 nm light and regeneration of eosin by molecular oxygen.

In Figure A.5 we show the plot for absorbance vs. time for the peak at 410 nm during irradiation of a solution of eosin and TEA in water. The solution was initially purged with argon gas and the chamber in which the reaction took place was purged with N_2 gas (~ 10 psi) at the beginning of the reaction. Then at about 840 s the nitrogen flow was topped and oxygen from air was let into the reaction chamber. It can be observed that at approximately 840 s the signal at 410 nm decays sharply. We hypothesized that the semi-reduced eosin radical is stabilized via resonance from the pi-structure in the xanthene center, similarly to what happens with Methylene Blue. Then, molecular oxygen is going to act as an efficient reductant to abstract that electron and regenerate eosin quickly. No peak at 410 nm was observed if the reaction is performed under air.

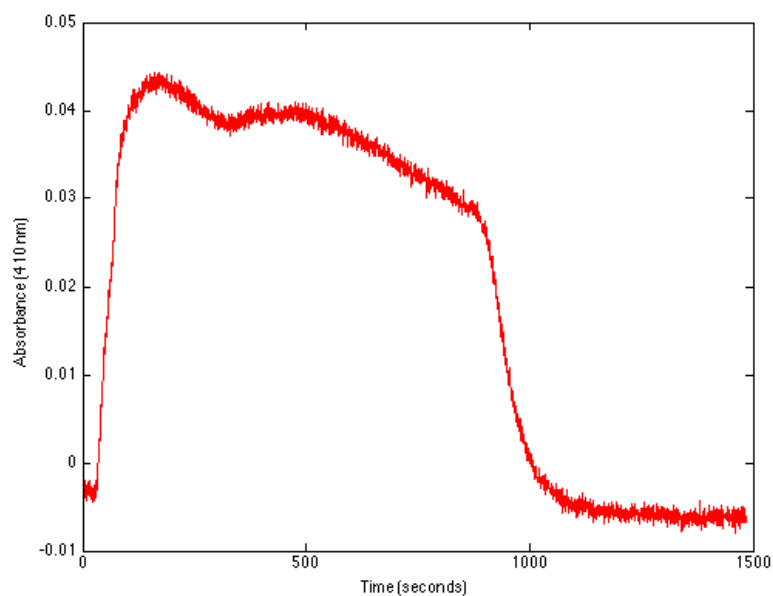


Figure A.5 Photoreduction of eosin by triethanolamine upon irradiation with 500 nm light and regeneration of eosin by molecular oxygen.

Additionally, we observed that the regeneration of the peak at 517 nm (corresponding to eosin) grows back the moment we opened the chamber to air and stopped N_2 flow. The decay of the peak at 410 nm and the growth at 517 nm coincide. However, more experiments need to be performed to assess whether or not the protonated version of the eosin is also produced, depending on the pH of the solution (Figure A.6). These findings along with additional experimental work will be published later.

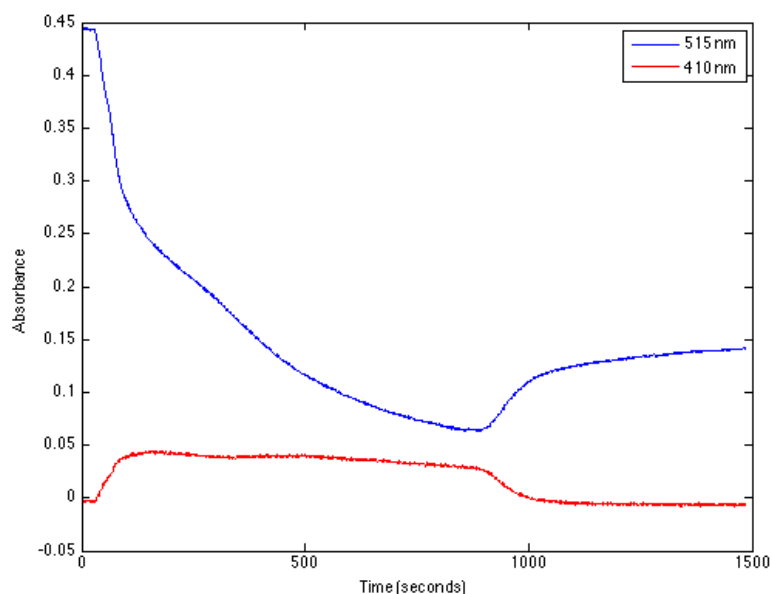


Figure A.6 Photoreduction of eosin by triethanolamine upon irradiation with 500 nm light and regeneration of eosin by molecular oxygen.

A.1.4 Use of photocatalysis for the conversion of CO₂ to methanol

Lastly, we are currently collaborating with the Musgrave group in a project where the capability of the full-spectrum analysis that we integrated into our probing device was employed. Figure A.7 shows preliminary data for the decay of the acridine orange peak at ~ 450 nm and the growth of a peak at around 300 nm that has been previously associated with the formation of the leuco form of this dye. The goal is to see if we can use the leuco form of the dye to convert CO₂ into methanol photochemical. If achieved, this could be the first time that methanol is produced from CO₂ with such a photocatalytic approach. The latter can have an immense impact in the way we produce fuels and raw chemicals.

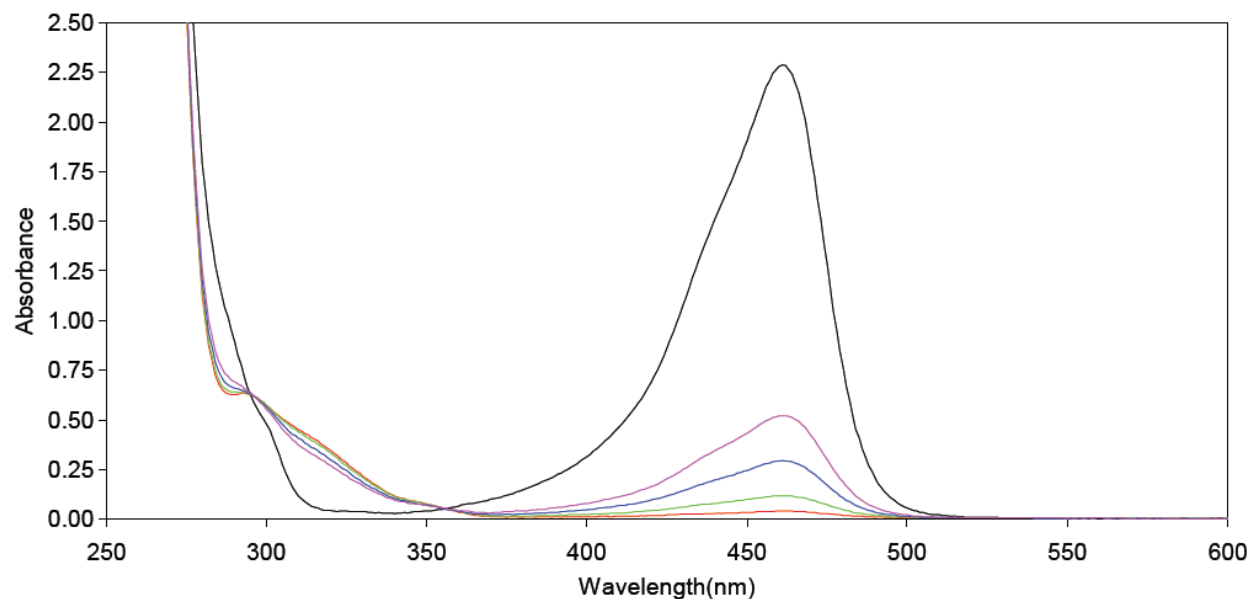


Figure A.7 Photoreduction of acridine orange and production of the leuco dye with an absorbance at ~300 nm.

A.2 References

1. Meng, Y., Fenoli, C. R., Aguirre-Soto, A., Bowman, C. N. & Anthamatten, M. Photoinduced Diffusion Through Polymer Networks. *Adv. Mater.* **26**, 6497–6502 (2014).
2. Scott, T. F., Schneider, A. D., Cook, W. D. & Bowman, C. N. Photoinduced plasticity in cross-linked polymers. *Science* **308**, 1615–1617 (2005).
3. Xi, W. *et al.* Spatial and Temporal Control of Thiol-Michael Addition via Photocaged Superbase in Photopatterning and Two-Stage Polymer Networks Formation. *Macromolecules* **47**, 6159–6165 (2014).
4. Avens, H. J. & Bowman, C. N. Mechanism of cyclic dye regeneration during eosin-sensitized photoinitiation in the presence of polymerization inhibitors. *J. Polym. Sci. A Polym. Chem.* **47**, 6083–6094 (2009).
5. Avens, H. J., Randle, T. J. & Bowman, C. N. Polymerization behavior and polymer properties of eosin-mediated surface modification reactions. *Polymer* **49**, 4762–4768 (2008).
6. Kaastrup, K., Chan, L. & Sikes, H. D. Impact of Dissociation Constant on the Detection Sensitivity of Polymerization-Based Signal Amplification Reactions. *Anal. Chem.* **85**, 8055–8060 (2013).
7. Kaastrup, K. & Sikes, H. D. Polymerization-based signal amplification under ambient conditions with thirty-five second reaction times. *Lab Chip* **12**, 4055 (2012).
8. Lee, J. K., Heimer, B. W. & Sikes, H. D. Systematic Study of Fluorescein-Functionalized Macrophotoinitiators for Colorimetric Bioassays. *Biomacromolecules* **13**, 1136–1143 (2012).

9. Lee, J. K. & Sikes, H. D. Balancing the Initiation and Molecular Recognition Capabilities of Eosin Macroinitiators of Polymerization-Based Signal Amplification Reactions. *Macromol. Rapid Commun.* **35**, 981–986 (2014).